CLIMATE IMPACTS OF AUSTRALIAN LAND COVER CHANGE

Peter Lawrence

(Bachelor of Science with Honours)

School of Geography, Planning and Architecture

Degree of Doctor of Philosophy

March 2004

This is a signed statement of originality that the work presented in the thesis is, to the best of the candidate's knowledge and belief, original and the candidate's own work, except as acknowledged in the text, and that the material has not been submitted, either in whole or in part, for a degree at this or any other university.

Peter Lawrence

Abstract

Australian land cover has been significantly altered since European settlement, primarily for agricultural utilisation, with native vegetation widely replaced or modified for cropping and intensive animal production. While there have been numerous investigations into the regional and near surface climate impacts of Australian land cover change, these investigations have not included the climate impacts of larger-scale changes in atmospheric circulation and their associated feedbacks, or the impacts of longer-term soil moisture feedbacks. In this research the CSIRO General Circulation Model (GCM) was used to investigate the climate impacts of Australian land cover change, with larger-scale and longer-term feedbacks included.

To avoid the common problem of overstating the magnitude and spatial extent of changes in land surface conditions prescribed in GCM land cover change experiments, the current Australian land surface properties were described from finer-scale, satellite derived land cover datasets, with land surface conditions extrapolating from remnant native vegetation to pre-clearing extents to recreate the pre-clearing land surface properties. Aggregation rules were applied to the fine-scale data to generate the land surface parameters of the GCM, ensuring the equivalent sub-grid heterogeneity and land surface biogeophysics were captured in both the current and pre-clearing land surface parameters.

The differences in climate simulated in the pre-clearing and current experiments were analysed for changes in Australian continental and regional climate to assess the modelled climate impacts of Australian land cover change. The changes in modelled climate were compared to observed changes in Australian precipitation over the last 50 and 100 years to assess whether modelled results could be detected in the historical record. The differences in climate simulation also were analysed at the global scale to assess the impacts of local changes on larger scale circulation and climate at distance from the land cover changes.

The Australian continental and regional analyses demonstrated that Australian land cover change did have statistically significant impacts on air temperature and precipitation simulated in the CSIRO GCM. The statistically significant DJF warming and drying modelled over south east Queensland, with causal links back to historical land cover change in the region, corresponded with strong drying trends over the last 50 years for the region. As this region and the areas to the north and west, continue to be actively cleared, this has significant implications for land use management planning in Queensland.

The statistically significant increase in JJA precipitation modelled over south west Western Australia was opposite to the observed drying trends identified from 100 and 50 year analyses of observed precipitation. This result was significant for the region, as it demonstrated that the increased JJA latent heat fluxes over agricultural land had the potential to increase cloud cover and precipitation. This finding supported field studies and satellite observations over the region that showed winter latent heat fluxes were higher over agricultural land than over adjacent native vegetation, and preferentially formed cumulus clouds with higher water content

over the agricultural land. The modelling results therefore suggest the strong drying trend over south west Western Australia has been in response to other climatic forcing, rather than from historical land cover change.

The global analysis identified global scale changes in atmospheric circulation responding to the changes in circulation around Australia. A change in the DJF Australian monsoon flow appeared to influence the wind flow across the Indian and Pacific oceans, with impacts on air temperature and precipitation in Asia, Europe and North America, as well as in Australia. The changes in cloud cover, soil moisture and snow cover over these areas resulted in larger changes in surface fluxes than occurred over the regions of Australian land cover change. A northward shift in JJA mid latitude westerly wind flow around Australia, had impacts over Australia and further to the north, resulting in a northward shift and increased flow in the JJA Asian monsoon. The increased Asian monsoon flow impacted the wind flow and circulation over the Indian and Pacific oceans, with impacts on air temperature, and precipitation over Asia, Europe and North America. Again the changes in cloud cover and soil moisture over these areas resulted in larger changes in surface fluxes than occurred over the regions of Australia land cover change.

Dedicated to my wife Alison, whose love, understanding and support made it all possible, and to our little boy Perry who was born during the final stages of writing it.

Acknowledgements

This research was supported by an Australian Research Council, Strategic Partnership with Industry, Training and Research award with the University of Queensland, School of Geography, Planning and Architecture, and the Queensland Department of Natural Resources and Mines, Climate Impacts and Natural Resources System group. I would like to thank all my supervisors for their support and direction through out the PhD. From the University of Queensland I wish to thank Clive McAlpine as my principal supervisor, for all his work in organising the research and help and dedication to developing this thesis, and to Hamish McGowan and Stuart Phinn for your help and support through out my time there. From the Queensland Department of Natural Resources and Mines I wish to thank Jozef Syktus for teaching me everything I needed to know about the Cray, the CSIRO models, and analysing the mountains of data, and to Steve Crimp and Greg McKeon thank you for your support and advice along the way.

I wish to thank my family for all their love, support and belief in taking on and finish this endeavour, as family makes all things possible. I would especially like to thank my wife Alison who has supported me emotionally, intellectually and financially through this journey of discovery, now it is your time to have some fun. Special thanks also go to my parents John and Janet for automating and formatting the tables of contents, figures and tables, when it all seemed too overwhelming. I would also like to thank my parents and Alison's parents Geoff, Joan and Pam for all your help in finishing everything in Brisbane and our move to Colorado. Lastly, I wish thank all my friends and colleagues who provided support, encouragement and perspective when it was needed.

Table of Contents

INTRODUCTION 1
1.1 Problem Statement 1
1.1.1 Australian Land Cover Change and Climate Change 1
1.1.2 Australian Land Cover Change and Climate Change Investigations 3
1.1.3 Specific Problem Statement 4
1.2 Aims and Objectives 4
1.3 Background to the Problem 6
1.3.1 General Land Cover and Climate Interaction 6
1.3.2 Temporal and Spatial Time Frames of Vegetation and Climate Interaction 7
1.4 Project Scope 9
1.4.1 Land Cover Influences Beyond the Scope of the Project 10
1.5 Thesis Structure 10
LAND COVER INFLUENCES ON CLIMATE REVIEW 13
2.1 Chapter Aims and Rationale 13
2.1.1 Aims and Structure 13
2.1.2 Rationale 13
2.2 Land Cover Impacts on Land Surface and Atmosphere Interaction 14
2.2.1 The Surface Radiation Budget and Vegetation 14
2.2.2 Surface Hydrology and Vegetation 18
2.2.3 Surface Energy Balance and Vegetation 20
2.2.4 Atmospheric Fluxes and Vegetation 21
2.2.5 Surface Fluxes and the Eddy Diffusion Model 22
2.2.6 Surface Roughness and Vegetation 23
2.2.7 Impacts of Changes in Surface Roughness on Surface Fluxes 25
2.2.8 Section Summary 26
2.3 Atmospheric Process And Land Surface Conditions 26
2.3.1 Introduction 26
2.3.2 Local Scale 27
2.3.3 Meso or Regional scale 28
2.3.4 Macro or Global scale 29
2.3.5 Section Summary 32
2.4 Australian Land Cover Change and Climate Case Studies 33
2.4.1 Introduction 33
2.4.2 Investigating South West Western Australia Land Cover Change 34
2.4.3 Modelling of Near Surface Climate Impacts of Australian Land Cover Change 36
2.4.4 Modelling Climate Impacts Australian Soil Moisture Anomalies 38
2.4.5 Section Summary 40
2.5 Synthesis, Conceptual Model And Postulated Relationships 41
2.5.1 Synthesis 41
2.5.2 Postulated Relationships 41
2.6 Chapter Summary 44
AUSTRALIAN LAND COVER CHANGE REVIEW 45
3.1 Chapter Aims and Rationale 45
3.1.1 Aims and Structure 45
3.1.2 Rationale 45
3.2 AUSLIG Historical Australian Land Cover Change 47
3.2.1 Australian Vegetation Mapping by AUSLIG 47
3.2.2 Australian Native Vegetation 47
3.2.3 Australian Vegetation Changes 56
3.2.4 Section Summary 61
3.3 Evaluation Against Other Historical Australian Land Cover Change Studies 61
3.3.1 CSIRO Australian Land Cover Disturbance Assessment 62
3.3.2 Bureau of Rural Sciences Historical Australian Land Cover Change Assessment 64
3.3.3 National Land and Water Resources Audit Australian Vegetation Assessment 65
3.3.4 ANU CO_2 and Land-use Effects on Australian Vegetation 66
3.3.5 National Land and Water Resources Audit Australian Agriculture Assessment 67
3.3.6 Section Summary 68
3.4 Ongoing Australian Land Cover Change Monitoring 68
3.4.1 Bureau of Rural Sciences 1990 – 1995 Australian Land Cover Change Assessment 69
3.4.2 Queensland Statewide Landcover and Tree Study 72
3.4.3 Seasonal and Inter-annual Australian Land Cover Variability 76
3.4.4 Section Summary 77
3.5 Chapter Summary 78
CSIRO GENERAL CIRCULATION MODEL REVIEW AND MODIFICATION 80
4.1 Chapter Aims and Rationale 80
4.1.1 Aims and Structure 80
4.1.2 Rationale 81
4.2 CSIRO Model Review and Land Surface Data Evaluation 83
4.2.1 Review of CSIRO General Circulation Model and Land Surface Representation 83
4.2.2 Evaluation of Global Land Surface Data 84
4.2.3 Section Summary 89
4.3 New Land Surface Parameter Generation Methods 90
4.3.1 Methods 90
4.3.2 CSIRO GCM Land Surface Parameter Results 94

4.3.3 Section Summary 111
4.4 New Land Surface Parameter Sensitivity Experiments 112
4.4.1 Methods 112
4.4.2 Global and Continental Modelling Evaluation 113
4.4.3 Processes Driving Global and Continental Differences 117
4.4.4 Detailed Australian Modelling Evaluation 127
4.4.5 Processes Driving Australian Differences 133
4.4.6 Section Summary 138
4.5 Chapter summary 140
CLIMATE IMPACTS OF AUSTRALIAN LAND COVER CHANGE EXPERIMENTS 142
5.1 Chapter Aims and Rationale 142
5.1.1 Aims and Structure 142
5.1.2 Rationale 143
5.2 Australian Land Cover Change Data And Extrapolation Methods 144
5.2.1 Australian Land Cover Change Data 144
5.2.2 Land Surface Parameter Generation Methods 149
5.2.3 Extrapolation 149
5.2.4 Fine-Scale Data Extrapolation Results 150
5.2.5 GCM Land Surface Parameters Results 154
5.2.6 GCM Regional Land Surface Parameters Analysis 159
5.2.7 Section Summary 163
5.3 Climate Impacts of Australian Land Cover Change Experiments 164
5.3.1 Experimental Methods 164
5.3.2 Australian Continental Results 166
5.3.3 Australian Regional Results 169
5.3.4 Observed Changes in Australian Annual Precipitation 172
5.3.5 Processes Driving Australian Results 176
5.3.6 Global Teleconnectioned Changes 189
5.3.7 Section Summary 196
5.4 Chapter Summary 198
EVALUATION AND CONCLUSION 201
6.1 Chapter Aims and Rationale 201
6.2 Thesis Conclusions 201
6.2.1 Postulated Relationship 1 201
6.2.2 Postulated Relationship 2 205
6.2.3 Postulated Relationship 3 210
6.2.4 Postulated Relationship 4 213
6.2.5 Postulated Relationship 5 215
6.3 Implications 217
6.4 Future Research 218
APPENDICES 220
BIBLIOGRAPHY 232

List of Illustrations and Diagrams

1. Figure 1.1. Australian Climate and Land Cover Changes: (a) Major changes in the structural form of Australian vegetation between the natural (pre-European) and current (mid 1980s) vegetation maps of AUSLIG (1990); (b) Bureau of Rural Sciences (BRS) assessment of Australian land cover change between 1990 and 1995 from Barson et al. (2000) (c) Annual Rainfall Trend Analysis from Linear Regression of Rainfall Data from 1910 – 1999 from Manins et al. (2001); and (d) Annual Rainfall Trend Analysis 1950 – 1999 from Manins et al. (2001). (State names: WA Western Australia; NT Northern Territory; SA South Australia; QLD Queensland; NSW New South Wales; VIC Victoria; and TAS Tasmania) 2

2. Figure 1.2. Conceptual model of the Climate System showing the interacting components and processes, with internal and external forcings for climate change. (from CSIRO Atmospheric Research web site) 7

3. Figure 1.3. Temporal and spatial scale definitions for processes affecting the climate system through changes in the atmosphere (blue) and terrestrial ecosystems (green) (adapted from Trenberth (1992)) 8

4. Figure 1.4. Thesis Chapter Structure and Linkages 11

5. Figure 2.1. Global radiation and energy balances as a percentage of incoming solar radiation at the top of the atmosphere (after Sturman and Tapper (1996)) 15

6. Figure 2.2 Solar radiation dynamics for: (a) individual leaves (after Trenberth (1992)); (b) bare soil; and (c) dense vegetation canopy (adapted from Pielke, (2001b)) 17

7. Figure 2.3 Long wave radiation dynamics for: (a) bare soil; and (b) dense vegetation canopy (adapted from Pielke (2001b)) 18

8. Figure 2.4 Hydrological processes for: (a) bare soil; (b) dense vegetation canopy (only processes additional to bare soil hydrology shown) (adapted from Pielke (2001b)) 19

9. Figure 2.5 Surface Energy Balance processes for: (a) bare soil; (b) dense vegetation canopy (only processes additional to bare soil shown) (adapted from Pielke (2001b)) 20

10. Figure 2.6 Idealised vertical structure of the atmosphere from the earth surface (adapted from Oke (1987) and Peixoto and Oort (1992)) 21

11. Figure 2.7 Logarithmic wind profile (u_z) (blue line) for a wind speed of 5 ms^{-1} at a height of 30m for: (a) bare soil; and (b) dense vegetation canopy (adapted from Pielke (2001b) and Monteith and Unsworth (1990)) 24

12. Figure 2.8 A typical day time meso-scale circulation formed between land and a water body. The uplift over the land is due to strong sensible heat fluxes from surface heating. The subsidence over the water body is from small or negative sensible heat fluxes resulting from the cooler surface temperature, and large evaporative fluxes (from Sturman and Tapper (1996)) 29

13. Figure 2.9 Conceptual model of the immediate biophysical changes in land surface properties that may have resulted from Australian land cover change, and the atmospheric responses in climate that may have resulted from these land surface changes 43

14. Figure 3.1 Australian Natural (pre-European) vegetation from AUSLIG (1990) showing: (a) Structural Form as a generalised subset of the original classification; and (b) Dominant Floristic Type, with only major floristic types listed 48

15. Figure 3.2 Current (mid 1980s) Australian vegetation from AUSLIG (1990) showing: (a) Structural Form as a generalised subset of the original classification; and (b) Dominant Floristic Type, with only major floristic types listed 49

16. Figure 3.3 (a) 1990-91 Landsat Multi Spectral Scanner (MSS) composite image from Graetz et al. (1995a) shown in standard False Colour Composite; and (b) AUSLIG Topographic map of Australia from NLWRA (2001a) 51

17. Figure 3.4 (a) Australian Median Annual Rainfall from Australian Bureau of Meteorology web site. (Median is based on 100 years of data for 1900 – 1999); and (b) CSIRO Atlas of Australian Soils from the Australian Bureau of Rural Sciences web site 52

18. Figure 3.5 Australian forests: (a) Mountain Ash (Eucalyptus regnans) forest with Tree-ferns (Dicksonia antartica), Alpine National Park, Victoria; (b) Sub-tropical rainforest with Grass Trees (Xanthorrhoea glauca) in the foreground, Bunya Mountains National Park, Queensland; (c) Monsoon Rainforest, Kakadu National Park, Northern Territory; and (d) Tropical Rainforest featuring a Strangler fig (Ficus destruens), Atherton tablelands, Queensland. (All photos except those credited otherwise are from the author) 54

19. Figure 3.6 Australian open forests and woodlands: (a) Salmon Gum (Eucalyptus salmonopholia) woodland with understorey of low shrubs, Western Australia, photo courtesy of Robert Hassett; (b) Lancewood (Acacia shirleyi) open forest, near St George, Queensland; (c) Poplar box (Eucalyptus populnea) woodland, near Roma, Queensland; and (d) White Gum (Eucalyptus alba) woodland with grass understorey, Kakadu National Park, Northern Territory 54

20. Figure 3.7 Australian shrublands, grasslands and heathlands: (a) Mulga tall shrubland of Acacia aneura, central Australia, photo courtesy of Robert Hassett; (b) Hummock grassland of Trodia spp., central Australia, photo courtesy of Robert Hassett; (c) Mallee tall shrublands of Eucalyptus oleosa, near Kalgoorlie, Western Australia, photo courtesy of Robert Hassett; and (d) Banksia Heathland, near Perth, Western Australia, photo courtesy of Alison Lawrence 55

21. Figure 3.8 Major changes in Australian vegetation between the natural (pre-European) and current (mid 1980s) vegetation maps of AUSLIG (1990) for (a) structural form and (b) dominant floristic type 57

22. Figure 3.9 Agricultural transformation of Australian vegetation: (a) Recently cleared Eucalypt open forest, near Surat, Queensland; (b) Wheat cropping, Darling Downs, Queensland; (c) Buffel grass (Cenchrus ciliaris) sown pasture, near Surat, Queensland; and (d) Sown pastures with uncleared ranges in the background, near Canberra, Australian Capital Territory 58

23. Figure 3.10 Australian historical land cover change maps: (a) Vegetation clearing and tree thinning between the natural (pre-European) and current (mid 1980s) vegetation maps of AUSLIG (1990); (b) CSIRO Wildlife and Ecology assessment of disturbance by clearing in the Australian Intensive Landuse Zone (ILZ) since European settlement from Graetz et al. (1995a); (c) Bureau of Rural Sciences (BRS) assessment of changes in woody vegetation since European settlement from Barson et al. (2000); and (d) National Vegetation Information System (NVIS) assessment of extent of native vegetation clearing from NLWRA (2001b) 62

24. Figure 3.11 Australian agricultural production maps from NLWRA (2001a): (a) Percentage of Australian beef cattle by Statistical Local Area; (b) Percentage of Australian sheep by Statistical Local Area; (c) Australian grain growing areas; and (d) Australian irrigated farming areas by Statistical Local Area 63

25. Figure 3.12 Bureau of Rural Sciences (BRS) assessment of Australian land cover change between 1990 and 1995 from Barson et al. (2000) showing the percentage of each 50 km grid cell newly cleared of woody vegetation 70

26. Figure 3.13 Bureau of Rural Sciences (BRS) assessment of Australian land cover change between 1990 and 1995 from Barson et al. (2000) showing the percentage of each 50 km grid cell with newly regenerated woody vegetation 71

27. Figure 3.14 Queensland Statewide Land and Tree Study (SLATS) clearing maps. The maps show the percentage of each 0.25 degree grid cell newly cleared of woody vegetation over the corresponding time periods: (a) 1991 to 1995 from

DNR (1999a); (b) 1995 to 1997 from DNR (1999b); (c) 1997 to 1999 from DNR (2000); and (d) 1999 to 2001 from DNRM (2003). Clearing is derived by computer classification and visual interpretation with an accuracy of ±10% 74
28. Figure 3.15 Queensland Statewide Land and Tree Study (SLATS) regrowth maps. The maps show the percentage of each 0.25 degree grid cell with new regrowth woody vegetation on cleared land over the corresponding time periods: (a) 1991 to 1995 from DNR (1999a); (b) 1995 to 1997 from DNR (1999b); (c) 1997 to 1999 from DNR (2000); and (d) 1999 to 2001 from DNRM (2003). Regrowth is derived by computer classification and visual interpretation with an accuracy of ±10%..... 75
29. Figure 3.16 Australian seasonal and inter-annual changes in vegetation greeness from NOAA Pathfinder Advanced Very High Resolution Radiometer (AVHRR) satellite imagery using the Normalized Difference Vegetation Index (NDVI) for: (a) May 1988; (b) September 1988; (c) May 1989; and (d) September 1989..... 77
30. Figure 4.1 Vegetation Mapping: (a) Original CSIRO GCM Parameters, Vegetation in Simple Biosphere (SiB) classification; (b) Detailed view of (a) over the Australian Region; (c) IGBP GLCC Vegetation in SiB classification; and (d) Detailed view of (c) over the Australian Region..... 85
31. Figure 4.2 Soil Mapping: (a) Original CSIRO GCM Parameters, Soil in the GCM soil classification; (b) Detailed view of (a) over the Australian Region; (c) UN FAO Soil Texture reclassified to the GCM soil classification; and (d) Detailed view of (c) over the Australian Region..... 86
32. Figure 4.3 Broadband Snow Free Surface Albedo Mapping: (a) Original CSIRO GCM Parameters, July Surface Albedo; (b) Detailed view of (a) over the Australian Region; (c) MODIS derived July Surface Albedo; and (d) Detailed view of (c) over the Australian Region..... 88
33. Figure 4.4 Global Leaf Area Index Mapping: (a) Original CSIRO GCM Parameters, July Leaf Area Index Map; (b) Detailed view of (a) over the Australian Region; (c) AVHRR derived monthly green leaf area index map for July; and (d) Detailed view of (c) over the Australian Region..... 89
34. Figure 4.5 Original CSIRO GCM land surface parameter generation methods compared with the new parameter generation methods using relatively fine-scale land surface data with physical surface models, and parameter aggregation. The parameterisation methods are shown for a single T63 Grid Increment (1.875 degree) GCM grid cell. . 91
35. Figure 4.6 New CSIRO GCM Parameters: (a) Vegetation Map in Simple Biosphere (SiB) classification; (b) Detailed view of (a) over the Australian Region; (c) Soil Map in the GCM soil classification; and (d) Detailed view of (c) over the Australian Region..... 95
36. Figure 4.7 CSIRO GCM Albedo Evaluation: (a) January zonal average land surface albedo for the new and original CSIRO GCM parameters; (b) same as (a) for July; (c) Average monthly land suface albedo for all land for new and original CSIRO GCM parameters; and (d) same as (c) for the Australian continent..... 96
37. Figure 4.8 New CSIRO GCM Surface Albedo Parameter Evaluation: (a) New Parameters, January Albedo; (b) Detailed view of (a) over the Australian Region; (c) Difference between New Parameters and Original CSIRO January Albedo; (d) Detailed view of (c) over the Australian Region; (e) New Parameters, July Albedo; (f) Detailed view of (e) over the Australian Region; (g) Difference between New Parameters and Original CSIRO July Albedo; and (h) Detailed view of (g) over the Australian Region..... 97
38. Figure 4.9 CSIRO GCM Leaf Area Index Evaluation: (a) January zonal average leaf area index for the new and original CSIRO GCM parameters; (b) same as (a) for July; (c) Average monthly leaf area index for all land for new and original CSIRO GCM parameters; and (d) same as (c) for the Australian continent..... 99
39. Figure 4.10 New CSIRO GCM Leaf Area Index Parameter Evaluation: (a) New Parameters, January Leaf Area Index; (b) Detailed view of (a) over the Australian Region; (c) Difference between New Parameters and Original CSIRO January Leaf Area Index; (d) Detailed view of (c) over the Australian Region; (e) New Parameters, July Leaf Area Index; (f) Detailed view of (e) over the Australian Region; (g) Difference between New Parameters and Original CSIRO July Leaf Area Index; and (h) Detailed view of (g) over the Australian Region..... 100
40. Figure 4.11 CSIRO GCM Vegetation Fraction Evaluation: (a) January zonal vegetation fraction for the new and original CSIRO GCM parameters; (b) same as (a) for July; (c) Average monthly vegetation fraction for all land for new and original CSIRO GCM parameters; and (d) same as (c) for the Australian continent..... 101
41. Figure 4.12 New CSIRO GCM Vegetation Fraction Parameter Evaluation: (a) New Parameters, January Vegetation Fraction; (b) Detailed view of (a) over the Australian Region; (c) Difference between New Parameters and Original CSIRO January Vegetation Fraction; (d) Detailed view of (c) over the Australian Region; (e) New Parameters, July Vegetation Fraction; (f) Detailed view of (e) over the Australian Region; (g) Difference between New Parameters and Original CSIRO July Vegetation Fraction; and (h) Detailed view of (g) over the Australian Region..... 102
42. Figure 4.13 CSIRO GCM Unrestrained Stomatal Evaluation: (a) January zonal stomatal resistance for the new and original CSIRO GCM parameters; (b) same as (a) for July; (c) Average monthly stomatal resistance for all land for new and original CSIRO GCM parameters; and (d) same as (c) for the Australian continent..... 104
43. Figure 4.14 New CSIRO GCM Parameters Evaluation: New Parameters Unrestrained Stomatal Resistance; (b) Detailed view of (a) over the Australian Region; (c) Difference between New Parameters and Original CSIRO Unrestrained Stomatal Resistance; and (d) Detailed view of (c) over the Australian Region..... 105
44. Figure 4.15 CSIRO GCM Unrestrained Canopy Resistance Evaluation: (a) January zonal canopy resistance for the new and original CSIRO GCM parameters; (b) same as (a) for July; (c) Average monthly canopy resistance for all land for new and original CSIRO GCM parameters; and (d) same as (c) for the Australian continent..... 106
45. Figure 4.16 New CSIRO GCM Canopy Resistance Parameter Evaluation: (a) New Parameters, January Canopy Resistance; (b) Detailed view of (a) over the Australian Region; (c) Difference between New Parameters and Original CSIRO January Canopy Resistance; (d) Detailed view of (c) over the Australian Region; (e) New Parameters, July Canopy Resistance; (f) Detailed view of (e) over the Australian Region; (g) Difference between New Parameters and Original CSIRO July Canopy Resistance; and (h) Detailed view of (g) over the Australian Region 107
46. Figure 4.17 CSIRO GCM Surface Roughness Evaluation: (a) January zonal surface roughness for the new and original CSIRO GCM parameters; (b) same as (a) for July; (c) Average monthly surface roughness for all land for new and original CSIRO GCM parameters; and (d) same as (c) for the Australian continent..... 109
47. Figure 4.18 New CSIRO GCM Surface Roughness Parameter Evaluation: (a) New Parameters, January Surface Roughness; (b) Detailed view of (a) over the Australian Region; (c) Difference between New Parameters and Original CSIRO January Surface Roughness; (d) Detailed view of (c) over the Australian Region; (e) New Parameters, July Surface Roughness; (f) Detailed view of (e) over the Australian Region; (g) Difference between New Parameters and Original CSIRO July Surface Roughness; and (h) Detailed view of (g) over the Australian Region 110
48. Figure 4.19 Average Austral Summer (DJF) and Winter (JJA) Air Temperature for 1975 – 1999: Differences (a and c) and spatial correlations (b and d) for Original CSIRO and New Parameters experiments compared with University of Delaware observed precipitation. (All land; Australia (Aust); North America (NorthAm); South America (SouthAm); Asia; and Africa) 115

49. Figure 4.20 Average Austral Summer (DJF) and Winter (JJA) Precipitation for 1975 – 1999: Differences (a and c) and spatial correlations (b and d) for Original CSIRO and New Parameters experiments compared with University of Delaware observed precipitation. (All land; Australia (Aust); North America (NorthAm); South America (SouthAm); Asia; and Africa) 116
50. Figure 4.21 Global differences in average climate between the Original CSIRO and New Parameters experiments (New – Old) for Austral Summer (DJF) and Winter (JJA) 1975 – 1999 for: Average Air Temperature (a) and (b); Average Precipitation (c) and (d); Average Mean Sea Level Pressure (e) and (f); and Average Soil Moisture (g) and (h) 120
51. Figure 4.22 Global 850 hPa wind fields for 1975 – 1999 for: the Original CSIRO for (a) Austral Summer (DJF) and (b) Winter (JJA); the New Parameters experiments for (c) Austral Summer (DJF) and (d) Winter (JJA) and the Difference between the experiments (New – Old) for (e) Austral Summer (DJF) and (f) Winter (JJA) 121
52. Figure 4.23 Global differences in average climate between the Original CSIRO and New Parameters experiments (New – Old) for Austral Summer (DJF) and Winter (JJA) 1975 – 1999 for: Average Cloud Cover (a) and (b); Average Snow Depth (c) and (d); Average Model Calculated Albedo (e) and (f); and Average Short Wave Radiation Flux (g) and (h) 122
53. Figure 4.24 Global differences in average climate between the Original CSIRO and New Parameters experiments (New – Old) for Austral Summer (DJF) and Winter (JJA) 1975 – 1999 for: Average Sensible Heat Flux (a) and (b); and Average Latent Heat Flux (c) and (d) 123
54. Figure 4.25 Seasonal model performance compared with Australian 1975 – 1999 observations: Differences and spatial correlations for the Original CSIRO and New Parameters experiments compared with observed average Australian temperature, precipitation and mean sea level pressure. Seasons shown are: Annual; Austral Summer (DJF); Autumn (MAM); Winter (JJA); and Spring (SON) 129
55. Figure 4.26. Average Air Temperature for Australia 1975 - 1999: Difference between Observed data from the SILO database, and the Original CSIRO and New Parameters Experiments for Austral Summer (DJF) (a) and (b); Autumn (MAM) (c) and (d); Winter (JJA) (e) and (f); and Spring (SON) (g) and (h) 130
56. Figure 4.27. Average Precipitation for Australia 1975 - 1999: Difference between Observed data from the SILO database, and the Original CSIRO and New Parameters Experiments for Austral Summer (DJF) (a) and (b); Autumn (MAM) (c) and (d); Winter (JJA) (e) and (f); and Spring (SON) (g) and (h) 131
57. Figure 4.28 Average Mean Sea Level Pressure for Australia 1975 - 1999: Difference between Observed data from the SILO database, and the Original CSIRO and New Parameters Experiments for Austral Summer (DJF) (a) and (b); Autumn (MAM) (c) and (d); Winter (JJA) (e) and (f); and Spring (SON) (g) and (h) 132
58. Figure 4.29 Differences in average climate between the Original CSIRO and New Parameters experiments for Australia – Asia Austral Summer (DJF) and Winter (JJA) 1975 – 1999 for: Average Air Temperature (a) and (b); Average Precipitation (c) and (d); Average Mean Sea Level Pressure (e) and (f); and Average Cloud Cover (g) and (h) 135
59. Figure 4.30 Average 850 hPa winds over Australia – Asia 1975 – 1999 for: The Original CSIRO experiment (a) Austral Summer (DJF) and (b) Winter (JJA); The New Parameters experiment (c) Summer (DJF) and (d) Winter; And the difference between the experiments (e) Summer (DJF) and (f) Winter (JJA) 136
60. Figure 4.31 Surface energy flux differences over Australia – Asia between the Original CSIRO and New Parameters experiments for Austral Summer (DJF) and Winter (JJA) 1975 – 1999 for: Average Short Wave Radiation Flux (a) and (b); Average Sensible Heat (c) and (d); and Latent Heat Flux (e) and (f) 137
61. Figure 5.1 (a) Current AUSLIG (1990) Vegetation Map and (b) Natural Vegetation Map, in Land Cover Classes of Graetz et al. (1995) 146
62. Figure 5.2 (a) Clearing Map developed in Chapter 3 and (b) Pre-clearing Vegetation Map in Land Cover Classes of Graetz et al. (1995) 147
63. Figure 5.3 Current and Pre Clear Vegetation Maps in Simple Biosphere Classes. These maps are used for generating the vegetation specific parameters used in calculating the new CSIRO GCM land surface parameters 148
64. Figure 5.4 Extrapolation techniques for generating Pre-clearing land surface parameters from Current Parameters and Vegetation Maps. The parameterisation methods are shown for a single T63 Grid Increment (1.875 degree) GCM grid cell 150
65. Figure 5.5 (a) Extrapolated Pre-clearing January Surface Albedo and (b) Difference between Pre-clearing and Current Albedo Maps 151
66. Figure 5.6 (a) Extrapolated Pre-clearing January Vegetation Fraction Map and (b) Difference between Pre-clearing and Current Vegetation Fraction Maps 152
67. Figure 5.7 (a) Extrapolated Pre-clearing January Leaf Area Index Map and (b) Difference between Pre-clearing and Current Leaf Area Index Maps 153
68. Figure 5.8 Average Australian Monthly Land Surface Parameters for Current and Pre-clearing Experiments 155
69. Figure 5.9 January Difference in Land Surface Parameters between Current and Pre-clearing Experiments 156
70. Figure 5.10 July Difference in Land Surface Parameters between Current and Pre-clearing Experiments 157
71. Figure 5.11 Australian Regions for Regional Investigation with Land Cover Change experiments and for Historical Climate Record Analysis 159
72. Figure 5.12 Average Monthly Land Surface Parameters for Current and Pre-clearing Experiments for South East Queensland 160
73. Figure 5.13 Average Monthly Land Surface Parameters for Current and Pre-clearing Experiments for Eastern New South Wales 161
74. Figure 5.14 Average Monthly Land Surface Parameters for Current and Pre-clearing Experiments for South West Western Australia 162
75. Figure 5.15 Average Air Temperature for Australia 1975 – 1999: Difference between Current and Pre-clearing Experiments for Austral Summer (DJF) (a), Autumn (MAM) (b), Winter (JJA) (c), and Spring (SON) (d) 167
76. Figure 5.16 Average Precipitation for Australia 1975 – 1999: Difference between Current and Pre-clearing Experiments for Austral Summer (DJF) (a), Autumn (MAM) (b), Winter (JJA) (c), and Spring (SON) (d) 168
77. Figure 5.17 Annual Rainfall Trend Analysis from Linear Regression of SILO Rainfall Data for (a) 1900 – 1999 and (b) 1950 – 1999 174
78. Figure 5.18 Yearly Average Annual Precipitation for Australia for 1900 – 1999 with 10 year running mean and regression line for the period 175
79. Figure 5.19 Differences in average climate between the Current and Pre-clearing experiments for Australia – Asia in Austral Summer (DJF) and Winter (JJA) 1975 – 1999 for: Average Air Temperature (a) and (b); Average Precipitation (c) and (d); Average Mean Sea Level Pressure (e) and (f); and Average Soil Moisture (g) and (h) 182
80. Figure 5.20 Average 850 hPa winds over Australia – Asia for: Pre-clearing experiment (a) Austral Summer (DJF) and (b) Winter (JJA); The Current experiment (c) Austral Summer and (d) Winter; And the difference between the experiments (e) Summer and (f) Winter 183

81. Figure 5.21 Surface energy flux differences over Australia – Asia between the Current and Pre-clearing experiments for Austral Summer (DJF) and Winter (JJA) 1975 –1999: for Average Cloud Cover (a) and (b); Short Wave Radiation Flux (c) and (d); Average Sensible Heat Flux (e) and (f); and Average Latent Heat Flux (g) and (h) 184
82. Figure 5.22 Global Differences in average climate between the Current and Pre-clearing experiments for Austral Summer (DJF) and Winter (JJA) 1975 – 1999 for: Average Air Temperature (a) and (b); Average Precipitation (c) and (d); Average Mean Sea Level Pressure (e) and (f); and Average Cloud Cover (g) and (h)..... 191
83. Figure 5.23 Global 850 hPa wind fields for 1975 – 1999 for: the Pre-clearing experiment for (a) Austral Summer (DJF) and (b) Winter (JJA); the Current experiment for (c) Austral Summer (DJF) and (d) Winter (JJA) and the Difference between the experiments (Current – Pre-clearing) for (e) Austral Summer (DJF) and (f) Winter (JJA) 192
84. Figure 5.24 Global Differences in average climate between the Current and Pre-clearing experiments for Austral Summer (DJF) and Winter (JJA) 1975 – 1999 for: Average Air Temperature (a) and (b); Average Precipitation (c) and (d); Average Mean Sea Level Pressure (e) and (f); and Average Cloud Cover (g) and (h)..... 193
85. Figure 5.25 Surface energy flux differences over Australia – Asia between the Current and Pre-clearing experiments for Austral Summer (DJF) and Winter (JJA) 1975 –1999: for Average Short Wave Radiation Flux (a) and (b); Average Sensible Heat Flux (c) and (d); and Average Latent Heat Flux (e) and (f) 194
86. Figure A.1 Broadband Surface Albedo (α) plotted against Solar Zenith Angle (θ) and Leaf Area Index (L) using the Two-Stream Radiation model solutions of Sellers (1985) with Clear Sky Radiation calculated from the methods of Dorman and Sellers (1989) and Vegetation Parameters taken from Sellers et al. (1996a). 222
87. Figure A.2 Fraction of absorbed short wave radiation, absorbed by the vegetation (σ_c) plotted against Solar Zenith Angle (θ) and Leaf Area Index (L) using the Two-Stream Radiation model solutions of Sellers (1985) with Clear Sky Radiation calculated from the methods of Dorman and Sellers (1989) and Vegetation Parameters taken from Sellers et al. (1996a).223
88. Figure C.1 Schematic of stomatal gas exchanges and photosynthesis within a C3 plant leaf (after Trenberth (1992)) ... 225
89. Figure E.1 (a) Surface Roughness (z0) and (b) Displacement Height (d) plotted against Canopy Height (h) and Leaf Area Index (L) using the simplified expressions of Raupach (1994)..... 230

List of Tables

1. Table 2.1 General rules for changes in short wave radiation dynamics from changing from native to agricultural vegetation 17
2. Table 2.2 General rules for changes canopy evaporation and transpiration from changing from native to agricultural vegetation 19
3. Table 2.3 General rules for changes in surface roughness from changing from native to agricultural vegetation 24
4. Table 3.1 Changes in Australian vegetation by structural form between the Natural (pre- European) and Current (mid 1980s) vegetation maps of AUSLIG (1990) in thousands of km^2 56
5. Table 3.2 Australian woody vegetation clearing between 1990 and 1995 from Barson et al. (2000). The table shows the area cleared by state and land use for the five year period 70
6. Table 3.3 Australian woody vegetation regeneration between 1990 and 1995 from Barson et al. (2000). The table shows the area regenerated by state and land use for the five year period 71
7. Table 3.4 Queensland Yearly Clearing Rates in hectares per year by land use from SLATS survey time periods, from DNRM (2003). 74
8. Table 3.5 Queensland Yearly Regrowth Rates in hectares per year from SLATS survey time periods, from DNR (1999a), DNR (1999b), DNR (2000), and DNRM (2003). 75
9. Table 3.6 Australian Land Cover Change and Land Use Studies Reviewed 79
10. Table 4.1 Evaluation of average continental Air Temperature statistics for the New Parameters and the Original CSIRO Experiments against Delaware observational data for 1975 – 1999. Seasons shown: Austral Summer (DJF) and Winter (JJA). Statistics shown: continental climatic mean values and spatial correlations between climatic mean maps of Models and Delaware observations 115
11. Table 4.2 Evaluation of average continental Precipitation statistics for the New Parameters and the Original CSIRO Experiments against Delaware observational data for 1975 – 1999. Seasons shown: Austral Summer (DJF) and Winter (JJA). Statistics shown: climatic mean values, and spatial correlations between climatic mean maps of Models and Delaware observations 116
12. Table 4.3 Global average Austral Summer (DJF) climate statistics for the New Parameters, Original CSIRO, and NCEP reanalysis data for the climate period 1975 – 1999 118
13. Table 4.4 Global average Austral Winter (JJA) climate statistics for the New Parameters, Original CSIRO, and NCEP reanalysis data for the climate period 1975 – 1999 124
14. Table 4.5 Evaluation of Australian average climate statistics for the New Parameters and the Original CSIRO Experiments against SILO observational data for the climate period 1975 – 1999. Seasons shown Annual; Austral Summer (DJF); Autumn (MAM); Winter (JJA); and Spring (MAM). Statistics shown are Australian climatic mean values and spatial correlations between Australian climatic mean maps of Model and SILO observations 128
15. Table 4.6 Differences in CSIRO GCM Land Surface Parameters between Original and New Parameters 141
16. Table 5.1 Australian Land Cover Equivalence from the Classifications of Graetz et al. (1995) to Simple Biosphere biome classes 145
17. Table 5.2 Time Series analysis of Australian Average Air Temperature and Precipitation for Current and Pre-clearing Experiments 1975 –1999. Seasons shown are: Annual, Austral Summer (DJF), Autumn (MAM), Winter (JJA) and Spring (SON). * indicates statistical significant result 166
18. Table 5.3 Time Series analysis of south east Queensland average Air Temperature and Precipitation for Current and Pre-clearing Experiments. Seasons shown are: Annual, Austral Summer (DJF), Autumn (MAM), Winter (JJA) and Spring (SON). * indicates statistical significant result 169
19. Table 5.4 Time Series analysis of eastern New South Wales Average Air Temperature and Precipitation for Current and Pre-clearing Experiments. Seasons shown are: Annual, Austral Summer (DJF), Autumn (MAM), Winter (JJA) and Spring (SON). * indicates statistical significant result 170
20. Table 5.5 Time Series analysis of south west Western Australia Average Air Temperature and Precipitation for Current and Pre-clearing Experiments. Seasons shown are: Annual, Austral Summer (DJF), Autumn (MAM), Winter (JJA) and Spring (SON). * indicates statistical significant result 171
21. Table 5.6 Comparison of Modelled Precipitation Changes and Linear Regression of Historical Precipitation Records for Australia and Regions. Differences are shown as total changes in annual precipitation for the period investigated * indicates statistical significant result 172
22. Table 5.7 General Differences in CSIRO GCM Land Surface Parameters between Pre-Clearing and Current Experiments199

CHAPTER 1.
INTRODUCTION

1.1 Problem Statement

The concept that land cover plays a major role in local and larger scale climate is a contentious issue that originated in the late 18th and early 19th Centuries, following the widespread environmental degradation that accompanied the exploitation of newly discovered lands by colonial powers. Studies by scientific societies of the time drew on the repeated experiences of deforestation on the Indian subcontinent and tropical islands, to develop theories linking deforestation with drastic reductions in rainfall and larger scale general desiccation (*Groves*, 1992). In Australia in the late 19th and early 20th Centuries these ideas were debated bitterly, with George Goyder and John Brown publicly arguing the value of trees in increasing rainfall for Australia (*Forestry and Timber Bureau*, 1972). Brown was convinced of the value of planting trees in inland Australia, while Goyder was adamantly opposed to the idea.

In recent years, field observations, atmospheric profiling, satellite monitoring and climate modelling have been used to investigate the impacts that land cover changes have on the earth surface and how changes in land surface properties influence near surface atmospheric processes. Reviews by *Sellers* (1997), *Pielke et al.* (1998), *Betts et al.* (1996), *Field and Avissar* (1998), and others document the complex relationships that exist between land surface properties, atmospheric processes and vegetation cover. These reviews detail how changes in vegetation impact land surface and near earth atmospheric processes by altering the fluxes of radiation, momentum, energy, and moisture, between the soil, the vegetation, and the atmosphere.

Reviews of land cover and climate interations at larger scales by *Pielke* (2001b), *Sellers* (1997), *Avissar* (1995), and *Stohlgren et al.* (1998) describe how changes in the land surface fluxes resulting from the land cover changes influence atmospheric processes operating over various temporal and spatial scales with numerous feedback mechanisms. Studies by *Chase et al.* (2001), *Lawton et al.* (2001), and *Zhao et al.* (2001) provide further indications that the local changes in surface fluxes interact with larger scale atmospheric conditions to impact weather and climate remotely through changes in global atmospheric circulation and moisture transport.

1.1.1 Australian Land Cover Change and Climate Change

In Australia, the clearing of native forest and woodland and the cultivation of native grasslands have been central to the production of rural commodities (*McAlpine et al.*, 2002). Since European settlement, there has been a gradual but continuous transformation of the landscape, from production that exploited the pre-existing natural resources such as logging and grazing, to the wholesale replacement of natural vegetation with intensive production systems such as cropping and improved pastures. Analysis by *AUSLIG* (1990) into the differences

between the pre-European and mid 1980s vegetation cover, found that one third of the continent had undergone structural changes in vegetation as a result of land use (*figure 1.1 a*). In the mid 1980s, extensive grazing covered approximately 60% of the continent, and intensive cropping and improved pastures covered approximately 10%. The intensive land use changes were concentrated in the south west and south east of the continent, coinciding with the Australian sheep-wheat belts and extending north into the Brigalow Belt bioregion of Queensland. Overall, approximately half the native woody vegetation within this intensive land use zone has been cleared (*AUSLIG*, 1990 and *Barson et al.*, 2000).

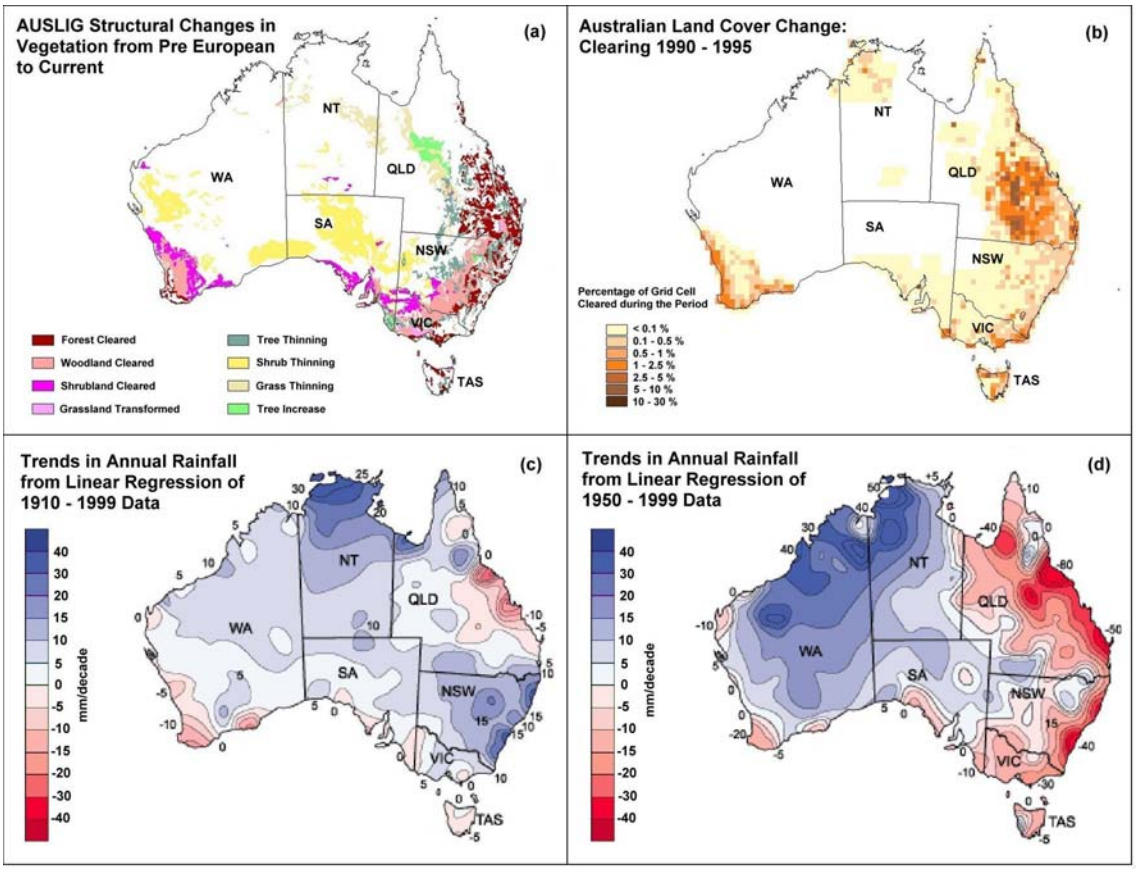

Figure 1.1. Australian Climate and Land Cover Changes: (a) Major changes in the structural form of Australian vegetation between the natural (pre-European) and current (mid 1980s) vegetation maps of AUSLIG (1990); (b) Bureau of Rural Sciences (BRS) assessment of Australian land cover change between 1990 and 1995 from Barson et al. (2000) (c) Annual Rainfall Trend Analysis from Linear Regression of Rainfall Data from 1910 – 1999 from Manins et al. (2001); and (d) Annual Rainfall Trend Analysis 1950 – 1999 from Manins et al. (2001). (State names: WA Western Australia; NT Northern Territory; SA South Australia; QLD Queensland; NSW New South Wales; VIC Victoria; and TAS Tasmania)

The transformation process continued through the last decade of the 20th Century, with current clearing rates still in excess of 250,000 hectares per year (*Barson et al.*, 2000 and *DNR*, 2000) (*figure 1.1 b*). The majority of current clearing is concentrated in the state of Queensland (73.5% of the national figure), with the largest source of clearing grazing (91.7% of statewide clearing), followed by agriculture (4%). Western Australia was the second largest contributor to

clearing, (10.1% of the national figure) with the majority of clearing for agriculture (72.4%). Clearing in the remaining states (16.4% of the national figure) was significantly lower; however, the different sizes of the states masked clearing intensity, with Victoria and Tasmania having intense areas of clearing, primarily as a result of expansion of plantation forestry.

Long-term trends in Australian climate are difficult to separate from the background variability, with rainfall revealing strong seasonal, inter-annual and inter-decadal variability over much of the continent (*Manins et al.*, 2001). Linear regression of Australian rainfall records show historically, mean annual rainfall since 1900 has had a weak upward trend that is primarily the result of dry years in the early 1900s and wet years in the 1970s. Regional rainfall trends from 1910-1999 (*figure 1.1c*) show significant increases in rainfall over eastern and northern New South Wales and over monsoonal northern Australia, with significant decreases over eastern Queensland (> 20 mm per decade) and south west Western Australia (> 10 mm per decade). During the last 50 years (*figure 1.1d*), large increases occurred in north west Australia (>30 mm per decade), while large decreases have occurred across eastern Australia, especially coastal Queensland and New South Wales. *Crimp and Day*, (2003) raise the question as to whether the declines in these coastal regions of Queensland are a function of natural variability or are a function of long term climate change.

1.1.2 Australian Land Cover Change and Climate Change Investigations

The strong spatial correlations between regional patterns of land cover change and decline in annual rainfall, especially south west Western Australia since 1910, and eastern Queensland and New South Wales since 1950, has generated hypotheses that land cover change may be a contributing to rainfall decline. There is a growing body of research attempting to address this hypothesis, through investigating the impacts of Australian land cover changes on land surface dynamics and the flow on impacts to the atmosphere.

Lyons et al. (1993), *Xinmei et al.* (1995), *Ray et al.* (2003) and others conducted field investigations and regional climate modelling studies into the climate impacts of large scale clearing of native vegetation in the Western Australian wheat belt, a region which has experienced extensive clearing and a significant decline in rainfall since 1910. These studies showed significant differences in land surface conditions, surface fluxes and atmospheric responses between agricultural land and adjacent native vegetation in the region. The regional modelling studies demonstrate that the changes in land surface properties do have strong impacts on air temperature, boundary layer structure, and cloud formation. These studies also indicate there may be impacts on precipitation and soil moisture which may account for some of the observed changes in winter rainfall.

Most recently, *Narisma and Pitman* (2003) investigated the impacts of historical Australian land cover change on near surface climate over the Australian continent through comparative regional climate modelling experiments. The study found there were strong

impacts on the modelled surface fluxes under present day vegetation, compared to conditions that may have existed prior to European arrival. The study also found there were statistically significant changes in regional air temperatures in the south east, south west, and north east of the continent, however, changes in precipitation between the two simulations were not found to be statistically significant.

1.1.3 Specific Problem Statement

In spite of the recent Australian land cover and climate research, there are still significant knowledge gaps and uncertainties of the role land cover and land cover change plays in the Australian regional and continental climate. Specifically, the modelling experiments of *Narisma and Pitman* (2003) suggest that warming from changed Australian land surface conditions propagates to altitude, which may have the potential to influence larger-scale circulation over Australia. This component of the climate modelling was prescribed/fixed from historical analysis of observed atmospheric conditions for all the Australian land cover and climate experiments conducted so far. As a consequence, the impact of Australian land cover changes on regional and continental climate involving larger scale atmospheric circulation and associated feedbacks, as well as the longer term feedbacks through changes in soil moisture have not been investigated. To address this gap in knowledge the climate impacts of Australian land cover change need to be investigated in a manner that not only captures the direct impacts of changes in land surface fluxes, but also incorporates the larger scale atmospheric dynamics and soil moisture feedbacks.

1.2 Aims and Objectives

The primary aim of this thesis is to investigate and identify possible causal explanations, of how the changes in Australian land cover since European arrival have altered the land surface properties, and whether the changes in land surface properties have impacted on Australian regional and continental long-term climate. This is achieved through climate modelling experiments using the CSIRO General Circulation Model (GCM) with the land surface as it may have existed prior to European arrival and as it is for the current day. The key questions addressed are:

1. How has Australian land cover changed, what are the key land surface properties associated with land cover change, and can these changes be consistently represented in the CSIRO GCM?
2. How do the changes in Australian land cover influence land surface and atmosphere interaction, and how do these changes influence atmospheric processes and regional climate?

3. How do the changes in atmospheric processes and climate from Australian land cover change influence larger scale atmospheric circulation, and do these changes in atmospheric circulation feedback to influence regional and continental climate?
4. How do the changes in atmospheric processes and atmospheric circulation induce cloud and radiation feedbacks, and precipitation and soil moisture feedbacks? And how do these feedbacks impact climate at a range of scales?
5. Do the modelled changes reflect observed changes in regional precipitation over the past 100 years and also the past 50 years?

The secondary aim of this thesis is to investigate how land cover and land surface properties (e.g. albedo, surface roughness and stomatal resistance) are represented in the CSIRO GCM and to investigate and explain how this representation affects: (i) fluxes of radiation, energy, and moisture, between the land surface and the overlying atmosphere, and (ii) the simulation of regional, continental and global climate in the model.

These aims are implemented in the research project through the following objectives:

Objective 1: Review the literature of international and Australian land cover change and climate change studies, and synthesise the theory and case studies into a conceptual model of Australian land cover change and climate impacts. This objective will develop a strong theoretical basis to the research, to ensure sound evaluation of the climate modelling experiments and to show how changes in Australian land cover affect modelled climate at a range of scales.

Objective 2: Compile a comprehensive record of land cover changes that have occurred across Australia since European arrival (1788). The best available land cover mapping needs to be acquired from a variety of sources and transformed into a consistent land cover change framework to assess both historical and contemporary Australian land cover change.

Objective 3: Review and adapt the CSIRO GCM to include land surface characteristics that capture the scale and nature of Australian land cover change. This will involve integration of current global land surface data at similar resolutions and attribution to the Australian land cover change data.

Objective 4: Perform sensitivity experiments with the CSIRO GCM using the new global land surface data and the original CSIRO land surface parameters, to evaluate the suitability of using the climate modelling framework with the new relatively fine-scale land surface data. The

performance of the model will be evaluated by comparing historical weather records for the 1975 – 1999 period with the global climate modelled in the GCM with the two land surface representations for the same period. Observed sea surface temperatures and sea ice distributions for this period will be prescribed in both experiments to provide the same climatic forcings in both simulations.

Objective 5: Extrapolate pre-European monthly land surface conditions from current global land surface data and pre-European and current day vegetation mapping. Extrapolation from current to pre-clearing is necessary as there is no way of spatially and seasonally describing the pre-European vegetation cover and physiology as can be done with current day satellite imagery and field data. In this manner the properties of remnant native vegetation are used as a surrogate to describe the properties of adjacent native vegetation prior to clearing.

Objective 6: Perform land cover change climate modelling experiments with the CSIRO GCM with current day land cover and with pre-European land cover in the same manner as the sensitivity studies of Objective 4. Comparative analysis of changes in the climate modelled in the CSIRO GCM against the changes in the land surface parameters of the two experiments will be performed to identify and quantify the relationships between Australian land cover change and climate at regional, continental and global scales.

Objective 7: Integrate and synthesise the modelling and theoretical relationships to identify the extent to which Australian historical land cover changes may have impacted Australian climate. Australian climate records and Australian land cover change records will be used to verify whether the modelled relationships can be observed in historical records.

1.3 Background to the Problem

1.3.1 General Land Cover and Climate Interaction

The influence of land cover on climate is incorporated in more recent conceptual models of the climate system by explicitly included vegetation as a dynamic interacting component of the system. These conceptual models have been formalised by *Trenberth* (1992), *Peixoto and Oort* (1992), *Henderson-Sellers and McGuffie* (1987) and others, and define the climate system as the complex interaction of the atmosphere, the hydrosphere (oceans, lakes and rivers), the cryosphere (glaciers, sea ice, permafrost and snow), the biosphere (all marine and terrestrial ecosystems including vegetation), the pedosphere (soils), and the lithosphere (the Earth's crust and upper mantle). The details and the dynamic nature of the climate system with interacting components and processes are shown in *figure 1.2*.

Trenberth (1992), *Huggett* (1997), *Peixoto and Oort* (1992) and others, describe how the components of the climate system interact with each other over a variety of temporal and spatial scales with numerous feedback mechanisms between the components. In this model the atmosphere and the oceans are the dynamic fluid components distributing energy, momentum and moisture between themselves and other components of the climate system through organised circulations, chaotic motions and random turbulence.

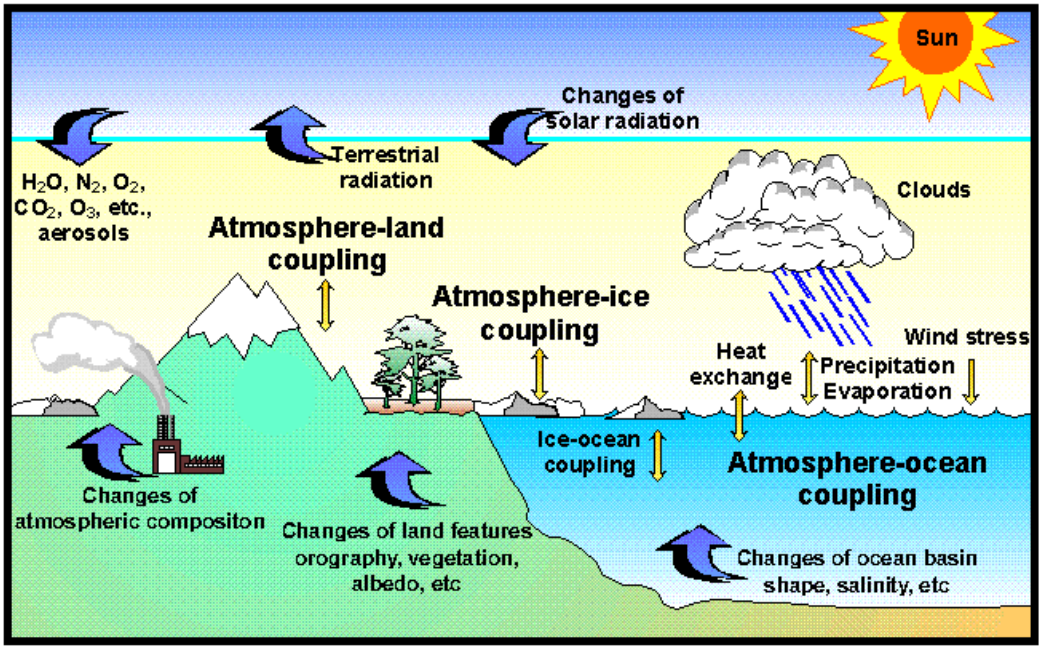

Figure 1.2. Conceptual model of the Climate System showing the interacting components and processes, with internal and external forcings for climate change. (from CSIRO Atmospheric Research web site)

1.3.2 Temporal and Spatial Time Frames of Vegetation and Climate Interaction

Pielke et al. (1998), *Gurevitch et al.* (2002) and many other describe how within the climate system the distribution, structure, and function of the terrestrial ecosystems of the biosphere change over various time frames, influenced by climate, soils, topography, and disturbance. *Trenberth* (1992), *Pielke et al.* (1998), and *Kabat et al.* (2004) also describe how terrestrial ecosystems and the atmosphere are coupled over a range of time scales through the exchanges of radiation, heat, water, CO_2, and other trace elements. Human disturbance, through land use, has significantly altered the distribution and function of vegetation from the previously natural ecosystems, resulting in man made landscapes over much of the Earth. This process of landscape modification has accelerated in intensity and scale over the last few centuries, with recent estimates suggesting around 10% of the Earth surface is directly used for some form of cultivation, and nearly another 50% used for pastures and rangelands (*Ramankutty et al.*, 2000).

The changes in land cover and the subsequent changes in interactions between the land surface and the atmosphere impact other components of the climate system at a range of temporal and spatial scales with numerous feedback mechanisms. Classification of the

interactions between terrestrial ecosystems and the atmosphere can therefore be based on the spatial scales on which they occur, and the time frames over which they operate. *Kabat et al.* (2004) categorised the vertical and horizontal scales at which the land surface interacts with the atmosphere and therefore climate, into the three classes of: the climate near the ground (micro and local); regional climate (meso); and global climate (macro). *Pielke et al.* (1998) categorised the time frames that these interactions occur as: short-term interactions (minutes to a few weeks); long-term interactions (months to 100 years); and very long-term interactions (greater than 100 years). Investigating the physical processes of the atmosphere *Orlanski* (1975) suggested there were clear links between spatial and temporal scales at which atmospheric processes operated, with vertical motion dominating the micro-scale, horizontal motion dominating the macro-scale, and horizontal and vertical motions equally important at the meso-scale (*Sturman and Tapper*, 1996) (*figure 1.3*).

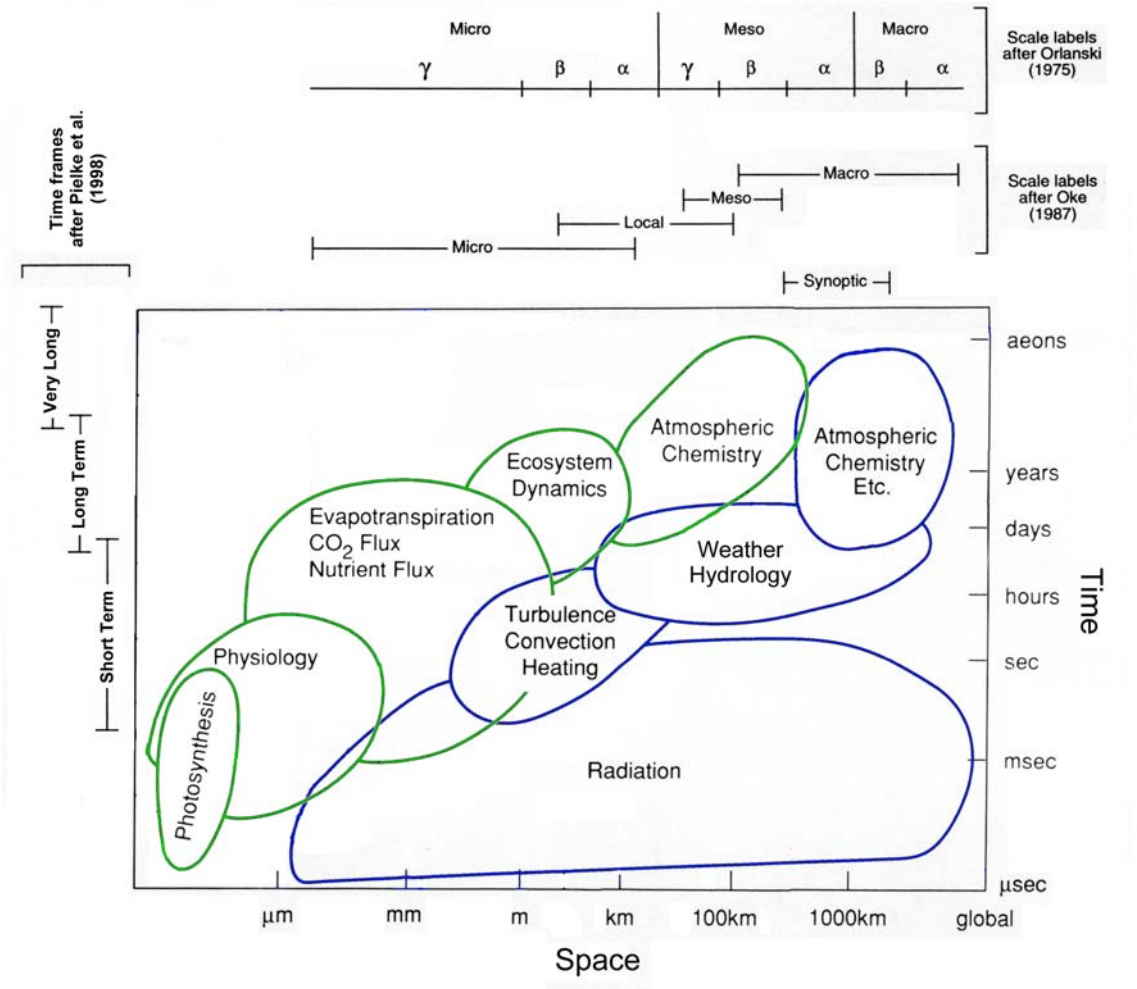

Figure 1.3. Temporal and spatial scale definitions for processes affecting the climate system through changes in the atmosphere (blue) and terrestrial ecosystems (green) (adapted from Trenberth (1992))

Trenberth (1992) recognised that the processes of the atmosphere and terrestrial biosphere were strongly coupled, again with the processes interacting on a range of different

spatial and temporal scales. By integrating the spatial scales of *Kabat et al.* (2004) with the temporal scales of *Pielke et al.* (1998) and the atmosphere and terrestrial ecosystem processes of *Orlanski* (1975) and *Trenberth* (1992) a formal basis to classify these processes and feedbacks can be made. *Figure 1.3* shows how the hierarchical framework simplifies some of the complexity of the interactions between the terrestrial ecosystems and the atmosphere, by separating them out into components operating at distinct space and time scales.

1.4 Project Scope

Australian land cover is defined for this study following *Graetz et al.* (1992), as "the surface that mediates the exchanges of energy and matter between the Earth's crust, and the overlying atmosphere". In this definition, the land cover includes the vegetation, soil, snow and ice present at the Earth's surface, and is used following *Graetz et al.* (1995b), at the spatial scales of landscapes (tens to hundreds of square kilometers). The description of Australian land cover is predominantly the distribution of vegetation and soil, as bare soils, snow and ice are far less common in distribution and coverage than vegetated land. Australian land cover change is defined in the study as the historical changes in land cover that have occurred since European arrival.

The climate impacts of Australian land cover change are investigated through comparative climate modelling experiments with the CSIRO GCM, with Australian land cover change represented through biophysical changes in land surface properties from Australian land cover prior to European settlement compared to current day. The changes in land surface properties are investigated at the local to meso spatial scales (*figure 1.3*), with atmospheric responses to the changed land surface conditions studied at the meso to macro-scale, over the short to long term time frame.

The changes in land surface dynamics are represented through changes in the physiological properties of vegetation, and through changes in the storage of soil moisture and surface water within the climate models. The changes in land surface conditions represent changes in the short term properties of short wave and long wave radiation at the surface, the turbulent exchange of momentum, energy and moisture between the surface and the atmosphere, and the transfer of moisture from the soil and vegetation to the atmosphere through evaporation and transpiration.

The modelling experiments investigate the climate impacts of Australian land cover change by representing changes in average monthly land surface conditions through differences in land surface parameter files. The climate modelling experiments remove other sources of climate forcing by prescribing sea surface temperatures and sea ice distribution from observed climate data for 1969 – 1999 period. While the modelling framework incorporates differences in average seasonal dynamics of the changed land surface conditions, this framework cannot address changes in land surface properties that result from the dynamics of vegetation over

longer time frames, or involve complex feedback processes from components of the climate system other than the atmosphere.

1.4.1 Land Cover Influences Beyond the Scope of the Project

To place this research in context to the larger role that vegetation plays in the climate system the many direct and indirect feedbacks not included in the research must be considered, if only briefly. Other processes that directly effect the distribution and composition of vegetation include: inter-annual responses of vegetation to climate variability; ecosystem dynamics from long term climatic changes in water availability and temperature; and ecosystem dynamics in response to disturbance and succession of vegetation.

Other indirect processes not covered by the scope of the study include feedbacks from: changes in atmospheric fluxes of energy and matter to and from the oceans and the cryosphere as a result of vegetation changes; changes in soil moisture and surface water from irrigated farming, river damming and altered drainage; changes in atmospheric chemistry from gas exchanges with vegetation; vegetation responses to changes in atmospheric chemistry; nutrient availability resulting from the process of soil formation and denudation; vegetation responses to very long term changes in solar radiation over the earth associated with Milankovitch mechanisms and solar variability; and vegetation responses to very long term geological processes associated with volcanic activity, plate tectonics, sedimentation, weathering and erosion.

1.5 Thesis Structure

The climate impacts of Australian land cover change introduced in this chapter are investigated through the series of linked chapters shown in *figure 1.4*. The outcomes and findings of the theory and review chapters are used to develop conceptual models, postulated relationships, and Australian historical and ongoing land cover change statements, which form the basis of the experimental climate modelling of later chapters. The results from modelling experiments are evaluated in the context of the conceptual model and postulated relationships, as well as historical climate and climate changes, and Australian and international land cover change and climate research. The final findings of this research are assessed against the aims and objectives as a series of conclusions at the end of the thesis. The details of each of these chapters are listed below:

Chapter 2. Land Cover Influences on Climate Review: addresses the requirements of Objective 1 to develop a strong theoretical background to investigate the climate impacts of Australian land cover change. The chapter details the theory of land surface and biosphere interaction with the atmosphere from the impacts that vegetation has on the surface fluxes of radiation, sensible and latent heat, to the impacts that changes in these surface fluxes have on

atmospheric processes and larger scale atmospheric circulation. The review also compiles international and Australian case studies of land cover change and climate to put this study in context with other research performed in this field. The findings of the review are integrated into a conceptual model with postulated relationships developed for the climate impacts of Australian land cover change at the end of the chapter.

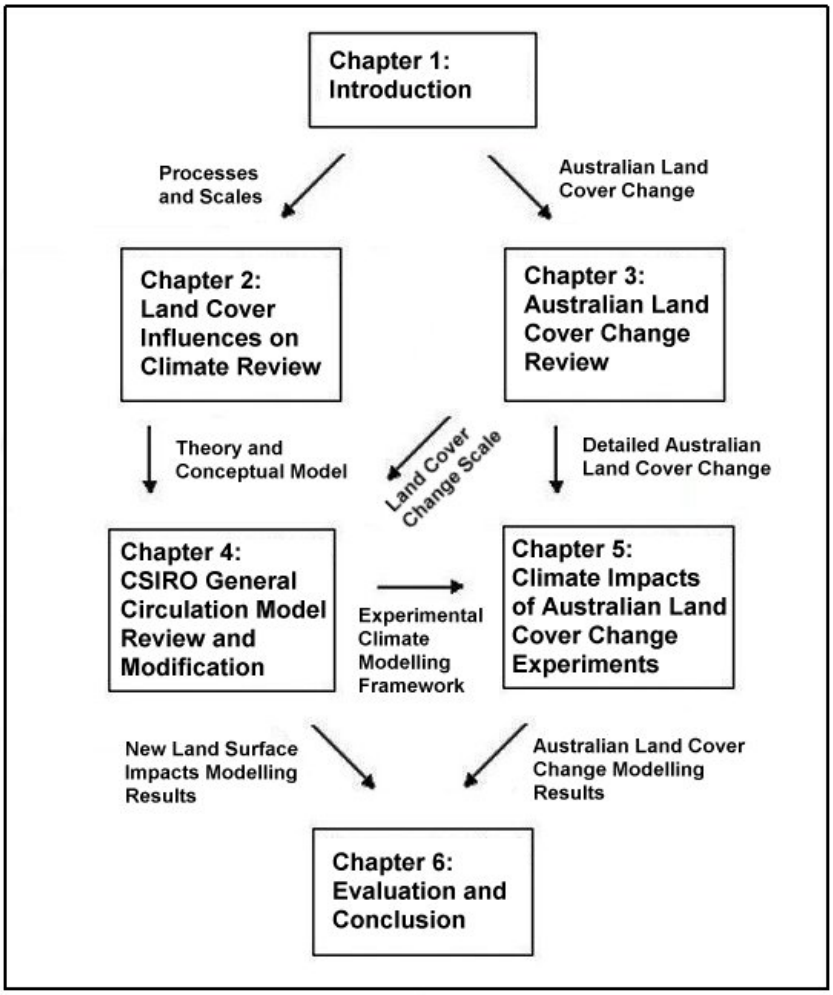

Figure 1.4. Thesis Chapter Structure and Linkages

Chapter 3. Australian Land Cover Change Review: addresses the requirements of Objective 2 to develop a consistent land cover change framework for both historical and contemporary Australian land cover change. The chapter describes Australian native vegetation prior to European settlement and the history of Australian land use and land cover change. The chapter also provides a review of current land cover change, as well as the variability of Australian vegetation in response to seasonal and inter-annual climate variation monitored from satellite observation.

Chapter 4. CSIRO General Circulation Model Review and Modification: addresses the requirements of Objective 3, by reviewing the CSIRO GCM and by making modifications to the model that allow land surface characteristics that describe the scale and nature of Australian

land cover changes to be represented in the model. The requirements of Objective 4 are addressed through assessing the impacts of using the climate modelling framework with the new relatively fine-scale land surface data. Sensitivity experiments compare the performance of the modified GCM with new global data sets to the performance of the GCM with the original CSIRO parameters. The experimental climate modelling framework developed in this chapter is used in Chapter 5 for the Australian land cover change climate modelling experiments.

Chapter 5. Climate Impacts of Australian Land Cover Change Experiments: addresses Objectives 5 by extrapolating pre-clearing land surface properties from the land surface properties of current remnant native vegetation to pre-clearing native vegetation extents. The requirements of Objective 6 are addressed through performing sensitivity experiments with the CSIRO GCM, with Australian land cover change represented by replacing the Australian pre-clearing land surface parameters with the current day land surface parameters. The results of the two experiments are compared and statistically analysed for the Australia continent, three Australian regions with significant land cover change, and over the larger Australian and global contexts. The results of the Australian land cover change experiments are evaluated against observed changes in precipitation, and in the context of the postulated relationships presented in Chapter 2.

Chapter 6. Evaluation and Conclusion: integrates the findings from Chapters 2, 3, 4 and 5 to address Objective 7 by developing Australian land cover change and climate change relationships from the climate modelling experiments, and by placing these findings in context with other research, and observed climate changes. The findings of the research are outlined against the thesis aims and objects at the end of the chapter as a series of conclusions to state how this thesis contributes to the understanding of the climate impacts of Australian land cover change research. From these conclusions the climate implications of historical and ongoing land cover change are assessed with future research requirements identified.

CHAPTER 2.
LAND COVER INFLUENCES ON CLIMATE REVIEW

2.1 Chapter Aims and Rationale

2.1.1 Aims and Structure

The aims of this chapter are to: (i) review the theory on how land cover influences the interaction between the land surface and the atmosphere; (ii) review international and Australian case studies investigating the impact that land cover change has on climate; and (iii) based on these reviews, develop a conceptual model and postulated relationships between Australian land cover change and climate. The reviews and conceptual model underpin the new land surface parameterisation framework used for investigating the possible climate impacts of Australian land cover change using the CSIRO climate models in subsequent chapters. The conceptual model is applied in Chapter 4 for the review of the CSIRO climate models, and to evaluate the climate impacts of adapting the model to incorporate Australian land cover change data. The conceptual model also is applied in Chapter 5 to develop and assess the Australian land cover change climate modelling experiments, and in Chapter 6 to evaluate the findings of Chapters 4 and 5.

The chapter is divided into four main sections. Section 2.2 reviews how land cover modifies land surface and atmosphere interaction processes. Section 2.3 reviews how the atmosphere responds to the changes in fluxes of moisture and energy from the land surface and how these responses impact climate at various scales. Section 2.4 reviews the status of Australian land cover change and climate research to identify and describe what work has been previously determined about these relationships and what is currently uncertain. Section 2.5 provides a synthesis of the chapter with a conceptual model and postulated relationships on how Australian land cover change may influence climate.

2.1.2 Rationale

To understand how Austrailan land cover change impacts climate, the details of how land cover change influences land surface properties and how these changes flow on to impact the climate system need to be identified. From the definition of the scope of the study provided in Chapter 1, the review of the land cover interactions with climate can be limited at the land surface spatially to the micro-scale, and temporally over the short-term timescale. At these spatial and temporal scales, *Trenberth* (1992) suggests that land cover has biophysical controls on the physical properties of the land surface, determined by the physiology and structure of vegetation present within the land cover. The different land surface properties associated with

different vegetation influence the interactions of the land surface with the near earth atmosphere and the underlying soil, with impacts on the surface energy balance and surface water balance.

The complex interacting nature of the climate system suggests that the climate response to the changes in vegetation structure and physiology present at the land surface will occur at a range of scales with numerous feedback through changes in the state of other components of the climate system. Again, given the definition of the scope of the study provided in Chapter 1, the review of climate responses to land cover change can be limited to the response of the atmosphere to changes in land surface fluxes of momentum, energy and moisture over the short to long term time frame.

Before undertaking climate modelling experiments to investigate the climate impacts of Australian land cover change it is necessary to develop a conceptual model of the systems and processes involved in these experiments to ensure that the representation of these complex interacting systems is realistic and represents actual changes at the land surface and possible responses in the climate system. The conceptual model and the postulated relationships at the end of this chapter provide a formal framework for assessing how the atmosphere, substrate and land surface conditions are affected by changes in Australian land cover in the simulated climate of the CSIRO GCM. The theory, field studies and modelling experiments detailed in this chapter form the basis for this formal framework.

2.2 Land Cover Impacts on Land Surface and Atmosphere Interaction

2.2.1 The Surface Radiation Budget and Vegetation

Following *Peixoto and Oort* (1992), all energy entering the climate system comes from the sun, with the exception of relatively negligible amounts of energy produced from the radioactive heating of the planet's core. As solar energy is the primary source of energy for the climate system, the influence of vegetation on the dynamics of solar radiation reaching the surface is important in determining the energy available at the land surface. Solar radiation covers the entire electromagnetic spectrum, with most of the energy falling in the wavelengths of the ultraviolet, visible and infrared, collectively referred to as short wave radiation (0.1 – 2.0 μm).

Following the Stefan – Boltzmann law, radiant energy also is emitted by all components of the climate system, with the amount of radiation and the wavelengths emitted dependent on the temperature of the components and their emissivity. The range of temperatures experienced within the climate system result in all radiation being emitted in the long wave spectrum (> 4.0 μm). The emission of long wave radiation is significant as it transfers energy through out the climate system and radiates thermal energy from the climate system back to space.

The solar radiation reaching the earth surface is reduced from the amount of radiation that reaches the top of the atmosphere through absorption and scattering from clouds, gas molecules,

and aerosols in the atmosphere (*Peixoto and Oort*, 1992). The proportion of the solar radiation that reaches the land surface that is reflected back from the surface is referred to as the surface albedo. The average global proportions of solar radiation reflected, scattered and absorbed of by air, water vapour, dust, ozone, clouds and the land surface are shown on the left hand side of *figure 2.1.*

The surface albedo is strongly determined by the nature of the surface, with different optical properties resulting from vegetation, bare soils, snow cover and water (*Peixoto and Oort*, 1992). At any point in time, the same surface also has different properties of surface albedo for different wavelengths of radiation and for different sun angles. The relationship between short wave radiation flux ($SW\downarrow$ Wm^{-2}) reaching the surface, to the short wave radiation flux ($SW\uparrow$) reflected from the surface, is expressed using the surface albedo (α) as:

$$SW\uparrow = SW\downarrow \alpha \tag{2.1}$$

The amount of long wave radiation energy emitted from the earth surface is proportional to the surface temperature by the Stephan-Boltzmann Law. This relationship between the long wave radiation flux from the surface ($LW\uparrow$ Wm^{-2}), the surface emissivity (ε_s), the Stefan-Boltzmann constant (σ), and the surface temperature (T_s K) is written as:

$$LW\uparrow = \varepsilon_s \sigma T_s^4 \tag{2.2}$$

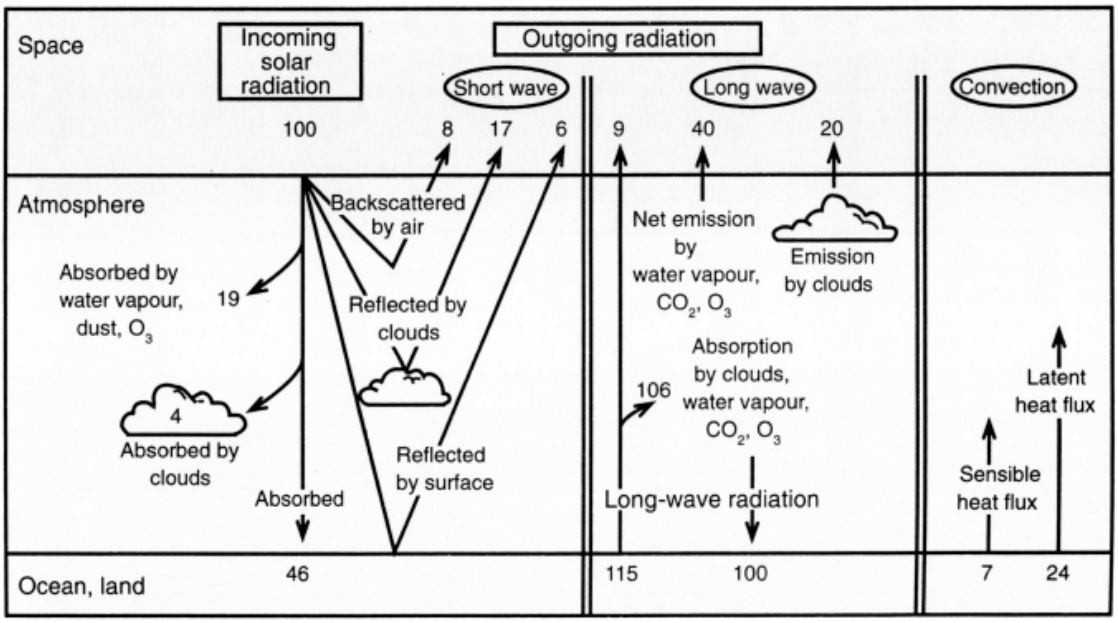

Figure 2.1. Global radiation and energy balances as a percentage of incoming solar radiation at the top of the atmosphere (after Sturman and Tapper (1996))

The downward long wave radiation flux ($LW\downarrow$) emitted by the atmosphere is dependant on the distribution of long wave radiation absorbing and emitting particles such as water vapour and CO_2, and the temperature of the lower atmosphere (*Peixoto and Oort*, 1992). The average global proportions of emission and absorption of long wave radiation by CO_2, water vapour, ozone, clouds and the land surface are shown in the center of *figure 2.1*.

The net amount of energy available at the earth surface from short wave (solar) radiation and from long wave (terrestrial) radiation is known as the surface radiation budget. The surface radiation budget accounts for all incoming solar radiation absorbed and reflected by the land surface, as well as, all long wave radiation emitted from the surface and emitted from the sky down to the surface. Combining the short wave and long wave components, the net surface radiation budget (R_{net}) absorbed by the land surface is written as:

$$R_{net} = SW\downarrow(1-\alpha) + LW\downarrow - \varepsilon\sigma T_s^4 \qquad (2.3)$$

The optical properties of vegetation canopies alter surface albedo and the effective emissivity from values that occur with bare soil. The changes in surface albedo and emissivity affects the amount of short wave and long wave radiation absorbed, reflected and emitted by the land surface, which in turn impacts the net surface radiation budget. The changes in radiation budget also have direct implications for the amount of energy available in the surface energy balance for heating and evaporation.

Vegetation impacts the surface albedo by changing the dynamics of short wave radiation at the surface. These changes are a result of the optical properties of individual leaves and through the light trapping properties of collections of leaves within the canopy (*Trenberth*, 1992). The optical properties of leaves are strongly influenced by chlorophyll, which absorbs strongly at visible wavelengths (0.4 – 0.7 μm) to drive photosynthesis, but absorbs very little at near-infrared wavelengths (0.7 – 4.0 μm).

The difference in optical properties of the individual leaves, result in visible wavelengths of radiation being completely absorbed after being reflected only a few times within the canopy, but near-infrared wavelengths being scattered numerous times through the canopy before being absorbed, or reflected to the ground or back to the sky. *Figure 2.2 a*, illustrates the representation of leaves as scattering objects for a beam solar radiation. The additional radiation dynamics of vegetation over bare soil are shown in *figure 2.2 b* and *c*.

Goudriaan (1977), *Kimes* (1984) and *Myneni et al.* (1989) provide rigorous and realistic models for describing the radiation dynamics within vegetation canopies. These models have detailed optical properties for the leaf elements, and describe radiative transfer through numerical ray tracing methods. *Dickinson* (1983) reviewed the work of *Meador and Weaver* (1980) to provide a simpler two-stream approximation of the dynamics of short wave radiation

within vegetation canopies by representing the canopy as a cloud of leaves, where the scattering of light was modelled similarly to the particles of clouds (*Sellers*, 1985).

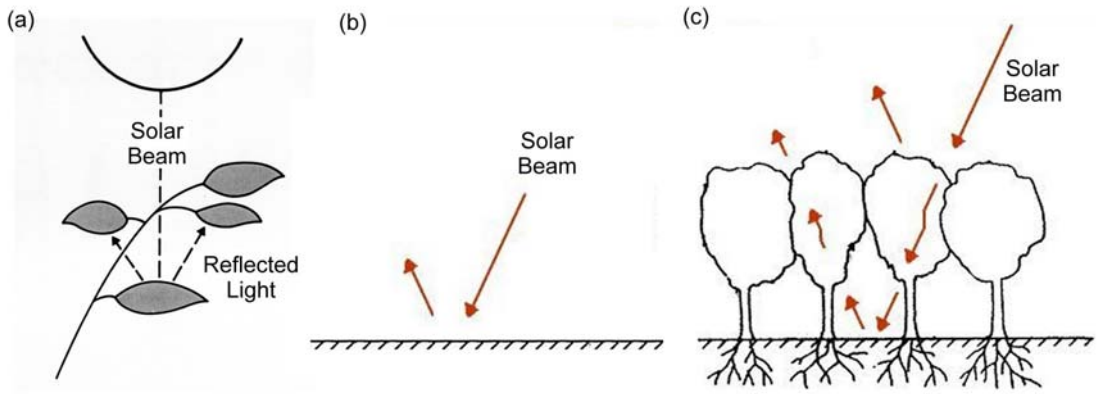

Figure 2.2 Solar radiation dynamics for: (a) individual leaves (after Trenberth (1992)); (b) bare soil; and (c) dense vegetation canopy (adapted from Pielke, (2001b))

In the two stream radiation model intercepted light is assumed to be absorbed, reflected or transmitted, dependant on the optical properties of the leaves for the wavelengths of the radiation, and the position and orientation of the leaves within the canopy. The properties of the two stream radiation model and the influence of vegetation properties, soil properties and sun angle on surface albedo and the division of radiation absorption between the vegetation and the soil are detailed in Appendix A. The relationships shown in Appendix A have been generalised and listed in *table 2.1*. The table shows that the net impact on surface albedo of changes in vegetation are complex, dependent on changes in the density of the vegetation, changes in optical properties of the vegetation, and the colour of the underlying soil.

Table 2.1 General rules for changes in short wave radiation dynamics from changing from native to agricultural vegetation

Vegetation Density	Vegetation Colour	Soil Colour	Albedo Impact
Native Vegetation Same Density as Agriculture	Native Vegetation Darker than Agriculture	No Impact	Higher
Native Vegetation Same Density as Agriculture	Native Vegetation Lighter than Agriculture	No Impact	Lower
Native Vegetation Denser than Agriculture	Same for both vegetation types	Soil Darker than Vegetation	Lower
Native Vegetation Denser than Agriculture	Same for both vegetation types	Soil Lighter than Vegetation	Higher
Native Vegetation Less Dense than Agriculture	Same for both vegetation types	Soil Darker than Vegetation	Higher
Native Vegetation Less Dense than Agriculture	Same for both vegetation types	Soil Lighter than Vegetation	Lower

Vegetation also affects the dynamics of long wave radiation at the surface. *Pielke* (2001b) demonstrated how the vegetation canopy acts as an intermediary layer absorbing and both sky and ground emitted long wave radiation, as well as emitting long wave radiation both upward and downward itself. *Figure 2.3 a* and *b* illustrates the intermediary nature of a dense vegetation canopy on the transfer of long wave radiation compared with bare soil.

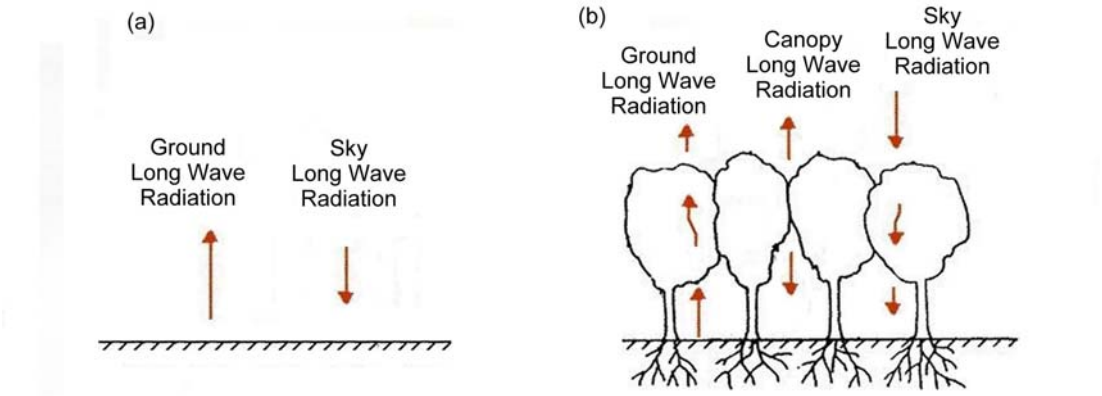

Figure 2.3 Long wave radiation dynamics for: (a) bare soil; and (b) dense vegetation canopy (adapted from Pielke (2001b))

Trenberth (1992) suggested that while the two-stream radiation model could be used to describe the fluxes of long wave radiation through the canopy from the sky, the ground, and the canopy itself, the closeness of these emissivities to unity made this an unnecessary component of the long wave radiation calculation. It was argued that the very high emissivity values ensure that long wave radiation incident on leaves is almost completely absorbed with almost no internal scattering. With the internal scattering of long wave radiation removed, the description of all components of long wave radiation absorption and emission were simplified to Beer's Exponential Extinction Law applied to the flux of long wave radiation from each source, with the long wave radiation emission calculated with the Stephan-Boltzmann Law. The impacts of vegetation change on the long wave radiation budget are therefore dependent on the soil temperature, the canopy temperature, the change in vegetation density and the downward flux of long wave radiation from the sky.

2.2.2 Surface Hydrology and Vegetation

The evaporative fluxes of moisture between the land surface and the atmosphere are limited by the availability of moisture at the surface, the supply of the latent heat of vaporisation, and the diffusion of the water vapour away from the surface (*Garratt*, 1992). *Trenberth* (1992), *Noilhan and Planton* (1989), *Pielke* (2001b), and others have demonstrated that the presence of vegetation at the land surface modifies the surface hydrology through deep-rooted vegetative transpiration, and through the interception of precipitation and dew by the canopy.

Figure 2.4 a and *b* illustrate the differences in the evaporative fluxes to the atmosphere, and the hydrological cycle of dense vegetation compared to bare soil.

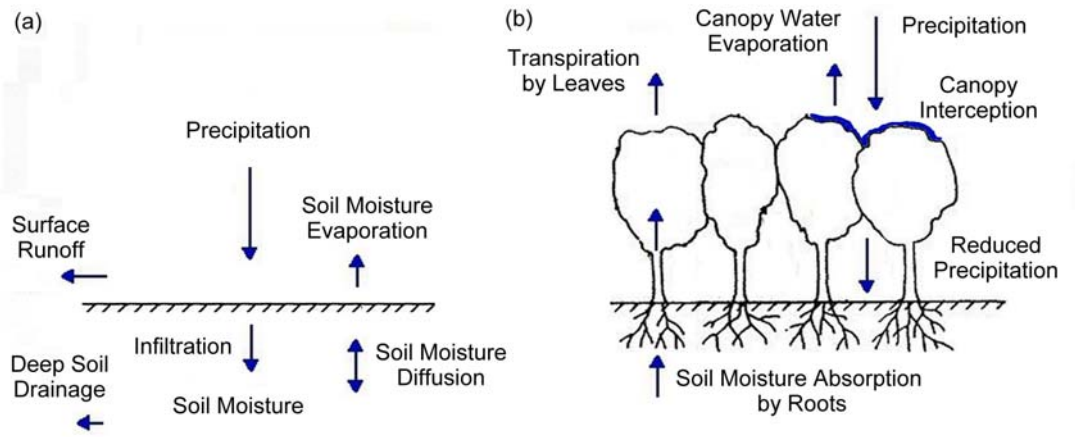

Figure 2.4 Hydrological processes for: (a) bare soil; (b) dense vegetation canopy (only processes additional to bare soil hydrology shown) (adapted from Pielke (2001b))

Evaporative processes are one of the main phases of the hydrological cycle, with significant impact on the water budget for a region. The evaporative fluxes also strongly influence the partition of surface energy into sensible heat and latent heat, which has impacts on the structure and atmospheric stability of the planetary boundary layer (*Pielke*, 2001b). The influence of changes in vegetation density and physiology on the evaporative flux from the canopy are detailed in Appendix B, C, and D, and are generalised in *table 2.2*.

Table 2.2 General rules for changes canopy evaporation and transpiration from changing from native to agricultural vegetation

Vegetation Density	Unrestrained Stomatal Resistance	Canopy Evaporation and transpiration Impact of Vegetation Change
Native Vegetation Same Density as Agriculture	Native Stomatal Resistance Higher than Agriculture	Higher transpiration from reduced canopy resistance to transpiration
Native Vegetation Same Density as Agriculture	Native Stomatal Resistance Lower than Agriculture	Lower transpiration from increased canopy resistance to transpiration
Native Vegetation Denser than Agriculture	Same for both vegetation types	Higher evaporation and transpiration from reduced canopy resistance and increased canopy interception of precipitation and dew
Native Vegetation Less Dense than Agriculture	Same for both vegetation types	Lower evaporation and transpiration from increased canopy resistance and decreased canopy interception of precipitation and dew

Table 2.2 shows that increasing vegetation density affects the canopy leaf area and therefore the number of stomatal pores present in the canopy for transpiration, resulting in a reduction in canopy resistance to transpiration. The vegetation density also affects the leaf area of the canopy for intercepting precipitation and dew, as well as the moisture storage capacity on the leaves. An increase in leaf area results in higher interception and larger moisture storage. The table also shows changes in physiology through unrestrained stomatal resistance impact transpiration, with higher stomatal resistance resulting in higher resistance to canopy transpiration and lower potential transpiration.

2.2.3 Surface Energy Balance and Vegetation

The energy available at the surface is a major limiting factor in sensible, latent, and ground heat fluxes, with the net energy available at the surface dependent on radiative fluxes. The balance of energy from each of the surface fluxes follows the First Law of Thermodynamics, such that energy must be conserved both instantaneously and averaged over time (*Garratt*, 1992). The division of energy into each of these fluxes is dependent on the direction of energy flow and the properties of the land surface, the atmosphere, and the substrate for the transfer moisture and energy. Following *Garratt* (1992), the surface energy balance can be calculated from the net surface radiation (R_{net}), the net sensible heat flux (SH_{net}), the net latent heat flux (LH_{net}), and the net ground heat flux (G) as:

$$R_{net} = SH_{net} + LH_{net} + G \qquad (2.4)$$

The presence of vegetation at the surface impacts the surface radiation budget, and the fluxes of sensible and latent heat through changes in surface hydrology and turbulent mixing. The differences in surface fluxes are illustrated in *figure 2.5 a* and *b* for bare soil compared with a dense vegetation canopy.

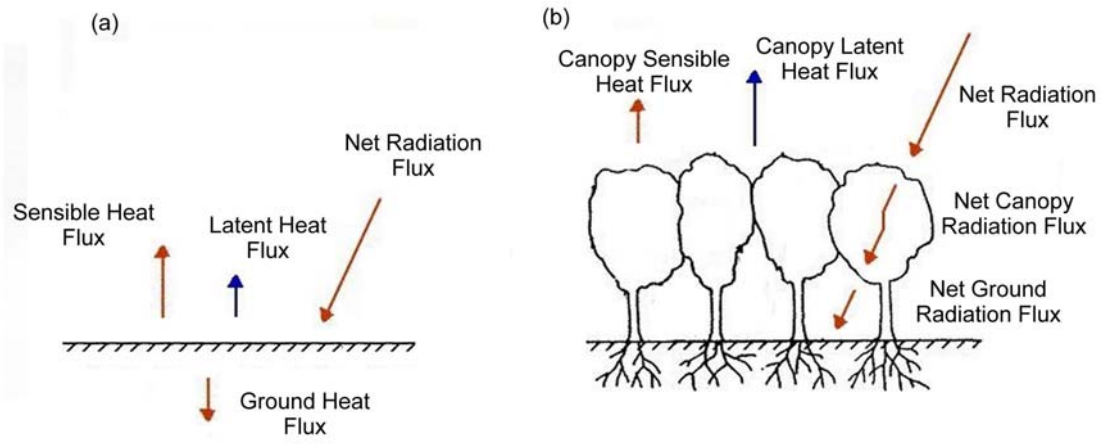

Figure 2.5 Surface Energy Balance processes for: (a) bare soil; (b) dense vegetation canopy (only processes additional to bare soil shown) (adapted from Pielke (2001b))

2.2.4 Atmospheric Fluxes and Vegetation

The influence the surface has on the atmosphere is effectively limited in height to the first 10 to 20 km of the atmosphere, known as the troposphere. The troposphere is the layer of the atmosphere in which most vertical motion and weather takes place, with the air strongly heated from the surface below through long wave radiation, and through sensible and latent heat transfer (*Sturman and Tapper*, 1996). The troposphere contains more than 80 percent of the air of atmosphere, and is characterised by temperature decreasing with height at a global average rate of 6.5 ^{O}C km^{-1}. The hydrological cycle is almost entirely confined within the troposphere due to the capping temperature inversion of the tropopause and stratosphere above.

Over time periods of a single day, however, the immediate influence of the surface is restricted to a shallower zone known as the planetary or atmospheric boundary layer. Within the atmospheric boundary layer, the exchange of momentum, matter, and energy is represented through the exchange of momentum and scalars, across a series of idealised boundary layers, which are approximately parallel to the surface (*Oke*, 1987 and *Peixoto and Oort*, 1992). The structure of these boundary layers are defined by the processes of motion that dominate the movement of air within the layers, and the temporal and spatial scales at which they operate. *Figure 2.6* shows the multi-layered structure of the atmosphere over the earth surface and within the planetary or atmospheric boundary layer.

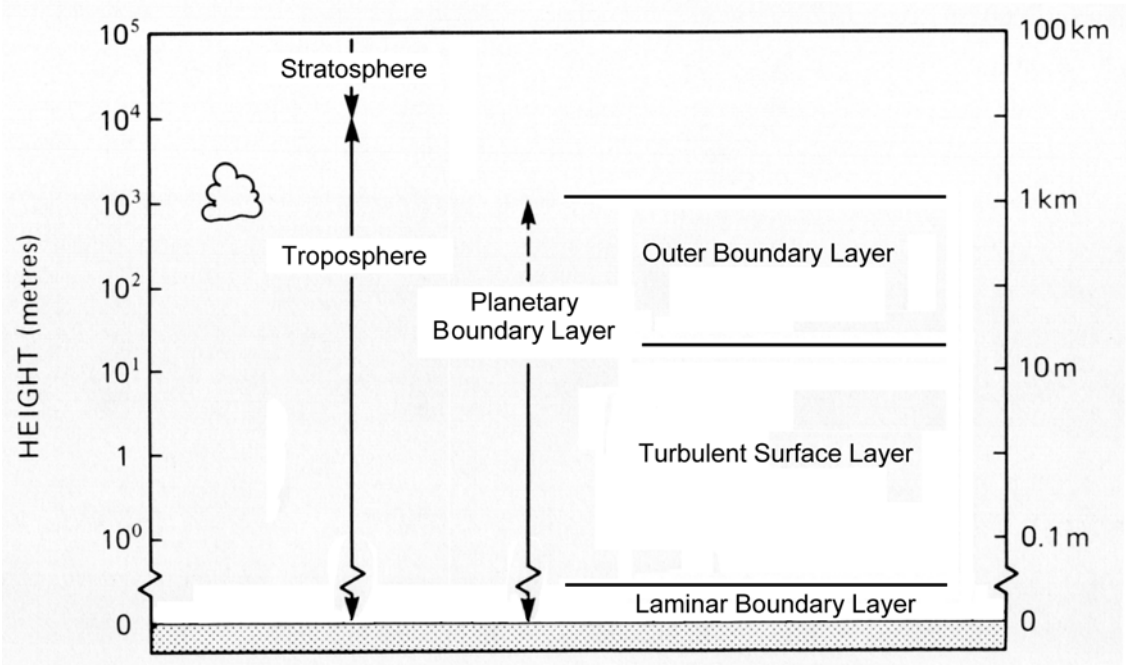

Figure 2.6 Idealised vertical structure of the atmosphere from the earth surface (adapted from Oke (1987) and Peixoto and Oort (1992))

In this model, the laminar boundary layer is the first layer immediately above the surface. This is a thin layer, where the air adheres to all surfaces for a depth of few millimetres through

laminar flows, without turbulence or convection. All non-radiative transfers of momentum and scalars within the layer are through molecular diffusion within the laminar flow. Beyond the laminar boundary layer, inertial and convective processes exceed viscous processes to produce turbulence within the airflow. The layer above laminar boundary layer is the turbulent surface layer, where small-scale turbulence dominates transfers of momentum and scalars. The vertical variation of the vertical fluxes within this layer is less than 10%, resulting in it also being called the constant flux layer (*Oke*, 1987 and *Peixoto and Oort*, 1992). The depth of the turbulent surface layer extends some tens of meters above the laminar boundary layer depending on the roughness of the surface, the wind speed and the atmospheric stability.

The turbulent region extending beyond the turbulent surface layer to the top of the planetary boundary layer is called the outer layer. The limit of the outer layer is conventionally set to the limit of turbulent activity, which is often set to the height of the lowest temperature inversion. The transfer of momentum and scalars in the outer layer is dominated by free convection involving large eddies associated with thermal convection and organised circulations. The large role of thermal convection in the outer layer results in large diurnal variations in the depth and structure of the layer, with the layer extending up to and beyond 2 km during the day, and often contracting to less than 100 m during the night (*Oke*, 1987).

The turbulent transport of momentum and scalars between the atmosphere and the surface through these boundary layers is complex, requiring eddy simulation techniques or high order closure models to describe all the processes involved with physically realism. *Garratt* (1992), *Trenberth* (1992), *Peixoto and Oort* (1992) and others suggest that eddy-diffusion can be used to provide a numerically adequate representation of these transfers without the complexities involved with higher order models.

2.2.5 Surface Fluxes and the Eddy Diffusion Model

The eddy-diffusion model extends the molecular diffusion model for transfers of momentum and scalars in laminar flows, to transfers involved in turbulent exchanges within the turbulent surface layer. In this model, fluid air flowing over a rough surface results in a profile of wind speeds from zero near the surface increasing with height to a point where wind speed is independent of surface friction. In this model the turbulent exchanges of momentum and scalars between levels in the wind profile are highly dependent of the rate of exchange of air between the layers and the properties of the two levels.

The exchange of momentum between the different layers is represented by the shearing stress (τ) caused by different wind speeds of the two levels in the wind profile. The amount of shearing stress is a product of the differences in horizontal velocities (u') of the wind between the two levels, the turbulent exchange (w') of air between the layers, and the mass per unit volume or density (ρ) of the air. Under neutral conditions in the turbulent surface layer, the turbulent mixing of the air between levels is equal in both the horizontal and vertical directions,

allowing both vertical and horizontal components to be represented by a single frictional velocity (u_*) for all levels in the wind profile. The relationship between the shearing stress and the wind speeds in the profile are written following *Monteith and Unsworth* (1990) as:

$$\tau = \rho u'w' = \rho u_*^2 \tag{2.5}$$

The properties of the wind speed profile are highly dependent on the roughness of the surface, with the wind speed profile following a logarithmic decay curve from a displacement height were the wind speed extrapolates to zero to the height were the profile is independent of surface friction. This relationship forms the basis for the logarithmic wind profile equation, written as:

$$u_z = \frac{u_*}{k} \ln\left(\frac{z-d}{z_0}\right) \tag{2.6}$$

where u_z is the mean wind speed (ms^{-1}) at height z (m), u_* is the frictional velocity for the wind profile, k is the von Karman's constant (≈ 0.4), d is the zero plane displacement that the wind profile is offset by roughness elements at the surface, and z_0 is the height the logarithmic wind speed profile extrapolates to zero above the displacement height, also known as the roughness length. For non-neutral conditions buoyancy can be included in the eddy-diffusion model to account for the effects of free convection within the surface layer following Monin-Obukhov similarity theory as detailed in *Garratt* (1992), however, these effects extend beyond the immediate influence of vegetation on turbulent exchanges.

2.2.6 Surface Roughness and Vegetation

Vegetation affects the properties of surface roughness and displacement height by changing the distribution of roughness elements over the surface, which in turn changes the surface friction imparted on the wind profile and the absorption of momentum by the vegetation and the surface. *Figure 2.7 a* and *b* demonstrate how the different surface roughness values (0.003 m and 1.5 m) and displacement heights (0.0 m and 10.0 m) for bare soil and a dense vegetation canopy produce very different wind speed profiles for the same wind speed (5 ms^{-1}) at the reference height (30 m).

The relationships between vegetation height and structure, with surface roughness and displacement height have been extensively examined through experiment and theory by *Raupach* (1992), *Shaw and Pereira* (1982), and others. *Raupach* (1994) provides simplified expressions for surface roughness and the displacement height that can be determined from canopy height and leaf area index. These relationships are detailed in Appendix E and generalised in *table 2.3*.

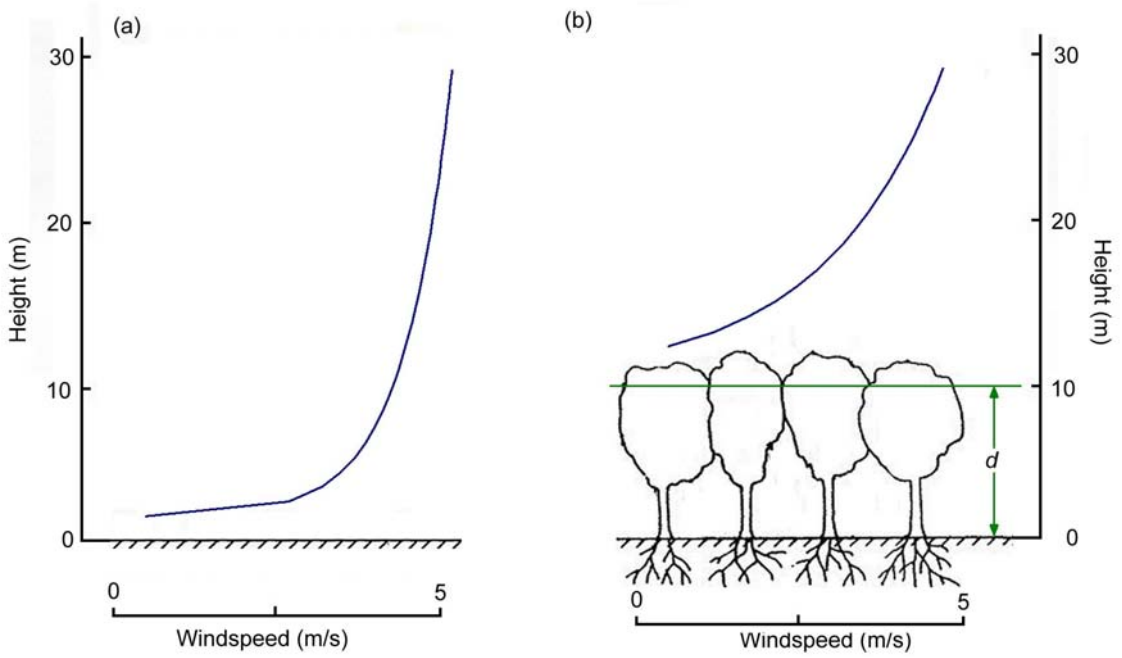

Figure 2.7 Logarithmic wind profile (u_z) (blue line) for a wind speed of 5 ms^{-1} at a height of 30m for: (a) bare soil; and (b) dense vegetation canopy (adapted from Pielke (2001b) and Monteith and Unsworth (1990))

Table 2.3 shows that surface roughness length and displacement height are both strongly influenced by vegetation density and vegetation height. The relationship with vegetation height shows that taller vegetation has larger surface roughness and displacement height, however, the relationship with vegetation density is more complex. Increasing leaf area index increases the surface roughness length and the displacement height to maximum value where the canopy starts to close. After this point increases in leaf area index decrease the surface roughness length but increase the displacement height.

Table 2.3 General rules for changes in surface roughness from changing from native to agricultural vegetation

Vegetation Density	Vegetation Height	Surface Roughness Impact of Vegetation Change
Native Same Density as Agriculture	Native Taller than Agriculture	Reduced surface roughness and displacement height
Native Same Density as Agriculture	Native Shorter than Agriculture	Increased surface roughness and displacement height
Native Denser than Agriculture	Same for both vegetation types	Reduced surface roughness and displacement height, unless closed canopy
Native Vegetation Less Dense than Agriculture	Same for both vegetation types	Increased surface roughness and displacement height, unless closed canopy

2.2.7 Impacts of Changes in Surface Roughness on Surface Fluxes

To quantify the influence of surface roughness on surface fluxes through the turbulent surface layer *Monteith and Unsworth* (1990) provide an alternative method for calculating the flux of momentum between different levels in the wind profile using a resistance model in the form of Ohm's Law. This model uses the concept of aerodynamic resistance (r_{aM}) as a limit for the flux of momentum between the different levels (z_1 and z_2) at different wind speeds (u_1 and u_2). This relationship can be written as:

$$\tau = \rho(u_2 - u_1)/r_{aM} \tag{2.7}$$

Assuming the flux of momentum is constant through the turbulent surface layer, the aerodynamic resistance between any levels within the layer can be assumed to be constant as well. If the aerodynamic resistance is evaluated between a reference level z_a and the level $z_0 + d$, where the wind speed is extrapolated to zero, the second wind speed term can be removed from the equation. With this term removed *equations 2.7*, *2.5* and *2.6* can be combined to rewrite the aerodynamic resistance for momentum as:

$$r_{aM} = \frac{\ln((z_a - d)/z_0)^2}{k^2 u_a} \tag{2.8}$$

Monteith and Unsworth (1990) extend the aerodynamic resistance model to the flux of sensible and latent heat, as well as other scalars, which maintain constant flux within the turbulent surface layer. The flux of these scalars between the levels z_1 and z_2 depend on the difference in the values between the levels and the resistance of the turbulent surface layer to mix the scalars between the levels. This relationship can be written for sensible (*SH*) and latent (*LH*) heat fluxes using the aerodynamic resistances for sensible heat (r_{aH}) and latent heat (r_{aE}), and the potential temperature (θ) and specific humidity (q) at both levels. These relationships are written as:

$$SH = \rho c_p(\theta_2 - \theta_1)/r_{aH} \tag{2.9}$$

$$LH = \rho L_e(q_2 - q_1)/r_{aE} \tag{2.10}$$

where c_p represents the specific heat of air at constant pressure, and L_e represents the latent heat of evaporation. The potential temperature and specific humidity are used to ensure that pressure differences between the two levels do not impact the measures of moisture and energy.

The atmospheric resistances for heat and moisture flux are closely related to the atmospheric resistance for momentum, with all three being highly dependent on the surface roughness length for momentum (z_0) and the displacement height (d). The dependence of the resistance terms on these values indicates different vegetation morphology and density have direct influences the potential turbulent transfers of latent and sensible heat from the surface through the turbulent surface layer to outer boundary layer.

2.2.8 Section Summary

1. Vegetation modifies the surface radiation budget by changing the net radiation flux into the canopy and the ground, by shading the ground, through absorbing short wave radiation more strongly in the visible than the near infrared wave length, and through absorbing and emitting long wave radiation.
2. Vegetation affects surface hydrology by deep rooted transpiration of soil moisture through the leaves of the canopy, and by intercepting and evaporating precipitation and dew before it reaches the underlying soil.
3. The changes in surface hydrology change the flux of sensible heat and latent heat flux through the latent heat of vaporisation.
4. The changes in surface radiation budget, surface roughness and surface hydrology all affect the surface energy balance with impacts on latent, sensible and ground heat fluxes, and through surface heating
5. Vegetation affects the exchange of momentum, and sensible and latent heat between the land surface and the atmosphere by increasing the mechanical turbulence in the turbulent surface layer with increased surface roughness from the canopy of branches and leaves.

2.3 Atmospheric Process And Land Surface Conditions

2.3.1 Introduction

As shown in the previous section, the changes in physical properties of the land surface associated with changes in vegetation, influence turbulence and convective heating of the near earth atmosphere and the transport of moisture through evaporation and transpiration. These changes have impacts on the vertical structure of moisture and energy in the daytime atmospheric boundary layer *Pielke* (2001b). These changes in boundary layer structure have strong impacts on the stability and the convective processes within the boundary layer, with impacts on cloud formation and precipitation. Regional scale wind circulations also develop as a result of differential heating and boundary layer composition over adjacent land surfaces with different physical characteristics and surface fluxes. These circulations can produce moisture convergence, cloud formation and precipitation with impacts on regional hydrology.

At macro-scales, changes in land surface properties associated with changes in vegetation can have impacts on continental and global atmospheric circulation, with possible large impacts on regional and continental climate. *Kabat et al.* (2004), *Pielke et al.* (1998), *Betts et al.* (1996) and others provide extensive reviews on the complex relationships that exist between vegetation and other components of the climate system at the local, regional, and global scales. These reviews detail the differences in magnitude and sign that similar vegetation change investigations have identified in different geographic localities over the Earth. The following section presents the general findings from a number of representative vegetation and climate studies over the three spatial scales identified in Chapter 1.

2.3.2 Local Scale

As reviewed in *Pielke et al.* (2002), turbulent heat fluxes near the ground are strongly affected by land surface characteristics, for the division of radiative energy into latent and sensible heat. Over dry bare land radiative energy is primarily transferred to sensible heat and ground heat fluxes through strong surface heating. Over wet bare land, the radiative energy is primarily transferred to latent heat fluxes through evaporation. For vegetated land, large latent heat fluxes can continue even with a dry soil surface through transpiration drawing moisture from deep within the soil profile.

The characteristics of the atmosphere above dry, and wet or vegetated land surfaces are significantly different. Over dry bare soils the strong sensible heat flux produces vigorous turbulent mixing, resulting in an unstably stratified planetary boundary layer. The strong turbulent mixing and heating result in a deep boundary layer extending to heights of 2000 – 3000 meters or more above the land surface in afternoon hours. The deep and thermally unstable boundary layer, also entrains dry air from the troposphere above further reducing the average moisture content of the boundary layer.

Over wet or vegetated land surfaces, the slower heating rate limits the growth of the planetary boundary layer to typically less than 1000 meters. Evaporation and transpiration supply additional moisture to the shallower boundary layer, which combines with significantly less entrainment of dry air to produce a moister boundary layer, than develops over dry bare soil. The shallower, cooler boundary layer with more moisture is unstable to moist convection and under favourable conditions may promote deep cumulus convection and heavy precipitation.

Pielke (2001a) presented the influences that land cover played on deep cumulus convection over the Central Plains of the United States from the modelling and field studies performed in *Pielke et al.* (1997). The modelling study looked at the convective processes associated with the current day land surface of irrigated cropping, compared with the same processes associated with the natural land surface of short prairie grass. The study found that the higher evaporation and transpiration rates of the current landscape produced higher convective

available potential energy (CAPE) in the boundary layer, which resulted in the development of a thunderstorm over the area during the simulation. The lower evaporation and transpiration of the natural landscape, however, only produced a shallow line of cumulus clouds under the same conditions.

2.3.3 Meso or Regional scale

At the regional scale, *Moore and Rojstaczer* (2002) studied the influence of irrigation on precipitation in the Texas High Plains of the United States. The study used rainfall gauges and radar tracking to follow storm events over the region for the summers of 1996 and 1997. The storm events were analysed for total precipitation and for intensity, in relation to the area that the storms originated. The study found that irrigation enhanced summer precipitation by between 6% and 18% for areas up to 90 kilometers downwind, with storms of greater duration, length, and total accumulation. The study also found that the irrigation was not a significant source of the moisture in the storms, rather the cool, wet surface increased low-level instability triggering the storms.

Lawton et al. (2001) investigated the impacts of lowland deforestation in Costa Rica on cloud immersion of adjacent tropical montane cloud forests during the dry season. The study used Landsat and Geostationary Operational Environmental Satellite imagery, and atmospheric modelling to assess changes in cloud formation, and the subsequent cloud immersion. The results of the study indicated that the pastures were relatively cloud free, while the remaining forests produced well developed cumulus cloud fields, with the cloud base heights significantly higher over the pastures than the forests. The study found the reduced cloud formation and higher cloud base height from deforestation, reduced the amount of cloud immersion experienced by the montane cloud forests with serious impacts on the moisture dependent ecosystem.

Differences in land surface characteristics at meso or regional scales also can produce organised circulations between areas with different surface fluxes, such as those between land and water, or irrigated crops and dry grassland. *Pielke and Avissar* (1990), *Avissar and Liu* (1996), and others have shown that these organised circulations and associated fluxes can generate clouds, alter precipitation patterns, and induce thunderstorms. *Figure 2.8* shows a meso-scale circulation between a warm dry land surface and a cool wet water body.

The scales at which heterogeneous landscapes with different land surface characteristics form organised circulations have been investigated by *Baidya Roy and Avissar* (2000), *Avissar and Schmidt* (1998), and others using large eddy simulation (LES). These experiments have modelled the dynamics of the convective boundary layer over a range of heterogeneity lengths within the meso-scale domain. The results of these modelling studies indicate that for land surface heterogeneity with homogeneous features less than 5 – 10 km in length, the vertical buoyancy caused by uneven heating is disturbed by horizontal pressure gradients caused by the

same uneven heating, preventing well organised circulations developing. With land surface heterogeneity greater than 5 – 10 km, however, the horizontal pressure gradients are too weak to disturb the vertical buoyancy, due to distance between the regions of uneven heating, and organised circulations are able to form between the areas of buoyancy and the areas of subsidence.

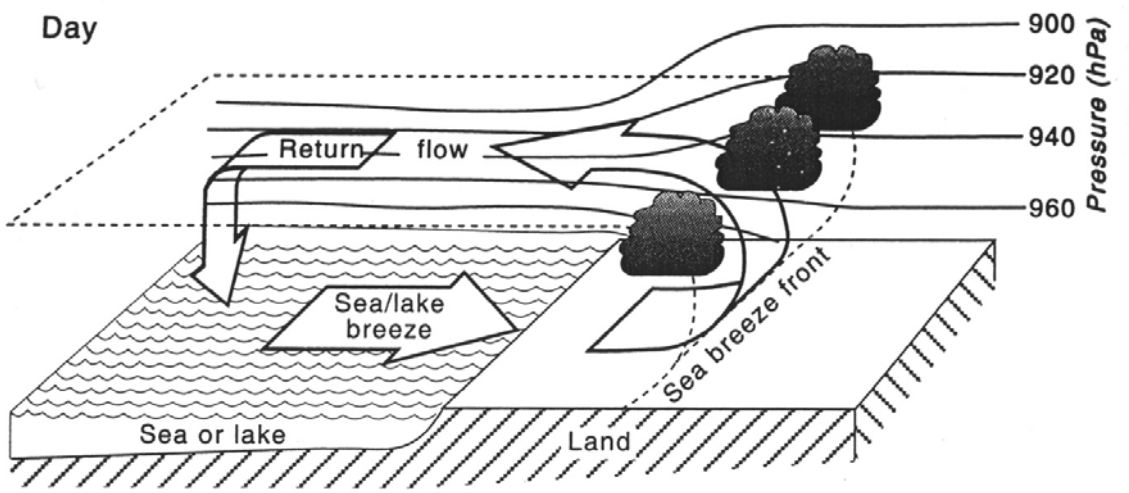

Figure 2.8 A typical day time meso-scale circulation formed between land and a water body. The uplift over the land is due to strong sensible heat fluxes from surface heating. The subsidence over the water body is from small or negative sensible heat fluxes resulting from the cooler surface temperature, and large evaporative fluxes (from Sturman and Tapper (1996))

2.3.4 Macro or Global scale

Researching the role of vegetation on surface albedo and climate, *Charney* (1975) investigated whether a reduction in darker vegetation over brighter soils in the Sahel region of the southern Sahara may lead to a decrease in the radiative heating of the surface and a relative cooling of the atmosphere above. The study suggested that atmospheric cooling resulted in a sinking motion that was superimposed on the descending branch of the Hadley cell, leading to increased stable descending air over the region, perpetuating arid conditions. The climate modelling by the study supported these hypotheses, with an increase in albedo over the Sahel shifting the Inter Tropical Convergence Zone several degrees south and reducing rainy season precipitation over the Sahel by 40%.

In similar research *Lofgren* (1995) used global scale climate models to show that thermally induced overturning circulations between oceans and land could be affected by albedo at low latitudes. The study found that decreased surface albedo increased radiative heating at the surface, resulting in enhanced upward atmospheric motion over the continent. The increased upward motion caused increased low level convergence of air over the continent and an associated low level divergence over the surrounding oceans. This circulation pattern resulted in enhanced moisture flux from the ocean to the continent, with increased precipitation over the

continent. The increased precipitation further enhanced the thermal forcing through latent heat release on condensation. At higher latitudes *Betts* (2000) and *Kabat et al.* (2004) suggest the effective surface albedo can be sensitive to the distribution of boreal forest, with a snow and albedo feedback resulting in warming and enhanced snow melt where forest is present. *Betts* (2000) suggests that the warming associated with the decreased surface albedo of boreal forestation, may offset any reduction in radiative warming that the growing forest would cause from sequestration of CO_2 from the atmosphere.

Investigating the climate impacts of different types of vegetation in tropical lands *Hales and Neelin* (2002) performed a systematic investigation into the comparative roles of surface albedo and moisture conductance using a Quasi-equilibrium Tropical Circulation Model. The investigation found that both higher albedo and lower surface conductance resulted in lower precipitation over all vegetation types of the model. The impacts on temperature, however, were opposite, with higher albedo resulting in lower surface temperatures due to a reduced radiation budget, and lower surface conductance resulting in higher surface temperatures due to reduced evaporation. The precipitation changes from surface conductance were shown to be from local rainfall recycling, where as, albedo effects where more likely to be caused by moisture convergence from changes in atmospheric circulation from the ocean to the land.

The study found the combined effects of albedo and surface conductance tended to be near linear, with the independent albedo and conductance effects combining to give a final result that was nearly equal to their total. These relationships also where reasonably symmetrical, with increases in either property having the opposite effect to a decrease. This was true for their impact on both precipitation and temperature. The experiments showed that low density vegetation was more sensitive to changes in albedo, dense vegetation was more sensitive to changes in conductance, and medium vegetation was a combination of the two.

Modelling investigations into the climate impacts of tropical deforestation in South America, Africa, and South East Asia, by *Zhang et al.* (1995), *Polcher and Laval* (1994) and others, support the findings of *Hales and Neelin* (2002) for dense vegetation. These studies identified the main impact of removing tropical forests was on the hydrological cycle through reduced transpiration. The reduction in atmospheric moisture combined with the increase in sensible heat flux, resulted in reduced cloud formation and precipitation. The reduced cloud cover significantly increased solar radiation flux which offset the increased albedo associated with the deforestation, to result in further increases in sensible heat flux and further reduction in precipitation and cloud cover.

Bounoua et al. (2000) investigated the sensitivity of the CSU GCM to global changes in NDVI by comparing climate simulated with the minimum and maximum NDVI values observed for the 1982 – 90 period. The increase in NDVI from the minimum to maximum value resulted in increased albedo in tropical and subtropical areas, but decreased albedo at higher latitudes. The increase in NDVI also resulted in a 46% increase in global absorbed visible radiation, with

similar increases in photosynthetic uptake of CO_2 and transpiration. The increase in transpiration combined with the increase in albedo to produce a cooling of tropical and subtropical surface climate by 0.8 ^{O} C. During the growing season in northern latitudes the increased transpiration also resulted in cooling of surface climate by 1.8 ^{O} C, despite the reduced albedo. In winter however, the reduced albedo resulted in a slight warming of the surface climate. The increase in transpiration also was larger than the increase in precipitation resulting in an overall deficit of soil moisture with the increased NDVI.

In similar work with the same GCM and land surface model *Bounoua et al.* (2002) compared the climate modelled with a modern day land surface derived from satellite observation, to the climate modelled with a reconstructed land surface representing vegetation as it may have existed in the absence of human disturbance. The land cover conversion experiments reinforced the findings of the previous NDVI experiments. The impact of converting forests to grasslands in tropical and subtropical areas was a year round warming of surface climate by 0.8^{O} C. The impact of converting forests and grasslands to crops was a cooling of summer surface climate by 0.7 ^{O} C and a cooling of 1.1^{O} C in winter. As the sign of the changes in surface climate were opposite for temperate and tropical latitudes the overall impact of land cover conversion on global surface climate was small. At regional scales however, the changes in surface climate were significant and highly dependent on the type of land cover conversion represented.

Looking over the longer term at global deforestation *Brovkin et al.* (1999) used a climate system model of medium complexity to progressively clear forests and replace them with crops and grasslands over the last millennium. The modelling experiments found that the land cover conversion resulted in overall global cooling of surface climate of 0.35^{O} C, with a more notable 0.5^{O} C cooling in the northern hemisphere. *DeFries et al.* (2002) investigated how possible future deforestation out to the year 2050 may impact surface climate. Their study found that the majority of future deforestation will likely occur in tropical and subtropical regions. In these areas the modelling experiments suggested this deforestation would result in reduced evaporation and transpiration with in increased surface temperatures up to 2^{O} C and a drier hydrological cycle.

Reale and Dirmeyer (1998) investigated land cover and climate changes in northern Africa from 2000 years ago to see whether historical changes in land cover could be responsible for changes in Mediterranean climate. Climate proxies from the region suggested a widespread drying trend across the Mediterranean since the Roman Classical Period (RCP). The study also showed the desert areas of northern Africa corresponding with modern Egypt, Tunisia and Algeria were significantly moister during the RCP, with wealthy agricultural economies making the area the most productive in the Roman World.

To investigate if land cover changes associated with deforestation and cultivation across the Mediterranean may have contributed to the widespread drying, the study modelled the

climate of the region with a fine grid increment general circulation model using vegetation that existed in the RCP compared with the climate modelled with the vegetation representing modern day cover. The modelling experiments showed significant changes in the climate under the two vegetation scenarios, with a northward shift in the Inter Tropical Convergence Zone, and the creation of a sea-land circulation over northwestern Africa under the RCP vegetation. The changed atmospheric circulation resulted in substantially moister conditions in northern Africa, with the speculation that the vegetation of the RCP would be sustained under the wetter conditions in areas that under current day conditions are too dry. The conclusion from the research was that clearing of the Mediterranean by human activity since the RCP may have triggered a positive climate feedback with a drift towards the dryer conditions of modern day.

Investigating the global climate impacts of land cover change, *Pielke et al.* (2002) suggested that changes in surface fluxes due to land cover change in tropical areas may have global impacts similar to those associated with changes in sea surface temperatures of El Niño events. This was supported by modelling experiments performed by *Chase et al.* (1996) and again by *Chase et al.* (2000), that indicated changes in tropical land surface conditions changed tropical convection, impacting on upper level tropical outflow, in turn influencing the Northern Hemisphere westerly jet, with impacts on high latitude climates. *Pielke et al.* (2002) also suggested that the climate impacts of land cover change were less obvious than El Niño conditions, which reverse to back average and La Niña conditions on relatively short time spans, due to the gradual nature of land cover changes and their relatively permanent impact on climate.

2.3.5 Section Summary

1. Changed fluxes of moisture and energy affect the atmospheric boundary layer, with strong impacts on the convective processes within the boundary layer.
2. At the local scale, dry bare land results in deep stable boundary layers while vegetated or saturated land results in shallower, unstable boundary layers that may promote deep cumulus convection.
3. At the meso-scale, case studies have shown irrigation and land cover change affect regional circulation and precipitation patterns through meso circulations and altered moisture transport and cloud formation.
4. At the macro-scale, both albedo and surface conductance through evaporation and transpiration have been demonstrated to alter the larger-scale atmospheric circulation, changing wind flows and altering the flux of moisture from the oceans to the adjacent land.
5. There is a growing body of evidence suggesting that changes in atmospheric circulation resulting from land cover change may propagate and influence global circulations at a distance from the initial land cover change.

2.4 Australian Land Cover Change and Climate Case Studies

2.4.1 Introduction

The main focus of field investigation into the climate impacts of Australian land cover change have concentrated on the large scale clearing of native vegetation for the Western Australian wheat belt. In this region clearing has resulted in large homogeneous tracts of agricultural land and native vegetation meeting at a strong transition line known as the "Bunny Fence". Statistical analysis of historical precipitation records for this area of Western Australia, show significant decreases in May to October precipitation coinciding with the major clearing period from 1945 – 1990 (*Lyons et al.*, 1993).

Modelling and field studies investigating the land surface conditions, surface fluxes and atmospheric responses over agricultural land and adjacent native vegetation in this area, demonstrate that the changes in land surface properties do have strong impacts on air temperature, boundary layer structure, and cloud formation. These studies also indicate there may be impacts on precipitation and soil moisture which may account for some of the observed changes in winter rainfall.

Recently *Narisma and Pitman* (2003) investigated the impacts of historical Australian land cover change on near surface climate over the Australian continent through comparative regional climate modelling experiments. The study found there were strong impacts on the modelled surface fluxes under present day vegetation, compared with conditions that may have existed prior to European arrival. The study also found there were statistically significant changes in regional air temperatures in the south east, south west, and north east of the continent. Changes in precipitation between the two simulations, however, were found not to be statistically significant.

Yang (1995) also investigated the impacts on Australian climate of anomalously dry or wet soil moisture conditions. While this study was not interested in land cover change the changes in land surface conditions associated with the soil moisture changes were similar to those that occur with land cover change. The study found that the altered soil moisture conditions had strong impacts on the surface fluxes of sensible and latent heat, with large impacts on precipitation and air temperature. The study also found that the soil moisture anomalies were short lived in the modelling experiments, rapidly converging back toward the control experiment values.

The following subsections describe each of these Australian case studies in detail to evaluate the scope of research performed for Australian land cover change and climate, and to help develop the land cover change and climate experimental framework used in Chapter 5.

2.4.2 Investigating South West Western Australia Land Cover Change

The first major study into the climate impact of land cover changes in south west Western Australia was conducted by *Lyons et al.* (1993), as part of a larger program called the "Bunny Fence" experiment (BuFex). The initial study was a combined field campaign and modelling exercise to investigate differences in surface fluxes over adjacent agricultural land and native vegetation during the winter of 1991. The study used surface, aircraft and satellite sensors over a study site near Lake King at the eastern margin of cleared land in south west Western Australia. The study site encompassed the transition from agricultural land to native vegetation, with heterogeneity lengths well in excess of 10 km either side of the transition.

The satellite imagery for the region showed that for August 1991 agricultural lands had higher NDVI values and latent heat fluxes than adjacent native vegetation. The rationale for these differences was that the rapidly transpiring, dense, green pastures and wheat crops produced higher latent heat fluxes compared to the darker, dryer and rougher native vegetation, with the higher sensible heat flux. Modelling experiments with the different surface fluxes showed a deeper boundary layer developed over the native vegetation, with boundary layer development suppressed over the growing crops and pastures. In agreement with the modelled results, satellite imagery from the same time period showed the preferential development of convective cumulus cloud over the dark native vegetation compared with the lighter crops and pastures.

Xinmei et al. (1995) continued the work of the BuFex program with further investigation into the seasonal changes in surface conditions and surface fluxes at the Lake King field site. This work used NOAA AVHRR satellite imagery and regional climate models to investigate monthly changes associated with the two vegetation types. From the satellite imagery the native vegetation showed significantly smaller variations in NDVI than the agricultural land, with the agricultural land having strong seasonal cycles associated with cropping. The NDVI values over agricultural land were very low in summer when the soil was left bare. These values increased through autumn and winter, peaking in early spring with the growing crop. This was followed by decreasing values through late spring and early summer as the crop senesced, returning to the low values of summer after harvest.

Surface albedo for agricultural lands was markedly higher than native vegetation for all months, with values consistently more than 10% higher. Both native vegetation and agricultural lands had seasonal variations in albedo, with both having the highest values in summer and the lowest values in winter. Modelling experiments of boundary layer development over the two vegetation types showed the sensible heat flux was greater over native vegetation than agricultural land for all months. Latent heat flux, however, was greater for agricultural crops in winter and early spring with the growing crop, but greater for native vegetation in summer after the harvest.

The differences in surface fluxes resulted in different modelled boundary layer development over the two vegetation types, with the boundary layer height greater over native vegetation for all months. The modelled boundary layer heights where compared with the monthly lifting condensation level to investigate conditions for convective cloud formation. The lifting condensation levels were estimated from mean monthly air temperature and relative humidity profiles observed by the Bureau of Meteorology at nearby Lake Grace.

The study found that the mean lifting condensation level was higher than the modelled boundary layer height for both vegetation types for December to February, and lower for both vegetation types for August to October. For the remaining months, however, the mean lifting condensation level was lower than the modelled boundary layer height for native vegetation, but higher for the agricultural land. The study suggested that this indicated that the conditions for convective cloud formation were more favourable over native vegetation than over agricultural land for these months. The modelled relationships between boundary layer height and vegetation type supported the preferential cloud formation over native vegetation observed by *Lyons et al.* (1993). The study noted that the linkage between changes in precipitation and boundary layer height associated with the lifting condensation level were beyond the scope of the research, warranting further investigation.

More recently, *Ray et al.* (2003) extended the work of the BuFex experiment to regional scales using Moderate Resolution Imaging Spectrometer (MODIS), Advanced Spaceborne Thermal Emission and Reflection Radiometer (ASTER) and Geostationary Meteorological Satellite 5 (GMS5) satellite imagery over the August 2000 to December 2000 period. The MODIS data was used to measure surface properties such as NDVI, albedo, soil moisture availability, surface temperature, sensible and latent heat flux, with the ASTER data used for more detailed measurement of these surface properties along the fence line. The GMS5 data was used to construct monthly cumulus cloud frequency occurrence maps for 1999 to 2000, with the MODIS data also used to investigate cloud optical thickness, droplet size and liquid paths over the different land surface properties.

In agreement with *Xinmei et al.* (1995), the new satellite data showed that the NDVI values were higher over agricultural land for August, and higher over the native vegetation following the harvest in December. Again the albedo values were consistently lower for native vegetation than agricultural land for all months. The study also found the latent heat fluxes and soil moisture availability were higher over native vegetation in summer, and higher over agricultural land in winter. The higher latent heat fluxes coincided with increased likelihood of cumulus clouds formation, with cumulus clouds with higher optical depth and more liquid content, preferentially forming over native vegetation in summer and over agricultural land in winter and spring.

In conjunction with the surface and cloud observations, one dimensional boundary layer simulations were performed with the RAMS atmospheric model, to generate atmospheric

profiles of temperature and moisture over the different vegetation types for 3 January 1999, a day where GMS5 imagery shows preferential cloud development over native vegetation. The RAMS simulations produced atmospheric profiles over the native vegetation with higher CAPE, with lower lifting condensation level and lower level of free convection, than the adjacent agricultural land. The higher convective energy and lower levels of condensation and free convection suggested the different land surface characteristics were responsible for the higher cloud formation potential, in agreement with the observed cumulus cloudiness.

Also investigating the impacts of landscape changes on summer weather in south west Western Australia, *Li et al.* (2000) used the Japan Spectral Model to perform regional modelling experiments with current vegetation compared with a range of hypothetically altered landscapes. The experiments were performed at 45 and 15 km grid increments over a 500 x 500 km area for two days in January 1990 with atmospheric conditions conducive to unstable convection. The model boundary conditions for all experiments were taken from global analysis data for the days simulated.

The land surface alterations where performed as a series of sensitivity experiments investigating the impacts of changes in albedo, transpiration efficiency, and surface roughness on weather over the area. The experiments found that increasing albedo decreased precipitation and evaporation, while increasing transpiration efficiency increased precipitation and evaporation. The impact of increasing surface roughness, however, was more complex, with small increases in surface roughness producing small initial increases in precipitation, however larger increases in surface roughness resulted in a slight decrease in precipitation.

2.4.3 Modelling of Near Surface Climate Impacts of Australian Land Cover Change

Narisma and Pitman (2003) investigated the impacts of Australian historical land cover change on near surface climate using the NCAR Mesoscale Model (MM5). The regional climate model was run at a 50 km grid increment to simulate January and July climate from 1987 to 1995. The impacts of land cover change were included in the experiments by prescribing land surface conditions for current day Australian vegetation compared with the land surface conditions that may have existed prior to European settlement.

The land surface parameters representing pre-European arrival and current day vegetation were derived from the vegetation mapping of *AUSLIG* (1990), with the model parameters generated from a subjective allocation of the mapped pre-European and current day floristic codes to the USGS vegetation classes used by the MM5 land surface model. Both land cover experiments had the same model boundary conditions prescribed from the National Centers for Environmental Prediction (NCEP) Global Data Assimilation System (GDAS) analysis data for the months simulated.

The 50 km grid increment of the model experiments was used to include regional land cover changes, as well as changes in meso-scale fluxes in the experiments. The changes in

climate variables between the two experiments were investigated for statistical significance using the spatial field comparison methods of *Wigley and Santer* (1990). These methods use univariate and multivariate statistics to investigate differences in time mean values, differences in grid point means, grid point temporal variance, and comparison of temporal and spatial variance, to assess the statistical significance of land cover change perturbations.

The major historical land cover changes represented in the experiments were from the USGS vegetation classes of evergreen broadleaf forest to grassland following the clearing of native vegetation for the wheat belts of south west Western Australia and south east Australia, and from sparse to shrubland following the invasion of *Acacia nilotica* into the Mitchell grasslands of central Queensland. Historical land cover changes in other areas of Queensland were a mixture of clearing of shrub land and evergreen broadleaf forest for grassland, and the replacement of shrub land with evergreen broadleaf forest.

In south west Australia, the clearing of evergreen broadleaf forest to grassland resulted in an increase in surface albedo of 0.06, a decrease in leaf area index (LAI) of 2.53 and a decrease in surface roughness of 0.23. In general these changes between pre-European and current day vegetation, were consistent with the differences in land surface conditions between current day native vegetation and agricultural land found by *Lyons et al.* (1993), *Xinmei and Lyons* (1995), and *Ray et al.* (2003). Clearing of evergreen broadleaf forest to grassland in south east Australia was represented with the same land surface changes as in south west Australia, with the exception of the decrease in LAI, which was marginally smaller at 2.48. The study noted that the use of grassland to represent crops in both areas, did not capture the strong seasonal cycles associated with winter cropping, followed by summer harvest.

The modelling experiments produced both increases and decreases in net radiation over the cleared areas of south west and south east Australia, but produced a general increase in net radiation in central Queensland. The changes in net radiation were much stronger in summer, with areas with up to 30 Wm^{-2} difference between the experiments. The changes in winter values were in general less than 10 Wm^{-2}. The modelling experiments showed significantly larger changes in latent heat flux, with decreases up to 60 Wm^{-2} in summer over south west and south east Australia, reducing to 10 Wm^{-2} in winter, and increases of around 20 Wm^{-2} for both summer and winter in central Queensland. Statistical analysis showed the changes in latent heat flux were statistically significant over Australia, and for each of the major areas of land cover change.

The modelled changes in latent heat flux and net radiation flux resulted in changes in sensible heat flux and air temperature. Over south west and south east Australia, the reduced latent heat flux was larger than the reduced radiation flux, resulting in a warming of mean air temperature of 1 – 1.5^{O} C in summer, while the increased latent heat flux over central Queensland was larger than the increased radiation flux, resulting in marginal cooling of around 0.2^{O} C. In winter the warming over south west and south east Australia was removed, however,

over central Queensland the cooling increased to around 0.5^{O} C. The changes in air temperature were shown to be statistically significant for Australia and for each of the land cover change areas, for both summer and winter.

The changes in surface fluxes and air temperature produced no consistent changes in precipitation. There were areas with small reductions in summer precipitation, but these were contrary to long term observed regional and continental changes. There also were areas with small reductions in winter precipitation, but these did not reflect the magnitude of the observed changes. The changes in precipitation were not significant in the temporal mean values for Australia or for any of the areas of land cover change.

Analysis of changes in the vertical profiles showed warming of summer air temperatures over south west and south east Australia propagated to the 0.7 sigma level, equating to around 2.6 km in altitude, with net cooling above this level. This higher level warming indicated that land cover change impacts were not isolated to the near surface climate and may have had the potential to influence larger circulation patterns of Australia. Changes in wind fields also were strongest near the surface, however they propagated to altitude with clear impacts on local and regional circulations.

2.4.4 Modelling Climate Impacts Australian Soil Moisture Anomalies

Yang (1995) investigated the impacts of anomalous soil moisture on Australian climate by using the Bureau of Meteorology Research Centre (BMRC) General Circulation Model (GCM) to simulate Australian summer and winter weather conditions for 1984 with various soil moisture conditions. The investigation compared 60 to 90 day weather simulations of a control experiment with Australian soil moisture initialised from global analysis data, against experiments with Australian soil moisture initialised as saturated (WET) and desiccated (DRY).

For January of the summer WET experiment, the study found the saturated soil moisture increased latent heat flux over the entire continent, with the increases up to 200 Wm^{-2} higher than the control experiment. In general the increases in latent heat flux were accompanied by increased precipitation, with the largest increases in precipitation up to 4 mm/day, corresponding with the largest increases in latent heat flux. Large cool surface temperature anomalies also were associated with the increased latent heat flux over the entire continent, with the largest cool anomalies up to -8.5^{O} C. The study also suggested there were areas where cooling may have been enhanced by reduced radiation flux from increased cloud cover.

The study found the summer soil moisture and latent heat flux anomalies converged rapidly with the control experiment, with latent heat flux anomalies for February, a half to a third the January values. The precipitation anomalies decayed more quickly than latent heat flux, with only one localised area of increased precipitation remaining in February. The temperature anomalies also decayed with the latent heat flux anomalies, with cool temperature anomalies greatly reduced or changed to slight warm anomalies in February.

The study found that July of the winter WET experiment also had increased latent heat flux over the entire continent, with values half the magnitude of the January WET experiment. Precipitation increases were restricted to the south of the continent, and northern Queensland, with the largest areas of precipitation increase not corresponding with the areas of largest latent heat flux increase. There also was general surface warming over the south of the continent, and cooling over the north of the continent.

The study found the wet soil moisture and latent heat flux anomalies did not converge with the control experiment for winter as they did for summer. In some areas self reinforcing increases in precipitation and soil moisture developed and by September, there was a large precipitation anomaly over eastern Australia of 4.2 mm/day, and a slightly smaller anomaly of 3.3 mm/day over south west Western Australia. Over the rest of Australia the precipitation anomalies converged back to the control experiment. The increased soil moisture also resulted in a general cooling over the entire Australian continent.

Analysis of atmospheric divergence over the continent for the different experiments suggested the increased soil moisture of the WET experiments, with higher evaporation and lower sensible heat flux, led to decreased continental low level convergence in summer and increased low level divergence in winter. The higher sensible heat fluxes of the DRY experiments had the opposite effect increasing low level convergence in summer and decreasing low level divergence in winter. These mechanisms were identified as being important for moisture transport, as the summer moisture flux from the surrounding oceans to the Australian continent is dependent on low level convergence, while low level atmospheric divergence in winter transports soil moisture evaporated over the continent back out to the oceans. The study suggested these mechanisms were a negative feedback for soil moisture anomalies, limiting their persistence and intensification. This was confirmed by analysis of moisture flux over the Australian continent for both the summer and winter WET experiments that showed there were net divergences of moisture with evaporation exceeding precipitation for all months, with the opposite true for summer and winter DRY experiments.

The study investigated the moisture divergence impacts of the persistence of wet and dry soil moisture anomalies by using a “halving time” measure for surface fluxes, soil moisture content and surface temperature. The “halving time” of summer and winter DRY experiments were found to be less than a month, with the breakdown of the summer anomaly quicker than the winter anomaly. The “halving time” of the summer WET anomaly was found to be a month, while the “halving time” of the winter WET anomaly was found to be two months.

2.4.5 Section Summary

1. Field and satellite monitoring campaigns in south west Western Australia show the region has experienced significant changes in land surface properties as a result of land cover change. Satellite imagery shows major changes in surface albedo, with native vegetation significantly darker than agricultural vegetation that replaces it.
2. The studies also show there were large changes in vegetation density and the seasonal cycles of the vegetation, with the native vegetation having lower seasonal and inter-annual variability compared to winter cereal crops that dominate the introduced vegetation.
3. The seasonal cycles of the introduced vegetation peaked with the late winter, spring growing cycle, where they had higher transpiration rates than the native vegetation. The vegetation cover of the introduced vegetation was lowest over summer, when crops were fallow, with the native vegetation having higher transpiration rates at that time.
4. Regional climate modelling over these areas indicate the differences in land surface properties of native and agricultural vegetation might have significant impacts on atmospheric boundary layer structure and therefore cloud formation and precipitation.
5. Investigation into the near surface climate impacts of Australian land cover change demonstrated that statistically significant changes in surface heating and surface fluxes are simulated in regional climate models when the land surface conditions are changed from pre-European to current day land cover. Precipitation changes in these experiments, however, were shown to be small and not statistically significant for all regions.
6. The modelling experiments suggested that the warming from the changed land surface conditions propagated to altitude, which may have had the potential to influence larger-scale circulation over Australia. As this component of the climate models was prescribed/fixed from historical analysis data for both experiments, the larger scale influence of these changes were not investigated in the study.
7. Australian soil moisture studies showed that soil moisture anomalies result in large differences in air temperature, precipitation and sensible and latent heat flux in climate model simulations.
8. The studies also found that there were regions where feedbacks between increased soil moisture anomalies and increased precipitation resulted in the persistence of the soil moisture anomalies. However, in most cases the soil moisture anomalies converged with the control experiment.

2.5 Synthesis, Conceptual Model And Postulated Relationships

2.5.1 Synthesis

The Australian case studies described in section 2.4 show that while the Australian continent has experienced significant changes in land cover since European settlement, however, the impacts that land cover changes have had on land surface properties and on regional and continental climate, still are not well understood. The limited number of empirical and modelling studies provide a good starting point for understanding how key processes and impact the near surface atmosphere over short time frames, however, there remains a significant gap in the research investigating how land cover changes influence regional and continental climate, as the larger scale circulation dynamics have not been incorporated in the land cover change experiments, nor have the feedbacks on climate through long-term soil moisture changes been included.

From the previous three sections of this chapter the immediate biophysical changes in land surface properties associated with Australian land cover change are shown to be complex with land surface property changes impacting the interaction of the land surface with the lower atmosphere through changes in the surface radiation budget, surface hydrology, and the surface energy balance. The wide range of land cover and climate studies from different regions of the world, suggest that the impacts these changes in Australian land surface fluxes have on the atmospheric boundary layer and larger scale atmospheric processes, also will be complex as these systems are closely coupled with the land surface fluxes, with numerous feedback mechanisms operating at a range of spatial and temporal scales.

Disentangling these interacting systems requires an understanding of how changes in Australian land cover affect Australian land surface properties at the local scale, and how these properties influence land surface and atmospheric processes at the local, meso and macro-scales. The relationships between land cover change, land surface properties, land surface and near earth atmosphere interaction, and larger scale atmospheric processes have been integrated into the conceptual model shown in *figure 2.16*, with the key relationships of the conceptual model formalised in the postulated relationships below.

2.5.2 Postulated Relationships

Based on the theoretical and empirical evidence synthesised in the conceptual model captured in *figure 2.16*, the following relationships are postulated between Australian land cover change and Australian climate:

Postulated Relationship 1: Australian land cover change has modified Australian land surface properties through changing:

a. surface albedo;
b. the split of radiation between the canopy and the underlying soil;
c. unrestrained canopy resistance to transpiration through changes in canopy density and unrestrained stomatal resistance;
d. canopy moisture storage capacity and interception rate for precipitation and dew, through changed canopy density; and
e. surface roughness and displacement heights through changes in canopy density and height.

Postulated Relationship 2: Australian land cover change has modified Australian land surface and lower atmosphere interaction processes through changes in:

a. surface radiation budget resulting from changes in surface albedo and the split of radiation between the canopy and the underlying soil;
b. surface hydrology by altered transpiration due to: changes in canopy density; unrestrained stomatal resistance; and the interception and evaporation of precipitation and dew;
c. surface energy balance with impacts on latent, sensible and ground heat fluxes; and
d. mechanical turbulence in the turbulent surface layer resulting from changes in surface roughness and displacement heights.

Postulated Relationship 3: The changes in Australian land surface and lower atmosphere interaction processes have directly influenced the atmospheric boundary layer and troposphere through changes in:

a. local scale fluxes of moisture and energy affecting the atmospheric boundary layer, with strong impacts on the convective processes within the boundary layer; and
b. meso-scale circulation and moisture transport impacting cloud formation and precipitation.

Postulated Relationship 4: The changes in the atmospheric boundary layer and troposphere indirectly influence climate at a distance beyond the location of the land cover changes through larger scale atmospheric circulation changes as a result of changes in:

a. humidity and temperature of the air masses that cross the Australian continent under the altered atmospheric circulation; and
b. larger scale pressure systems and atmospheric circulation processes such as monsoon flows.

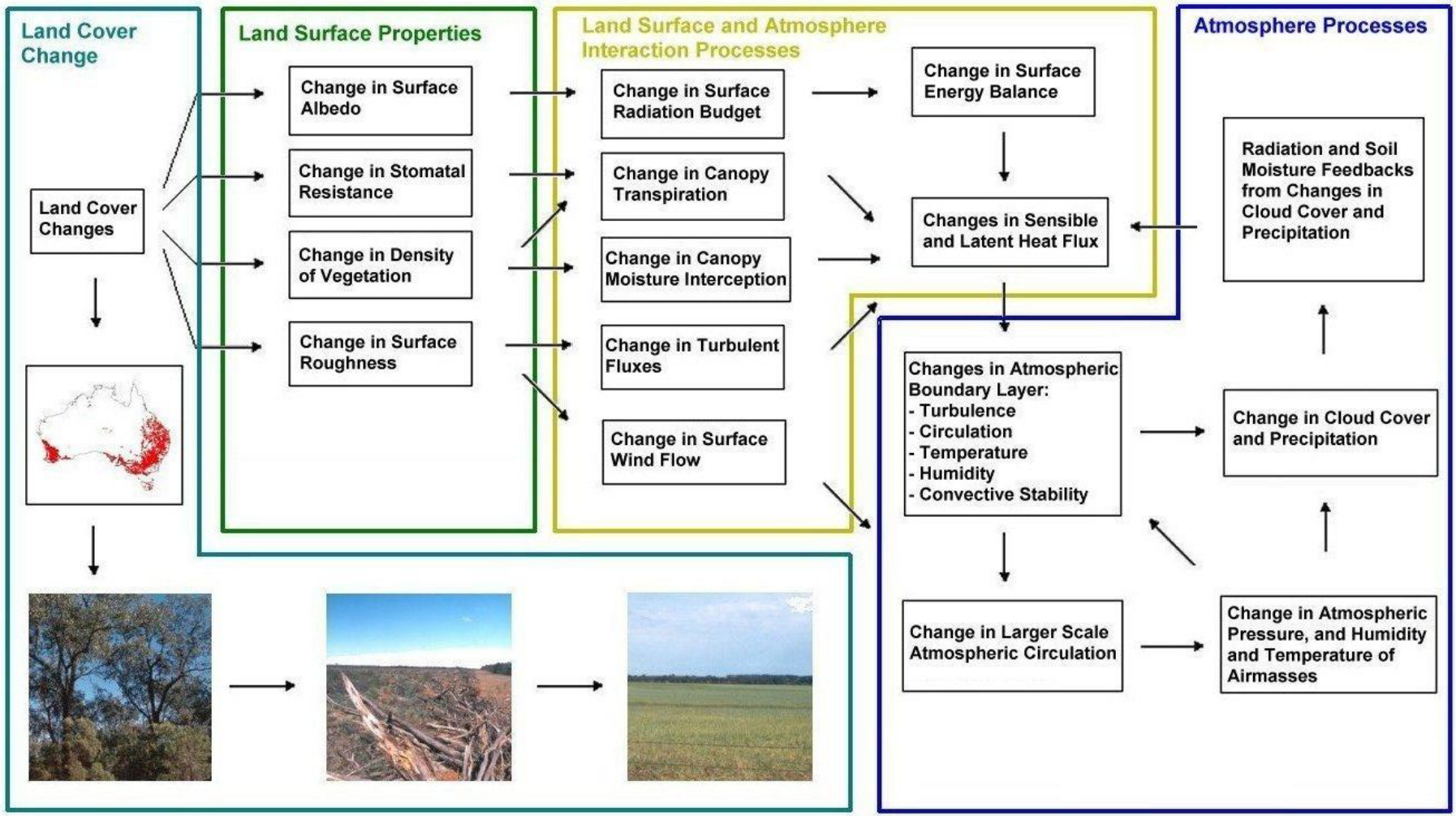

Figure 2.9 Conceptual model of the immediate biophysical changes in land surface properties that may have resulted from Australian land cover change, and the atmospheric responses in climate that may have resulted from these land surface changes

Postulated Relationship 5: The changes in climate resulting from changes in the atmospheric boundary layer and troposphere will have significant feedback mechanisms through changes in:

a. cloud cover impacting surface radiation budgets which have further impacts on sensible and latent heat fluxes to the atmosphere boundary layer; and
b. changes in precipitation impacting on soil moisture which then impacts on transpiration and evaporation which also have further impacts on latent heat fluxes and the surface energy balance.

2.6 Chapter Summary

The aim of this chapter was to review the theory on how land cover influences the interaction between the land surface and the atmosphere, including international and Australian case studies, and from this review develop a conceptual model and postulated relationships between Australian land cover change and climate. Firstly, the review of the influences of vegetation cover on surface properties has established key land surface attributes and lower atmosphere processes that would be affected by changes in Australian land cover. Secondly, the review of international case studies into the effects of land cover change on climate demonstrated that land cover change can potentially result in changes in atmospheric processes at a range of scales with cumulative impacts on regional and continental climate. Thirdly, the review of the research of Australian land cover change impacts on climate provided the context for this study by identifying current status of what is well understood and what is not so well understood. Finally, these reviews have been synthesised into a set of postulated relationships embedded in a conceptual framework of the impact of Australian land cover change on climate.

The chapter aims have been achieved with the theory and conceptual framework model providing a robust theoretical basis for investigating potential climate impacts of Australian land cover change. The framework captures and conceptualises the key points outlined in the chapter, dividing the interacting systems within the climate system into distinct elements that can be investigated individually and as part of the larger system. The framework and conceptual model are used as the basis for assessing the climate modelling experiments investigating of land surface representation and Australian land cover change in Chapter 4 and 5.

CHAPTER 3.
AUSTRALIAN LAND COVER CHANGE REVIEW

3.1 Chapter Aims and Rationale

3.1.1 Aims and Structure

The aims of this chapter are to: (i) review the historical Australian land cover changes described by *AUSLIG* (1990) for descriptions of Australian land cover as it may have existed prior to European arrival and how it exists for the current day; (ii) review other historical Australian land cover change and land use studies, to evaluate the land cover changes described by *AUSLIG* (1990), and to provide a consensus view on Australian land cover change; (iii) review ongoing Australian land cover change to provide perspective on how current land use practice continue to change Australian vegetation; and (iv) investigate satellite observations of the impacts of seasonal and inter-annual climate variability on land cover to assess the natural variability of Australian land cover independently from human induced land cover changes. The land cover changes detailed in these reviews form the basis for the climate impacts of Australian land cover change modelling experiments performed in later chapters of this thesis.

The chapter is divided into four main sections. Section 3.2 reviews the Australian land cover changes described by *AUSLIG* (1990). The review provides a descriptive assessment of the structure and floristic composition of Australian vegetation as it may have existed prior to European arrival and how human land use has altered the natural vegetation to produce the current vegetation of Australia. Section 3.3 reviews other historical Australian land cover change and land use studies. These studies form the basis of the evaluation of the AUSLIG study and help build a consensus view of Australian land cover change and land use since European arrival. Section 3.4 reviews projects assessing ongoing Australian land cover change from satellite observation as well as projects assessing the dynamic nature of vegetation in response to seasonal and inter-annual changes in precipitation and temperature.

3.1.2 Rationale

In the absence of human disturbance, *Graetz et al.* (1992), *AUSLIG* (1990) and *Gurevitch et al.* (2002) describe how the distributions of Australian vegetation communities were primarily determined by climate through temperature and moisture availability, with soils and environmental disturbances from fire and weather events playing strong secondary influences on the function, growth and survival of plants within vegetation communities. *Graetz et al.* (1992) and *AUSLIG* (1990) also suggest that prior to the arrival of Europeans, Aboriginal Australians had substantial influence on Australian vegetation in many areas through the use of

fire as a landscape management tool, although the exact extent of burning and the impacts that it had on Australian vegetation are still of debate.

To investigate how historical Australian land cover changes may have impacted climate it is essential that the land surface properties of the Australian continent can be described accurately and consistently for pre-European conditions and for current day. Current day distributions of Australian vegetation and land cover have been compiled at a range of spatial scales, with national and statewide maps produced from fine-scale satellite imagery and aerial photography, combined with field and ancillary data. Determining the distribution of vegetation prior to European arrival, however, is more difficult in many areas of Australia, as the natural vegetation was cleared before adequate historical records were kept on the original state of the vegetation.

The AUSLIG vegetation maps provide a consistent basis for assessing land cover change and for describing the land surface properties, as they may have existed prior to European settlement, and how they exist for current day. The vegetation maps were produced consistently across the continent, with the same scale and vegetation classifications for both natural and current vegetation. This consistent approach ensures the differences between the maps represent the land cover changes that the principal author Dr John Carnahan believed had occurred since European arrival. This means unlike many other assessments the land cover changes of the vegetation maps are not affected by differences in mapping scale or methodology.

Satellite imagery has shown that Australian land cover change was still highly active in the early 1990s, with clearing rates in excess of 250,000 hectares per year (*Barson et al.*, 2000). The majority of the clearing was shown to be concentrated in the state of Queensland, accounting for 73.5% of the national total. More recent satellite monitoring of land cover change assessments for Queensland show there was a general increase in the clearing rates in the state through the 1990s, starting at the 1991 – 1995 rate of 288,800 hectares per year, increasing up to the 1999 – 2000 peak rate of 757,800 hectares per year at the end of the decade (*DNRM*, 2003). Given the ongoing nature of land cover change in Australia, it is important to assess whether current land use practices may be further contributing to the climate impacts of historical land cover change.

The dynamic nature of vegetation in response to seasonal and inter-annual changes in precipitation and temperature also has been captured by satellite imagery, with Australian vegetation cover constantly monitored by daily satellite observation since 1981 by the NOAA/NASA Pathfinder Land project (*Goddard*, 1994). If climate impacts are found to result from human induced Australian land cover changes, it is important to describe the natural variability in Australian vegetation cover to assess whether these changes also have impacts on climate.

3.2 AUSLIG Historical Australian Land Cover Change

3.2.1 Australian Vegetation Mapping by AUSLIG

Vegetation mapping was undertaken by *AUSLIG* (1990) to produce maps for Australian vegetation as it may have been in a prior to European colonisation (natural) and as it is for the current day (mid 1980s). The two maps were developed using the same continental spatial scales of 1:5,000,000, and the same structural and floristic classifications, based on the structural types of *Specht* (1970) and the notation used by *Beard and Webb* (1974). Broad changes in vegetation between the pre-European and current day were assessed by comparative analysis of the two maps. The natural or pre-European vegetation maps for structural form and dominant floristic type are shown in *figure 3.1 a* and *b*, with current day vegetation maps shown in *figure 3.2 a* and *b*.

The vegetation mapping provides a descriptive assessment of the vegetation structure and floristic composition of native vegetation, as it may have existed prior to European arrival and as it exists for the current day. The Pre-European vegetation mapping was largely reconstructed from remnant natural vegetation and historical sources, with vegetation boundaries drawn from the soils, climate and other landscape features. In areas where there were limited historical records and little remnant vegetation, the mapping was largely speculative. Present day vegetation was mapped primarily from Landsat Multi Spectral Scanner (MSS) imagery to identify broadly homogenous vegetation types spatially, with information about the structure and floristic composition obtained from a wide range of secondary sources. The secondary information came mainly from larger scale vegetation mapping and reports, with a limited amount of information derived from field verification, soil, topography and climate.

A composite Landsat MSS image similar to that used in the current vegetation mapping is shown in *figure 3.3 a* in False Colour Composite. The image highlights the distinct spectral characteristics that identify vegetation boundaries between different relatively homogeneous vegetation types and between remnant and cleared vegetation. The major Australian topographic features and agricultural areas are shown in digital elevation map in *figure 3.3 b*, with median annual precipitation shown in *figure 3.4 a* and Australian soils in broad dominant soil types shown in *figure 3.4 b*.

3.2.2 Australian Native Vegetation

The natural vegetation maps of *AUSLIG* (1990) (*figure 3.1*) show the floristic composition and structural form of Australian native vegetation is largely determined by water availability, with the amount of plant cover generally decreasing inline with precipitation from the wetter coastal areas to the arid interior. The seasonal distribution of precipitation also plays an important role, with the northern summer maximum and the southern winter maximum giving rise to separate monsoonal and mediterranean vegetation north and south.

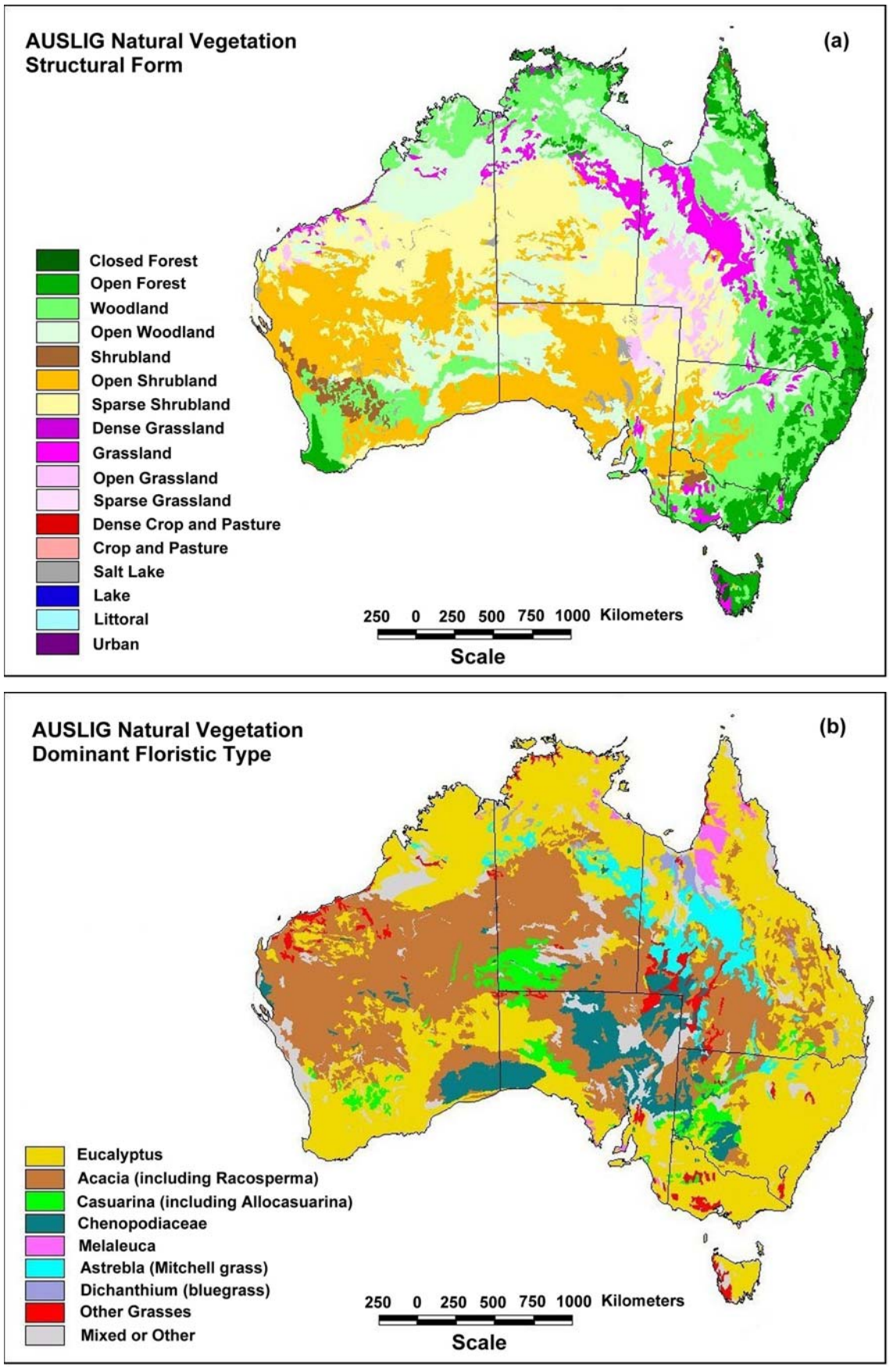

Figure 3.1 Australian Natural (pre-European) vegetation from AUSLIG (1990) showing: (a) Structural Form as a generalised subset of the original classification; and (b) Dominant Floristic Type, with only major floristic types listed

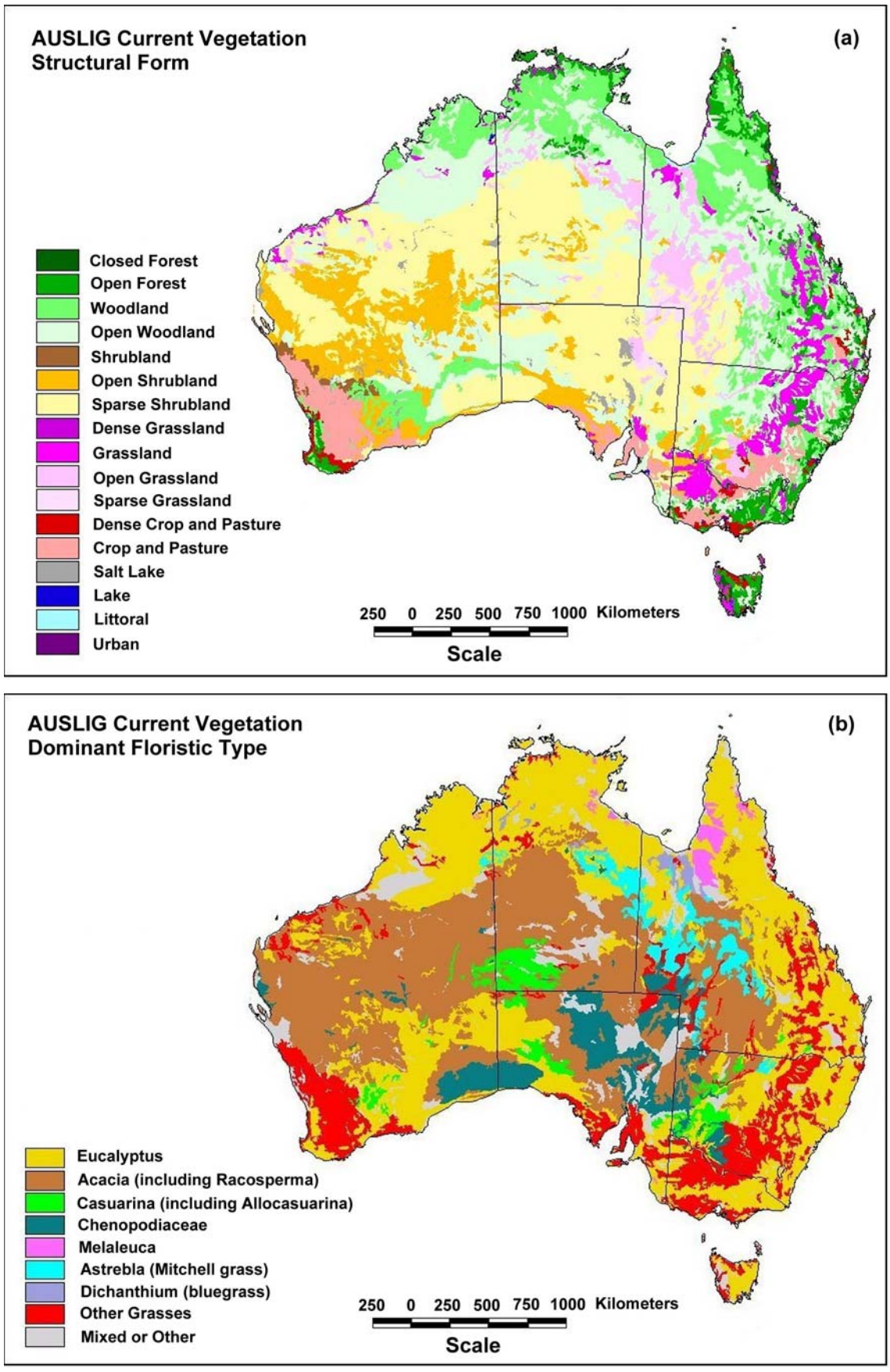

Figure 3.2 Current (mid 1980s) Australian vegetation from AUSLIG (1990) showing: (a) Structural Form as a generalised subset of the original classification; and (b) Dominant Floristic Type, with only major floristic types listed

Australian trees and shrubs are predominantly evergreen with hard and tough (sclerophyll) leaves, with ordinary (orthophyll) leaves prominent only in moist forests. The native vegetation is dominated by a few widespread genera, with *Eucalyptus* and *Acacia* trees and shrubs forming the dominant vegetation for over 75% of the continent. In other regions, *Casuarina* trees and shrubs, low shrubs of the *Chenopodiaceae* family, and tussock grasses of the *Astrebla* and *Dichanthium* genera also are spatially important.

Australian Forests

As shown in the natural and current vegetation structural form maps (*figure 3.1 a* and *figure 3.2 a*), the distribution of Australian forests are in general limited to the relatively high precipitation areas of the coastal margins of the continent. Open forests form the bulk of Australian forests, with closed forests or rainforests, restricted to a few areas of higher precipitation (greater than 1200 mm annually) along the eastern coast of mainland Australia and the west coast of Tasmania. The major exception to the dependence on higher precipitation occurs in central Queensland, where *Acacia* open forests extend well inland into areas of low precipitation (as low as 400 mm annually).

Australian rainforests are floristically diverse with complex environmental relationships with climate and soils. From these relationships, Australian rainforests are separated into four broad climatic groupings. Tropical rainforest occur in north Queensland as 'mesophyll vine forest' (*figure 3.5 d*); Sub-tropical rainforest occur from central Queensland to northern New South Wales as 'notophyll vine forest' (*figure 3.5 b*); Warm temperate rainforest, occur from central New South Wales to eastern Victoria as 'microphyll fern forest'; and cool temperate rainforest occur in other areas of Victoria and Tasmania as 'nanophyll moss forest'. Small patches of monsoon rainforest (*figure 3.5 c*), also occur in the Top End of the Northern Territory and in the Kimberley area of Western Australia in areas that have year round water availability and are protected from fire.

Eucalyptus is the most widespread floristic type of open forests, however, as shown in the natural vegetation floristic map (*figure 3.2 b*), *Acacia* and *Casuarina* were regionally important prior to clearing. In areas of high, reliable precipitation (greater than 1000 mm annually) tall *Eucalyptus* forests, such as the Mountain Ash (*Eucalyptus regnans)* forests of south eastern Australia and Tasmania (*figure 3.5 a*), reach heights nearing 100 meters, making them the tallest flowering plants in the world. In areas with lower or less reliable precipitation, *Eucalyptus* open forests have lower canopies reaching 10 – 30 meters in height. In areas with low precipitation such as inland Queensland, *Acacia* open forests (*figure 3.6 b*), have low canopies below 10 meters in height.

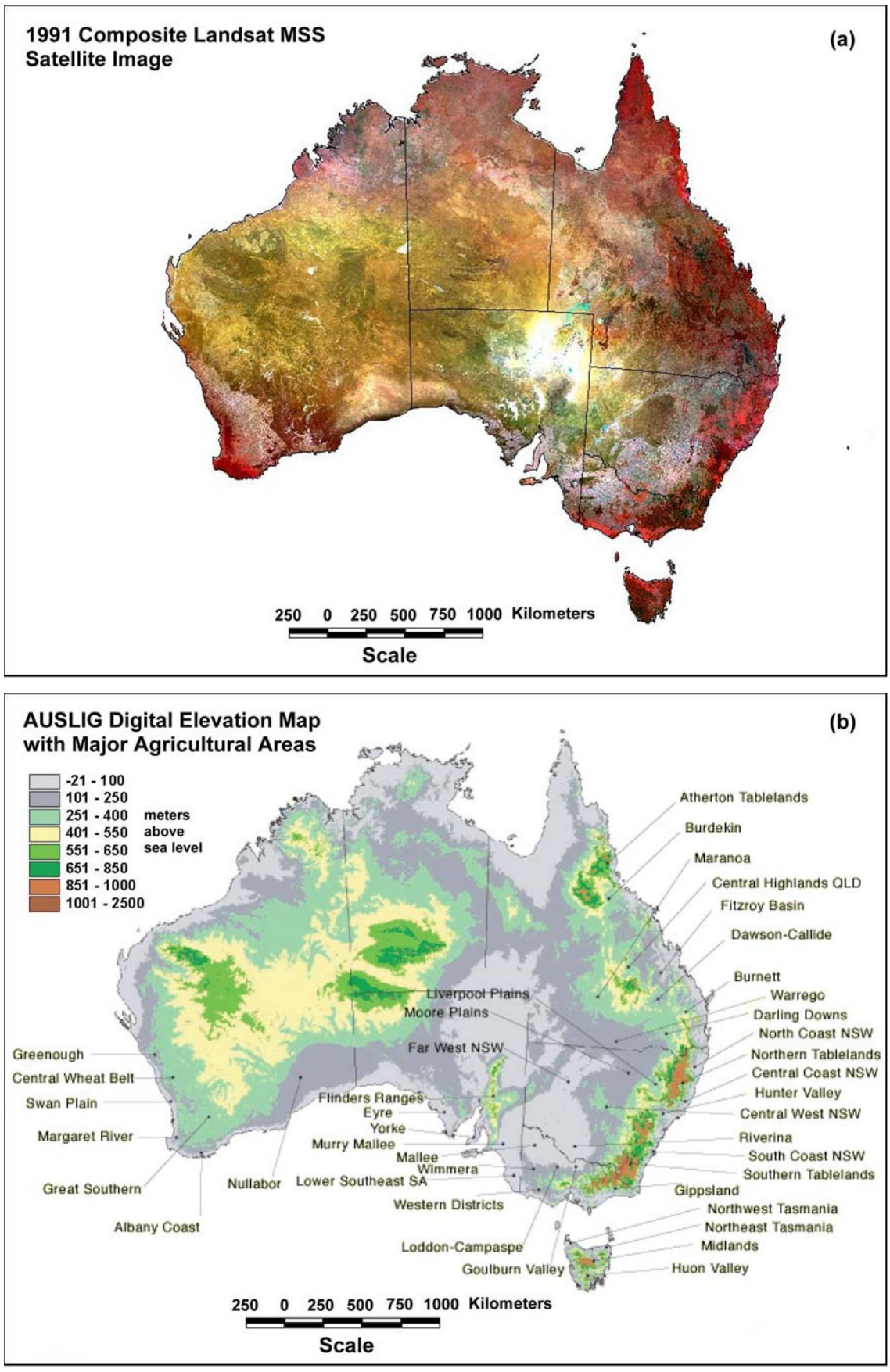

Figure 3.3 (a) 1990-91 Landsat Multi Spectral Scanner (MSS) composite image from Graetz et al. (1995a) shown in standard False Colour Composite; and (b) AUSLIG Topographic map of Australia from NLWRA (2001a)

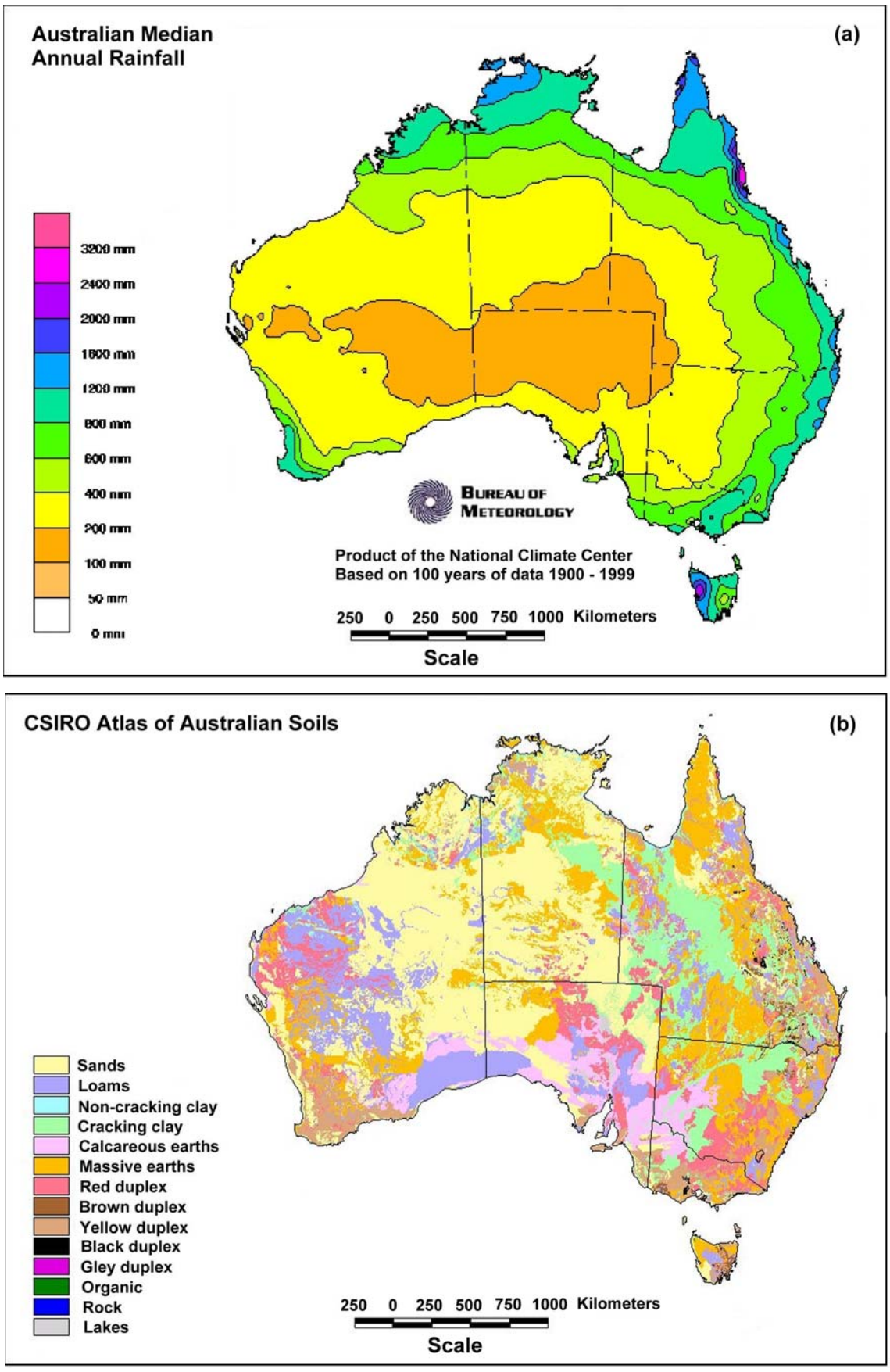

Figure 3.4 (a) Australian Median Annual Rainfall from Australian Bureau of Meteorology web site. (Median is based on 100 years of data for 1900 – 1999); and (b) CSIRO Atlas of Australian Soils from the Australian Bureau of Rural Sciences web site

The understoreys of open forests also are strongly influenced by precipitation, with soils and fire playing major roles in many areas. In areas with higher precipitation and fertile soils the open forests have understoreys of low trees and shrubs including palms, tree-ferns, and rainforest species, which may reach heights exceeding 10 meters. On less fertile soils and with lower precipitation (down to 600 mm annually) the understorey often is comprised of a dense stratum of sclerophyllous low shrubs, which grow to less than 2 meters in height. In areas of heavy soils or regular fire, grassy understoreys replace shrubs and trees, and in areas of low precipitation, *Acacia* and *Callitris* open forests have bare or very sparse understoreys.

Australian Woodlands

The distribution of woodlands is primarily driven by precipitation, with soils playing a larger role in the better watered areas of northern and eastern Australia. As shown in the current and natural vegetation structural form maps (*figure 3.1 a* and *figure 3.2 a*), woodlands form a transitional zone between the forested margins of the continent and the arid interior. *Eucalyptus* forms the most widespread tree component, however, in more arid areas of inland Queensland, New South Wales, and Victoria *Acacia, Casuarina* and *Calitris* form the tree components of low woodlands in many areas.

There are a wide range of understorey types associated with precipitation and soils. Woodlands with low trees and tall shrubs (*figure 3.6 c*) are widespread in the coastal regions of northern Australia and in inland eastern Australia; In areas with heavier, more fertile soils, grassy understoreys commonly replace the trees and shrubs (*figure 3.6 d*); And woodlands with low shrubs, (*figure 3.6 a*), mainly occur in areas of low precipitation and poor soils in south west and south east Australia.

Australian Shrublands

Shrublands are the widest structural form of vegetation, covering large areas of inland and western Australia, as shown in the natural and current vegetation maps (*figure 3.1 and 3.2*), *Eucalyptus* and *Acacia* most commonly dominate the tall shrublands, however *Casuarina* was regionally significant prior to clearing. *Eucalyptus* dominated shrublands are widely referred to as ‘mallee’, (*figure 3.7 c*) and *Acacia* dominated shrublands are widely referred to as ‘mulga’ (*figure 3.7 a*).

The understoreys of tall shrublands range from dense low shrubs in better watered areas, to hummock grasses in areas of lower precipitation. In arid areas low sparse shrublands are predominantly composed of species of the *Chenopodiaceae* family such as salt bush, blue bush and samphires, with understoreys ranging from grasses to bare soils. In coastal and alpine areas low shrublands form as dense floristically diverse heaths (*figure 3.7 d*).

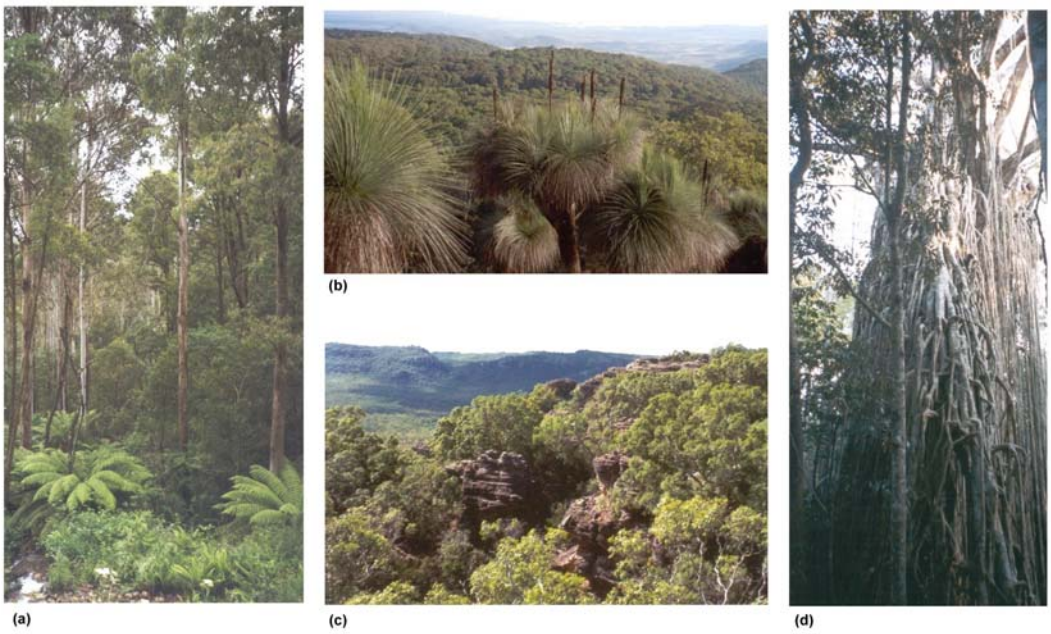

Figure 3.5 Australian forests: (a) Mountain Ash (Eucalyptus regnans) *forest with Tree-ferns* (Dicksonia antartica)*, Alpine National Park, Victoria; (b) Sub-tropical rainforest with Grass Trees* (Xanthorrhoea glauca) *in the foreground, Bunya Mountains National Park, Queensland; (c) Monsoon Rainforest, Kakadu National Park, Northern Territory; and (d) Tropical Rainforest featuring a Strangler fig* (Ficus destruens)*, Atherton tablelands, Queensland. (All photos except those credited otherwise are from the author)*

Figure 3.6 Australian open forests and woodlands: (a) Salmon Gum (Eucalyptus salmonopholia) *woodland with understorey of low shrubs, Western Australia, photo courtesy of Robert Hassett; (b) Lancewood* (Acacia shirleyi) *open forest, near St George, Queensland; (c) Poplar box* (Eucalyptus populnea) *woodland, near Roma, Queensland; and (d) White Gum* (Eucalyptus alba) *woodland with grass understorey, Kakadu National Park, Northern Territory*

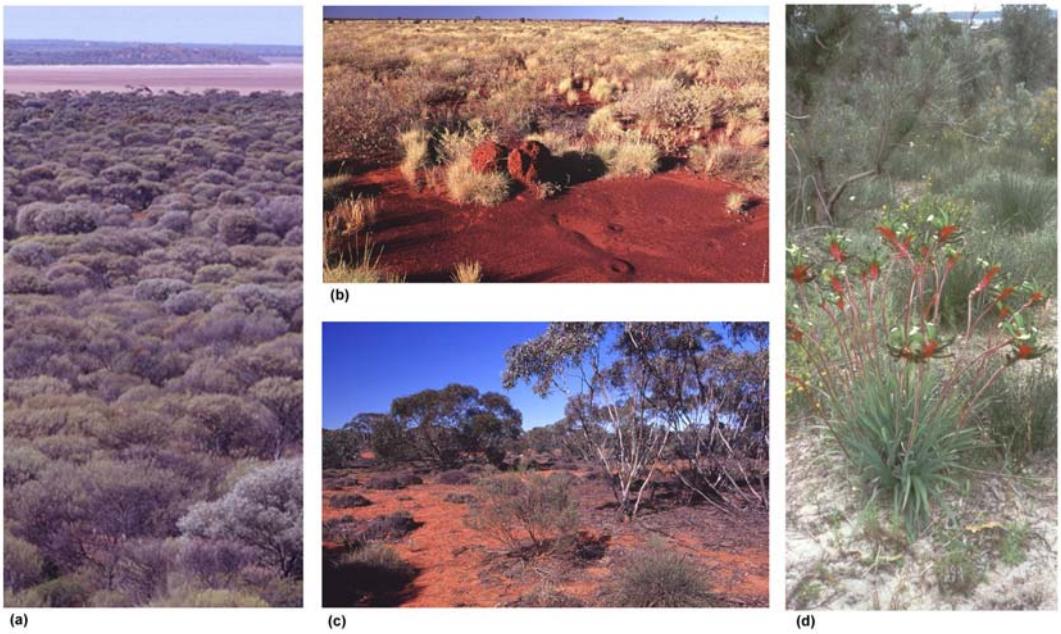

Figure 3.7 Australian shrublands, grasslands and heathlands: (a) Mulga tall shrubland of Acacia aneura*, central Australia, photo courtesy of Robert Hassett; (b) Hummock grassland of* Trodia spp*., central Australia, photo courtesy of Robert Hassett; (c) Mallee tall shrublands of* Eucalyptus oleosa*, near Kalgoorlie, Western Australia, photo courtesy of Robert Hassett; and (d) Banksia Heathland, near Perth, Western Australia, photo courtesy of Alison Lawrence*

Australian Grasslands

Large areas of native grasslands occur in central and western Queensland, and the Northern Territory, with smaller areas of grasslands in other areas of the continent. As shown in the natural vegetation maps (*figure 3*.2), the most extensive of these native grasslands are the *Astrebla* (Mitchell grass) tussock grasslands, primarily associated with the cracking clays of northern Australia.

In higher precipitation areas of northern Australia *Dichanthium* (blue grass) and other species of tussock grass replace *Astrebla* as the dominant grass. In southern regions, native tussock grasslands were composed of *Themeda*, *Danthonia*, *Poa*, and *Stipa* prior to replacement with sown pastures. Hummock grasslands of *Trodia* (*figure 3.7 b*) are restricted to small areas of Western Australia, the Northern Territory, and South Australia, however, hummock grasslands form the understorey vegetation for large areas of inland Australia, covering 25% of the continent.

Sparse open herbfields occur in arid areas (less than 200 mm precipitation annually) of north east South Australia and south west Queensland, dominated by herbaceous members of the *Chenopodiaceae* family. Vegetation cover and composition fluctuate greatly with precipitation. In dry years virtually all vegetation disappears, while after rain it thickens rapidly with a wide range of genera.

3.2.3 Australian Vegetation Changes

Analysis by *AUSLIG* (1990) into the differences between the natural and current vegetation maps, found that one third of the continent had undergone structural changes in vegetation as a result of land use since European colonisation. The area used for agriculture and forestry was identified as covering more than 5,000,000 km^2, or 70% of the Australian continent. The most intensive changes in vegetation were identified where forest and woodland were cleared to create pasture and cropping land. These changes were concentrated in the south west and south east of the continent, following the Australian "wheat belts" and north in the east into the former "brigalow lands" of Queensland.

The major vegetation changes between the two vegetation maps are shown in the Australian historical changes in structural form map (*figure 3.8 a*) and the Australian historical changes in floristic type map (*figure 3.8 b*). The process of clearing native vegetation to create pasture and cropping land is shown in the photos of *figure 3.9*. The area of vegetation mapped for both the natural and current maps as well as the changes between the maps are shown for each structural form in *table 3.1*.

Table 3.1 Changes in Australian vegetation by structural form between the Natural (pre-European) and Current (mid 1980s) vegetation maps of AUSLIG (1990) in thousands of km^2

Vegetation	Natural (1000 km^2)	Current (1000 km^2)	Lost (1000 km^2)	Gained (1000 km^2)	Net Change (1000 km^2)
Closed Forest	46	36	10	0	-10
Open Forest	642	358	299	15	-284
Woodland	1574	1066	602	94	-508
Open Woodland	1650	1985	55	390	335
Shrubland	103	54	67	18	-49
Open Shrubland	1510	798	730	18	-712
Sparse Shrubland	1464	2024	33	593	560
Dense Grassland	14	25	10	21	11
Grassland	359	326	185	152	-33
Open Grassland	160	393	0	233	233
Sparse Grassland	73	74	0	1	1
Dense Crops and Pastures	0	73	0	73	73
Crops and Pastures	0	374	0	374	374
Urban	0	7	0	7	7
Other	87	88	0	1	1

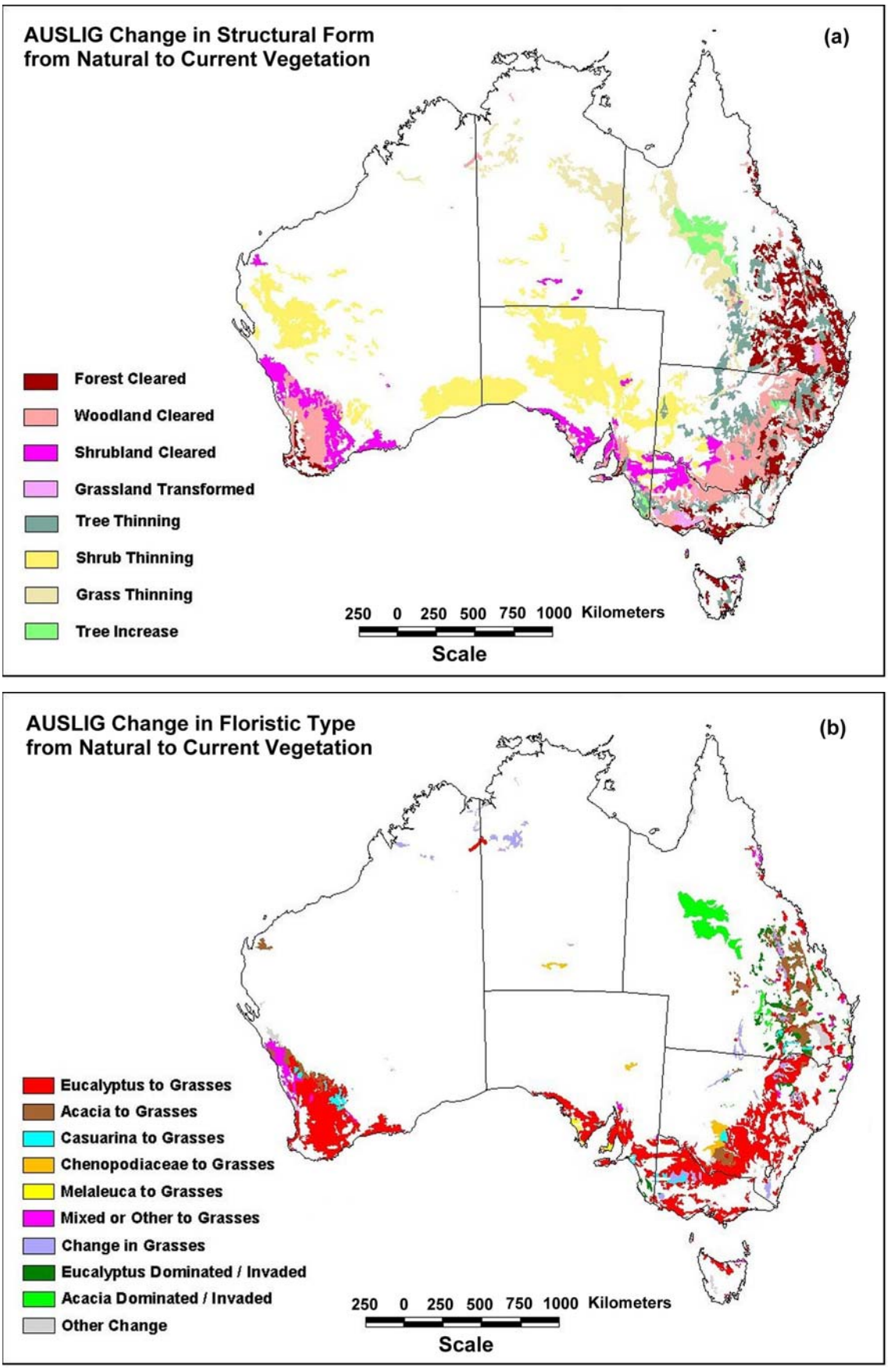

Figure 3.8 Major changes in Australian vegetation between the natural (pre-European) and current (mid 1980s) vegetation maps of AUSLIG (1990) for (a) structural form and (b) dominant floristic type

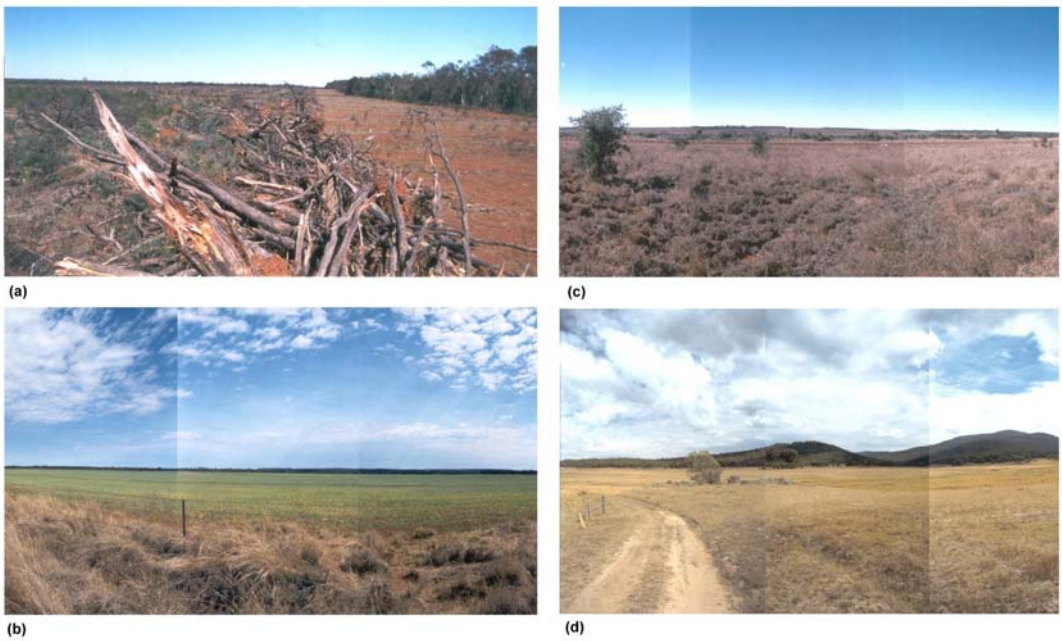

Figure 3.9 Agricultural transformation of Australian vegetation: (a) Recently cleared Eucalypt open forest, near Surat, Queensland; (b) Wheat cropping, Darling Downs, Queensland; (c) Buffel grass (Cenchrus ciliaris) *sown pasture, near Surat, Queensland; and (d) Sown pastures with uncleared ranges in the background, near Canberra, Australian Capital Territory*

The analysis identified that the major land uses that had driven land cover changes were: cropping and intensive animal production, covering just under 10% of the Australian continent; commercial forestry, covering around 2% of the continent; and extensive grazing, covering around 60% of the continent. Urban development also was identified as causing major changes in vegetation but with a much smaller extent than agricultural land use, with impacts covering around 0.1% of the continent.

Much of the remaining natural vegetation was shown to be in areas unsuitable for intensive agriculture. The analysis showed that remaining forests were usually found on rugged terrain such as the ranges of eastern Australia, which were still widely used for timber production. In the remaining areas the natural vegetation had been changed by grazing pressures due to either pastoral use, or in less fertile areas, from introduced feral grazers such as rabbits, horses, donkeys, camels and goats. The analysis also suggested that in areas identified as unchanged, there were possible changes in structure and floristic composition that were too subtle to be identified by the vegetation mapping classification or too small to be represented at the spatial scale.

Changes to Australian Forests

The comparison of pre-European and present day maps identified that the extent of Australian forests had declined by 40% from 688,000 km^2 to 395,000 km^2, with an increasing area of the existing forests composed of exotic and native plantations. The analysis identified

that in general, where forests occurred in agriculturally arable lands, they were widely cleared for this use. Along the Queensland coast, rainforest and eucalypt forests were cleared mainly for the cultivation of sugar cane. In the south west and the east of Australia, forests were mainly cleared for improved pastures, and in central Queensland, forests were widely cleared for exotic pastures and seasonal cropping. The areas of forest clearing are shown explicitly in the Australian historical change in structural form map (*figure 3.8 a*).

Timber extraction and forest management also have changed the structure and floristic composition of much of the remaining forests. Changes in wildfire frequency and intensity, prescribed burning, and grazing by cattle also have altered the understorey of many forest areas by replacing shrubs and low trees with grassy cover. Mining and recreational activity also were shown to have had localised impacts on forest cover and composition in some areas.

Changes to Australian Woodlands

The comparative analysis of the two vegetation maps showed the largest area of historical change has occurred in woodlands, with 587,000 km^2 identified as being converted from natural woodland to sown pastures and crops, tussock grasslands, and open woodlands. The area of woodland clearing represented 37% of their natural extent, with much of the clearing performed to create the wheat belts of inland south west and south east Australia.

In many areas, the transformation from woodland to agricultural land has almost eliminated all native vegetation, with remnant woodlands restricted to relictual patches and narrow roadside verges, surrounded by pastures and crops. Large areas of the woodlands had dense low tree and shrub understoreys, with biomass and transpiration rates equal to those of forested areas. The areas of woodland clearing and tree thinning are shown in the Australian historical change in structural form map (*figure 3.8 a*).

The area of open woodland has increased by 390,000 km^2 primarily as a result of thinning and partial clearing of forests and woodlands to increase livestock carrying capacity. In this process only the largest trees were left for shade and shelter for stock, with continuous grazing and additional stress ensuring that remnant trees were not replaced by regeneration. There also has been an increase of 50,000 km^2 in low open woodlands in north central Queensland with the invasion of prickly acacia (*Acacia nilotica*) into the Mitchell Grass Downs. The invasion is shown as tree increases of *Acacia* in the Australian historical changes in structural form and floristic type maps (*figure 3.8 a* and *b*).

Changes to Australian Shrublands

The study found that the total area of tall shrublands had fallen by 35% or 460,000 km^2 since European settlement. Of this change, roughly 160,000 km^2 was identified as being cleared for cropping and pastures in the *Eucalyptus* dominated mallee lands of south west and south east Australia. Much of the remaining change in tall shrubland was identified as thinning from sheep

grazing in the *Acacia* dominated mulga lands of inland Australia. The areas of shrubland clearing and shrub thinning are shown in the Australian historical change in structural form map (*figure 3.8 a*).

Grazing in mulga lands also resulted in selective elimination of palatable species and secondary succession by annual grasses such as species of *Astrida* and *Enneapogon* that leave the soil largely bare during dry times. The mulga foliage also was used as an important source of drought relief fodder and was often felled for that purpose during dry times. The study suggested it was difficult to assess the total effects of grazing on the mulga lands as they naturally undergo a cyclic pattern of decline and regeneration in response to prolonged drought, making it difficult to determine the combined impacts of drought, grazing and felling for fodder.

Areas of low chenopod shrublands were found to have had reduced cover density from continual grazing by sheep, however, these areas were shown to recover even from intense grazing pressures. The alpine shrublands of south eastern Australia also were thinned by summer grazing and autumn burning, however this practice was phased out in the 1960's. Other areas of low shrubland which have had limited grazing by sheep, such as the Nullarbor Plain also had signs of thinning, the cause of which was speculated as being the combined effects of rabbits, fire and drought.

Changes to Australian Grasslands

The study found that sown pastures, crops, and tussock grasslands dominate the new landscapes created for agricultural production. Sown pastures and crops covered 474,000 km^2, and sown pastures formed the understorey of another 50,000 km^2 of open woodland. In many areas a variety of crops were alternated with annual pastures, but in the wetter coastal valleys the sown pastures were mostly perennial. Tussock grasslands were also increased by 200,000 km^2 to cover 674,000 km^2, with a general decline in the density and floristic composition of pre-European grasslands as a result of continuous grazing by cattle and sheep.

In southern Australia, sown pastures were composed of introduced legumes such as *Trifolium subterraneum* (subterranean clover) and grasses such as *Stipa falcata* and several species of *Danthonia.* In many areas these replaced the taller perennial native grasses such *Themeda australis* and *Stipa aristiglumis*. In northern Australia, sown pastures were composed of legumes such as *Macroptilium atropurpureum* (siratro) and several species of *Stylosanthes*, and with grasses such as *Cenchrus ciliaris* (buffel grass), *Panicum maximum* (Guinea grass), and *Chloris gayana* (Rhodes grass). The study found that long term changes in the density of grasslands were hard to evaluate in inland Australia as the foliage cover was subject to enormous natural fluctuations in response to weather events such as sporadic rains and prolonged droughts.

3.2.4 Section Summary

1. Australian native vegetation was largely determined by water availability, with plant cover decreasing with precipitation from coastal areas to the arid interior.
2. *Eucalyptus* and *Acacia* trees and shrubs formed the dominant vegetation for over 75% of the continent prior to clearing.
3. Australian forests are in general restricted to higher precipitation margins of the continent, with open forests the most common form of forest and closed forest restricted to areas of higher precipitation.
4. Woodlands form a transition between the wetter forested margins of the continent and the arid interior.
5. Shrublands are the most widespread structural form covering large areas of inland Australia.
6. Tussock grasslands naturally occurred in large areas of northern Australia on cracking clays. Hummock grasslands were restricted to small areas, however they formed the understorey for large areas of inland Australia
7. One third of the continent has undergone structural change in vegetation as a result of land use since European colonisation.
8. 5,000,000 km^2 or about 70% of the Australian continent is used for agriculture or forestry, with 60% used for extensive grazing, 10% used for cropping and intensive animal production, and 2% used for commercial forestry.
9. The most intensive and widespread changes in vegetation occurred in the "Australian wheat belts" and the former Brigalow lands of Queensland, where forest and woodland have been cleared to create pasture and cropping land.
10. Forests have reduced in extent by 40%, woodlands have reduced by 37%, open woodlands have increased by 23% primarily for improved grazing, and tall shrublands have reduced by 35%.
11. Sown pastures, crops and tussock grasslands dominate the new landscapes created for agricultural production.
12. Long term changes in the density of grasslands and shrublands are difficult to assess as they are subject to large natural climate induced variability.

3.3 Evaluation Against Other Historical Australian Land Cover Change Studies

To evaluate and support the land cover changes described in the AUSLIG study, the findings of four other land cover change assessments and an Australian land use assessment were reviewed and compared to the AUSLIG study. While each of the other studies had different objectives with a range of methods and data used, the findings of the studies show a high degree of consensus with the general changes identified by the AUSLIG study. *Figure 3.10* shows the areas identified as cleared or with trees thinned for each of these studies against those

areas identified as cleared or with trees thinned in the AUSLIG study. *Figure 3.11* shows current day agricultural land use over the Australian continent.

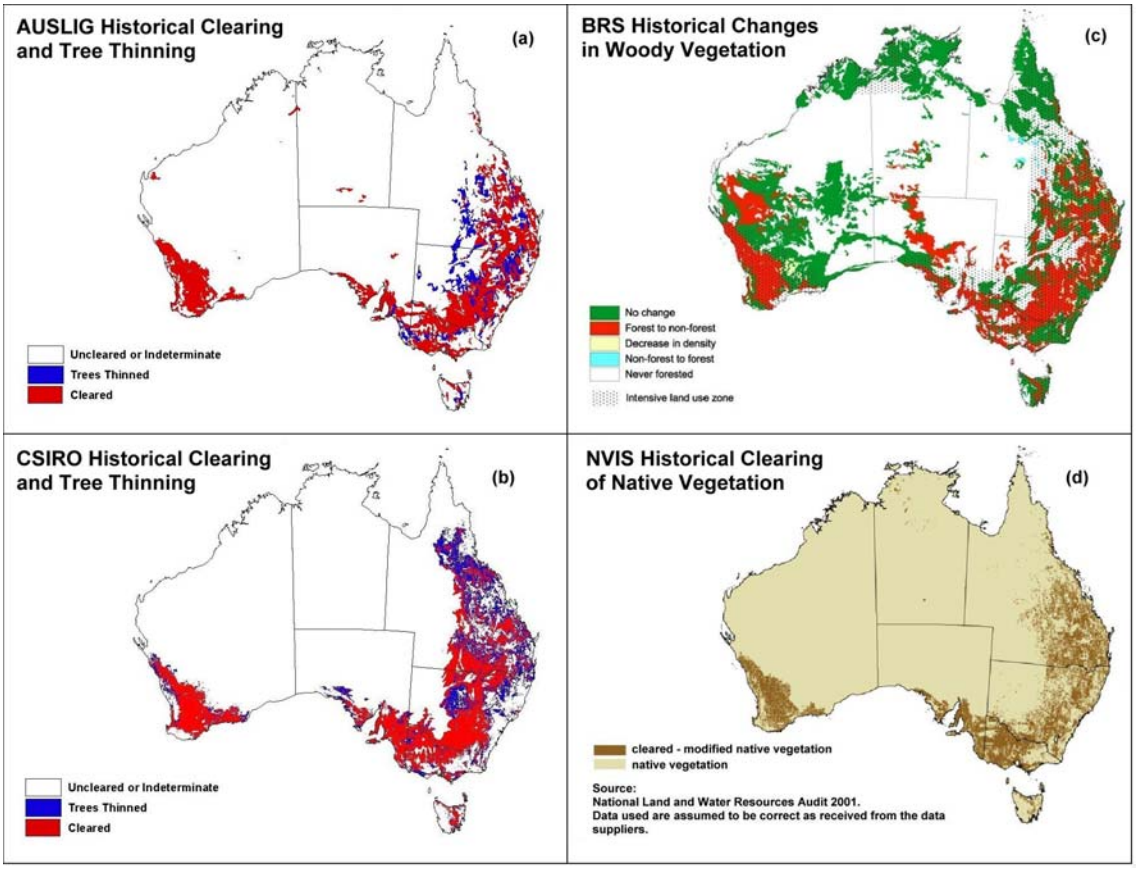

Figure 3.10 Australian historical land cover change maps: (a) Vegetation clearing and tree thinning between the natural (pre-European) and current (mid 1980s) vegetation maps of AUSLIG (1990); (b) CSIRO Wildlife and Ecology assessment of disturbance by clearing in the Australian Intensive Landuse Zone (ILZ) since European settlement from Graetz et al. (1995a); (c) Bureau of Rural Sciences (BRS) assessment of changes in woody vegetation since European settlement from Barson et al. (2000); and (d) National Vegetation Information System (NVIS) assessment of extent of native vegetation clearing from NLWRA (2001b)

3.3.1 CSIRO Australian Land Cover Disturbance Assessment

Graetz et al. (1995b) performed a national assessment of the changes in Australian land cover since European settlement using Landsat MSS imagery from the early 1990s (*figure 3.3 a*), contrasted with the natural (pre-European) vegetation map of *AUSLIG*, (1990) (*figure 3.1*). The study found the most significant land use impacts were from the clearing of native vegetation and the replacement with crops and pastures. Using native vegetation clearing as a basis, the study divided the continent into two zones of different land use intensities.

The Intensive Land use Zone (ILZ) boundary was delineated by eye from the Landsat MSS imagery, using a 100 km buffer around areas identified as cleared, with the boundary then aligned to the national 1:250,000 map grid. The area of clearing that defined the ILZ was found to extend across the southern areas of the continent, including Tasmania, and northwards

through central Queensland. In general, southern areas of clearing were associated with cereal cropping and improved pastures, where as in northern New South Wales and in central Queensland clearing was mostly for the establishment of pastures.

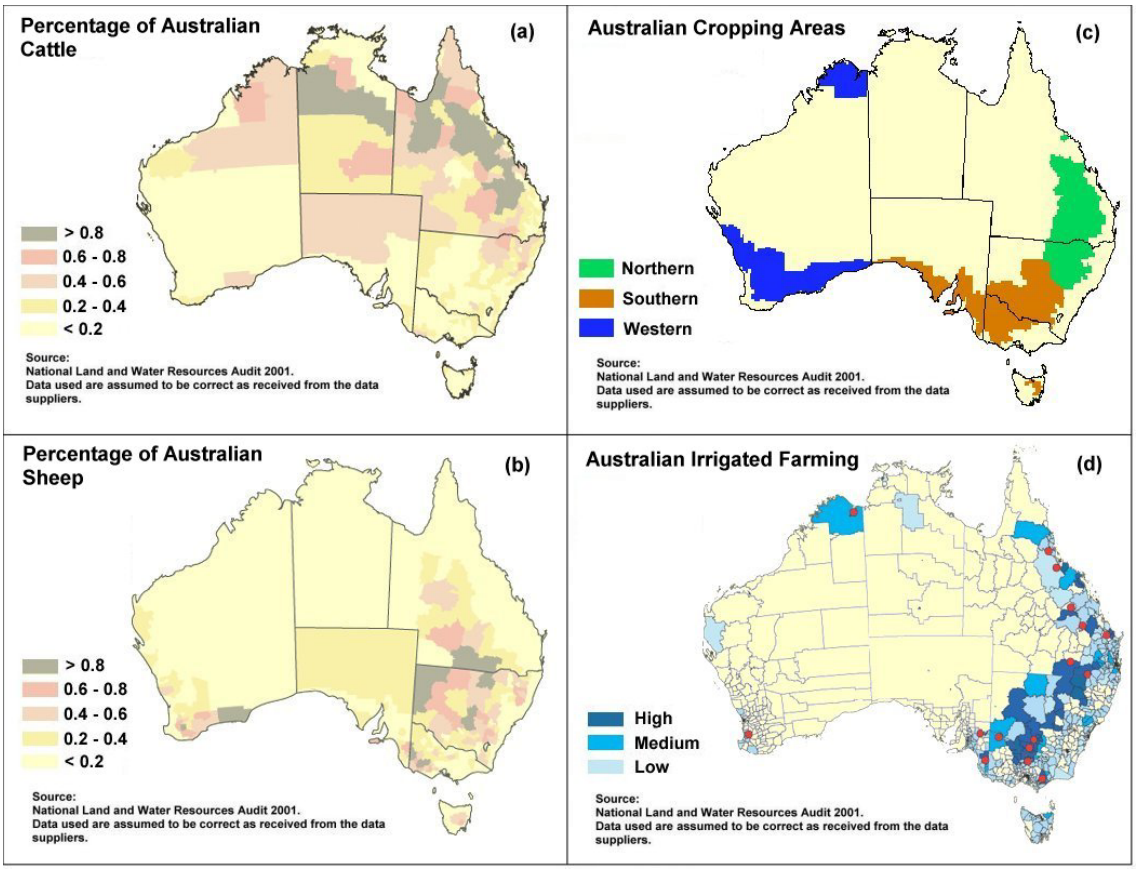

Figure 3.11 Australian agricultural production maps from NLWRA (2001a): (a) Percentage of Australian beef cattle by Statistical Local Area; (b) Percentage of Australian sheep by Statistical Local Area; (c) Australian grain growing areas; and (d) Australian irrigated farming areas by Statistical Local Area

Within the ILZ, Landsat MSS imagery was used to infer vegetation cover and greenness using the near infrared band #5. Land cover and climatic specific thresholds in band #5 were generated for all vegetation types based on the values of remnant natural vegetation for the band. Using the natural vegetation threshold values, all vegetation in the ILZ was categorised into the three classes of uncleared, thinned and cleared. The extent of clearing and tree thinning found by the study in the ILZ are shown in the Australian Intensive Landuse Zone map (*figure 3.10 b*).

The analysis found that 51.9% of the ILZ area of 2,984,000 km^2 was cleared, with another 17.4% identified as thinned. Further analysis found the largest area of clearing occurred in open Eucalypt woodlands, followed by eucalypt shrublands, eucalypt forests, and eucalypt open woodlands, with the area cleared of eucalypt woodlands and shrublands accounting for 45% of the total area cleared.

The remainder of the continent was termed the Extensive Land use Zone (ELZ) where the land cover was identified as being largely intact, with extensive land use reducing the vegetation cover through grazing by live stock and repeated burning in many areas. In the ELZ a more subjective, expert opinion based assessment of disturbance was performed using the Landsat MSS imagery. The analysis categorised the level of disturbance of vegetation into slight, substantial and significant. The study found that 62% of the ELZ area of 4,708,000 km^2 was slightly disturbed, 15% was substantially disturbed, and 26% was significantly disturbed.

The study reported in some areas there were limitations in the analysis of cleared and thinned areas, with large and consistently occurring errors resulting from the values assigned to the Landsat MSS band #5 clearing thresholds. In many areas green and actively growing pastures or crops were miscategorised as uncleared, and changing the thresholds to eliminate this problem, produced the opposite effect of categorising remnant vegetation as thinned or cleared. To minimise the overstatement of clearing, thresholds were set conservatively, however, even with this precaution, there are areas falsely marked as cleared along clearing boundaries in Western Australia, South Australian, Tasmania and northern Queensland. These errors of classification may explain some of the differences in clearing and thinning identified by the study in northern and central Queensland, that are not found in the other three studies.

3.3.2 Bureau of Rural Sciences Historical Australian Land Cover Change Assessment

As part of their assessment of Australian land cover change, *Barson et al.* (2000) reviewed Australian land cover change from European settlement to current day. The main focus of their review was the change in woody vegetation between the natural (pre-European) map of *AUSLIG* (1990) (*figure 3.1*), and current day woody vegetation derived from Landsat TM imagery from 1990 and various sources of structural vegetation data.

Comparing the differences between the current and natural woody vegetation, historical changes in woody vegetation were identified and mapped, as shown in the BRS changes in woody vegetation since European settlement map (*figure 3.10 c*). As the Landsat imagery used for current day woody vegetation was very similar to the imagery used as the basis of the current map by *AUSLIG* (1990), it was not surprising that many of the areas identified as being changed from forest to non-forest are the same as those marked as cleared or having had trees thinned in the AUSLIG study. Additional areas identified as changing from forest to non-forest but not included in the areas of clearing and tree thinning by the AUSLIG study, were in general associated with thinning of denser tall shrublands. The inclusion of areas of shrubland thinning can be traced to the study's definition of woody vegetation including all vegetation greater than 2 meters in height with a crown cover of greater than 20%.

The review found that the principle driver of historical land cover change was agricultural development, with other sources of land cover change resulting from mining, forestry and urban development. The study found data from *Graetz* (1998) indicated that early clearing (prior to

1950) was principally for cropping, with clearing for pastures increasing in importance from the 1950s on. Clearing rates were found to have peaked during the 1970s, during the clearing of extensive areas of south west Western Australia and Queensland for grain production, as well as for pasture improvement in Queensland.

3.3.3 National Land and Water Resources Audit Australian Vegetation Assessment

The National Land and Water Resources Audit (NLWRA) performed a national assessment of Australian native vegetation using the best available regional scale vegetation data from Australian state and territory mapping agencies, with the findings from the study published in the *NLWRA* (2001b) assessment report. The mapping process involved over 100 data sets of pre-European and present day native vegetation to form a national extent. The assessment summarised the disparate data sets into common structural and floristic groupings based on the hierarchical classification scheme of the National Vegetation Information System (NVIS).

The assessment found that between European colonisation and present day, native vegetation clearing primarily had occurred for human settlement and agriculture in the higher precipitation regions with relatively fertile soils, and in general had excluded the arid interior and the tropical far north. The areas identified by the study as cleared of native vegetation are shown in the extent of native vegetation clearing map (*figure 3.10 d*).

The report suggested the impacts on native vegetation varied with different land uses, with broad acre clearing for cultivation and grazing, native forest harvesting for timber, rangeland grazing with changes in fire regime, exotic plant invasion, and urbanisation identified as the major drivers of change. The affects of intensive land use were found to be greatest in: south west Western Australia; southern South Australia; western and central Victoria; the midlands and northern Tasmania; central and eastern lowlands of New South Wales; northern and eastern areas of the Australian Capital Territory; central and south east Queensland; and small patches of the Northern Territory.

The assessment found clearing of eucalypt woodlands and open woodlands accounted for the greatest area of clearing at 45% of the total area cleared, with 31% and 25% of their pre-European extents cleared respectively. Mallee woodlands and shrublands accounted for 14% of all clearing, with 35% of their pre-European extent cleared. Inland *Acacia* forests and woodlands accounted for 10% of all clearing, with 15% of their pre-European extent cleared. Native tussock grasslands, rainforest communities, and heath communities also were sighted as having been extensively cleared, although having smaller spatial extent.

The report identified limitations with the vegetation mapping arising from consistency issues with the wide range of data sets used. The resulting continental maps of pre-European and present day native vegetation were combined from very broad to detailed mapping, with mapping methods having different levels of reliability and temporal currency. Despite these

limitations, the clearing of native vegetation identified by the assessment was highly consistent with the clearing and tree thinning map from the AUSLIG study.

3.3.4 ANU CO_2 and Land-use Effects on Australian Vegetation

Berry and Roderick (2002a) performed an analysis of the combined impacts of increased concentrations of atmospheric CO_2 and land-use on Australian vegetation. The study noted that while the most obvious changes to Australian vegetation came from the clearing of woody vegetation and replacement with herbaceous vegetation for intensive cropping and improved pastures, there where many extensively grazed areas that had subsequently increased in woody vegetation.

The study suggested that the increase in woody vegetation in these areas may be partially due to the increased water use efficiency of vegetation under increased atmospheric CO_2. The higher water use efficiency would allow higher rates of photosynthesis with similar moisture availability, and the increased carbohydrate production would result in increased dry matter concentration in stems. To assess the impact of increased atmospheric concentration of CO_2 in combination with land-use, the study investigated changes in vegetation composition using the present (current) and natural (pre-European) maps of *AUSLIG* (1990), with methods for estimating leaf functional type from *Berry and Roderick* (2002b), and monthly Normalized Difference Vegetation Index (NDVI) data from 1981 – 1991 NOAA/NASA Pathfinder satellite imagery.

The leaf functional type methods of *Berry and Roderick* (2002b) divided vegetation composition into three classes based on leaf properties. Turgor (T) leaves relied on turgor pressure of protoplasm for support; they were short lived, had high rates of photosynthesis and had high water availability requirements. Mesic (M) leaves were evergreen and required a good supply of light, water and nutrients throughout the year; they were slower growing than T leaves, with lower maximum rates of photosynthesis. Sclerophyll (S) leaves were evergreen and replaced M leaves where the supply of nutrients was limited; they were longer lived than M leaves and had lower rates of photosynthesis than M and T leaves.

The composition of the three leaf types within vegetation was assessed by the composite breakdown of the fraction of photosynthetically active radiation (Fpar) absorbed by each of the leaf types. This was assessed from the NDVI satellite imagery for each vegetation class of the current AUSLIG vegetation map. The fraction of Fpar absorbed by T leaves (F_T) was assigned as the raingreen component obtained from the NDVI in conjunction with climate data. The remaining Fpar was assigned to M and S leaves based on the original Fpar value. For Fpar values of greater than 0.75 the residual Fpar was assigned to M leaves (F_M); for Fpar values less than 0.2 the residual Fpar was assigned to S leaves (F_S); and for Fpar values between 0.2 and 0.75 the F_M value increased linearly with increasing Fpar.

The study used the current vegetation class compositions of T, M and S leaves (F_T, F_M and F_S) in combination with the AUSLIG natural vegetation map to reconstruct natural distributions of T, M and S leaves and the natural Fpar values. The natural Fpar values where then extrapolated back from the current day 350 ppm atmospheric concentration of CO_2 to the pre-industrial value of 280 ppm for 1788. The extrapolation technique assumed that the total Fpar value of the vegetation decreased linearly with decreased CO_2, and the Fpar of evergreen leaves (F_S, and F_S) also linearly decreased with CO_2. The residual difference between the reduced total Fpar value and the reduced Fpar of evergreen leaves was assigned as the reduced Fpar for T leaves (F_T).

In the absence of changed atmospheric CO_2 the study found that the greatest land-use impact on Australian vegetation was the clearing of woody vegetation for cropping and improved pastures. In these areas the regular disturbance suppressed the M and S forms of vegetation and promoted the T forms. Where disturbance was less frequent, such as where grazing occurred in range lands, increases in T forms of vegetation were only temporary before M and S forms restored to pre-disturbance cover, resulting in little long term change.

When the impacts of increased atmospheric CO_2 were included in the analysis, the study predicted that the increased atmospheric CO_2 would have resulted in an increase in the M and S forms of vegetation, with similar quantities of the T form. The S form of vegetation would have increased over most of the continent, while the increase in the M form would have been confined to regions of higher precipitation. The study suggested that while the increased CO_2 may have exacerbated the increase in woody vegetation, the association with pastoralism suggested that other factors associated with European settlement also would have been important. The study also found there was little evidence of increased photosynthesis or vegetation cover from field studies or satellite observations, suggesting that natural climatic variability may have swamped longer term trends.

3.3.5 National Land and Water Resources Audit Australian Agriculture Assessment

The NLWRA also performed a comprehensive national assessment of contemporary Australian agriculture from a wide range of sources, with the findings published in the *NLWRA*, (2001a) assessment report. The distribution of agricultural activity detailed in the report was highly supportive of the agricultural drivers of vegetation change suggested by the AUSLIG study. The distributions of cattle, sheep and grain production, as well as the use of irrigation are shown in the maps of *figure 3.11*.

The majority of the clearing of forests, woodlands and shrublands identified in the Australian historical changes in structural form map (*figure 3.8 a*), can be identified as the cropping regions in the Australian grain growing areas (*figure 3.11 c*) and as the irrigated farming areas of the Australian irrigated farming areas map (*figure 3.11 d*). The extensive grazing of cattle and sheep widely discussed in the AUSLIG study also can be seen to be

concentrated in the northern woodlands and grasslands for the Australian beef cattle map (*figure 3.11 a*), and in southern shrublands and woodlands for the Australian sheep map (*figure 3.11 b*)

3.3.6 Section Summary

1. The CSIRO Australian land cover disturbance assessment found the most significant changes to Australian land cover were from clearing of native vegetation for replacement with crops and pastures.
2. Based on clearing Australia was divided into the Intensive Landuse Zone (ILZ) and the Extensive Landuse Zone (ELZ).
3. The study found 51.9% of ILZ (1,549,000 km^2) was cleared, with 17.4% (520,000 km^2) thinned of trees.
4. 26% of the ELZ (1,224,000 km^2) was significantly disturbed, 15% (706,000 km^2) substantially disturbed, and 62% (2,919,000 km^2) slightly disturbed.
5. The mapping of clearing and tree thinning was in general supportive of AUSLIG study, with the exception of areas that where identified as having unreliable change detection in the CSIRO study.
6. The historical component of the Australian Land Cover Change project also identified changes in woody vegetation that were highly supportive of the clearing and tree thinning identified by the AUSLIG study.
7. Historical Australian vegetation clearing from the independent vegetation mapping of the National Land and Water Resources Audit study, also was highly supportive of the of the clearing and tree thinning identified by the AUSLIG study.
8. Studies into the impact of increased atmospheric CO_2 on vegetation, suggest that increased water use efficiency may result in increased evergreen vegetation over much Australia, however, this cannot be confirmed by field or satellite observation.
9. Independent agricultural assessment of the Australian grain growing regions, irrigated farming, and cattle and sheep grazing by the National Land and Water Resources Audit, also was supportive of the agricultural drivers of land cover change suggested by the AUSLIG study.

3.4 Ongoing Australian Land Cover Change Monitoring

The advent of satellite monitoring, has allowed the changes in vegetation and land cover to be systematically detected between various periods of observation. The resolution of satellite imagery, the frequency of observation and spectrum of light sampled all influence the ability to detect change and the time periods over which the change can be assessed. In this section, recent Australian continental and state wide studies for detecting ongoing changes in Australian land cover are detailed to compile a picture of absolute changes in land cover as well as demonstrate the seasonal and inter-annual changes in land cover in response to climatic variation.

3.4.1 Bureau of Rural Sciences 1990 – 1995 Australian Land Cover Change Assessment

To assess recent Australian land cover change, *Barson et al.* (2000) used higher spatial resolution Landsat Thematic Mapper (TM) imagery in conjunction with structural vegetation mapping to identify changes in Australian woody vegetation between 1990 and 1995. Ancillary data was used in conjunction with the detected changes in land cover, to attribute the changes to a range of land uses.

The study covered the Intensive Landuse Zone as defined by *Graetz et al.* (1995b), using 158 Landsat TM scenes for each of the two time periods. The data for the 1990 time period included satellite imagery from November 1989 up to March 1992, with data for the 1995 time period including imagery from March 1994 up to December 1996. Structural vegetation mapping was derived from Australian state and territory mapping agencies, the National Forest Inventory, and the current (mid 1980s) vegetation map of *AUSLIG* (1990). The total areas of woody vegetation clearing and regeneration are shown for each state and land use in *table 3.2* and *table 3.3*. The distribution of woody vegetation clearing and regeneration from all sources excluding fire are shown in the Australian land cover change between 1990 and 1995 clearing and regeneration maps (*figure 3.12* and *3.13*).

Clearing and regeneration were defined in the study as the change between woody and non-woody vegetation, where woody vegetation was defined as native or exotic vegetation greater than 2.0 meters in height, with a crown cover of greater than 20%. The changes detected by the study were extensively verified by state and territory agencies using aerial photography, other satellite imagery, ancillary thematic data, and field work.

The study found that between 1990 and 1995, in the Australian Intensive Landuse Zone, a total of 1,372,370 ha were cleared for agriculture, grazing, forestry, plantation management, and other activities excluding fire, with another 414,070 ha cleared as a result of fire. The study also found in the same time period, 442,540 ha were regenerated on land cleared for land use, with 480,710 ha regenerated on land cleared by fire.

Nationally grazing was the largest source of clearing for land use, resulting in 929,280 ha or 67.7% of the total area cleared excluding fire. Agriculture was the second largest source of clearing at 213,680 ha or 15.6% of the total. Forestry, plantation management and other sources accounted for the remaining 229,410 ha or 16.7%. Woodlands and open woodlands represented 75% of the area cleared, with open forests representing 16% of the area cleared, and tall shrublands representing 7%.

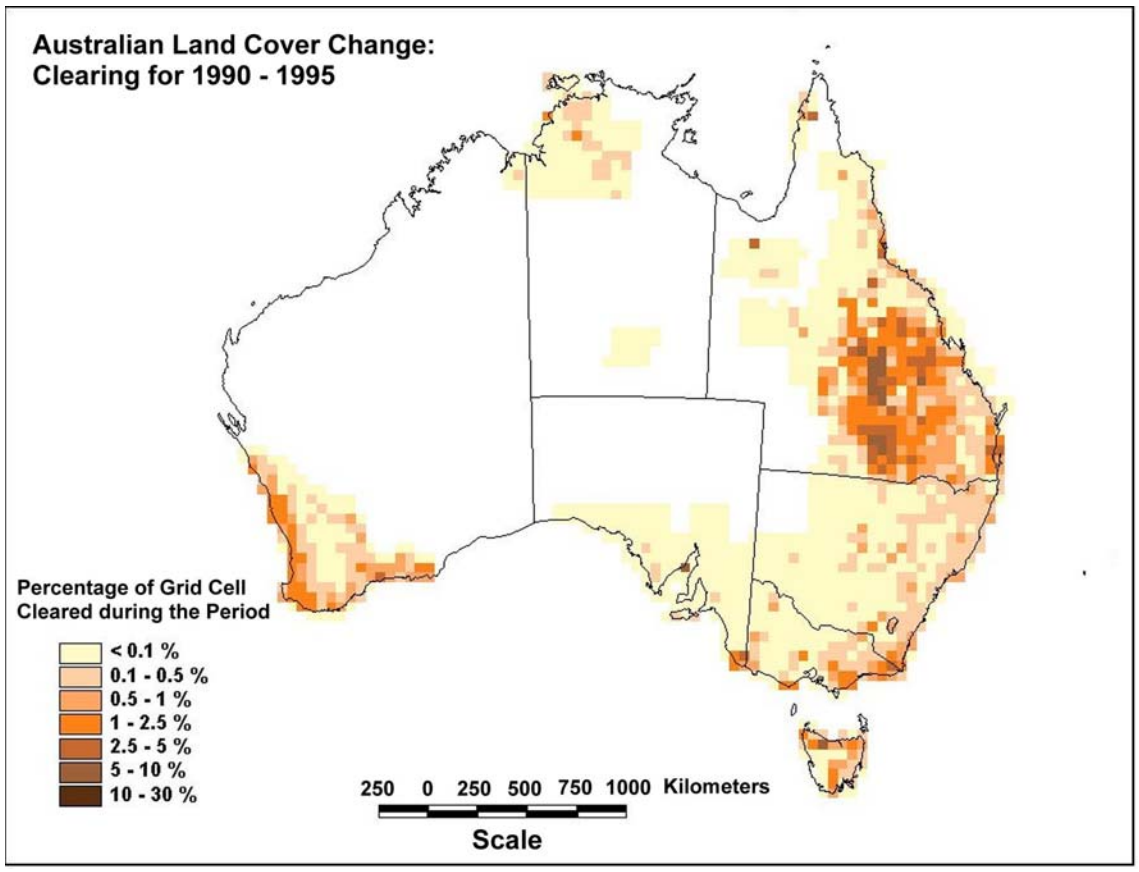

Figure 3.12 Bureau of Rural Sciences (BRS) assessment of Australian land cover change between 1990 and 1995 from Barson et al. (2000) showing the percentage of each 50 km grid cell newly cleared of woody vegetation

Table 3.2 Australian woody vegetation clearing between 1990 and 1995 from Barson et al. (2000). The table shows the area cleared by state and land use for the five year period

State	Agric-ulture (ha)	Grazing (ha)	Other (ha)	Forestry (ha)	Plant-ation (ha)	Fire (ha)	Total with out Fire (ha)
Queensland	40510	924410	27380	3970	12300	140	1008570
Western Australia	99930	0	20280	12290	5590	198140	138090
New South Wales	51860	0	8070	16130	7580	123040	83640
Victoria	9240	0	3480	30280	21640	25120	64640
Tasmania	230	3800	1500	27270	8280	1310	41080
Northern Territory	5870	1070	9550	0	20	0	16510
South Australia	6040	0	1160	10	8030	66320	15240
Australian Capital Territory	0	0	0	210	4390	0	4600
Australia	213680	929280	71420	90160	67830	414070	1372370

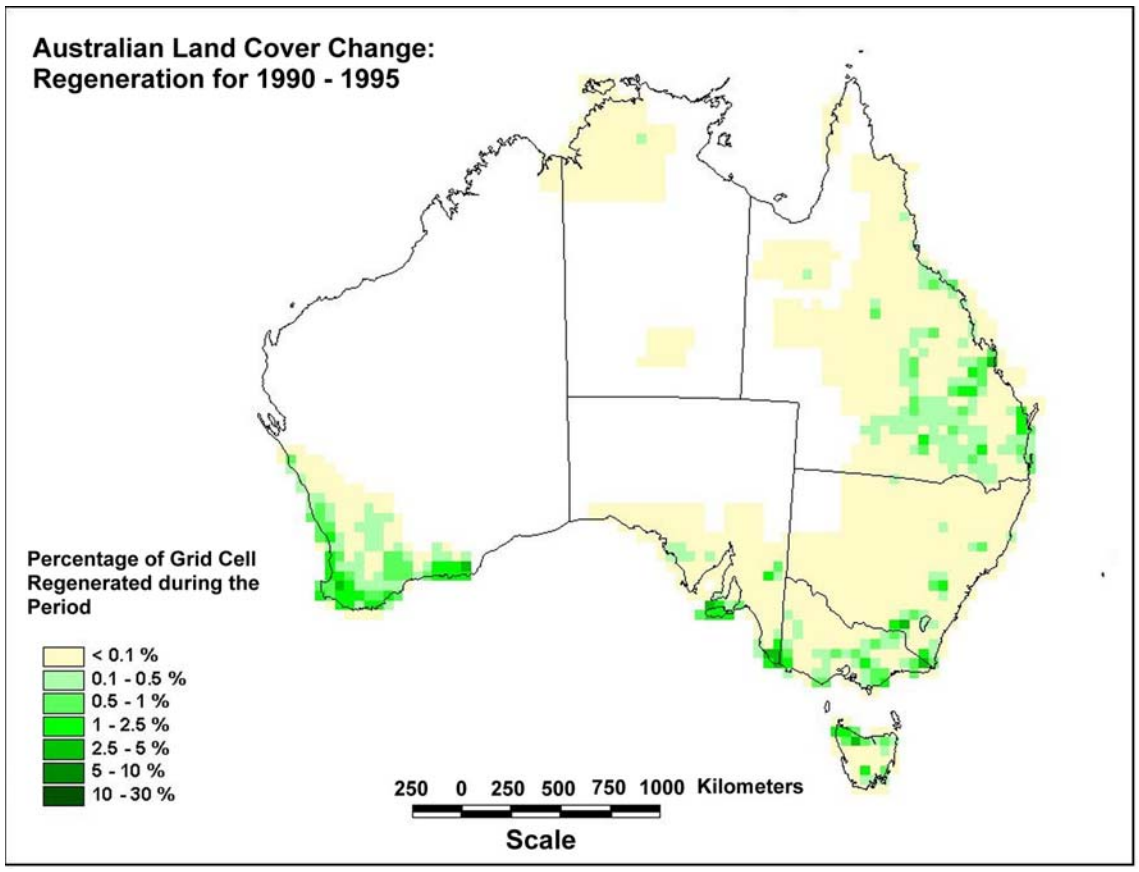

Figure 3.13 Bureau of Rural Sciences (BRS) assessment of Australian land cover change between 1990 and 1995 from Barson et al. (2000) showing the percentage of each 50 km grid cell with newly regenerated woody vegetation

Table 3.3 Australian woody vegetation regeneration between 1990 and 1995 from Barson et al. (2000). The table shows the area regenerated by state and land use for the five year period

State	Agric-ulture (ha)	Grazing (ha)	Other (ha)	Forestry (ha)	Plant-ation (ha)	Fire (ha)	Total with out Fire (ha)
Western Australia	95720	0	22340	6900	38950	76570	163910
Queensland	0	113090	0	1180	12960	0	127230
Victoria	0	0	3370	13400	33350	206970	50120
New South Wales	1140	30	230	5670	31810	13690	38880
South Australia	15140	0	1370	0	19190	183410	35700
Tasmania	120	0	280	1380	22560	0	24340
Australian Capital Territory	0	0	0	0	1790	70	1790
Northern Territory	420	0	0	0	150	0	570
Australia	112540	113120	27590	28530	160760	480710	442540

As shown in the Australian 1990 to 1995 clearing map (*figure 3.12*) and *table 3.2*, the largest area of clearing occurred in the state of Queensland, with most clearing concentrated in the south east and central areas of the state. The total area cleared in Queensland from all sources excluding fire was 1,008,570 ha, which accounted for 73.5% of the national figure. The largest source of clearing in Queensland was grazing, accounting for 91.7% of the state's clearing, followed by agriculture with 4% of the state's clearing.

Western Australia was the second largest contributor to clearing for land use, with 138,090 ha, accounting for 10.1% of the national figure. The largest source of clearing in Western Australia came from agriculture, with 72.4% of the state's clearing. The remaining states, combined, contributed 16.4% of the national figure, however, the different sizes of the states masked clearing intensity in some states, with Victoria and Tasmania having intense areas of clearing, primarily as a result of forestry and plantation management.

Nationally the largest increase in woody vegetation came from plantation management, with 160,760 ha representing 36.3% of regeneration, excluding regeneration from fire. This was closely followed by regeneration on land cleared for grazing at 113,120 ha or 25.6% of regeneration, and regeneration on land cleared for agriculture at 112,540 ha or 25.4%.

As shown in the Australian 1990 to 1995 regeneration map (*figure 3.13*) and *table 3.3*, the largest area of regeneration on land cleared for land use, occurred in Western Australia, with 163,910 ha or 37% of the national total. The largest source of regeneration for Western Australia was on land cleared for agriculture, representing 58.4% of the state's regeneration. The next largest source of regeneration came from plantation management at 23.8%. The second largest area of regeneration occurred in Queensland, with 127,230 ha or 28.7% of the national total. The largest source of regeneration in Queensland was on land cleared for grazing at 88.9% of the state's total, followed by plantation management at 10.2%.

3.4.2 Queensland Statewide Landcover and Tree Study

The Queensland Statewide Landcover and Tree Study (SLATS) is one of many land cover change studies currently conducted across Australia using a range of satellite imagery, aerial photography and field data. The Queensland Department of Natural Resources and Mines (NRM) has undertaken the SLATS study with the objective of compiling accurate mapping of woody vegetation cover and land cover change for the state of Queensland. The study uses Landsat MSS, Landsat TM, and Landsat Enhanced Thematic Mapper (ETM+) satellite imagery to compare vegetation cover between the years of 1988, 1991, 1995, 1997, 1999, 2000, and 2001 (DNRM, 2003).

Woody vegetation changes between image dates were assessed using the differences in a multiple regression vegetation index and the differences in band #3 and band #5 of the satellite imagery. All changes in perennial woody vegetation were mapped down to the level distinguishable by the imagery, with field verification performed for a high percentage of the

changes, with particular focus on areas where change was uncertain. Changes in woody vegetation included changes to native vegetation, disturbed native vegetation, regrowth vegetation, native and exotic plantations, and domestic woody vegetation. Replacement land cover was assigned to all areas of change to identify the land use associated with the change. Areas affected by fire, were in general, not mapped.

The minimum level of woody vegetation identifiable from the satellite imagery was strongly dependent on the season the imagery was taken from. Dry season imagery provided better discrimination between woody vegetation and the understorey allowing for measurement of changes in woody vegetation down to 7% foliage projected cover. Wet season imagery, however, reduced the level of discrimination due to the presence of green understorey grasses, only allowing detection of woody vegetation down to 12% foliage projected cover. Long term changes such as woodland thickening as described by *Burrows et al.* (2002) were not reliably detected using the Landsat imagery and were not mapped by the project.

The annual rates of change in woody vegetation for a range of time periods between 1991 and 2001 are shown for clearing by land use in *table 3.4* and for statewide regrowth in *table 3.5*. The distributions of woody vegetation clearing and regrowth over the same time period are shown in the Queensland clearing maps (*figure 3.14*) and the Queensland regrowth maps (*figure 3.15*).

The total statewide clearing rates in *table 3.4*, show there was a general increase in the clearing rates in Queensland through the 1990s, from the 1991 – 1995 rate of 288,800 ha per year, up to the 1999 – 2000 peak rate of 757,800 ha per year. After reaching the peak rate there was a return to clearing rates of the mid 1990s with the 2000 – 2001 rate of 377,800 ha per year. The major contributor to the peak in clearing rates in 1999 – 2000 was intensive clearing prior to regulation brought into place with the proclamation of Queensland Vegetation Management Act in September 2000.

The statewide regrowth rates in *table 3.5* show there was a general decrease in Queensland regrowth rates for the same time period. Analysis performed by the study into the projected foliage cover of vegetation cleared also showed there were changes in the density of the vegetation cleared through the study period. The median density of vegetation cleared for 1991 – 1995 had a foliage project cover 24%, compared with 28% for 1995 – 1997, 29% for 1997 – 1999, and 23% for 1999 – 2001.

Clearing for the 1991 – 1995 period was most intense in central Queensland (*figure 3.14 a*), with clearing during this period predominantly for pasture at 92% of the state total, followed by clearing for crops at 4%, and clearing for all other land uses at 4%. Clearing for the 1995 – 1997 period, again was most intense in central Queensland (*figure 3.14 b*), with clearing again predominantly for pasture, at 86% of the state total, however, clearing for crops was significantly higher at 9%, and clearing for all other land uses increased to 5%.

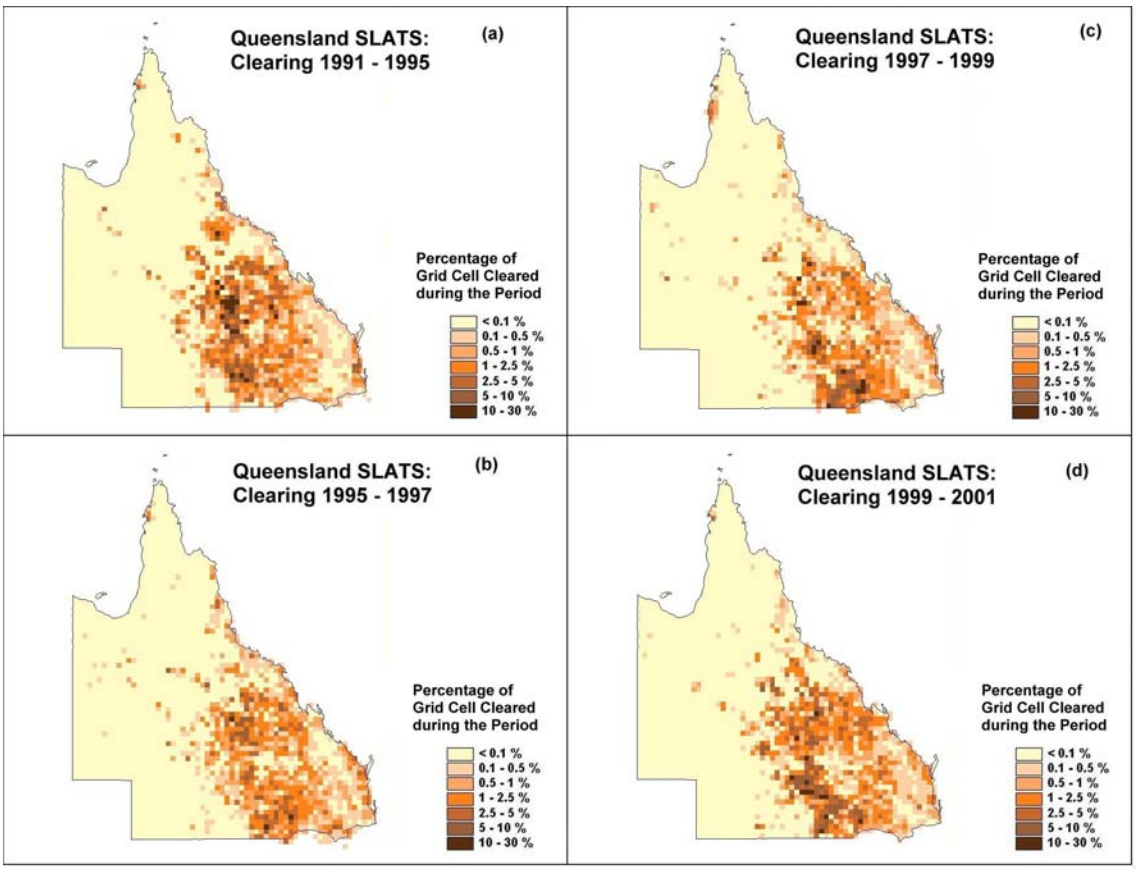

Figure 3.14 Queensland Statewide Land and Tree Study (SLATS) clearing maps. The maps show the percentage of each 0.25 degree grid cell newly cleared of woody vegetation over the corresponding time periods: (a) 1991 to 1995 from DNR (1999a); (b) 1995 to 1997 from DNR (1999b); (c) 1997 to 1999 from DNR (2000); and (d) 1999 to 2001 from DNRM (2003). Clearing is derived by computer classification and visual interpretation with an accuracy of ±10%

Table 3.4 Queensland Yearly Clearing Rates in hectares per year by land use from SLATS survey time periods, from DNRM (2003).

Time Period	Pasture (ha/yr)	Crop (ha/yr)	Forest (ha/yr)	Mining (ha/yr)	Infra-stucture (ha/yr)	Settle-ment (ha/yr)	Total (ha/yr)
1991 – 1995	265300	12500	4800	1500	2400	2300	288800
1995 – 1997	292600	29400	500	2700	8200	2500	335900
1997 – 1999	363800	40800	7400	2100	9900	1500	425500
1999 – 2000	716400	20000	6500	1400	11500	2000	757800
2000 – 2001	355300	2000	8200	1900	8900	1500	377800

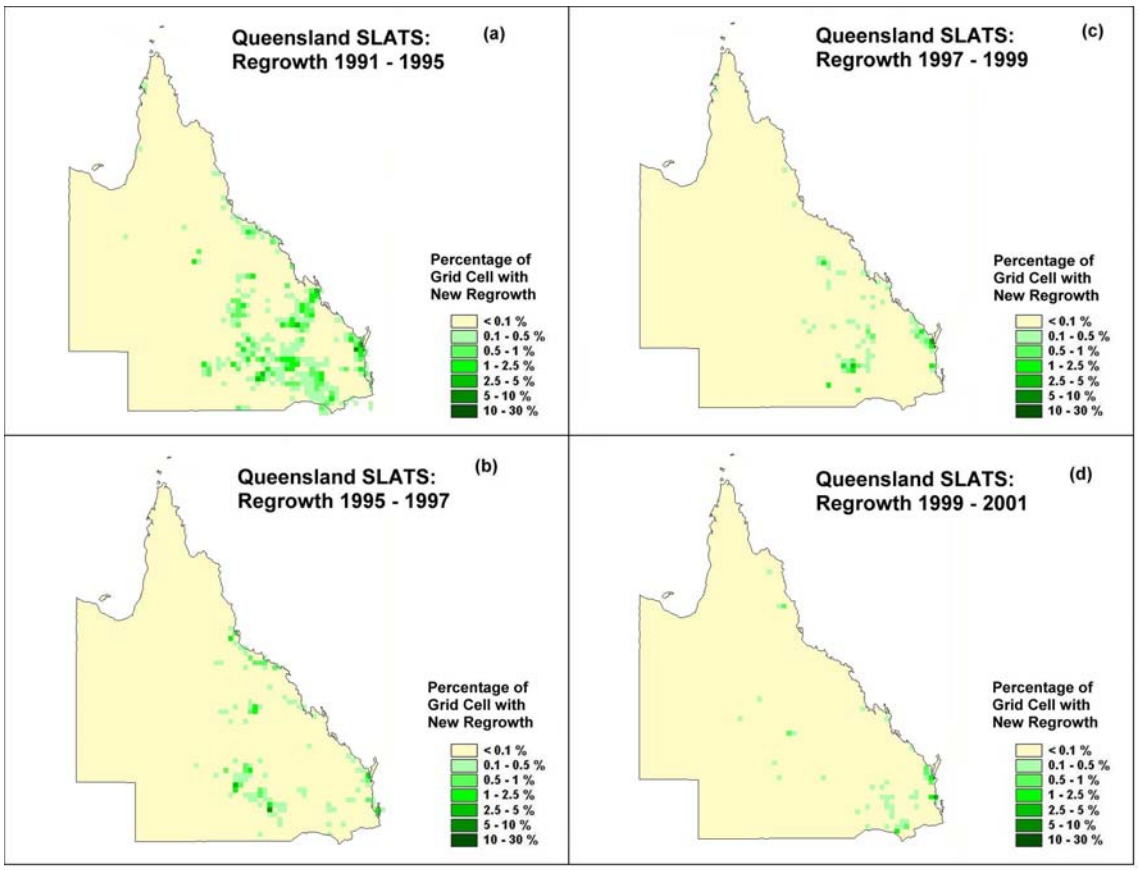

Figure 3.15 Queensland Statewide Land and Tree Study (SLATS) regrowth maps. The maps show the percentage of each 0.25 degree grid cell with new regrowth woody vegetation on cleared land over the corresponding time periods: (a) 1991 to 1995 from DNR (1999a); (b) 1995 to 1997 from DNR (1999b); (c) 1997 to 1999 from DNR (2000); and (d) 1999 to 2001 from DNRM (2003). Regrowth is derived by computer classification and visual interpretation with an accuracy of ±10%

Table 3.5 Queensland Yearly Regrowth Rates in hectares per year from SLATS survey time periods, from DNR (1999a), DNR (1999b), DNR (2000), and DNRM (2003).

Time Period	New Woody Regrowth (ha/yr)
1991 – 1995	37300
1995 – 1997	18860
1997 – 1999	9647
1999 – 2001	8811

Clearing for the 1997 – 1999 period, was most intense in the southern parts of Queensland (*figure 3.14 c*), with clearing predominantly for pasture at 86% of the state total, with another increase in clearing for crops to 10%. Clearing for the 1999 – 2001 period, returned to be most intense in central Queensland (*figure 3.14 d*), with a significant increase in the proportion of clearing for pasture, up to 94% of the state total, with a significant decrease in the proportion of clearing for crops down to 2%, and all other land uses to 4%.

3.4.3 Seasonal and Inter-annual Australian Land Cover Variability

Australian land cover is dynamic over time frames of months and years with vegetation cover responding to climatic factors effecting water availability and temperature (*Graetz et al.*, 1992). At the time scale of months, Australian vegetation shows general patterns of change associated with seasonal cycles of precipitation and solar radiation. At the time scale of years the vegetation shows noticeable changes associated with climatic variability manifested through droughts and above average precipitation episodes.

Seasonal and inter-annual changes in Australian and global vegetation cover have been constantly monitored using daily satellite observation since 1981 by the NOAA/NASA Pathfinder Land project (*Goddard*, 1994). Changes in vegetation cover are detected from the satellite imagery through changes in the amount of photosynthetically absorbed radiation, which is represented by the Normalized Difference Vegetation Index (NDVI), which is written as:

$$\mathrm{NDVI} = \frac{\rho_n - \rho_v}{\rho_n + \rho_v} \tag{3.1}$$

where ρ_n is the surface reflectance measured by the near infrared wavelength channel and ρ_v is the surface reflectance measured by the visible wavelength channel. The average monthly NDVI values over Australia for May and September 1988 and 1989 (*figure 3.16*) shows there are seasonal changes between May and September, and inter-annual changes between the same months in the two years.

In northern Australia the high NDVI values of May follow the northern summer wet season. These values are replaced by low NDVI values in September, nearing the end of the dry season. In the wheat belt areas of south west Western Australia the low NDVI values of May follow the hot dry summer. These values are replaced by high NDVI values of the growing wheat crop following the winter rains.

In other areas such as Tasmania, the forests of south west Western Australia, and much of eastern Australia, the differences in NDVI are more noticeable between the two years than the seasonal changes between May and September. In these areas the low NDVI values of 1988 are replaced by higher NDVI values in 1989. The inter-annual changes in these areas are almost entirely due to inter-annual variability in climate, with much of Australia experiencing significantly below average precipitation for 1988, but returning to average or significantly above average precipitation for 1989.

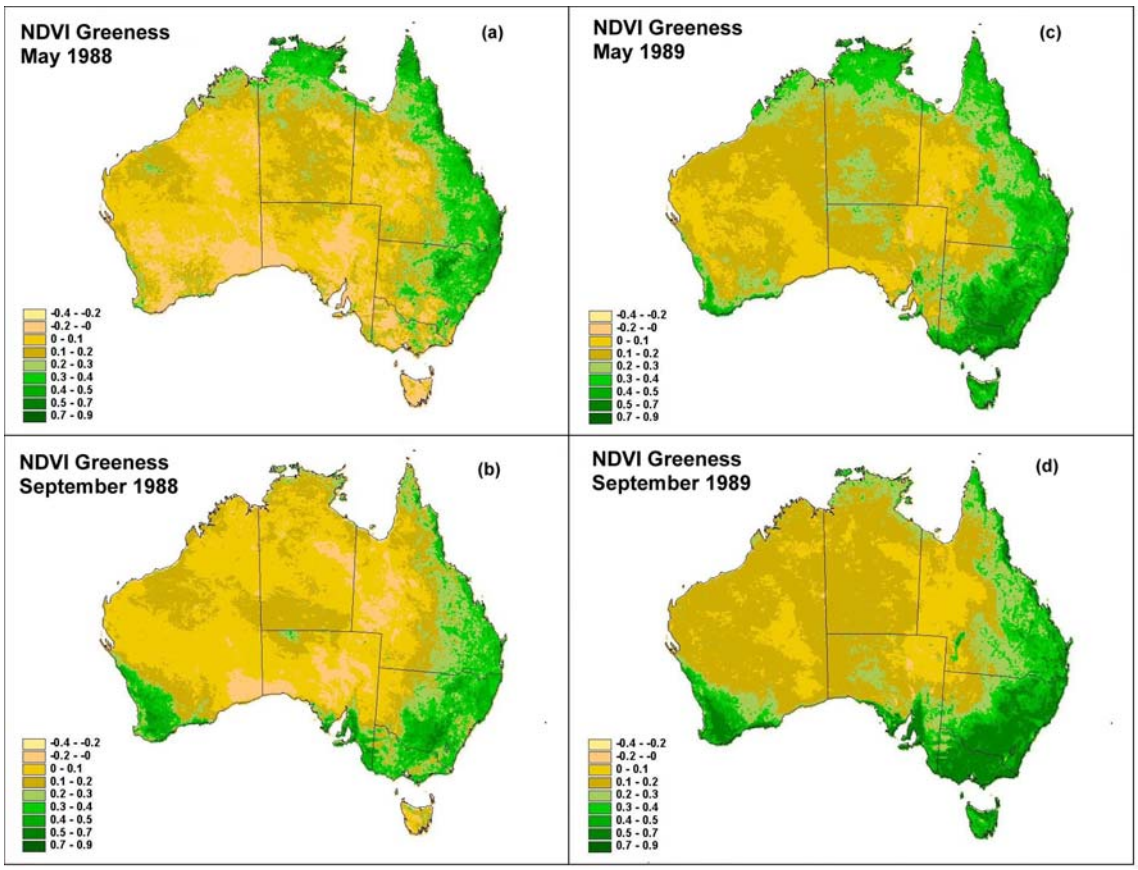

Figure 3.16 Australian seasonal and inter-annual changes in vegetation greeness from NOAA Pathfinder Advanced Very High Resolution Radiometer (AVHRR) satellite imagery using the Normalized Difference Vegetation Index (NDVI) for: (a) May 1988; (b) September 1988; (c) May 1989; and (d) September 1989

3.4.4 Section Summary

1. The Australian Land Cover Change assessment shows that across Australia between 1990 and 1995, 1,372,370 ha were cleared for land use, with 442,540 ha regenerated on land previous cleared for land use.
2. Nationally grazing was the largest source of clearing at 67.7% of the national total, followed by agriculture at 15.6%
3. The state of Queensland was the largest contributor to clearing, accounting for 73.5% of the national total, followed by Western Australia with 10.1%.
4. Western Australia was the largest contributor to regrowth accounting for 37% of the national total, followed by Queensland at 28.7%
5. The SLATS study showed there was a general increase in clearing rates in Queensland in the 1990s leading up to vegetation management legislation, with clearing rates of 288,800 ha/year for 1990 – 1995 increasing to 757,000 ha/year for 1999 – 2000.
6. The study also found there was a general decrease in regrowth rates over the same period, with regrowth rates of 37,300 ha/year for 1990 – 1995 decreasing to 8,811 ha/year for 1999 – 2001.

7. NOAA/NASA Pathfinder satellite imagery showed that land cover was dynamic over timeframes of months and years in response to changes in moisture availability and temperature arising from seasonal and inter-annual climate variability.

3.5 Chapter Summary

The aim of this chapter was to review historical Australian land cover change investigations, to develop a consensus description of Australian land cover as it may have existed prior to European arrival and how it exists for the current day. The aims of the review also encompassed ongoing Australian land cover change to provide perspective on how current land use practice continue to change Australian vegetation. The chapter described how Australian land cover has been dramatically altered since European settlement with a strong consensus from a range of studies assessing historical land cover change and agricultural utilisation. These studies showed that this intensive modification has been concentrated in the relatively fertile and climatically favourable areas of the continent. Native vegetation in these areas has been replaced or modified for cropping, intensive animal production, commercial forestry, urban development, mining, and other land uses. In the remaining areas of the continent, the vegetation is identified as being largely intact but disturbed from grazing by cattle and sheep, changes in the frequency and intensity of fire regimes, and the introduction of non-endemic plants and animals, and diseases.

The chapter also described how satellite monitoring of ongoing land cover change demonstrates that high land clearing rates continue through out Australia, with the largest areas concentrated in central and southern Queensland. These studies showed that clearing still was predominantly for grazing and agriculture, with clearing rates many time greater than regeneration. The satellite monitoring also demonstrated the dynamic nature of Australian land cover over months and years, as the vegetation responds to seasonal climatic cycles, and to droughts and above average precipitation.

The Australian land cover change and land use studies reviewed in this chapter are listed in *table 3.6* with the spatial and temporal extents, mapping methods and critical findings of each project. As shown in the table, these studies cover both historical land cover changes and ongoing changes with a high degree of consistency, providing a good consensus view of the Australian landscape and changes that have occurred since European arrival. The outcome of this chapter therefore is a robust consensus view of the extent and nature of change in Australian land cover since European arrival. The review also provides insight into the ongoing changes in land cover that result from current land use practices and natural variability. The Australian land cover changes compiled in the chapter form the basis for the climate impacts of Australian land cover change experiments in Chapter 5, and provide a basis to the assessment of whether current land use practices are contributing to the climate impacts of historical Australian land cover change in Chapter 6.

Table 3.6 Australian Land Cover Change and Land Use Studies Reviewed

Study	Area and Period Studied	Processing Approach and Source Data	Critical Findings
AUSLIG Australian Land Cover Change Assessment	Australia - From pre-European to mid 1980s	Pre-European from current remnant vegetation and historical sources Current Day mapped from mid 1980s Landsat MSS imagery and secondary data.	60% of Australian continent used for extensive grazing, with 10% used for intensive cropping or pastures. 40% of forests cleared; 37% of woodlands cleared; 23% increase in open woodlands primarily for improved grazing, and 35% of tall shrublands cleared
CSIRO Australian Land Cover Disturbance Assessment	Australia - From pre-European to 1990	Pre-European from AUSLIG mapping Current Day mapped from 1990 Landsat MSS imagery.	The study found 51.9% of ILZ was cleared, with 17.4% thinned of trees. 26% of the ELZ was significantly disturbed, 15% substantially disturbed, and 62% slightly disturbed.
BRS Australian Land Cover Change Assessment	Australia - Historical: from pre-European to 1990 Current: from 1990 to 1995	Pre-European from AUSLIG mapping 1990 land cover mapped from Landsat TM imagery 1995 land cover mapped from Landsat TM imagery	Historical component of the study supportive of the clearing identified by AUSLIG study 1990 – 1995 component found 1,372,370 ha were cleared for land use, with 442,540 ha regenerated on land previous cleared for land use. Queensland the largest contributor to clearing with 73.5% of total
National Land and Water Audit Vegetation Assessment	Australia - Preclearing to Current Day	State agency pre-clearing and current vegetation mapping compiled into national maps	Clearing identified between vegetation maps was highly supportive of the clearing identified by AUSLIG study
National Land and Water Audit Agricultural Assessment	Australia - Current Day	Wide range of sources of Agricultural activity	Australian grain growing regions, irrigated farming, and cattle and sheep grazing supportive of the agricultural drivers of land cover change suggested by the AUSLIG study
DNRM Statewide Landcover and Tree Study	Queensland 1990 - 1995 1995 - 1997 1997 - 1999 1999 - 2000 2000 - 2001	Landsat TM and ETM+ imagery used for change detection between start and end of time periods	General increase in clearing rates in Queensland in the 1990s: 288,800 ha/year for 1990 – 1995 increasing to 757,000 ha/year for 1999 – 2000 Decrease in regrowth rates: 37,300 ha/year for 1990 – 1995 decreasing to 8,811 ha/year for 1999 – 2001
NOAA Pathfinder NDVI Changes	Global - 1981 – Current Day	Monthly composites of Daily imagery using visible and near infrared spectrums	Land cover was dynamic in response to seasonal and inter-annual climate variability

CHAPTER 4.
CSIRO GENERAL CIRCULATION MODEL REVIEW AND MODIFICATION

4.1 Chapter Aims and Rationale

4.1.1 Aims and Structure

The aim of this chapter is to develop a climate modelling framework, using the CSIRO General Circulation Model (GCM) that can be used to investigate the climate impacts of changes in Australian land cover in Chapter 5. The modelling framework is required to realistically represent the relatively fine-scale changes in Australian land cover described in Chapter 3, in the land surface model of the CSIRO GCM. To achieve this, the CSIRO GCM required modification, as the original model represented the land surface by common homogeneous vegetation at the 1.875 degree grid increment of the model grid. The new climate modelling framework with the modified CSIRO GCM required evaluation for climate modelling performance, to assess the suitability of using the CSIRO GCM with the new land surface parameters for the Australian land cover change experiments of Chapter 5.

The chapter is divided into three sections. Section 4.2 reviews the CSIRO GCM, focusing on the land surface model and the monthly parameters currently used to represent the land surface. The current land surface parameters are compared with the best available land surface data to evaluate limitations in using the existing model to represent the land surface at the scales described in Chapter 3. Section 4.3 integrates the best available land surface data and physical models (canopy radiation, transpiration, surface roughness, etc) to produce the best available representation of current land surface conditions in the CSIRO GCM. The land surface theory of Chapter 2 is used to provide a sound basis for modifying the land surface model and to develop new parameter generation methods that incorporate the best available land surface data. A comparative analysis is performed of the original CSIRO GCM land surface parameters with the new land surface parameters to:

(i) demonstrate the limitations of the current CSIRO GCM land surface parameters in representing the land surface; and

(ii) provide an objective assessment of the implications of using a more accurate representation of the land surface for land surface processes such as physical radiation, evaporation and transpiration, and sensible heat flux.

Section 4.4 performs a sensitivity experiment to evaluate the performance of the CSIRO GCM using the original and new land surface representations. The performance of the two

experiments with prescribed sea surface temperatures and sea ice distributions is assessed against global and Australian climate observations for the period 1975-1999. Analysis of model outputs are performed for global, continental and Australian regional scales for a range of climate variables including surface temperature, precipitation and surface energy fluxes in order to:

(i) evaluate the impact of the new land surface properties on the GCM climate simulation;
(ii) assess the climate biases that the new land surface properties remove or introduce into the climate modeling framework; and
(iii) provide an assessment of the effect of these changes in biases on the Australian land cover change and climate modelling experiments conducted in Chapter 5.

4.1.2 Rationale

The CSIRO GCM is a fully coupled process based atmosphere, land surface, ocean, and sea ice climate model, simulating the global climate. These properties of the model make it suitable to systematically investigate the regional, continental and global climate impacts of Australian land cover change. The processes simulated in the model allow investigation into the direct impacts of changes in surface fluxes on the atmospheric boundary layer, and the indirect impacts of changes in larger scale atmospheric circulation and longer term feedbacks such as changes in soil moisture.

The problem with the current CSIRO GCM, however, is that the original land surface data of the model was captured at the very coarse spatial grid increment of the model (1.875 degrees), which can not realistically represent the fine-scale changes in Australian land cover described in Chapter 3. In addition to the scale issues, *Sellers et al.* (1996b) identified significant weaknesses in the methods and data used to compile the land surface parameters of *Dorman and Sellers* (1989), which are currently used to describe the land surface in the CSIRO GCM. Specifically, the arbitrary prescription of vegetation phenology from the mapping of *Kulcher* (1983) with data from ecological literature was deemed to be unrealistic for representing spatial and temporal patterns in vegetation.

Global Circulation Modelling experiments by *Polcher and Laval* (1994), *Zhang et al.* (1995), *Zhao et al.* (2001), *Bounoua et al.* (2002), and many others, have investigated possible climate impacts of global and regional land cover change by comparatively modelling of the global climate with control and altered land surface conditions. The differences in the simulated climate with the two land surface representations are used to identify the modelled climate response to the changes in the land cover. Originally the changes in land cover have been represented in GCM models by replacing the current dominant vegetation of a GCM model grid cell in the control experiment, with the dominant vegetation of natural vegetation in a pre-

cleared experiment in the areas of change. In these experiments the changes in land surface properties are represented by differences in internal GCM look up values referenced by the different vegetation types assigned to the climate model experiments.

More recently the differences between current day and natural land surface conditions have been represented through extrapolation of current day satellite derived land surface conditions to natural or pre-disturbance extents, such as in investigations by *Zhao et al.* (2001) and *Bounoua et al.* (2002). The extrapolation process assigns the natural land surface conditions for altered grid cells from surrounding grid cells identified as having remnant natural vegetation, similar to the natural vegetation of the altered grid cell. Both the dominant vegetation changes, and the more recent satellite derived land cover change investigations, however, represent changes in land cover by altering the land surface properties at the horizontal grid increment of the GCM model.

Raupach and Finnigan (1995), *Baidya Roy and Avissar* (2000), and others suggest that like the Australian land cover change investigations of Chapter 3, the scale at which human modification alters the landscape is several orders of magnitude finer than the horizontal grid increment of GCM land cover change experiments. Following on these scale issues *Shuttleworth* (1991), *Koster and Suarez* (1992), *Pitman* (1995), *Arain et al.* (1997), and others demonstrate that there are large differences in the surface fluxes calculated from highly heterogeneous land surfaces compared with the homogeneous land surfaces of the GCM experiments.

Investigating the issues of scale and land surface representation, *Oleson et al.* (2004) recently found that climate modelling experiments using satellite-derived land cover change datasets that capture sub-grid heterogeneity and land biogeophysics, diminish the magnitude and spatial extent of climate changes that result from changes in land surface conditions, compared to experiments conducted with biome-derived datasets at the model grid grid increment. The reduction in magnitude of the climate changes was attributed to the ecological similarity between land cover types involved in the land use change, and the reduced intensity of agriculture identified in the satellite-derived datasets. The study suggested that the realism of the datasets used to represent land cover change, and the parameterisations selected to represent land cover type biogeophysics, needed to be carefully considered to understand and quantify the impacts of land cover change on climate. In the context of this research the CSIRO GCM needs to be reviewed and modified to capture the fine-scale Australian land cover changes of Chapter 3, in order to realistically investigate the climate impacts of these land cover changes.

4.2 CSIRO Model Review and Land Surface Data Evaluation

4.2.1 Review of CSIRO General Circulation Model and Land Surface Representation

The CSIRO Mark 3 Climate System Model developed by CSIRO Atmospheric Research (CAR) and described in *Gordon et al.* (2002), is a coupled atmosphere, land surface, sea ice and ocean General Circulation Model (GCM). The atmosphere and land surface components of the model have horizontal grid increments of approximately 1.875 degrees as specified by the T63 truncation grid increment.

The atmosphere component consists of 18 vertical levels incorporating a hybrid vertical structure of atmospheric pressure relative to surface pressure at the lowest levels, reverting to isobaric levels with altitude. The surface fluxes of heat, moisture and momentum are parameterised following Monin-Obukhov similarity theory, assuming constant vertical fluxes in the surface layer. Atmospheric processes involving vertical mixing and shallow convection are parameterised in terms of stability dependent K theory following *Blackadar* (1962).

The land surface model of the GCM is implemented based on the land surface parameterisations of *Noilhan and Planton* (1989) and *Deardorff* (1978). The model represents the land surface as a single vegetation canopy covering bare soil. Soil is represented by a six-layer soil profile with deep-rooted vegetation, snow accumulation, surface runoff, and deep soil moisture drainage. Surface temperature and surface fluxes of momentum, sensible heat and moisture are calculated independently for the vegetation canopy and the bare soil for each model grid location. Vegetation fraction is used to weight the independent values from the bare soil and canopy to specify the average surface temperature and surface fluxes for each grid cell. A more comprehensive description of the CSIRO GCM and the land surface model can be found in *Gordon et al.* (2002).

The original land surface parameters of the CSIRO GCM were developed from the global land surface climatology of *Dorman and Sellers* (1989), with parameters derived from the dominant vegetation and soil type for each model grid cell. Each grid location in the land surface model is parameterised through land surface maps specifying:

(i) monthly broadband surface albedo;
(ii) annual mean vegetation fraction;
(iii) monthly surface roughness;
(iv) one of 13 Simple Biosphere (SiB) land surface types; and
(v) one of 9 model defined soil types.

The model uses the SiB land surface type to prescribe maximum leaf area index, the change in leaf area index with soil temperature, unrestrained stomatal resistance to transpiration,

and variation in vegetation fraction with soil temperature. All soil thermal and hydraulic properties are prescribed from the model soil class.

4.2.2 Evaluation of Global Land Surface Data

Current day global land surface data have recently become available with relatively fine spatial resolutions, covering longer, more representative time periods, than were used in generating the land surface parameters of *Dorman and Sellers* (1989). The new global land surface data describe characteristics of the land surface, such as land cover (*Loveland et al.*, 2000), soil texture (*Reynolds et al.*, 1999), leaf area index (*Buermann et al.*, 2001), and surface albedo (*Schaaf et al.*, 2002). These new land surface data are the products of long-term satellite monitoring and international data integration projects, representing the earth surface heterogeneously at scales of the order of 1km, and dynamically over seasonal and inter-annual time frames. The vegetation, soil and albedo parameters currently used in the CSIRO GCM are evaluated against this new global data to assess implications of the current representation of the land surface in the model.

Vegetation mapping

Fine-scale satellite derived global vegetation biome mapping developed by the International Geosphere Biosphere Project's (IGBP) Global Land Cover Characterisation (GLCC) (*Loveland et al.*, 2000) was selected for global vegetation mapping, as it was a globally coordinated, fine-scale satellite-derived land cover mapping project that accurately captures the global vegetation biomes used in the model. The vegetation mapping was developed from NOAA Pathfinder AVHRR satellite imagery over the 1992 – 1993 period at a 1 km resolution. The GLCC vegetation biome map is shown in the Simple Biosphere (SiB) classification, globally and for the Australian region, in *figure 4.1 c* and *d*.

The GLCC vegetation biome mapping process was based on clustering of AVHRR NDVI monthly composites to generate seasonally homogeneous greenness classes for each continent. The greenness classes were interpreted with extensive ancillary data to identify individual land cover classifications for each region. Using the relationships between greenness classes and land cover, the project performed land cover mapping for a number of different land cover classification systems, including the SiB classification.

The original CSIRO GCM vegetation map is shown in the SiB classification, globally and for the Australian region, in *figure 4.1 a* and *b*. Comparison of the original parameters with the more recent satellite derived vegetation mapping, shows good general agreement at the global scale, with consistent regions of tropical forest, savannah, bare desert, agriculture, and boreal forest for both maps. Closer inspection of the Australian region, however, identifies major discrepancies between the two maps. The most obvious of these differences are: large expanses of bare soil in the western center of the Australian continent; broadleaf-deciduous forests along

the eastern coastal margin; and needleleaf forests over the western half of Tasmania. The vegetation descriptions of Chapter 3, support the GLCC vegetation mapping, and challenge the accuracy of the original CSIRO GCM parameters in representing Australian land cover.

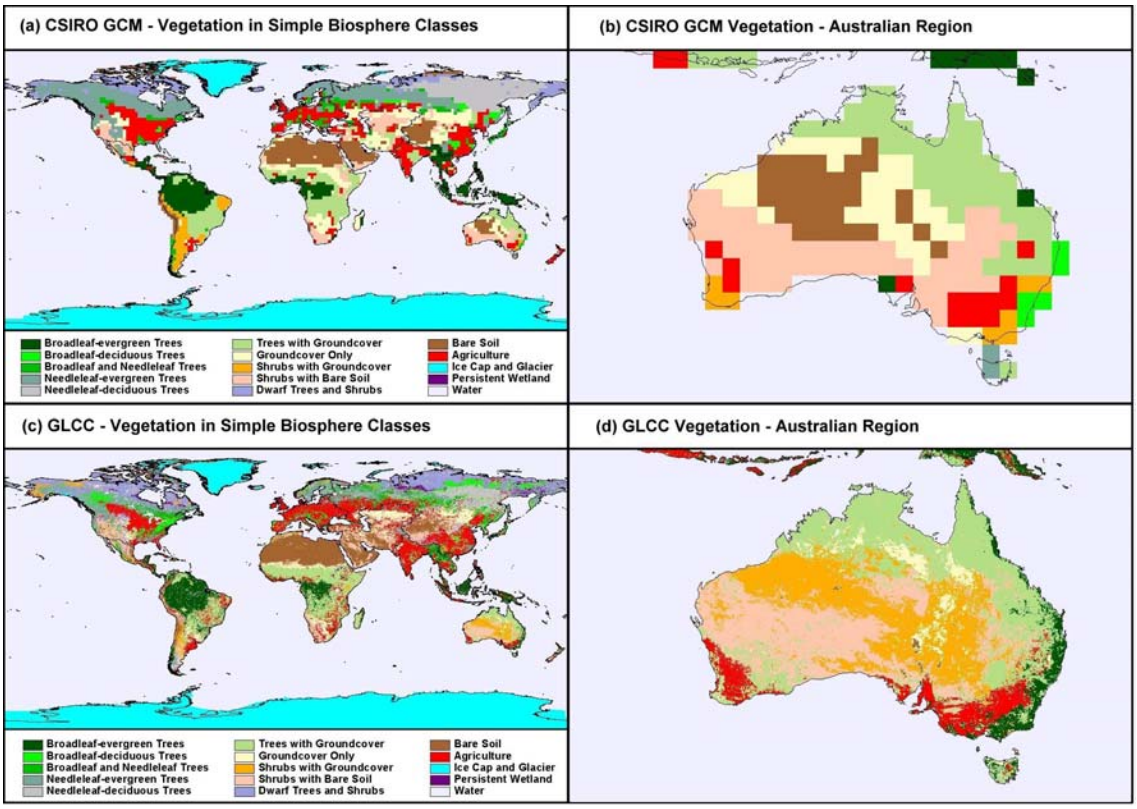

Figure 4.1 Vegetation Mapping: (a) Original CSIRO GCM Parameters, Vegetation in Simple Biosphere (SiB) classification; (b) Detailed view of (a) over the Australian Region; (c) IGBP GLCC Vegetation in SiB classification; and (d) Detailed view of (c) over the Australian Region

The biome based mapping of the Global Land Cover Characterisation was used for the comparison with the CSIRO GCM parameters as it was in the same classifications as model. Continuous vegetation function data, such as those produced by *DeFries et al.* (1994), *DeFries et al.* (1995), *DeFries et al.* (1999) and *DeFries et al.* (2000), could not be used as a comparison to the CSIRO GCM, as the land surface parameters of the model did not specify the percentage tree cover, the percentage composition of needle leaf and broadleaf trees, or the percentage composition of evergreen and deciduous trees. As both the continuous vegetation function data and the Global Land Cover Characterisation were processed from the same IGBP AVHRR satellite imagery, and the GLCC data was used as the basis for much of the continuous vegetation function data it assumed there is a high degree of consistency between the land surface parameters generated with both data sets.

Global Soil Mapping

Global soil texture mapping derived by *Reynolds et al.* (1999) from the United Nations, Food and Agriculture Organization's (UN FAO) global soil map and global soil profile database, was selected for the global soil mapping. The soil texture mapping provided the fractional composition of silt, sand and clay, at 10 km resolution, for the top 30 cm layer and for a deeper 30 cm to 100 cm layer. The fractional composition of soil in both layers were grouped into the CSIRO GCM soil classes by the matching the sand, silt and clay composition to the CSIRO classes. The top layer of the UN FAO soil map is shown in the CSIRO GCM soil classification, globally and for the Australian region, in *figure 4.2 c* and *d*.

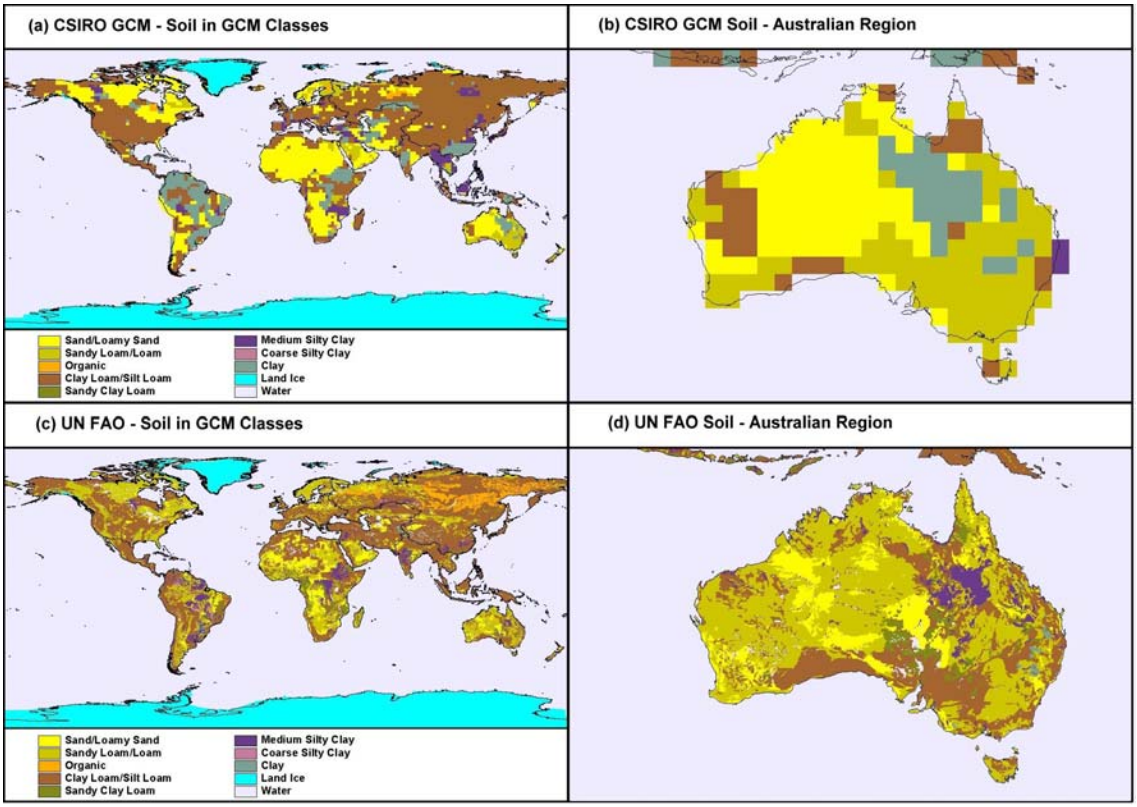

Figure 4.2 Soil Mapping: (a) Original CSIRO GCM Parameters, Soil in the GCM soil classification; (b) Detailed view of (a) over the Australian Region; (c) UN FAO Soil Texture reclassified to the GCM soil classification; and (d) Detailed view of (c) over the Australian Region

The original CSIRO GCM soil map is shown in the CSIRO GCM soil classification, globally and for the Australian region, in *figure 4.2 a* and *b*. At the global scale the largest differences in the maps occur in Africa and northern parts of North America, where the original CSIRO parameters are mapped with large areas of sand, but have higher compositions of silt and clay in the UN FAO mapping. There also are major differences in South America where the original parameters map large areas as clays that are not reflected in the UN FAO mapping. Across eastern Russia there also are areas with very high silt composition in the UN FAO mapping that are represented as clay loams/silt loams in the original CSIRO parameters.

Over the Australian region, there is general agreement between the two maps, with small differences the soil compositions in some areas. The major differences occur where the original CSIRO parameters map more sand in north western and central areas, more clay for areas of Queensland, and less silt over the south east. The Atlas of Australian soils, shown in Chapter 3, is generally supportive of the mapping of both the soil maps over Australia (*figure 3.4 b*).

Global Surface Albedo Mapping

The global fortnightly surface albedo mapping by *Schaaf et al.* (2002) generated from MODerate resolution Imaging Spectroradiometer (MODIS) satellite imagery, was selected for global albedo mapping. The surface albedo mapping used directional satellite observation coupled with semi-empirical models to produce Bi-directional Reflectance Distribution Function (BRDF) mapping for the period 2001 to 2003 at a 0.5 degree resolution. The BRDF mapping estimated spectral and broadband surface reflectance for black sky (direct beam) and white sky (diffuse) solar radiation corrected to the local solar noon for the day of observation.

To make the MODIS surface albedo mapping comparable with the single broadband snow free surface albedo parameter used in the CSIRO GCM, average monthly solar noon surface albedo was calculated from the fortnightly direct beam and diffuse albedo values. The calculation of the average monthly values required filtering to remove snow effected values and scaling by the relative amounts of direct beam and diffuse radiation reaching the surface at a given location at noon on the day of observation under clear skies.

The average July MODIS broadband albedo is shown globally and for the Australian region in *figure 4.3 c* and *d*. July broadband snow free surface albedo from the original CSIRO GCM parameters is shown globally and for the Australian region in *figure 4.3 c* and *d*. Comparison of the original CSIRO GCM parameters and the MODIS mapping, shows large discrepancies at both global and Australian regional scales.

At the global scale the MODIS derived albedo was significantly higher than the original CSIRO GCM parameters for the Sahara desert and the Arabian peninsula. For large areas of central Asia, South America, Africa and Australia, however, the MODIS derived albedo was significantly lower than the original parameters. The differences in albedo over the Australian region were significant, with the original CSIRO GCM parameters specifying albedo values similar to those of the Sahara desert (> 0.3) for much of inland Australia. The differences in albedo for the cropping areas of south west Western Australia, also were significant, with the original GCM parameters mapping these areas as being darker than the surrounding native vegetation. The MODIS derived albedo, however, showed these areas were lighter than the adjacent native vegetation in agreement with the numerous field and satellite observation studies of the area detailed in Chapter 2.

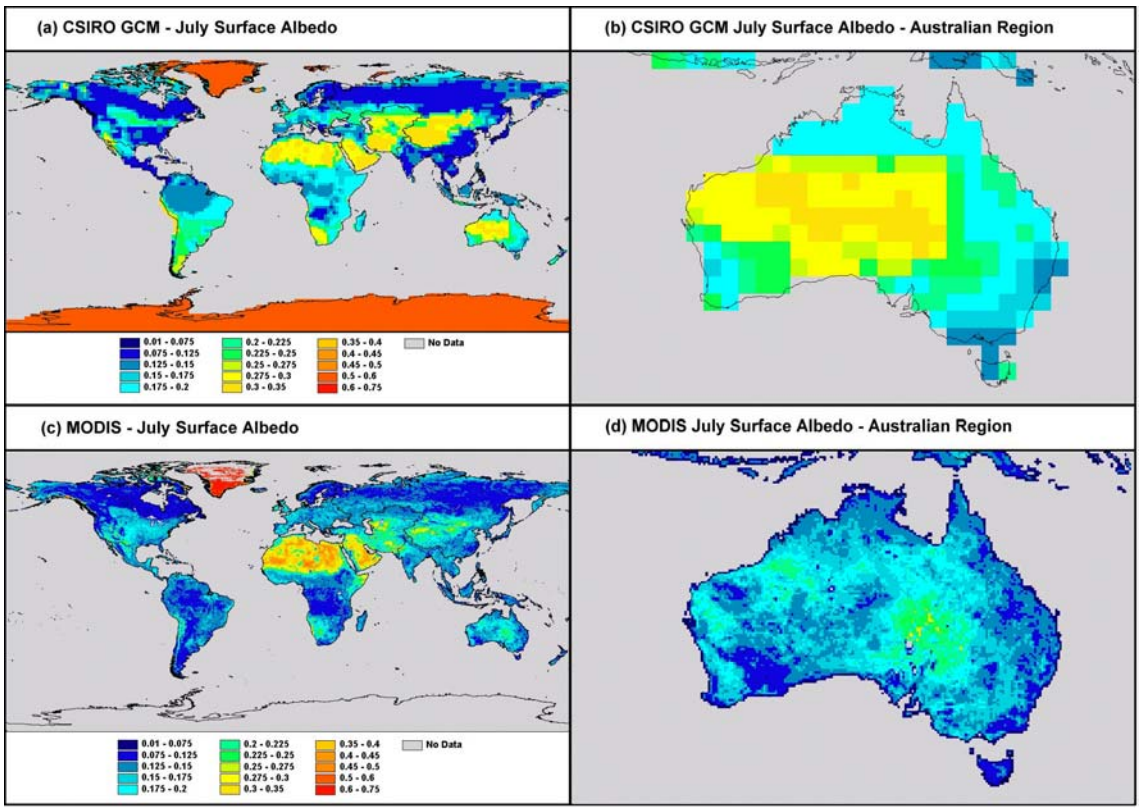

Figure 4.3 Broadband Snow Free Surface Albedo Mapping: (a) Original CSIRO GCM Parameters, July Surface Albedo; (b) Detailed view of (a) over the Australian Region; (c) MODIS derived July Surface Albedo; and (d) Detailed view of (c) over the Australian Region

Global Leaf Area Index Mapping

The global monthly green leaf area index (LAI) mapping of *Myneni et al.* (1997) was selected for global leaf area index mapping. The LAI mapping was derived from Pathfinder AVHRR satellite imagery for the period 1981 to 2001 at 8 km resolution, using vegetation specific relationships between the Normalised Difference Vegetation Index (NDVI) and LAI. The relationships were used in conjunction with global structural vegetation mapping and the monthly composite NDVI mapping, to calculate monthly LAI values. Mean monthly LAI values were calculated from the individual monthly values over the period 1981 to 1991 to reduce the bias of a single year given the inter-annual variability in the data. The July AVHRR derived green LAI maps are shown globally and for the Australian region in *figure 4.4 c* and *d*.

The original monthly LAI values used in the CSIRO GCM were calculated in the model based on vegetation specific parameters and soil temperature rather than specified explicitly. To compare the original monthly LAI values of the CSIRO GCM with the equivalent monthly mean leaf area index maps, it was necessary to calculate monthly LAI values from mean monthly soil temperatures, vegetation specific maximum leaf area index values, and the vegetation specific leaf area index variability functions of the model. The soil temperatures were sourced from climatological mean monthly soil temperatures taken from a 30 year model run with the original CSIRO GCM parameters.

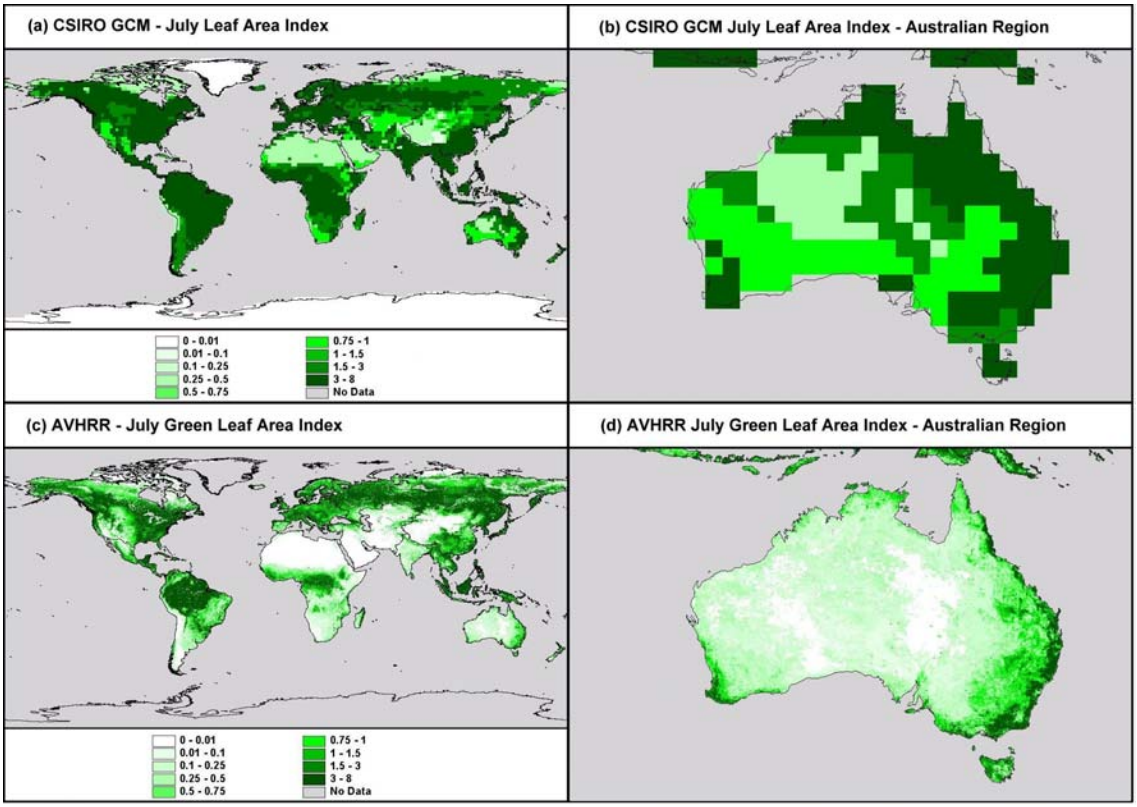

Figure 4.4 Global Leaf Area Index Mapping: (a) Original CSIRO GCM Parameters, July Leaf Area Index Map; (b) Detailed view of (a) over the Australian Region; (c) AVHRR derived monthly green leaf area index map for July; and (d) Detailed view of (c) over the Australian Region

The equivalent mean July LAI values calculated from the original CSIRO GCM parameters are shown globally and for the Australian region in *figure 4.4 c* and *d*. Both globally and over the Australian region there are large differences in leaf area mapping, with only the most densely vegetated tropical broadleaf forests and boreal needleleaf forests showing similar values. Over all other vegetation types the AVHRR derived values are significantly lower than the original CSIRO GCM values. Over the Australian region the LAI values have the same major discrepancies, with most of inland Australia having AVHRR derived values an order of magnitude lower than the original CSIRO GCM parameters. Only along the coastal margins of the south east and the south west of the continent do the values become comparable. Comparison of the monthly LAI values across inland New South Wales with field observations performed by *McVicar et al.* (1996) also is supportive of the much lower AVHRR derived values.

4.2.3 Section Summary

1. The CSIRO GCM is a fully coupled, process based, atmosphere, land surface, sea ice and ocean model designed to simulate global climate.

2. The model is suitable for investigating climate impacts of land cover change in Australia because its coupled, process-based structure captures the fundamental properties of the land surface, and how they interact with the atmospheric boundary layer (i.e. turbulent and convective fluxes of energy, moisture and momentum, radiation dynamics, and deep-rooted transpiration of soil moisture through vegetation).
3. The model also captures the dynamic feedbacks in the climate system from sub-grid processes to global atmospheric circulation resulting from changes in land surface properties and surface fluxes.
4. The original model parameters are unable to represent the fine-scale heterogeneity of the modified Australian land cover relative to its pre-clearing distribution due to the coarse nature of the original land surface parameters.
5. The original CSIRO vegetation parameters had good general agreement with IGBP GLCC vegetation mapping, at the global scale, however, more detailed inspection over the Australian region, there were major discrepancies between the two maps at finer scales.
6. The original CSIRO soil parameters had large discrepancies with the top layer of the UN FAO soil map for Africa, northern parts of North America, South America, and eastern Russia. For Australia there was general agreement between the two maps.
7. The original CSIRO July broadband surface albedo parameters had large discrepancies with the MODIS derived broadband surface albedo mapping, with CSIRO values lower for the Sahara desert and the Arabian peninsula, but significantly higher for large areas of central Asia, South America, Africa and Australia.
8. The original CSIRO July leaf area index values were significantly higher than the AVHRR derived values for most vegetation types, with only tropical broadleaf forests and boreal needleleaf forests showing similar values.

4.3 New Land Surface Parameter Generation Methods

4.3.1 Methods

The numerous differences between the new land surface mapping and the original parameters, as well as the fine-scale nature of Australian land cover change, described in Chapter 3, suggested that the original CSIRO GCM parameters would not be able to represent the land surface as required for the land cover change experiments. To overcome this limitation new land surface parameter generation methods were developed to incorporate the finer more representative data into the land surface model of the CSIRO GCM. The new methods used the two stream radiation model of *Sellers* (1985) and the simplified surface roughness model of *Raupach* (1994) to ensure that the vegetation, soil and radiation dynamics captured by the new

land surface data were represented as realistically as possible in the land surface of the CSIRO GCM.

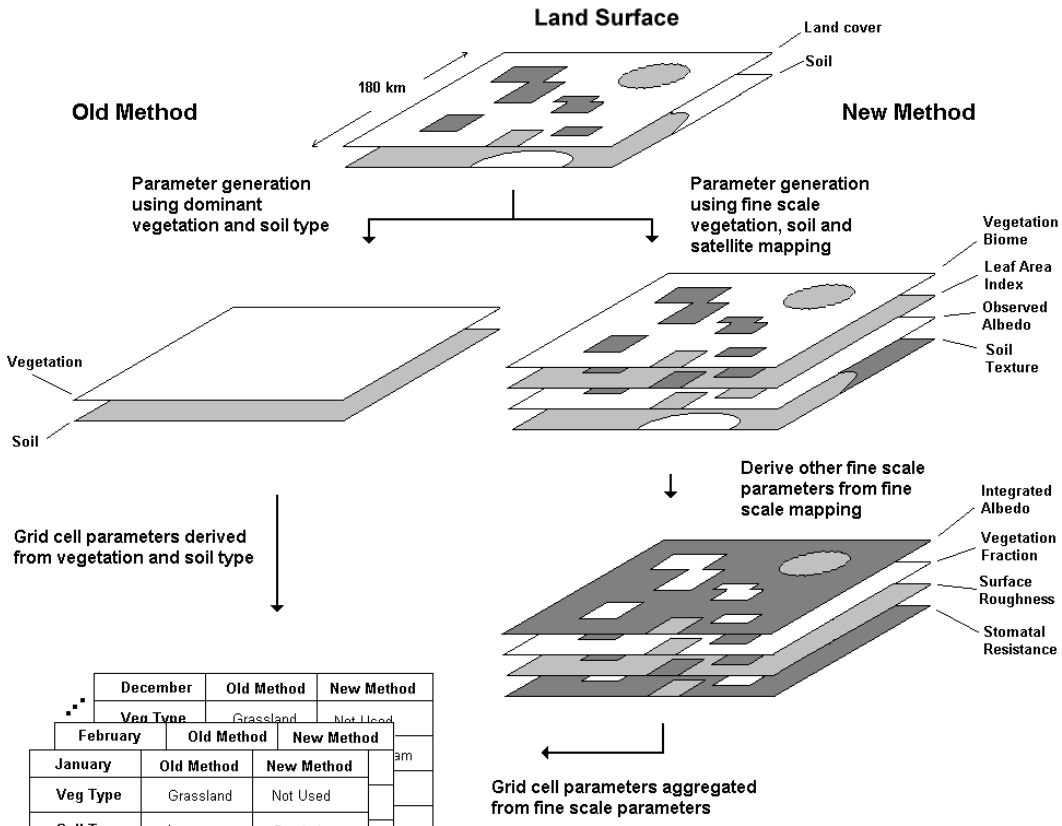

December	Old Method	New Method
Veg Type	Grassland	Not Used

February	Old Method	New Method

January	Old Method	New Method
Veg Type	Grassland	Not Used
Soil Type	Loam	Sandy loam
Albedo	0.23	0.18
Sigmaf	0.5	0.72
LAI	0.6	1.4
RSmin	150	130
Z0	0.2	0.75

Figure 4.5 Original CSIRO GCM land surface parameter generation methods compared with the new parameter generation methods using relatively fine-scale land surface data with physical surface models, and parameter aggregation. The parameterisation methods are shown for a single T63 Grid Increment (1.875 degree) GCM grid cell.

The new parameter generation methods also used the aggregation rules of *Arain et al.* (1997) and *Shuttleworth* (1991) to capture the fine-scale land surface heterogeneity represented in the new land surface data at the coarse grid increment of the GCM parameters. The CSIRO GCM was modified to directly specify LAI and vegetation fraction as monthly parameters rather than calculating these values based on vegetation type and soil temperature. *Figure 4.5* graphically illustrates the differences between the new land surface parameter generation methods and the original CSIRO GCM parameters.

By combining the physical land surface models with the new fine-scale mapping and aggregation rules the new land surface methods ensured that the land surface parameters used to calculate land surface fluxes in the models were consistent with the data collected in each of the mapping projects. These methods also ensured that differences in land surface conditions between Australian current day and pre-European land cover could be represented as accurately as possible for the Australian land cover change experiments performed in Chapter 5. The new land surface parameter generation methods were refined from extensive investigation using the CSIRO GCM with various land surface data and methods investigated.

Aggregation rules

The aggregation techniques of *Arain et al.* (1997) and *Shuttleworth* (1991) were applied to capture the relatively fine-scale land surface parameters and produce representative parameters at the 1.875 degree grid cell increment of the CSIRO GCM. These aggregation methods can be generally expressed through linear averaging by the expression:

$$Var_f = \sum Var_{f\,i}\ Fraction_i \qquad (4.1)$$

where: $Fraction_i$ is the fraction of the GCM grid represented by the source data and Var_f represents the parameters of:

1. Vegetation Type
2. Soil Texture (*Sand%, Silt%, Clay%*)
3. Surface Albedo;
4. Vegetation Fraction (*SigmaF*)
5. Leaf Area Index (*LAI*)
6. Unrestrained Stomatal Resistance (*RSmin*)

The linear averaging rules for were modified for a number of the parameters following *Arain et al.* (1997), and where aggregation rules were not previously defined. The aggregated soil texture values were converted to a CSIRO GCM soil class by matching aggregated soil composition for each GCM grid cell. Surface roughness length values for each grid cell where aggregated using a blending height method as described by *Hagemann et al.* (1999). And the vegetation parameter was aggregated by a most common vegetation type method. The role of the vegetation parameter, however, was removed from the modified model as the leaf area index and vegetation fraction were specified explicitly for each month.

Two Stream Radiation Model

The two stream radiation model of *Sellers* (1985) was used to model the dynamics of incoming solar radiation between the vegetation and the underlying soil to calculate mean monthly surface albedo and vegetation fraction. The model calculated the amount of direct and diffuse solar radiation absorbed and reflected by the vegetation and the soil in the visible and near infrared spectrums, for each grid cell at an 8 km resolution for every hour of the mid day of each month. The leaf optical properties used in the two stream radiation model were specified from the GLCC vegetation mapping of *Loveland et al.* (2000) and lookup tables provided by *Sellers et al.* (1996a). The monthly LAI values were specified from the average monthly AVHRR derived values of *Myneni et al.* (1997).

To ensure the albedo calculated by the two stream radiation model was consistent with the albedo derived from the MODIS observation, the soil reflectance used in the model was reverse calculated for each 8 km grid cell for each month. The soil reflectance calculation used a simple fitting algorithm applied over a range of soil reflectance values to find the soil reflectance that produced the closest value for solar noon albedo compared to the MODIS observed value for that month.

Following the methods of *Dorman and Sellers* (1989), the two stream radiation model was used to calculated the average monthly surface albedo using the monthly fitted soil reflectance and vegetation properties for the middle day of each month. This method weighted hourly surface albedo values through out the day, by the amount of solar radiation reaching the surface at each hour. The objective of the radiation weighted albedo was to reproduce the same daily solar radiation budget in the CSIRO GCM as was calculated with the two stream radiation model for the middle day of the month.

Vegetation fraction also was calculated using the two stream radiation model, following the definition of *Noilhan and Planton* (1989) as the radiation shielding factor of the vegetation over bare soil. Under this definition the vegetation fraction was calculated as the fraction of radiation absorbed by the vegetation compared to the total radiation absorbed by vegetation and soil together. Mean monthly vegetation fraction was calculated in the same manner as albedo using the hourly vegetation fraction values of the middle day of the month, weighted by the amount of solar radiation reaching the surface at each hour.

The use of the calculated soil reflectance rather than prescribed soil reflectance reduced the albedo differences reported by *Oleson et al.* (2003) between MODIS and the two stream radiation model, for all but heavily vegetated areas, where soil reflectance had little influence over surface albedo. Details on the two stream radiation model and the relationships of albedo and vegetation fraction with vegetation type, LAI, soil reflectance, and sun angle are described in detail in Appendix A.

Other Parameters

Most of the other parameters were derived directly from the global mapping and through lookup tables. The vegetation parameters were specified directly from the GLCC vegetation mapping, soil texture was specified directly from the interpretation of the UN FAO mapping, and LAI parameters were specified directly from the average monthly AVHRR derived values. Unrestrained stomatal resistance values were generated using the GLCC vegetation mapping and lookup table values for each SiB vegetation type, sourced from the first ISLSCP project web site (*Sellers et al.*, 1995).

The surface roughness length parameters, were calculated using the simplified roughness model of *Raupach* (1994), with canopy height specified from the GLCC vegetation mapping and lookup tables supplied by *Sellers et al.* (1996a), and LAI specified from the average monthly AVHRR derived values. Details on the simplified roughness model and the relationships of surface roughness with canopy height and LAI are described in detail in Appendix E.

4.3.2 CSIRO GCM Land Surface Parameter Results

Comparison of the new land surface parameters at the GCM grid increment with the finer scale mapping, illustrated how effectively the aggregation rules captured the nature of the new data. As a result of this, the comparison of the new land surface parameters with the original CSIRO GCM parameters reflected many of the differences already identified between the original parameters and the finer scale land surface mapping in the previous section.

Although the vegetation parameter was no longer used in the CSIRO GCM, the new vegetation parameters shown in *figure 4.6 a* and *b*, show the same discrepancies as were shown between the GLCC vegetation map and the original CSIRO GCM parameters in *figure 4.1*. The new soil parameters shown in *figure 4.6 c* and *d* also show the same discrepancies as shown between the UN FAO soil map and the original CSIRO GCM parameters in *figure 4.2*.

Unlike the vegetation parameters, the differences in the soil parameters, affected soil properties as the soil type was used to specify soil hydraulic and thermal parameters. In general soils with higher sand content had lower saturation and field capacity levels, with faster soil moisture drainage. Conversely soils with higher clay or silt content had higher saturation and field capacity, with higher soil moisture retention. These factors impact infiltration, surface runoff, deep soil drainage, soil moisture evaporation, and soil moisture availability for vegetation.

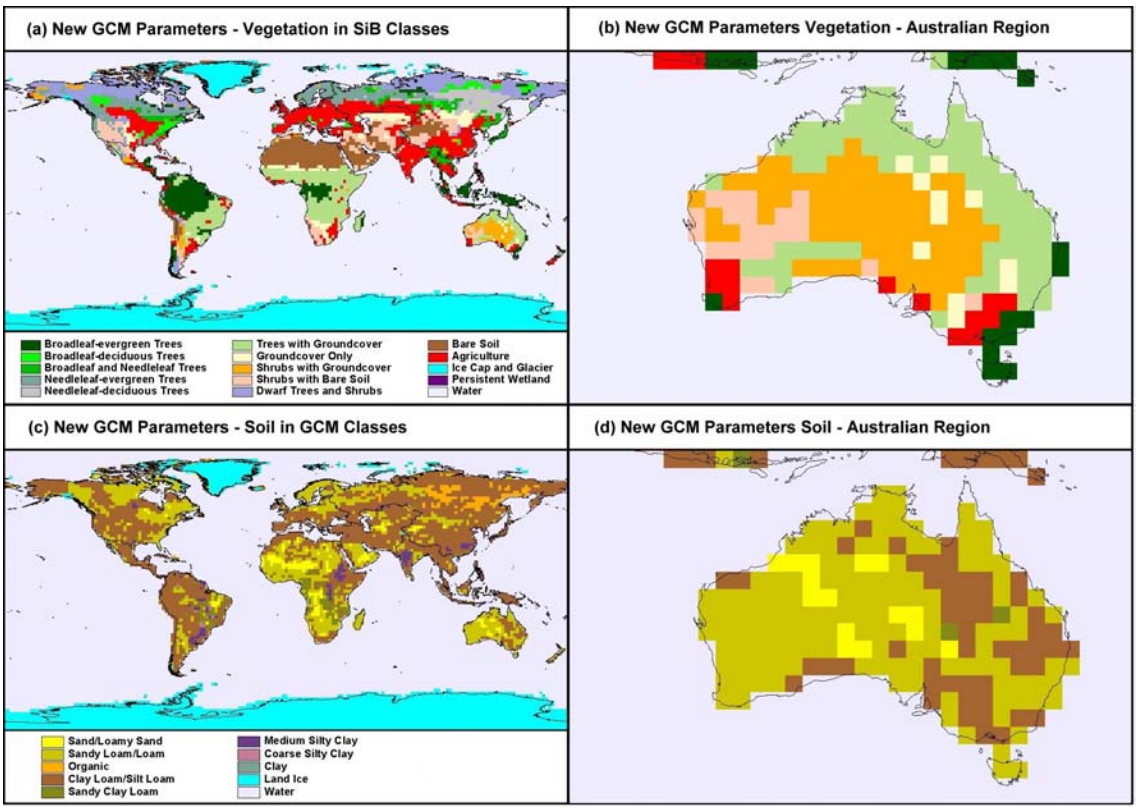

Figure 4.6 New CSIRO GCM Parameters: (a) Vegetation Map in Simple Biosphere (SiB) classification; (b) Detailed view of (a) over the Australian Region; (c) Soil Map in the GCM soil classification; and (d) Detailed view of (c) over the Australian Region

Evaluation of the parameters of surface albedo, leaf area index, vegetation fraction, unrestrained stomatal resistance, unrestrained canopy resistance, and surface roughness length were of greater significance to the land cover change experiments as they directly specified the properties of land cover. Consequently these parameters are evaluated in greater detail, globally and over the Australian region.

Albedo

The monthly average land surface albedo values of the new GCM parameters were evaluated against the original GCM parameters for January and July global zonal averages, as well as for monthly average values for all land over the Earth, and for Australia. The results from these evaluations are shown in the graphs of *figure 4.7*. The differences in zonal, global and Australian averages are shown geographically for January and July in the global and Australian land surface albedo maps of *figure 4.8*.

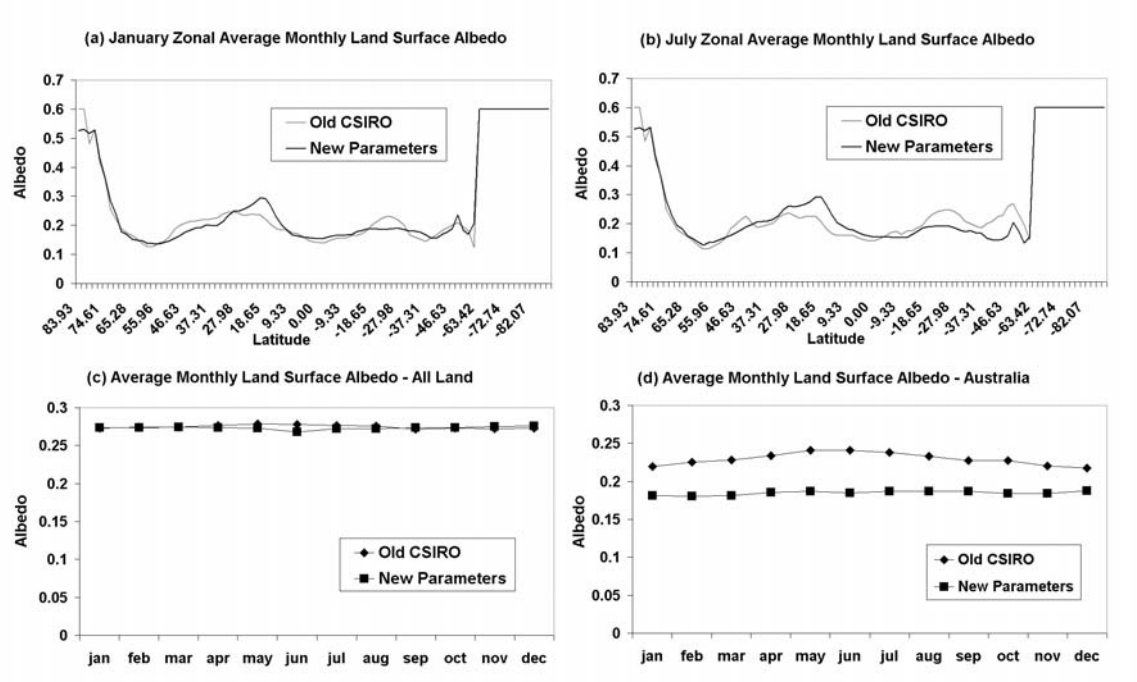

Figure 4.7 CSIRO GCM Albedo Evaluation: (a) January zonal average land surface albedo for the new and original CSIRO GCM parameters; (b) same as (a) for July; (c) Average monthly land suface albedo for all land for new and original CSIRO GCM parameters; and (d) same as (c) for the Australian continent

The global average land surface albedo graph (*figure 4.7 c*), shows values of the new parameters were similar to the original parameters for all months, with the difference between the two average values less than 0.01 for all months. The graphs also show the global average of the new parameters was closest to the original parameters in boreal winter and furthest apart in boreal summer.

The zonal average graphs (*figure 4.7 a* and *b*), show that in the northern hemisphere, between 10 N and 30 N the new parameters were higher for both January and July, with latitudes north and south of this range in general agreement for the two sets of parameters. The zonal average graphs also show that in the southern hemisphere, the new parameters had lower albedo for 10 S to 33 S for January, and for 0 to 54 S for July, with remaining areas again in general agreement for both parameters.

The global albedo difference maps (*figure 4.8 c* and *g*), show that the sparsely vegetated areas of southern South America, southern Africa, central Australia, and central Asia had significantly lower albedo (shown in red) in the new parameters than the original CSIRO parameters. The differences were larger in magnitude and spatial extent in July than January. The only areas where this general rule of lower albedo with sparse vegetation, was not true were for bright sandy areas over the Saharan and Arabian deserts, where the albedo was significantly higher with the new parameters (shown in blue). In general all other areas had higher albedo in the new land surface parameters.

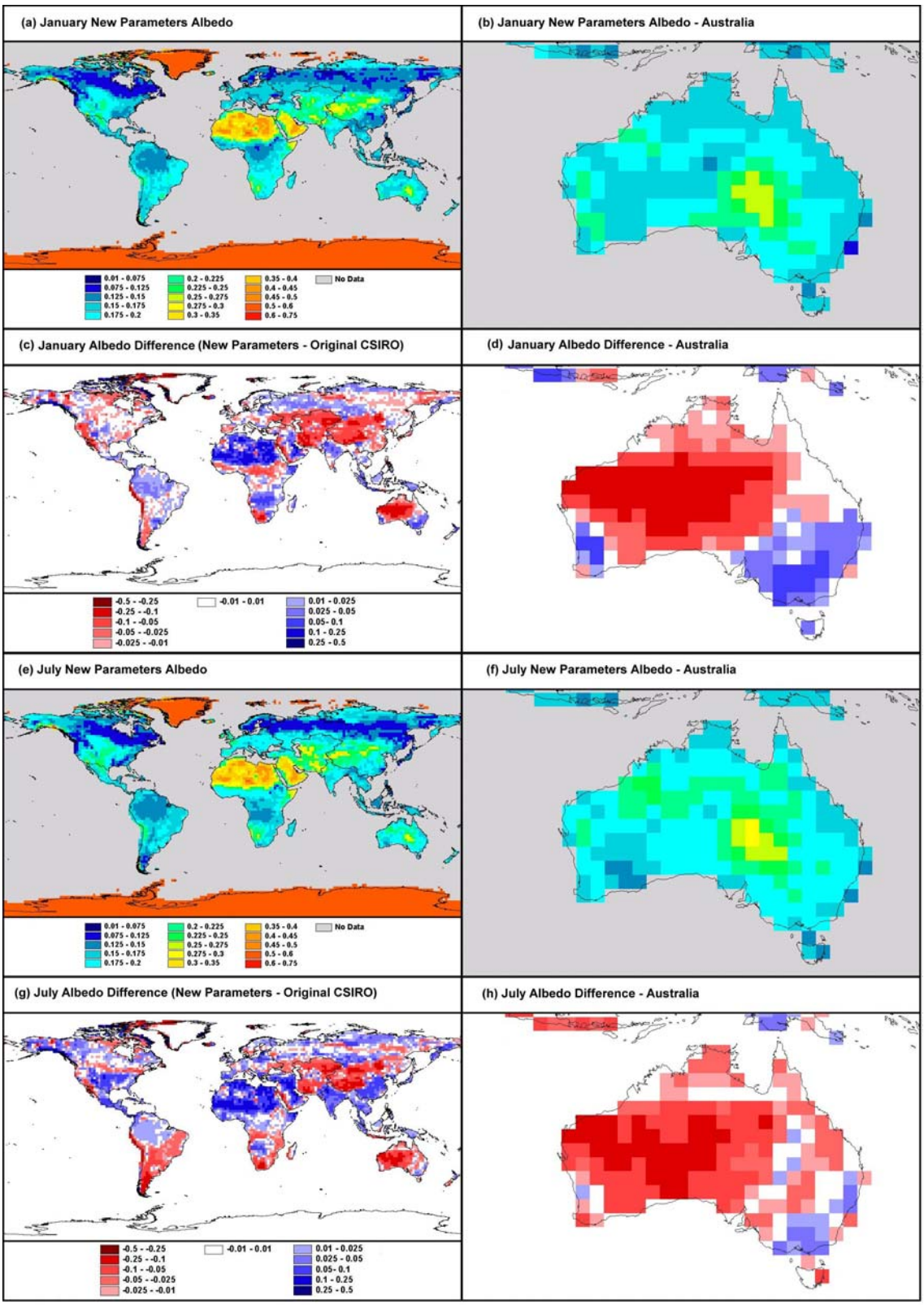

Figure 4.8 New CSIRO GCM Surface Albedo Parameter Evaluation: (a) New Parameters, January Albedo; (b) Detailed view of (a) over the Australian Region; (c) Difference between New Parameters and Original CSIRO January Albedo; (d) Detailed view of (c) over the Australian Region; (e) New Parameters, July Albedo; (f) Detailed view of (e) over the Australian Region; (g) Difference between New Parameters and Original CSIRO July Albedo; and (h) Detailed view of (g) over the Australian Region

The average Australian monthly albedo graph (*figure 4.7 d*) shows Australian albedo was significantly lower in the new parameters, with values 0.03 to 0.06 lower than the original parameters for all months. The largest differences between the parameters occurred in austral winter, with the closest values in austral summer. The Australian albedo differences maps (*figure 4.8 d* and *h*) show the largest differences were in central Australia where the new parameters were up to 0.18 lower than the original parameters. In the more densely vegetated areas of south eastern and south western Australia, the albedo of the new parameters was significantly higher with values up to 0.05 higher than the original CSIRO values. These differences were in general the same as those shown in the comparison of the original CSIRO parameters with the MODIS derived albedo.

Leaf Area Index

The monthly average leaf area index values of the new GCM parameters were evaluated against the original GCM parameters for zonal averages, and for the monthly average values for all land and for Australia, with the results of these evaluations shown in *figure 4.9*. The differences in the evaluations are shown geographically for January and July in the global and Australian LAI maps of *figure 4.10.*

The global average LAI graph (*figure 4.9 c*) shows the new parameters were 55 to 70 % lower than the original parameters for all months, with the largest difference in the boreal winter and the closest values in the boreal summer. The new parameters also had a stronger seasonal cycle with the boreal summer average LAI 33 % higher than the boreal winter average. In line with this seasonal cycle, the zonal average graphs (*figure 4.9 a* and *b*) show the smallest differences in the LAI were north of 40 N in the boreal summer, and south of 40S in austral summer. These same areas also had the greatest difference in winter LAI values, with the new parameters a fraction of the original parameters. For the remaining areas from 40 N to 40 S, the zonal average LAI of the new parameters was consistently less than 50 % of the value of the original parameters.

The global LAI difference maps (*figure 4.10 c* and *g*), show that the differences between the parameters were greatest in sparsely vegetated areas, such as deserts, shrublands and savannahs, where the new parameters were significantly lower than the original parameters. In densely vegetated areas, such as tropical forests, boreal forests and broadleaf forests, however, the LAI values of the two sets of parameters were very similar, and in some cases higher for the new parameters. These differences were consistent with the difference found between the original parameters and the AVHRR derived LAI mapping.

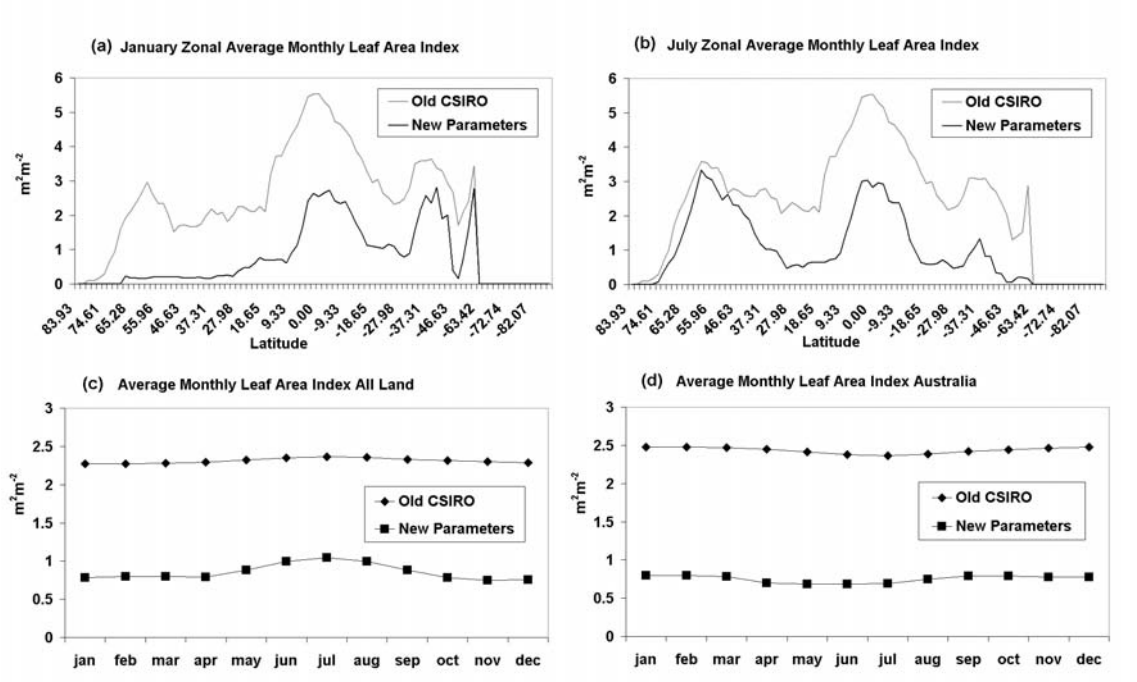

Figure 4.9 CSIRO GCM Leaf Area Index Evaluation: (a) January zonal average leaf area index for the new and original CSIRO GCM parameters; (b) same as (a) for July; (c) Average monthly leaf area index for all land for new and original CSIRO GCM parameters; and (d) same as (c) for the Australian continent

The average monthly Australian LAI graph (*figure 4.9 d*) shows the Australian LAI was 75 to 80 % lower for the new parameters than the original parameters for all months, with the largest difference in austral autumn and the smallest difference in austral spring. The graph shows the new parameters also had seasonal changes in average monthly Australian LAI, with austral autumn and winter up to 20 % lower than austral spring and summer. These seasonal changes appear to represent vegetation flushes in the north corresponding to the austral summer wet season, and vegetation flushes in the south with the austral spring.

The Australian LAI difference maps (*figure 4.10 d* and *h*) show that the greatest differences in LAI were in northern Australia, where the new parameters were up to 80 % lower than the original parameters. Only in the forested areas along the east coast margin and in the south west corner were the values of the two sets of parameters similar. Again this was consistent with the differences found between the original parameters and the AVHRR derived LAI mapping.

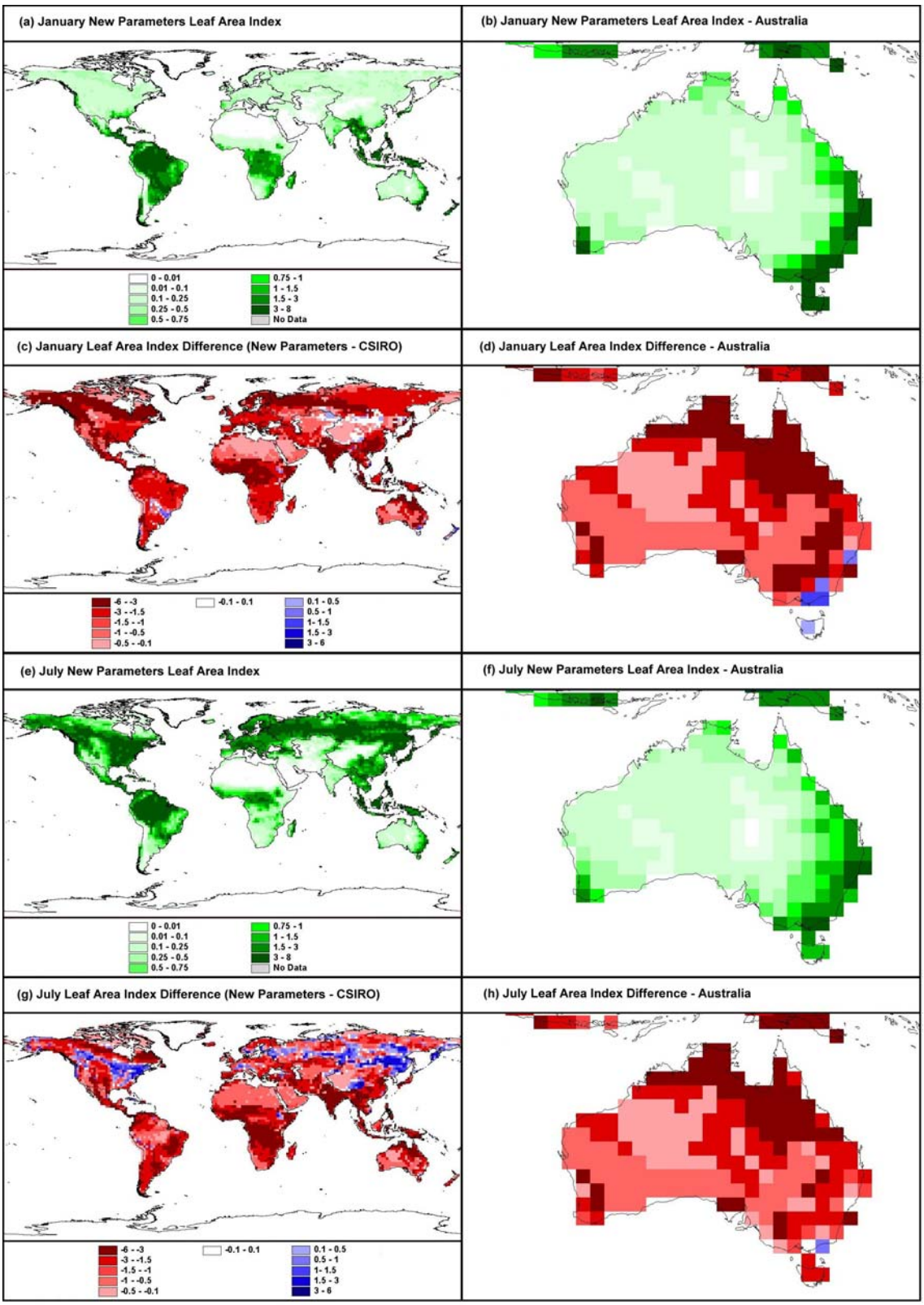

Figure 4.10 New CSIRO GCM Leaf Area Index Parameter Evaluation: (a) New Parameters, January Leaf Area Index; (b) Detailed view of (a) over the Australian Region; (c) Difference between New Parameters and Original CSIRO January Leaf Area Index; (d) Detailed view of (c) over the Australian Region; (e) New Parameters, July Leaf Area Index; (f) Detailed view of (e) over the Australian Region; (g) Difference between New Parameters and Original CSIRO July Leaf Area Index; and (h) Detailed view of (g) over the Australian Region

Vegetation Fraction

The monthly average vegetation fraction values of the new GCM parameters were evaluated against the original GCM parameters for zonal averages, and for the monthly average values for all land and for Australia. The results of these evaluations are shown in the graphs of *figure 4.11* and geographically for January and July in the global and Australian vegetation fraction maps of *figure 4.12*. The strong dependence of vegetation fraction on LAI, shown in Appendix A, suggested that the relationships between the new and original parameters for LAI would be reflected with vegetation fraction. This was supported by the zonal and average monthly vegetation fraction graphs, as well as in the global and Australian maps.

The global average vegetation fraction graph (*figure 4.11 c*) shows the new parameters had vegetation fraction 45 to 60 % lower for all months. The graph also shows the new parameters had the same strong seasonal cycle in vegetation fraction as they had in leaf area index, with boreal summer average vegetation fraction 29 % higher than the boreal winter average. The zonal average graphs (*figure 4.11 a* and *b*) show the zonal differences between the new parameters and the original parameters were in general the same as LAI for both January and July, however the differences between the two sets of parameters were proportionally smaller for vegetation fraction than they were for LAI.

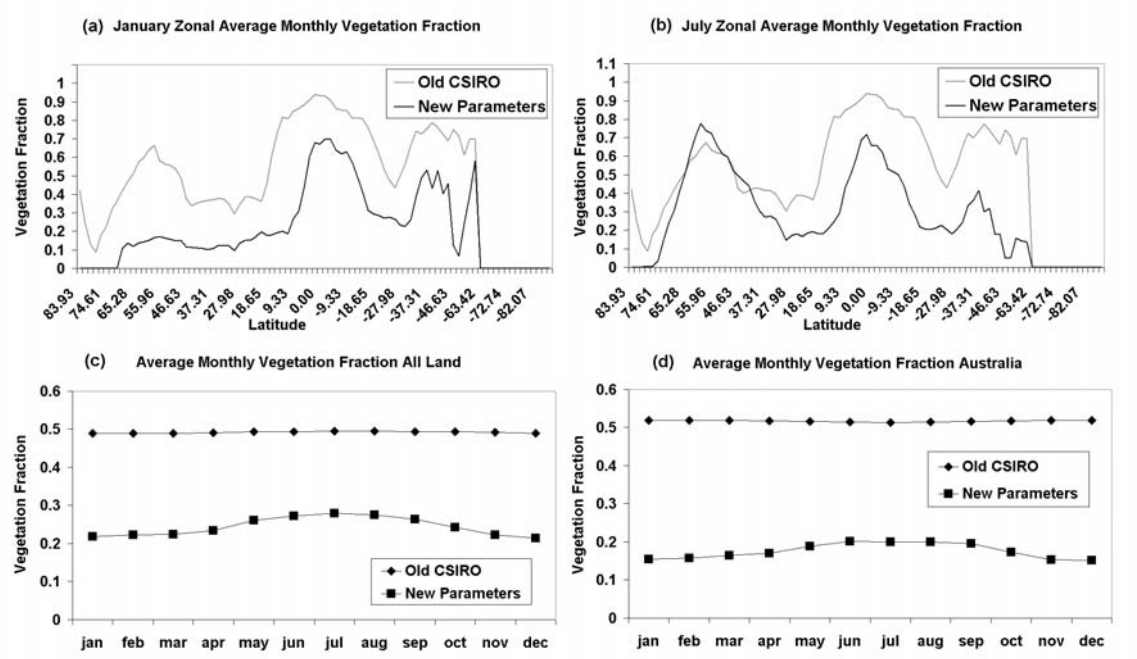

Figure 4.11 CSIRO GCM Vegetation Fraction Evaluation: (a) January zonal vegetation fraction for the new and original CSIRO GCM parameters; (b) same as (a) for July; (c) Average monthly vegetation fraction for all land for new and original CSIRO GCM parameters; and (d) same as (c) for the Australian continent

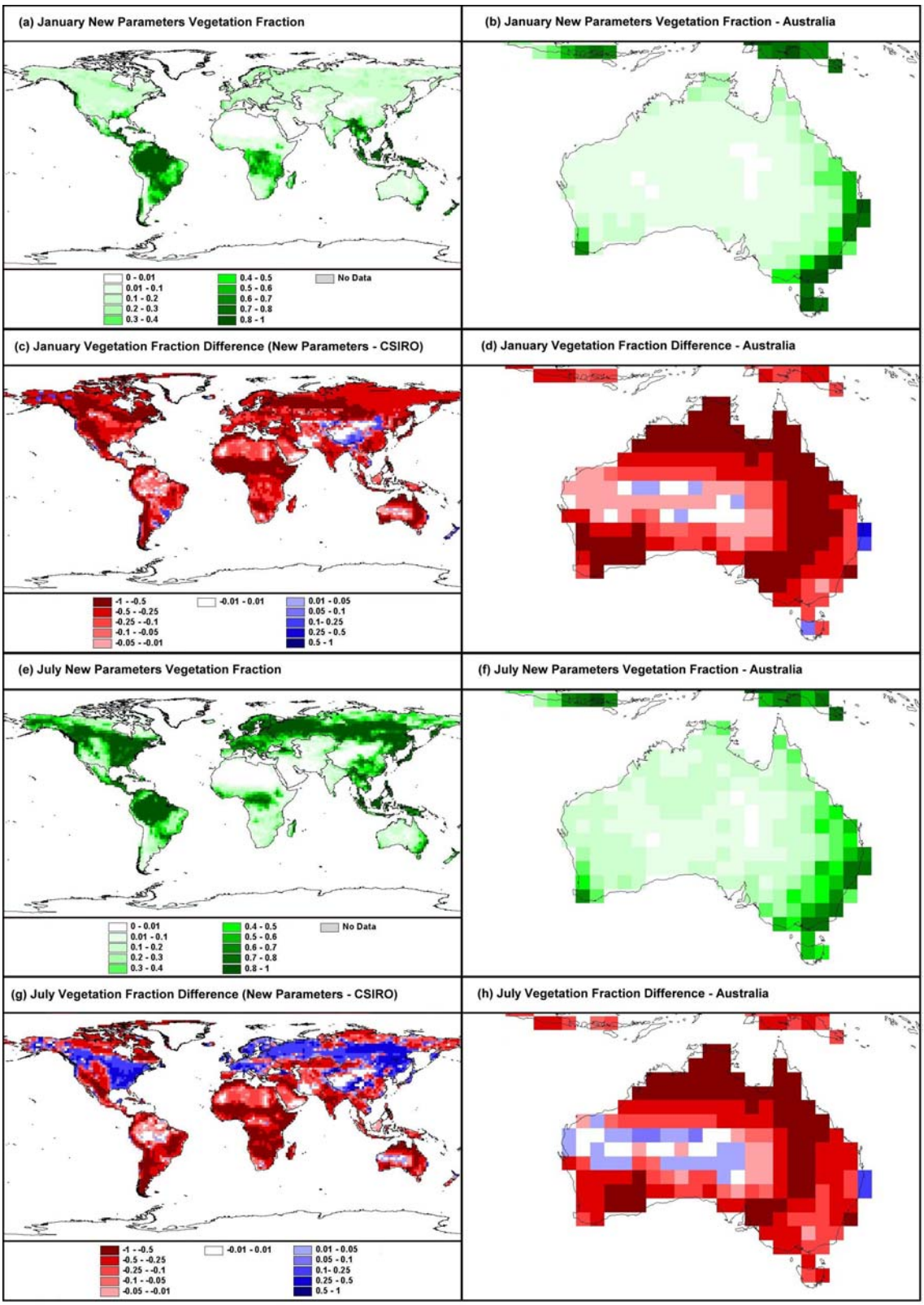

Figure 4.12 New CSIRO GCM Vegetation Fraction Parameter Evaluation: (a) New Parameters, January Vegetation Fraction; (b) Detailed view of (a) over the Australian Region; (c) Difference between New Parameters and Original CSIRO January Vegetation Fraction; (d) Detailed view of (c) over the Australian Region; (e) New Parameters, July Vegetation Fraction; (f) Detailed view of (e) over the Australian Region; (g) Difference between New Parameters and Original CSIRO July Vegetation Fraction; and (h) Detailed view of (g) over the Australian Region

The global vegetation fraction difference maps (*figure 4.12 c* and *g*) confirmed that the differences in vegetation fraction between the new and original parameters were geographically the same as the differences in LAI. The vegetation fraction was closest in areas with dense vegetation, such as tropical forests, boreal forests and broadleaf forests, and furthest apart in areas of sparse vegetation, such as deserts, savannahs, shrublands and grasslands.

The average monthly Australian vegetation fraction graph (*figure 4.11 d*) shows the new parameters had Australian vegetation fraction 60 to 70 % lower than the original parameters for all months, with the largest differences in austral summer and the smallest differences in austral winter. The graph shows the new parameters had different seasonal patterns in average vegetation fraction compared to LAI, with austral summer up to 28 % lower than austral winter. It is speculated the difference in the vegetation fraction seasonal cycle were predominantly due to the effect of lower sun angles in the austral winter, which increased vegetation fraction for a given LAI value, as shown in Appendix A. This effect appears to have greater influence on the vegetation fraction than the decrease in winter LAI.

The Australian vegetation fraction difference maps (*figure 4.12 d* and *h*) also show the differences in vegetation fraction between the new and original parameters were not geographically the same as the differences in LAI. The maps show the greatest differences in vegetation fraction were in a belt running from northern Australia south through western New South Wales and into South Australia, with a second area in south west Australia. In these areas the new parameters were a fraction of the original values. In central Australia, and the remainder of the south east and south west of the continent, the values of the two sets of parameters were much closer.

Unrestrained Stomatal Resistance

The monthly average unrestrained stomatal resistance values of the new GCM parameters were evaluated against the original GCM parameters for zonal averages, and for the monthly average values for all land and for Australia. The results of these evaluations are shown graphically in *figure 4.13* and geographically in the global and Australian unrestrained stomatal resistance maps of *figure 4.14*. Unrestrained stomatal resistance was used in the model to prescribe the minimum resistance to transpiration of a stomatal pore given optimum environmental conditions. The details of this relationship are described further in Appendix B.

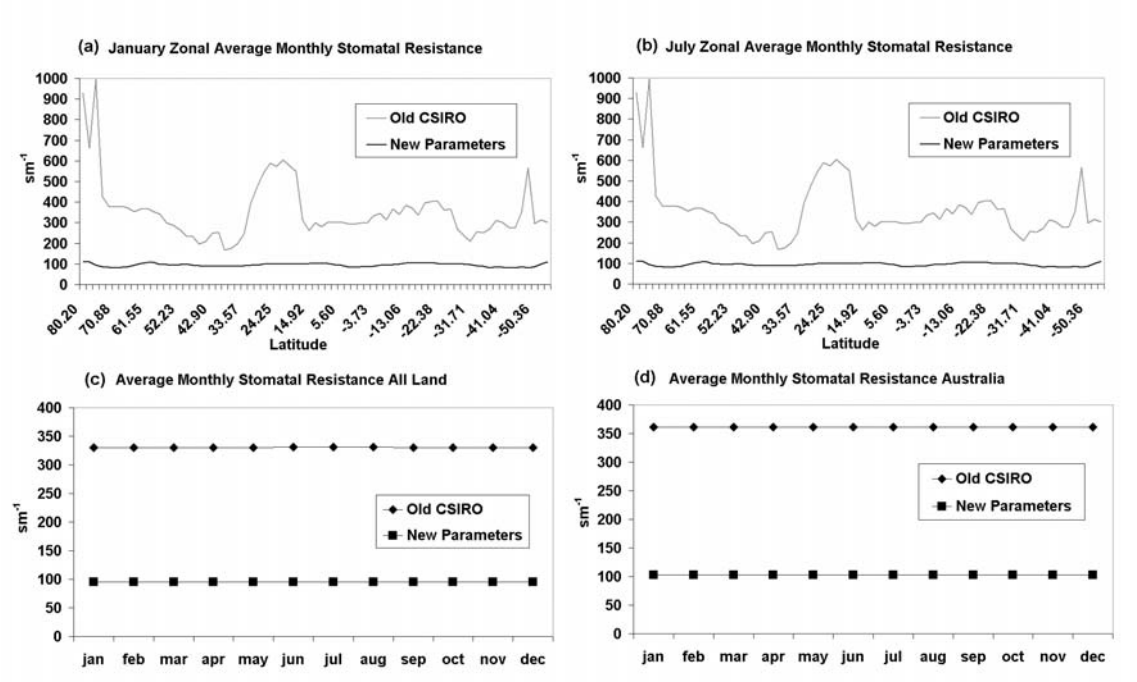

Figure 4.13 CSIRO GCM Unrestrained Stomatal Evaluation: (a) January zonal stomatal resistance for the new and original CSIRO GCM parameters; (b) same as (a) for July; (c) Average monthly stomatal resistance for all land for new and original CSIRO GCM parameters; and (d) same as (c) for the Australian continent

The average monthly global stomatal resistance graph (*figure 4.13 c*) shows the new parameters were on average 70 % lower than the original parameters for all months. There was no seasonal variation in unrestrained stomatal resistance in either set of parameters, as the stomatal resistance was derived from vegetation type in both cases. The zonal average stomatal resistance graphs (*figure 4.13 a* and *b*) show there were large peaks in unrestrained stomatal resistance for the original parameters north of 74 N, from 30 N to 15 N, and from 45 S to 50 S. These peaks were not evident in the new parameters. The global difference map (*figure 4.14 c*) shows these peaks correspond to areas dominated by bare soils such as the Artic, and the deserts of central Asia, Arabia and the Sahara. In these areas the original parameters prescribed stomatal resistance values of 995 sm^{-1} compared with the 110 sm^{-1} prescribed by the first ISLSCP project web site. In areas covered with vegetation, the new parameters were still significantly lower than the original parameters.

The average monthly Australian stomatal resistance graph (*figure 4.13 c*) shows the new parameters were 64 % lower than the original parameters for Australia. The Australian difference map (*figure 4.14 d*) shows that the difference in stomatal resistance was largest in northern and eastern Australia and closest in southern and central areas. The white areas in central Australia represent areas without vegetation in the original CSIRO parameters where the stomatal resistance is not used, and so is not comparable.

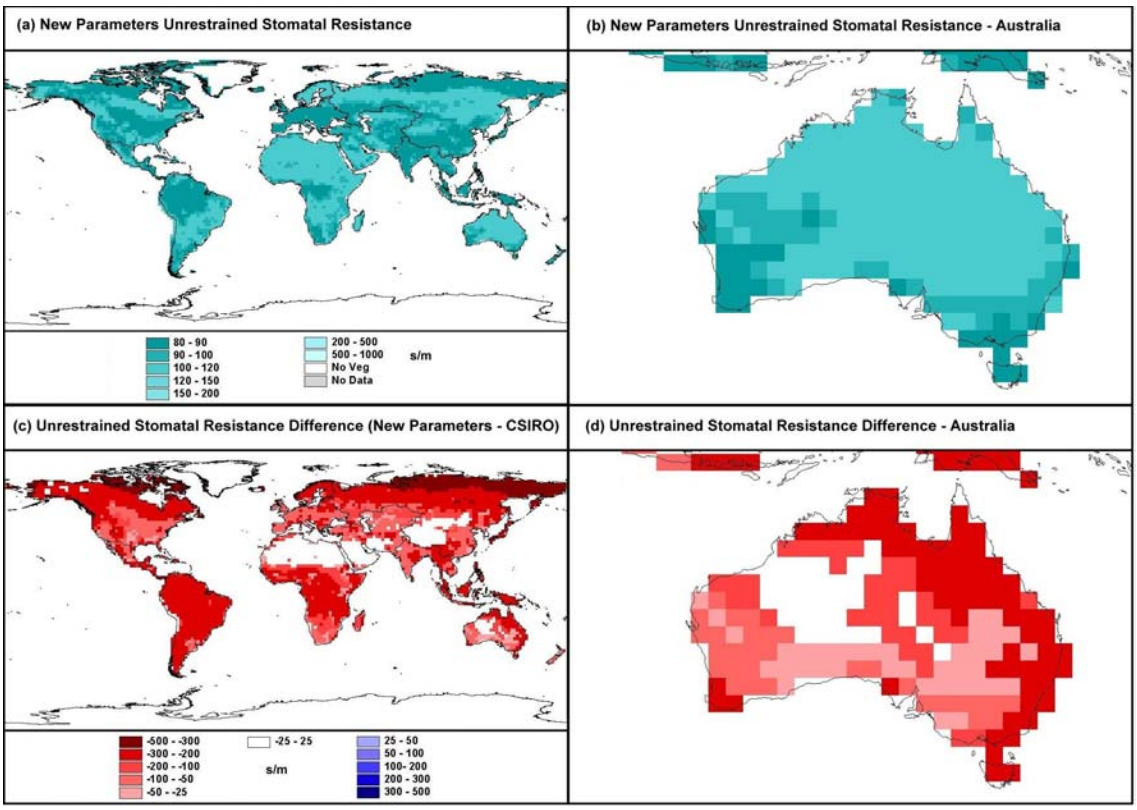

Figure 4.14 New CSIRO GCM Parameters Evaluation: New Parameters Unrestrained Stomatal Resistance; (b) Detailed view of (a) over the Australian Region; (c) Difference between New Parameters and Original CSIRO Unrestrained Stomatal Resistance; and (d) Detailed view of (c) over the Australian Region

Unrestrained Canopy Resistance

As the unrestrained stomatal resistance was used in the model to parameterise the resistance of the vegetation canopy to transpiration a more representative comparison of transpiration resistance was provided through unrestrained canopy resistance. Unrestrained canopy resistance was calculated following the transpiration model of *Noilhan and Planton* (1989) by dividing the unrestrained stomatal resistance by LAI. The relationship between unrestrained stomatal resistance, LAI, and unrestrained canopy resistance are described further in Appendix B.

The monthly average unrestrained canopy resistance derived from the new parameters was evaluated against the derived values from the original parameters for zonal averages, and for the monthly average values for all land and for Australia. The results of these evaluations are shown in the graphs in *figure 4.15* and geographically for January and July in the global and Australian unrestrained canopy resistance maps of *figure 4.16.*

The global average monthly unrestrained canopy resistance graph (*figure 4.15 c*) shows unrestrained canopy resistance of the new parameters was much closer to the original parameters than the unrestrained stomatal resistance. The primary reason for the closer values was the lower unrestrained stomatal resistance of the new parameters was divided by lower LAI resulting in a closer final value between the two sets of parameters. Consequently the new

parameters were only 10 to 35 % lower than the original parameters for all months. The graph shows the global average value of the new parameters also had strong seasonal variation in line with seasonal variation in global average LAI, with boreal summer average values 28 % lower than the boreal winter values.

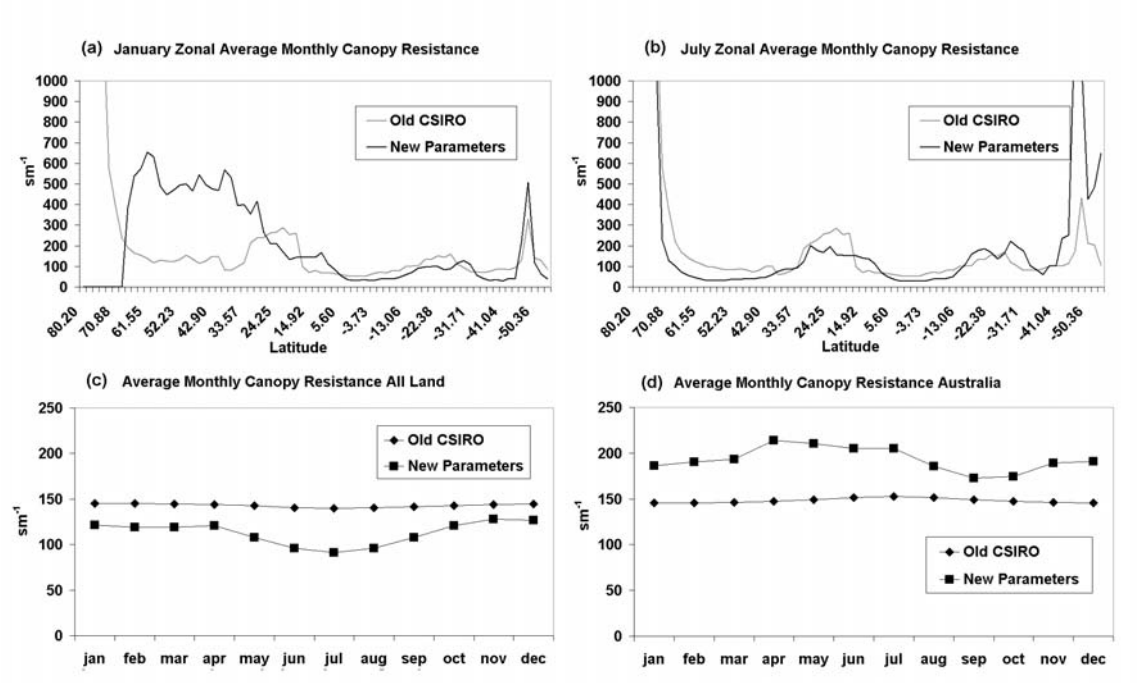

Figure 4.15 CSIRO GCM Unrestrained Canopy Resistance Evaluation: (a) January zonal canopy resistance for the new and original CSIRO GCM parameters; (b) same as (a) for July; (c) Average monthly canopy resistance for all land for new and original CSIRO GCM parameters; and (d) same as (c) for the Australian continent

The zonal averages graphs (*figure 4.15 a* and *b*) show that for most latitudes there was good general agreement in canopy resistance for both January and July. The largest difference between the two sets of parameters occur from 25 N to 65 N in boreal winter, with the new parameter canopy resistance significantly higher than the original parameters. The graphs show for the remaining areas in boreal winter, and for most areas in boreal summer, the canopy resistance of the new parameters was marginally lower than the original parameters.

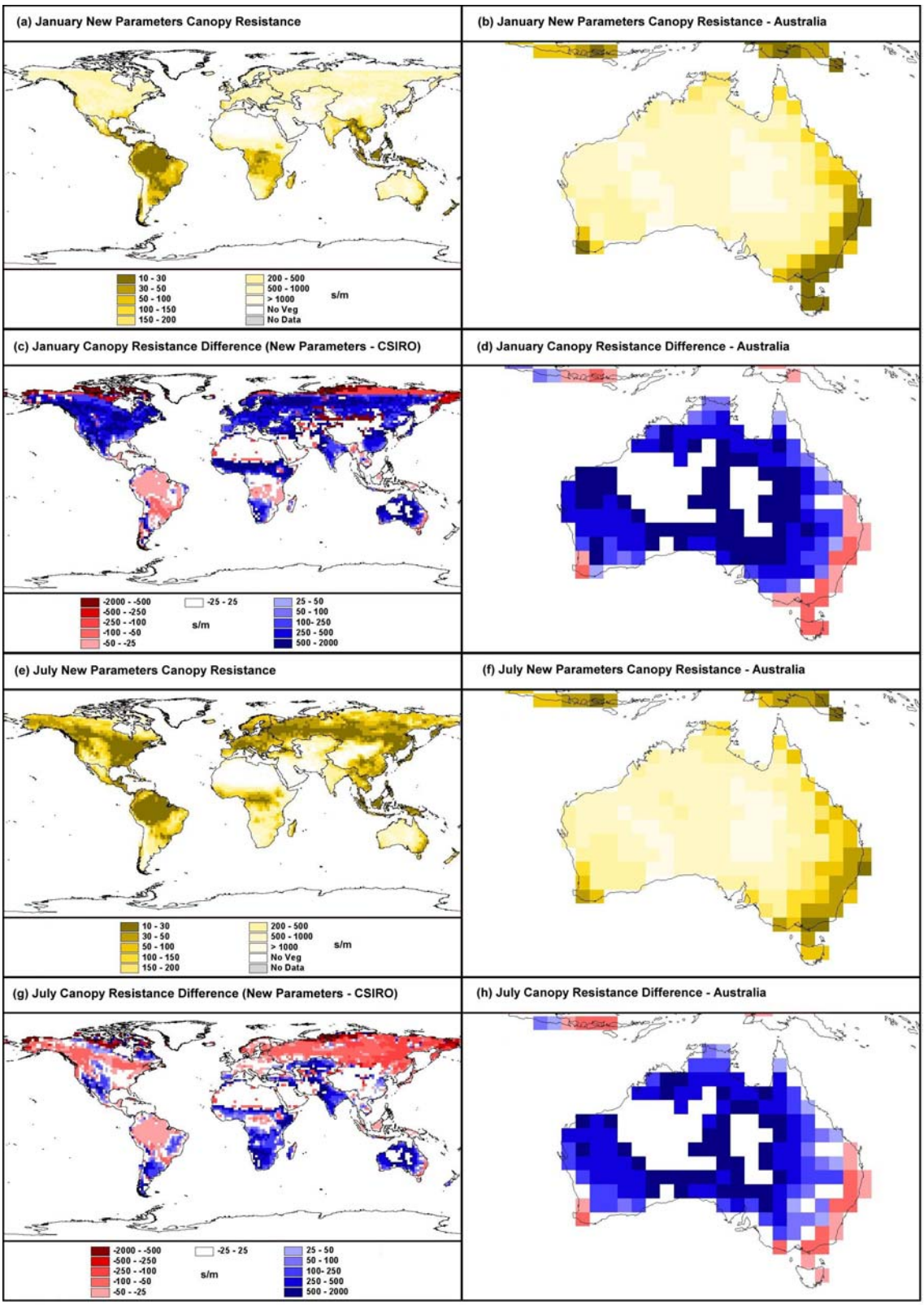

Figure 4.16 New CSIRO GCM Canopy Resistance Parameter Evaluation: (a) New Parameters, January Canopy Resistance; (b) Detailed view of (a) over the Australian Region; (c) Difference between New Parameters and Original CSIRO January Canopy Resistance; (d) Detailed view of (c) over the Australian Region; (e) New Parameters, July Canopy Resistance; (f) Detailed view of (e) over the Australian Region; (g) Difference between New Parameters and Original CSIRO July Canopy Resistance; and (h) Detailed view of (g) over the Australian Region

The global difference in canopy resistance maps (*figure 4.16 c* and *g*) show that while there was good general agreement in zonal average canopy resistance, there were major regional differences between the two sets of parameters. The new parameters had lower canopy resistance for dense vegetation, such as tropical forests, boreal forests and broadleaf forests, and higher canopy resistance for sparse vegetation, such as deserts, savannahs, shrublands and grasslands.

Following this trend the average monthly Australian unrestrained canopy resistance graph (*figure 4.15 d*) shows the new parameters were 15 to 45 % higher for Australia than the original parameters, with the largest differences in austral autumn and the smallest differences in austral spring. The graph shows the new parameters had seasonal changes in canopy resistance, with austral spring and summer up to 20 % lower than austral autumn and winter. These seasonal patterns reflect the dependence of canopy resistance on the seasonal patterns of LAI.

The Australian unrestrained canopy resistance maps (*figure 4.16 b* and *f*), show the lowest canopy resistance values for the new parameters were in forested areas along the eastern coastal margin and in the south west corner, with the canopy resistance increasing away from the coast, with the highest values in the arid center of the continent. The Australian difference in unrestrained canopy resistance maps (*figure 4.16 d* and *h*), show that the new parameters had lower canopy resistance over the forested areas than the original parameters, but significantly higher canopy resistance over the cropping lands, tropical savannahs, shrublands and grasslands of inland and northern Australia. The white areas of the difference maps in central Australia represent areas with no vegetation in the original parameters where canopy resistance is not calculated.

Surface Roughness

The monthly surface roughness of the new GCM parameters was evaluated against the original GCM parameters for zonal averages, and for the monthly average values for all land and for Australia. The results of these evaluations are shown in the graphs of *figure 4.17* and geographically for January and July in the global and Australian surface roughness maps of *figure 4.18.*

The global monthly average surface roughness graph (*figure 4.17 c*) shows the new land surface parameters had global surface roughness 10 to 25 % lower than the original parameters. The graph also shows the new parameters had strong seasonal cycles with maximum values in boreal spring and autumn, and minimum values in boreal summer and winter. The primary reason for these cycles was the dependence of the simplified roughness model on changes in LAI as described in Appendix E. The zonal average surface roughness graphs (*figure 4.17 a* and *b*) show that the new parameters had much higher surface roughness over the equator from 10 N to 10 S, but much lower values north and south in the areas from 10 N to 20 N and from 10 S to 35 S.

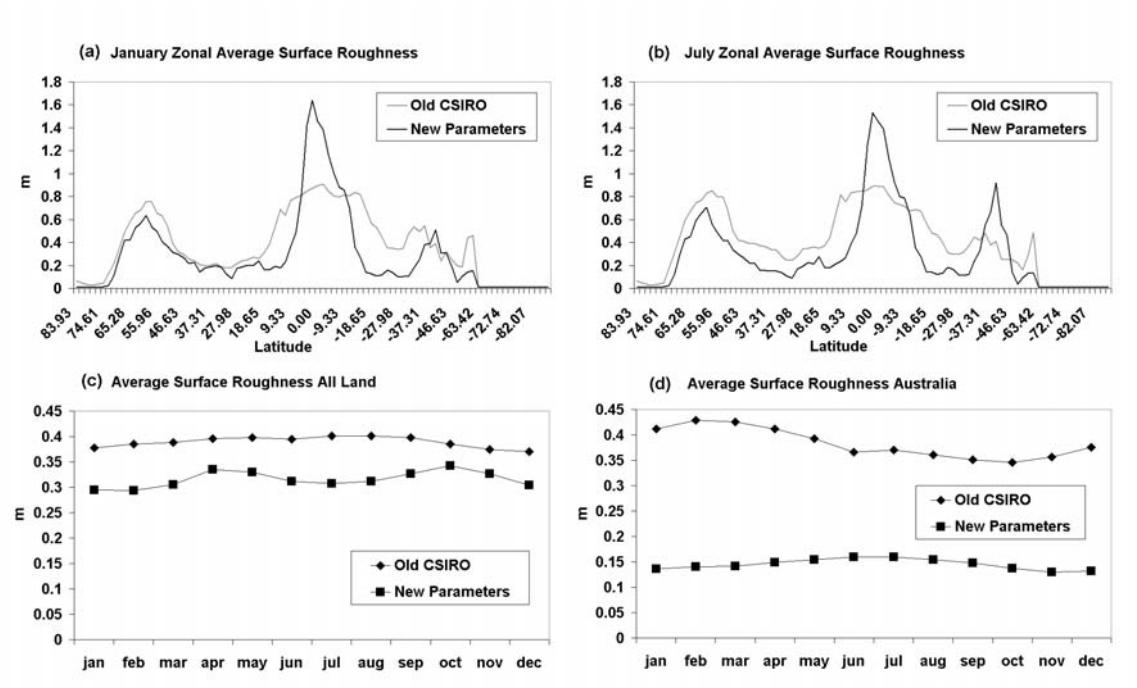

Figure 4.17 CSIRO GCM Surface Roughness Evaluation: (a) January zonal surface roughness for the new and original CSIRO GCM parameters; (b) same as (a) for July; (c) Average monthly surface roughness for all land for new and original CSIRO GCM parameters; and (d) same as (c) for the Australian continent

The global surface roughness difference maps (*figure 4.18 c* and g) show that the differences in surface roughness were related to vegetation density and height, with tall, more densely vegetated areas such as tropical forests, having significantly higher surface roughness in the new parameters than the original parameters. For low, sparse vegetation such as deserts, shrublands and grasslands, however, the relationship was reversed, with the new parameters having significantly lower surface roughness.

Following this trend, the monthly average Australian surface roughness graph (*figure 4.17 d*) shows the new parameters were 55 to 70 % lower than the original parameters for Australia. The new parameters also had a different seasonal cycle, with the highest surface roughness in austral winter, and the lowest values in austral summer. By comparison, the original parameters had the highest values in late austral summer and early austral autumn and the lowest values in austral spring. The Australian surface roughness difference maps (*figure 4.18 d* and *h*) show the new parameters were significantly lower than the original parameters for most of Australia, with the two sets of parameters similar only in the forested areas of the eastern coastal margin and the south west corner.

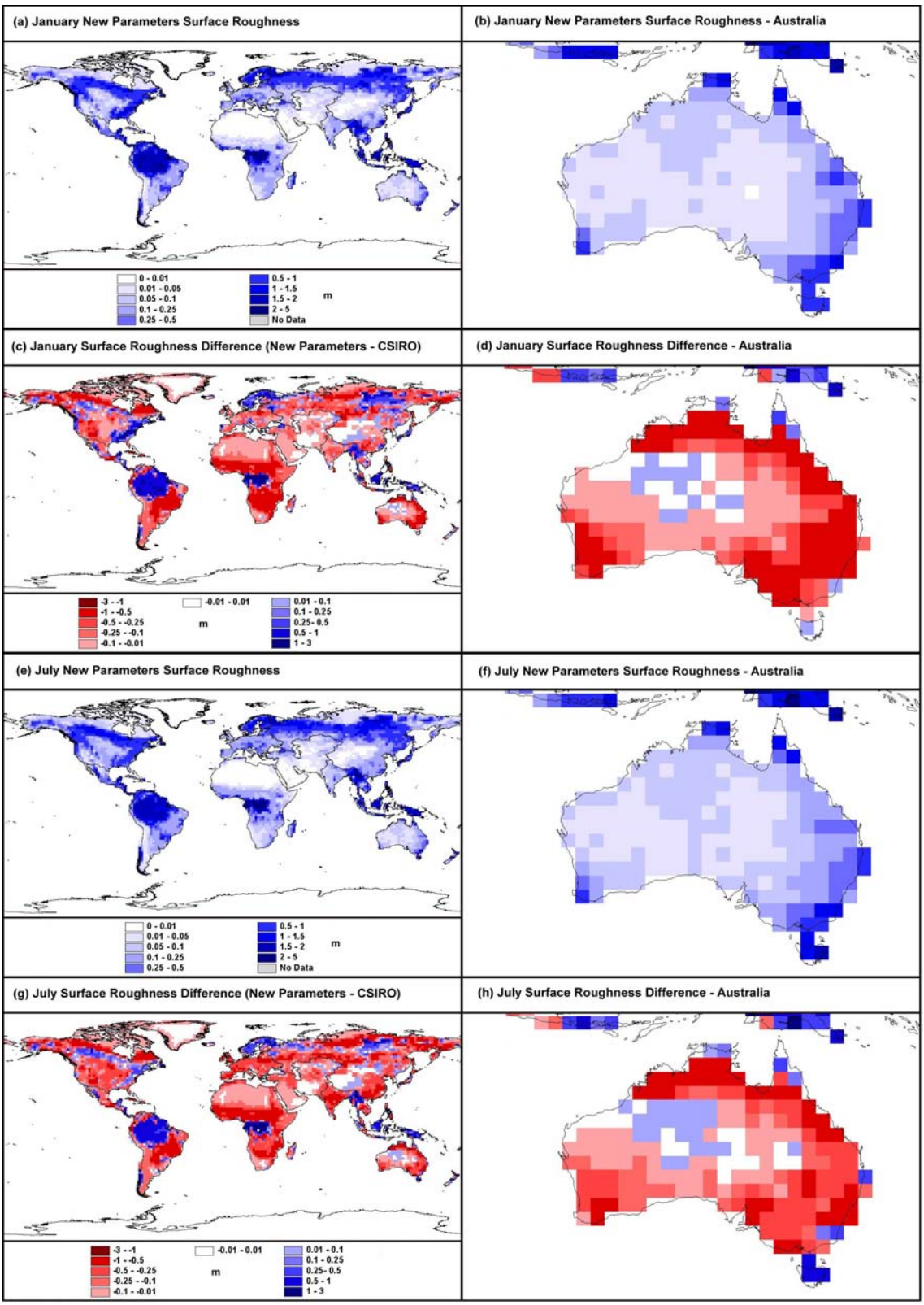

Figure 4.18 New CSIRO GCM Surface Roughness Parameter Evaluation: (a) New Parameters, January Surface Roughness; (b) Detailed view of (a) over the Australian Region; (c) Difference between New Parameters and Original CSIRO January Surface Roughness; (d) Detailed view of (c) over the Australian Region; (e) New Parameters, July Surface Roughness; (f) Detailed view of (e) over the Australian Region; (g) Difference between New Parameters and Original CSIRO July Surface Roughness; and (h) Detailed view of (g) over the Australian Region

4.3.3 Section Summary

1. New land surface data was integrated into physically based models to calculate fine-scale land surface parameters that would recreate the same land surface conditions in the CSIRO GCM as were observed in the data.
2. Radiation was calculated using the two stream radiation model, with vegetation and observed radiation dynamics prescribed from derived satellite data. Surface roughness was calculated using the simplified surface roughness model with vegetation properties prescribed from satellite derived data.
3. Linear averaging rules were applied to aggregate the fine-scale parameters to the grid increment of the model, capturing the fine-scale heterogeneity of the new data.
4. New parameters had similar global average land surface albedo for all months. Regionally new parameters had significantly lower albedo for sparsely vegetated areas of South America, Africa, Australia and Asia, with significantly higher albedo for Saharan and Arabian deserts. The rest of the land surface had similar or marginally higher albedo. Average Australian albedo was 0.03 to 0.06 lower, with largest differences in central Australia where the new parameters were up to 0.18 lower.
5. New Parameters had global average LAI 55 to 70 % lower. Regionally new parameters had significantly lower LAI in sparsely vegetated areas, and similar or marginally higher LAI in densely vegetated areas. Average Australian LAI was 75 to 80 % lower. The biggest differences were in northern Australia, with LAI values close only in forested areas.
6. New parameters had global average vegetation fraction 45 to 60 % lower. Regionally new parameters had significantly lower vegetation fraction in sparsely vegetated areas, and similar vegetation fraction in densely vegetated areas. Average Australian vegetation fraction was 60 to 70 % lower. Greatest differences were from northern Australia through central Australia, and in south west Australia. For the rest of the continent, the values were much closer.
7. New parameters had average global stomatal resistance 70 % lower. Regionally new parameters had largest differences in areas with bare soils in the Artic, and the deserts of central Asia, Arabia and the Sahara, however areas with dense vegetation also were significantly lower. Average Australian stomatal resistance was 64 % lower, with largest differences in northern and eastern Australia and closest values in southern and central areas.
8. New parameters had average global canopy resistance 10 to 35 % lower. Regionally new parameters had higher canopy resistance for sparse vegetation and lower canopy resistance for dense vegetation. Average Australian canopy resistance was 15 to 45 % higher, with significantly higher canopy resistance in inland and northern Australia, and lower canopy resistance over forested areas.

9. New parameters had average global surface roughness 10 to 25 % lower. Regionally new parameters had larger surface roughness for taller, denser vegetation and smaller surface roughness for low, sparse vegetation. Average Australian surface roughness was 55 to 70 % lower, with values lower for most of Australia, with values similar only in forested areas
10. Generating CSIRO GCM land surface parameters with physically realistic models from new relatively fine-scale land surface data, represents an important step in overcoming the limitations of using the existing model for the climate impacts of Australian land cover change experiments in Chapter 5.

4.4 New Land Surface Parameter Sensitivity Experiments

4.4.1 Methods

The impacts the new land surface parameters have on the climate simulated in the CSIRO GCM were evaluated by comparative sensitivity experiments with the new land surface parameters and with the original CSIRO land surface parameters. The experiments were performed as global climate simulations for 1969 to 1999, with the initial 6 year period of each climate simulation discarded as a "spin up" period. Average climatological means for each experiment were compared with observed climate records for the remaining 1975 to 1999 period to evaluate the performance of the CSIRO GCM with the new and original land surface parameters. Differences in a range of climate variables were compared to differences in land surface parameters to investigate and find possible explanations for how the new land surface parameters influenced climate simulation in the CSIRO GCM.

To ensure the experiments had the same initial conditions, the experiments were restarted with the new and original land surface parameters from a long-term climate simulation with the original land surface parameters. Other sources of climate variability unrelated to the land surface were kept consistent in both experiments by prescribing the same monthly observed sea surface temperatures and sea ice distributions for the 1969 to 1999 period, from the Hadley Centre global records (*Rayner et al.*, 1996). Other forcing factors, such as atmospheric concentration of CO_2, were also kept consistent by keeping their values unchanged for both experiments.

At the global and continental scale the climate simulated by the two experiments were compared to interpolated global historical weather records to assess the performance of the experiments in reproducing historical climate. The Terrestrial Air Temperature and Precipitation Monthly Time Series developed by the University of Delaware, Department of Geography (*Willmott and Robeson*, 1995) was sourced for global land climate records. To provide insight into the processes that may be driving the differences identified between the climate in the modelling experiments and the observed climate, global climatological maps of the two

experiments were assessed for differences in land surface characteristics, fluxes and climate. The differences in the maps were used in conjunction with global mean values for these properties and with NCEP reanalysis climate data (*Kistler et al.,* 2002), to assess the relative differences between the modelling experiments, compared to the difference between the CSIRO GCM, and other climate models and observations.

More detailed analysis was performed for Australia to assess the suitability of using the CSIRO GCM with the new land surface parameters in the Australian land cover change experiments of Chapter 5. The Queensland Department of Natural Resources and Mines' SILO database (*Jeffery et al.*, 2001) was sourced for historical weather records of air temperature, precipitation, and mean sea level pressure over the Australian continent for the 1975 to 1999 period. The differences between the climate observed in the Australian weather records and the modelling experiments, were investigated for regional differences by mapping the difference between the observed and modelled climatalogical means over Australia. To provide insight into the processes that may be driving the Australian continental and regional differences, climatological maps of the two experiments were assessed for differences in land surface characteristics, fluxes and climate for the area surrounding Australia. The differences in the maps were used in conjunction with Australian mean values for these properties to assess the influence of the new land surface parameters on climate and climatic processes over Australia.

4.4.2 Global and Continental Modelling Evaluation

The results of the global and continental assessments of the New Parameters and Original CSIRO GCM experiments against historical weather observations are shown for average climatological air temperature in *table 4.1*, and for average climatological precipitation in *table 4.2*. The differences between the experiments and observations, and the spatial correlations of the climatological means of the experiments to the observations are graphed for air temperature in *figure 4.19*, and for precipitation in *figure 4.20*. Spatial correlations were based on spatial differences between the modelled and observed climate values at the GCM grid increment.

The air temperature difference graphs (*figure 4.19 a* and *c*) show that over all land areas, the New Parameters experiment increased the cool air temperature biases of the Original CSIRO experiment, for both austral summer (DJF) and winter (JJA). The air temperature spatial correlation graphs (*figure 4.19 b* and *d*) show the spatial correlation of air temperature over all land was similar for the two experiments, with the New Parameters experiment marginally higher for DJF and the Original CSIRO experiment marginally higher for JJA.

Of the continents shown (*figure 4.19 a* and *c*), the largest increase in air temperature bias was in North America during DJF, where the cool bias the Original CSIRO experiment was increased from –1.2 ^{O}C to –2.9 ^{O}C in the New Parameters experiment. Africa, Asia and South America also experienced increased cool biases in DJF, however, in Australia there was a change from the marginal cool bias with the Original CSIRO parameters to a warm bias in the New Parameters experiment. The greatest reduction in continental air temperature bias also was in North America during JJA, where the warm bias of the Original CSIRO experiment was decreased from 1.2 ^{O}C to 0.6 ^{O}C in the New Parameters experiment. During JJA, there also were increases the warm bias in Asia, and the cool biases in Australia and Africa. In South America the marginal warm bias with the Original CSIRO parameters changed to a cool bias in the New Parameters experiment.

The air temperature spatial correlation graphs (*figure 4.19 b* and *d*) show the differences in spatial correlation with observed air temperature were mixed geographically and seasonally for the two experiments, with as many continents showing increased spatial correlation in the New Parameters experiment as decreased. All differences in continental air temperature spatial correlation between the two experiments, however, were small.

The precipitation difference graphs (*figure 4.20 a* and *c*) show that over all land areas, the New Parameters experiment had a marginal reduction in the wet bias of the Original CSIRO experiment for DJF, and a marginal increase in the dry bias for JJA. The precipitation spatial correlation graphs (*figure 4.20 b* and *d*) show spatial correlation with observed precipitation over all land was marginally higher in the New Parameters experiment than the Original CSIRO experiment for DJF, but marginally lower for JJA.

The largest increase in precipitation bias was in Australia over DJF, where the Original CSIRO experiment bias of 0.51 mm/day increased to 1.04 mm/day in the New Parameters experiment. Also over DJF, the New Parameters experiment had reductions in the wet bias of North America and the dry biases of South America, but had increases in the dry biases of Asia and Africa. During JJA the New Parameters experiment had a wet bias for Australia compared to the dry bias of the Original CSIRO experiment. Also during JJA the New Parameters increased the wet bias for North America, and increased the dry biases for Asia and Africa. Only over South America was the dry bias reduced, with the reduction relatively small compared to the size of the bias.

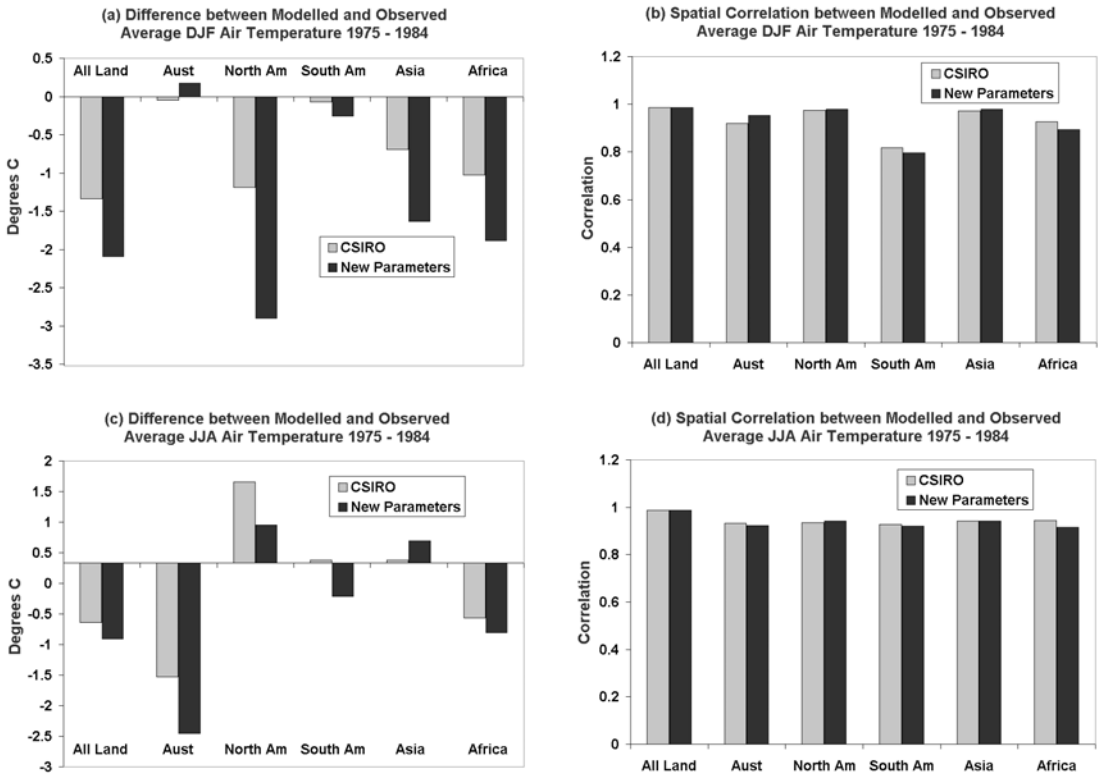

Figure 4.19 Average Austral Summer (DJF) and Winter (JJA) Air Temperature for 1975 – 1999: Differences (a and c) and spatial correlations (b and d) for Original CSIRO and New Parameters experiments compared with University of Delaware observed precipitation. (All land; Australia (Aust); North America (NorthAm); South America (SouthAm); Asia; and Africa)

Table 4.1 Evaluation of average continental Air Temperature statistics for the New Parameters and the Original CSIRO Experiments against Delaware observational data for 1975 – 1999. Seasons shown: Austral Summer (DJF) and Winter (JJA). Statistics shown: continental climatic mean values and spatial correlations between climatic mean maps of Models and Delaware observations

Continent	Season	CSIRO (^{O}C)	New Params (^{O}C)	Delaware (^{O}C)	CSIRO Corr.	New Params Corr.
All Land	DJF	2.0	1.2	3.3	0.986	0.985
	JJA	13.1	12.9	14.0	0.988	0.987
Australia	DJF	27.2	27.5	27.3	0.919	0.953
	JJA	13.2	12.3	14.9	0.931	0.923
North America	DJF	-10.5	-12.2	-9.3	0.975	0.979
	JJA	18.0	17.4	16.8	0.934	0.941
South America	DJF	23.1	22.9	23.2	0.817	0.797
	JJA	19.2	18.6	19.1	0.928	0.921
Asia	DJF	1.7	0.8	2.4	0.972	0.978
	JJA	21.6	21.8	21.5	0.941	0.943
Africa	DJF	20.4	19.6	21.4	0.926	0.894
	JJA	24.3	24.1	25.1	0.945	0.915

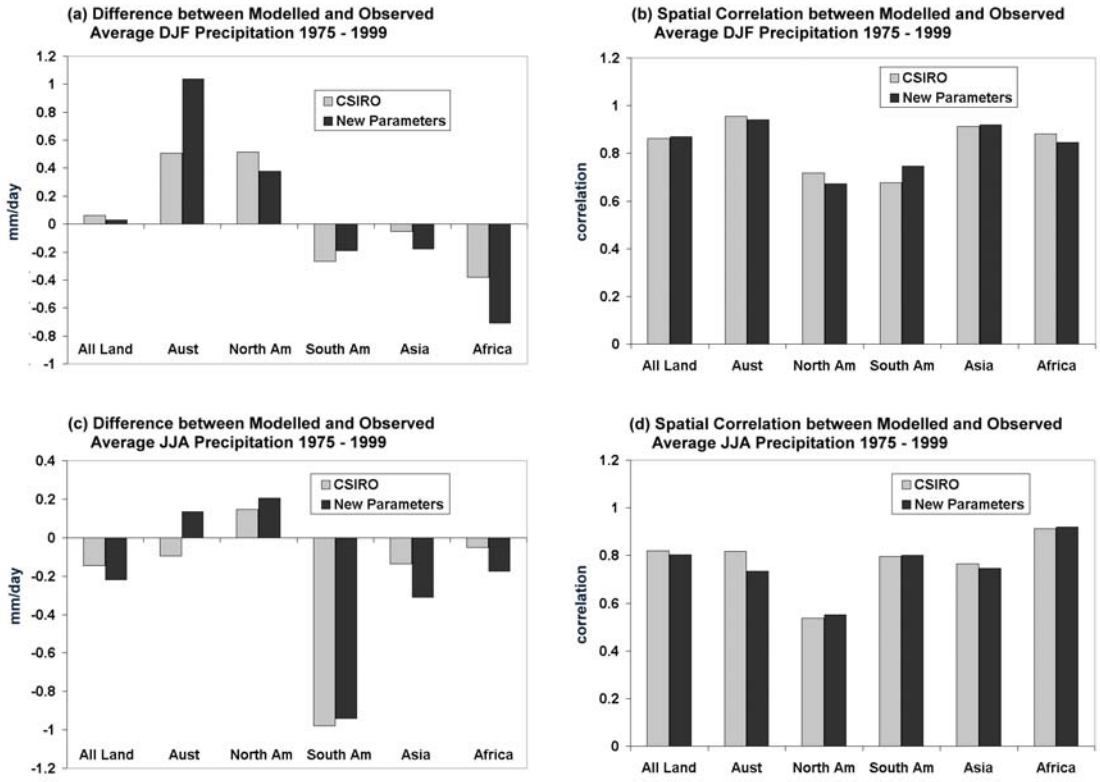

Figure 4.20 Average Austral Summer (DJF) and Winter (JJA) Precipitation for 1975 – 1999: Differences (a and c) and spatial correlations (b and d) for Original CSIRO and New Parameters experiments compared with University of Delaware observed precipitation. (All land; Australia (Aust); North America (NorthAm); South America (SouthAm); Asia; and Africa)

Table 4.2 Evaluation of average continental Precipitation statistics for the New Parameters and the Original CSIRO Experiments against Delaware observational data for 1975 – 1999. Seasons shown: Austral Summer (DJF) and Winter (JJA). Statistics shown: climatic mean values, and spatial correlations between climatic mean maps of Models and Delaware observations

Continent	Season	CSIRO (mm/day)	New Params (mm/day)	Delaware (mm/day)	CSIRO Corr.	New Params Corr.
All Land	DJF	1.94	1.91	1.88	0.863	0.871
	JJA	2.06	1.99	2.21	0.821	0.802
Australia	DJF	2.78	3.31	2.28	0.955	0.941
	JJA	0.60	0.83	0.70	0.817	0.735
North America	DJF	1.91	1.78	1.40	0.717	0.673
	JJA	2.35	2.41	2.20	0.538	0.551
South America	DJF	5.23	5.31	5.50	0.677	0.746
	JJA	1.92	1.96	2.90	0.796	0.801
Asia	DJF	1.05	0.92	1.10	0.911	0.919
	JJA	4.64	4.47	4.78	0.766	0.746
Africa	DJF	1.53	1.20	1.91	0.883	0.847
	JJA	1.03	0.90	1.08	0.911	0.919

Like air temperature, the differences in spatial correlation of experiments with observed precipitation (*figure 4.20 b* and *d*) were mixed geographically and seasonally, and again the changes in spatial correlation were relatively small. The largest differences were a decrease in spatial correlation for the New Parameters experiment in Australia during JJA, decreases in spatial correlation in North America and Africa during DJF, and a significant increase in spatial correlation for South America during DJF.

4.4.3 Processes Driving Global and Continental Differences

The differences between the climate simulated in the models were assessed at global scales to provide insight into the processes that may be driving the overall increase in cool biases over land, and the increases in wet and dry precipitation biases for Australia, Asia, and Africa. The global mean climate and surface fluxes of the two experiments and the NCEP reanalysis climate data are shown for austral summer (DJF) in *table 4.3* and for winter (JJA) in *table 4.4*. The global differences between the two experiments for climate variables, model calculated land surface characteristics, and surface fluxes are shown in the differences maps of *figure 4.21*, *4.22, 4.23* and *4.24* for DJF and JJA.

Austral Summer Analysis

The average 1975 to 1999 DJF climate statistics for the New Parameters and the Original CSIRO experiments are shown for global averages in *table 4.3* compared to NCEP reanalysis data for the same period. Both the average global surface temperature and the near surface air temperature were marginally cooler in the New Parameters experiment for DJF, with average global precipitation marginally higher. The average global DJF short wave surface radiation flux, and sensible heat flux both were marginally lower for the New Parameter experiment, with latent heat flux marginally higher.

These statistics suggest that the new parameters did have an influence on the CSIRO GCM producing a global DJF surface climate that was slightly cooler with less incoming solar radiation absorption and reduced sensible heat flux. The statistics also suggest that the surface climate was marginally wetter with increased precipitation and latent heat flux. The differences between the two experiments, however, were relatively small when compared to the differences between the CSIRO GCM experiments and the NCEP reanalysis data.

Making sense of the all the differences between the two models in the maps of *figure 4.21*, *4.22, 4.23* and *4.24*, requires interpretation and some conjecture as the processes are interacting, influencing each other at a range of scales, with direct causality hard to demonstrate. Using the theory of Chapter 2 along with the emerging patterns shown in the difference maps, hypotheses can be developed to explain how the new land surface parameters, which are the only climate forcing changes in the experiments, impact on the DJF climate simulated in the CSIRO GCM.

Table 4.3 Global average Austral Summer (DJF) climate statistics for the New Parameters, Original CSIRO, and NCEP reanalysis data for the climate period 1975 – 1999

Variable	CSIRO	New Parameters	New – CSIRO	NCEP
Surface Temperature (^{O}C)	12.60	12.39	-0.21	13.01
Screen Air Temperature (^{O}C)	11.72	11.48	-0.24	12.39
Precipitation (mm/day)	2.84	2.85	0.01	2.69
Surface SW Rad. Flux (Wm^{-2})	168.45	167.15	-1.30	163.63
Sensible Heat Flux (Wm^{-2})	23.66	22.91	-0.75	13.82
Latent Heat Flux (Wm^{-2})	80.68	81.11	0.43	80.00

The strong cooling over the Northern Hemisphere evident in DJF air temperature difference map (*figure 4.21 a*), appears to be due to the much higher calculated albedo (*figure 4.23 e*) over northern Asia, Europe and North America. Interestingly the differences in albedo do not come directly from the differences prescribed by the land surface parameters. It is speculated that for the New Parameters experiment, the marginally higher prescribed albedo (*figure 4.8 c* and *g*) produces year round reduced short wave radiation flux. The year round reduced radiation flux combines with increased boreal summer latent heat fluxes from the lower canopy resistance (*figure 4.16 g*) to produce cooler all year round temperatures in these areas. The cooler temperatures promote snow to fall and settle sooner in the boreal autumn/winter in these areas in New Parameters experiment, significantly increasing the effective surface albedo, with a snow and albedo feedback in same manner as suggested by *Kabat et al.* (2004). The colder temperatures penetrate south allowing snow to fall sooner reinforcing the snow and albedo feedback further to the south.

The reduced snow depth in higher latitudes shown in the DJF snow depth differences map (*figure 4.23 c*), appears to be the result of colder air temperatures reducing sensible and latent heat flux in these areas (*figure 4.24 a* and *c*), with the reduced convective activity resulting in the higher average mean sea level pressure shown in these areas (*figure 4.21 e*). The higher pressure and reduced convective activity results in reduced precipitation in these northern regions (*figure 4.21 c*), resulting in the reduced snow depth. To the south of these areas there is increased snow depth in Europe, central North America, China, the Korean Peninsula, and Japan, even though the precipitation is reduced in these areas. It is speculated that the colder temperatures from the snow and albedo feedback, result in more of the (reduced) precipitation falling as snow than falls as snow in the Original Parameters experiment. This is hypothesis further supported as the areas with large differences in snow depth correspond with the areas with significantly increased average calculated albedo.

The lower mean sea level pressure over the northern Pacific Ocean and the Atlantic Ocean (*figure 4.21 e*) are speculated to be products of the prescribed sea surface temperatures which are the same for both experiments. In the New Parameters experiment the air above the sea surface is relatively warmer than the colder surrounding land surface air. This relative difference also would account for the higher latent and sensible heat fluxes in these areas (*figure 4.24 a* and *c*). The relative increased temperature difference between the ocean and land air temperatures, may account for the lower short wave radiation fluxes over these areas due to increased cloud optical thickness associated with the increased precipitation (*figure 4.21 c*), and sea mist.

The differences in DJF calculated albedo for land away from the effects of snow cover, can be seen to be the direct result of differences prescribed by albedo in the land surface parameters of the two experiments (*figure 4.23 e* and *4.8 c*). Over the Sahara and the Arabian Peninsula, the increased albedo results in reduced short wave radiation flux (*figure 4.23 g*), with less radiative heating producing cooler air temperatures and reduced sensible heat flux (*figure 4.21 a* and *4.24 a*). As suggested by *Charney* (1975) and others the reduced sensible heat flux leads to enhanced subsidence over these areas, producing the higher mean sea level pressure (*figure 4.21 e*). The increased subsidence reduces precipitation and cloud cover to the south over Sub-Saharan Africa and over the Congo rainforests (*figure 4.21 c* and *4.23 a*). With the decreased cloud cover, air temperature differences in southern Africa appear to be the result of regional differences in surface albedo driving changes in short wave radiation flux, with all three having similar spatial patterns.

Over the Amazon the reduced canopy resistance of the New Parameters experiment, results in increased DJF latent heat flux (*figure 4.24 c* and *4.16 c*), with the increased latent heat resulting in the increase in DJF cloud cover and precipitation over the region (*figure 4.21 c* and *4.23 a*). The increased cloud cover combines with the increased albedo to reduce short wave radiation flux (*figure 4.23 e* and *g*), with the reduced short wave radiation resulting in cooling of air temperature and reduction in sensible heat flux over the area (*figure 4.21 a* and *4.24 a*). It appears the decrease in thermal convection is greater than the increase in moist convection with the net product an increase in mean sea level pressure over the area (*figure 4.21 e*).

In Australia the increased DJF short wave radiation flux, with associated increases in air temperature and sensible heat flux resulted in increased thermal convection, which produced the lower mean sea level pressure shown over the region (*figure 4.21 e*). The lower pressure over Australia combined with the higher pressure over Asia to increase the monsoon flow from southern Asia into northern Australia and into the South Pacific Convergence Zone (SPCZ) to the north east (*figure 4.22 e*). The increased monsoon flow increased moisture flux from the oceans to the north of Australia into the continent and into the SPCZ, which results in increased DJF precipitation and cloud in both regions (*figure 4.21 c* and *4.23 a*).

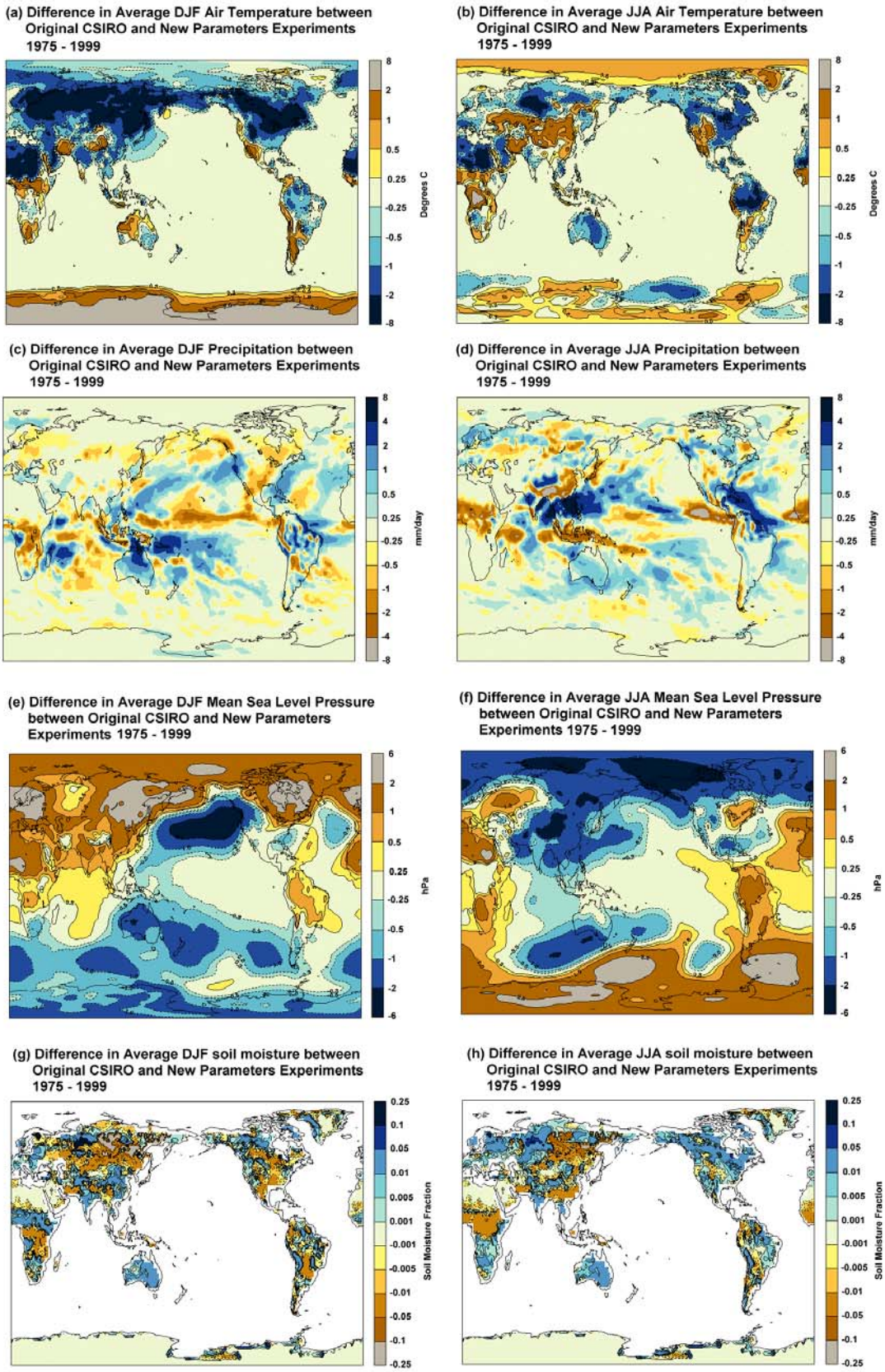

Figure 4.21 Global differences in average climate between the Original CSIRO and New Parameters experiments (New – Old) for Austral Summer (DJF) and Winter (JJA) 1975 – 1999 for: Average Air Temperature (a) and (b); Average Precipitation (c) and (d); Average Mean Sea Level Pressure (e) and (f); and Average Soil Moisture (g) and (h)

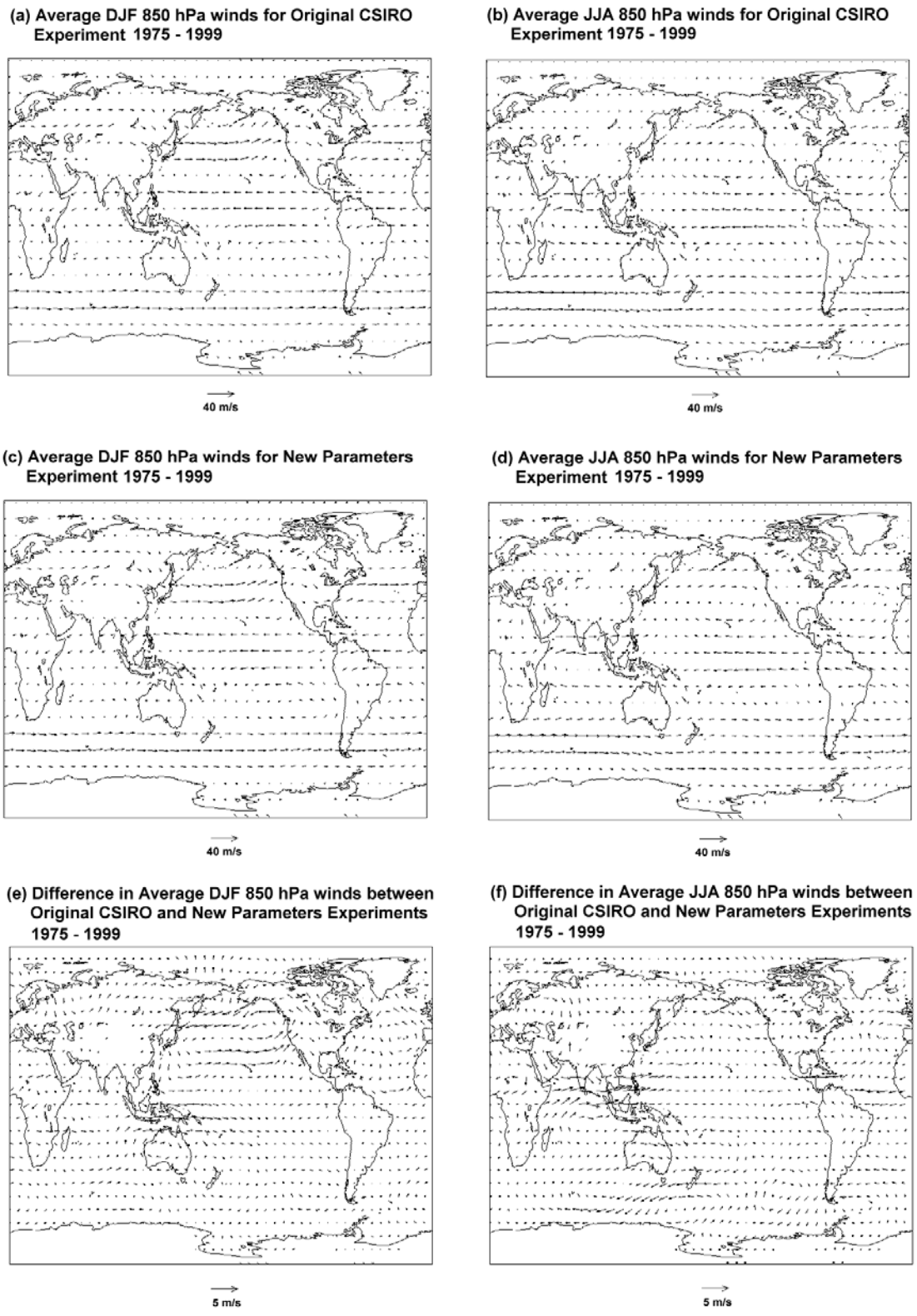

Figure 4.22 Global 850 hPa wind fields for 1975 – 1999 for: the Original CSIRO for (a) Austral Summer (DJF) and (b) Winter (JJA); the New Parameters experiments for (c) Austral Summer (DJF) and (d) Winter (JJA) and the Difference between the experiments (New – Old) for (e) Austral Summer (DJF) and (f) Winter (JJA)

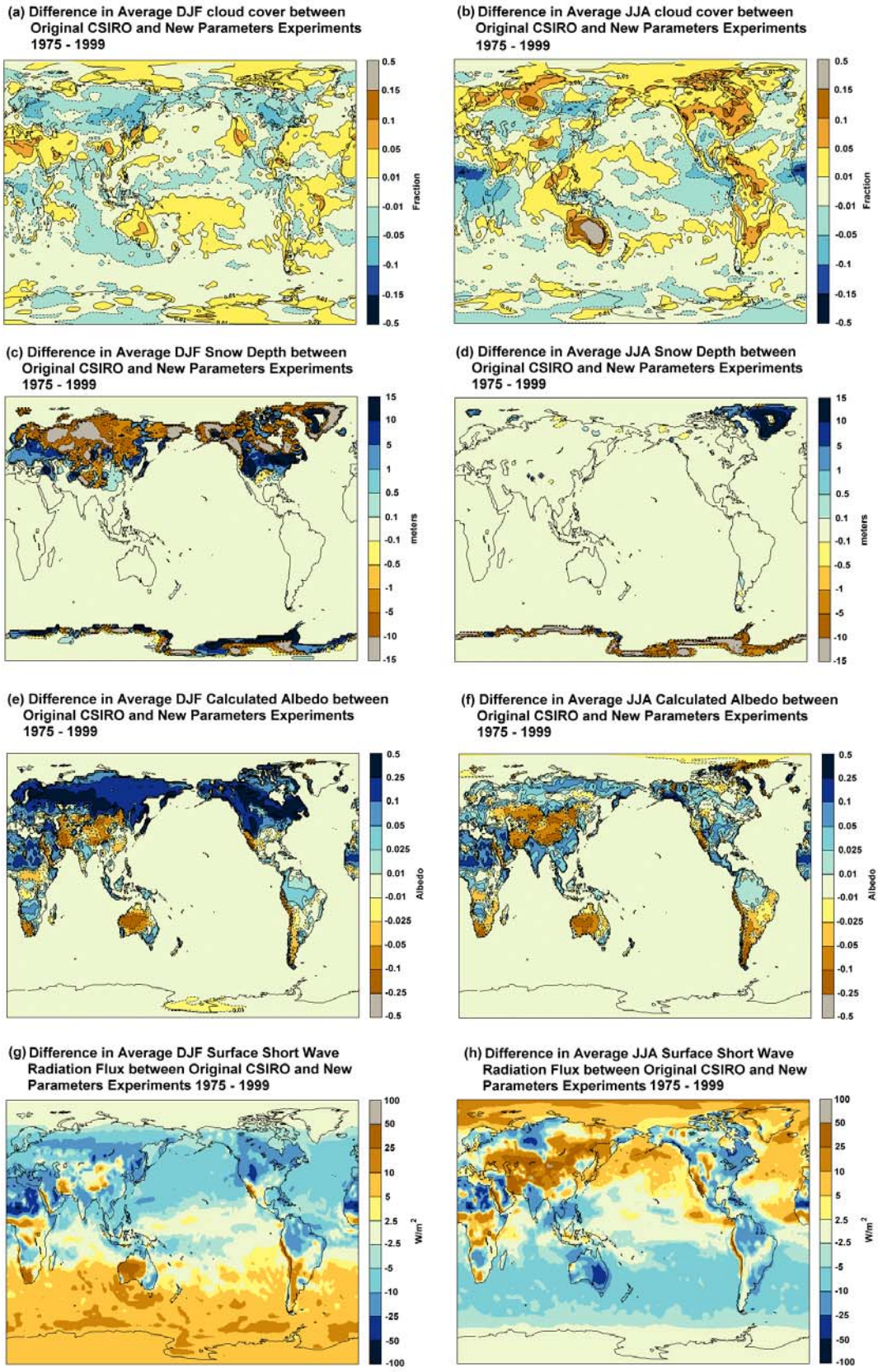

Figure 4.23 Global differences in average climate between the Original CSIRO and New Parameters experiments (New – Old) for Austral Summer (DJF) and Winter (JJA) 1975 – 1999 for: Average Cloud Cover (a) and (b); Average Snow Depth (c) and (d); Average Model Calculated Albedo (e) and (f); and Average Short Wave Radiation Flux (g) and (h)

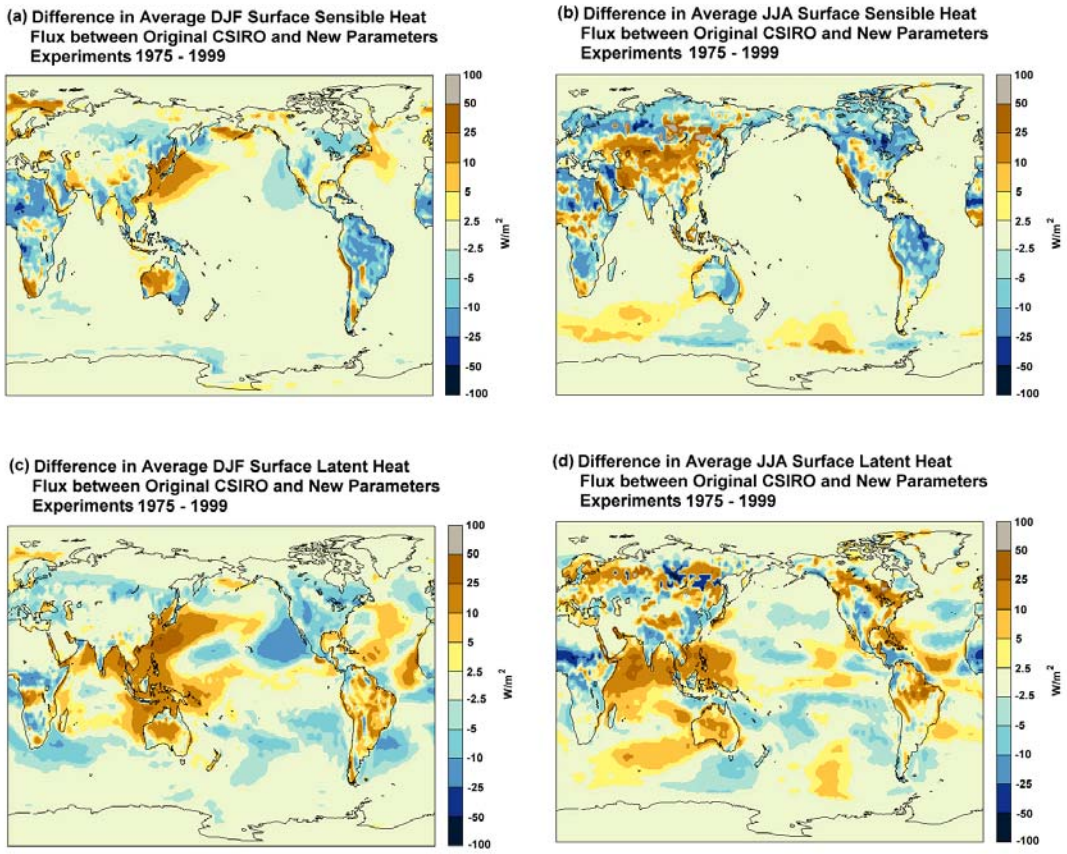

Figure 4.24 Global differences in average climate between the Original CSIRO and New Parameters experiments (New – Old) for Austral Summer (DJF) and Winter (JJA) 1975 – 1999 for: Average Sensible Heat Flux (a) and (b); and Average Latent Heat Flux (c) and (d)

The increased moisture flux also is indicated by the increased latent heat fluxes from the oceans to the north of Australia (*figure 4.24 c*). The increased precipitation in northern Australia results in increased soil moisture over the Australian continent (*figure 4.21 g*), which exceeds the effects of increased canopy resistance (*figure 4.16 c*), to increase the latent heat flux over Australia (*figure 4.24 c*). The increased latent heat fluxes further increase moist convection, with further increases in precipitation and decreases in mean sea level pressure. The details of these processes are further explored later in the chapter in the Australian investigations.

The remaining areas of the Southern Hemisphere have lower DJF mean sea level pressure (*figure 4.21 e*) in the New Parameters experiment. This can be partly accounted for due to the warmer air temperatures over Australia, southern areas of South America, and southern areas of Africa (*figure 4.21 a*), and partly as a response to the increased mean sea level pressure over the Northern Hemisphere (average global mean sea level pressure needs to be constant due to conservation of mass of the atmosphere). The warmer DJF air temperatures over Australia, southern areas of South America, and southern areas of Africa correspond to increased short wave radiation, associated with the lower albedo prescribed for sparsely vegetated areas of these continents. The DJF warming over Antarctica appears to be partly due to reduced atmospheric divergence from the continent associated with weakening of the mid latitude westerly winds and

the polar front due to the lower mean sea level pressure, and partly due to the increased short wave radiation flux. The reason for the increased short wave radiation flux can be speculated to be from reduced cloud optical thickness also associated with the reduced mixing of moist lower latitude air within the weakened mid latitude westerly winds.

Austral Winter Analysis

The average 1975 to 1999 austral winter (JJA) climate statistics for the New Parameters and the Original CSIRO experiments are shown for global averages in *table 4.4* compared to NCEP reanalysis data for the same period. The average global surface temperature in the New Parameters experiment was warmer for JJA, with the near surface air temperature remaining cooler. The magnitude of the near surface air temperature cooling, however was significantly reduced from the cooling in DJF. The average global annual precipitation was marginally higher for JJA as well, with the magnitude of the difference larger than in DJF.

The average global JJA short wave surface radiation flux, and sensible heat flux both were marginally lower for the New Parameter experiment, with the latent heat flux marginally higher. The decrease in short wave radiation flux was larger than DJF, while the decrease in sensible heat flux difference was smaller and the increase in latent heat flux larger. These statistics suggest that the new parameters have different influencing on the CSIRO GCM for JJA producing a global JJA surface climate that had increased surface warming, with less air temperature cooling, and less incoming solar radiation absorption. The increased warming resulted in smaller decreases in sensible heat flux, however the increased precipitation resulted in larger increases in latent heat flux. Again the differences between the two experiments were relatively small when compared to the differences between the CSIRO GCM experiments and the NCEP reanalysis data.

Table 4.4 Global average Austral Winter (JJA) climate statistics for the New Parameters, Original CSIRO, and NCEP reanalysis data for the climate period 1975 – 1999

Variable	CSIRO	New Parameters	New – CSIRO	NCEP
Surface Temperature (^{O}C)	16.15	16.18	0.02	16.06
Screen Air Temperature (^{O}C)	15.22	15.14	-0.08	15.48
Precipitation (mm/day)	2.91	2.94	0.03	2.88
Surface SW Rad. Flux (Wm^{-2})	162.51	160.64	-1.87	158.20
Sensible Heat Flux (Wm^{-2})	27.53	27.01	-0.53	18.29
Latent Heat Flux (Wm^{-2})	82.75	83.77	1.02	83.44

Like the DJF analysis, making sense of the differences between the two models in the maps of *figure 4.21*, *4.22, 4.23* and *4.24*, requires interpretation and conjecture to develop hypotheses that explain the emerging patterns shown in the JJA difference maps and how these patterns result from the new land surface parameters. As there were few differences in JJA snow depth between the experiments (*figure 4.23 d*), and the differences in calculated albedo reflected the differences prescribed in the land surface parameters (*figure 4.23 f* and *4.8 g*), the snow and albedo feedback effect was eliminated from the explanation of differences in JJA climate between the two experiments. This may partly explain why the surface and near surface air temperature differences were so much closer in JJA than in DJF. With the snow and albedo feedback removed, the processes driving the difference in JJA climate were confined to more direct influences, primarily involving differences in albedo and canopy resistance, and the feedbacks involving changes in soil moisture and cloud cover.

The largest increase in DJF short wave radiation flux occurred in central Asia (*figure 4.23 h*), as a result of lower albedo and reduced cloud cover (*figure 4.23 f* and *b*). The mixed differences in DJF soil moisture differences and latent heat flux (*figure 4.21 h* and *4.24 d*) ensured that the increased short wave radiation resulted in increases in air temperature and sensible heat flux (*figure 4.21 b* and *4.24 b*). The increased warming and sensible heat flux, resulted in increased thermal convection, contributing to the lower mean sea level pressure over the area (*figure 4.21 f*).

The higher DJF soil moisture and lower canopy resistance over North America and Europe (*figure 4.21 h* and *4.16 g*) resulted in increased latent heat flux over these areas (*figure 4.24 d*). The increased latent heat flux, enhanced precipitation and cloud cover over these areas (*figure 4.21 d* and *4.23 b*), with the increased cloud cover combining with higher albedo to significantly reduce short wave radiation flux (*figure 4.23 h*). The increased latent heat flux and reduced short wave radiation flux resulted in lower air temperatures and reduced sensible heat flux in these areas (*figure 4.21 b* and *figure 4.24 b*). It appears the reductions in thermal convection associated with the reduced sensible heat flux, were to some degree offset by the increases in moist convection associated with increased latent heat flux, with the differences in mean sea level pressure mixed, with some areas having increased pressure and others having reduced pressure (*figure 4.21 f*).

The increased albedo over the Sahara and Arabian Peninsula resulted in reduced short wave radiation flux over the area (*figure 4.23 f* and *h*), which resulted in cooler air temperature and reduced sensible heat flux (*figure 4.21 b* and *4.24 b*). In the same manner as suggested in the DJF analysis, the reduction in sensible heat flux increased atmospheric subsidence over the area, which is apparent in the increased mean sea level pressure over the area (*figure 4.21 f*). As suggested by *Charney* (1975) the impact of the increased subsidence was to reduce precipitation and cloud cover to the south in Sub-Saharan Africa (*figure 4.21 d* and *4.23 b*). The increase in canopy resistance over much of southern Africa (*figure 4.16 g*) resulted in reduced latent flux

over the area (*figure 4.24 d*), which appears to reduce moist convection over the area. The reduced moist convection combined with the increased mean sea level pressure over the Sahara to increase mean sea level pressure over the entire African continent.

Over the Amazon, the lower canopy resistance, resulted in increased latent heat flux (*figure 4.24 d* and *4.16 g*), which resulted in increased precipitation and cloud cover (*figure 4.21 d* and *4.23 b*). The increased cloud cover combined with the higher albedo over the area to reduce the short wave radiation flux (*figure 4.23 f* and *h*). The reduced short wave radiation flux combined with the increased latent heat flux resulted in cooler air temperature and reduced sensible heat flux (*figure 4.21 b* and *4.24 b*). It appears the reduction in thermal convection associated with reduced sensible heat flux was greater than the increase in moist convection associated with the increased latent heat flux, as there was a net reduction in convection resulting in an increase in mean sea level pressure over the South American continent (*figure 4.21 f*). The increased mean sea level pressure over South America combined with the increased pressure over Africa to increase pressure over the Atlantic Ocean, and into the Southern Ocean south of both continents. It is speculated the increase in mean sea level pressure south of South America and African, into the Southern Ocean perturbed the mid latitude westerly winds with increased northerly components near the two continents. The perturbation also influenced winds in other areas of the westerly wind flow, resulting in an increase in the southerly component of the wind flow to the south west of Australia and increased northerly component to the south of Australia (*figure 4.22*).

It is speculated the increased southerly component of the westerly wind flow to the south west of Australia also increased the penetration of mid latitude cyclones into southern areas of Australia, which increased the flux of cool moist air from the southern Indian Ocean into the continent. The increase in moisture flux from the south west resulted in the increased precipitation and cloud cover shown over the continent (*figure 4.21 d* and *4.23 b*). The increased precipitation resulted in increased soil moisture over most of Australia, which more than offset increased canopy resistance, resulting in increased latent heat flux over the continent (*figure 4.21 h* and *4.24 d*). The increase in cloud cover had greater impact than the lower albedo, resulting in a significant reduction in short wave radiation flux over much of Australia (*figure 4.23 f* and *h*). The lower short wave radiation flux combined with the increased latent heat flux resulting in significantly cooler air temperature and reduced sensible heat flux over the continent. It appears the increase in moist convection combined with the increased penetration of mid latitude cyclones compensated for the reduction in thermal convection associated with reduced sensible heat flux, with the mean sea level pressure lower over the southern half of the continent. Again the details of the JJA processes impacting Australian climate are further explored later in the chapter in the Australian climate investigations.

It is speculated the increased pressure over Antarctica was a result of the perturbation of the mid latitude westerly wind flow caused by the increased sea level pressure in the Southern

Ocean intensifying the polar front. The reduced short wave radiation flux over the Southern Ocean may also be the result of increased cloud optical thickness associated increased mixing of warmer moist air from lower latitudes in the mid latitude westerly wind flow with the increased northerly components of the wind flow south of Africa, South America and Australia.

Like Antarctica in the DJF analysis, it appears the decrease in mean sea level pressure over the Artic (*figure 4.21 f*) can be partly attributed to the increased warming over the area, and partly as response to the decreased mean sea level pressure over the Asian and North American continents. Like Antarctica in DJF, the increase in short wave radiation over the Arctic and Greenland and the associated warming over these areas (*figure 4.23 h* and *4.21 b*) occur with out decreases in albedo or cloud cover (*figure 4.23 f* and *b*). It is speculated therefore the increase in short wave radiation is the result of reduced optical thickness of the cloud associated with less moist air being mixed by the weaker polar front from the lower mean sea level pressure over the area.

4.4.4 Detailed Australian Modelling Evaluation

Given the climate modelling framework has been developed to investigate the climate responses to Australian land cover changes, more detailed evaluation of the climate modelled in the CSIRO GCM with the new land surface parameters was performed against Australian observed climate records. The average seasonal climate statistics for the New Parameters and Original CSIRO experiments are shown for Australia in *table 4.5* compared with observed climate statistics from the SILO database for the 1975 – 1999 period. The seasonal differences and spatial correlations of the model experiments compared to the observed records from the SILO database are graphed in *figure 4.25*, and mapped geographically in *figure 4.26*, *4.27*, and *4.28*.

The seasonal analysis of air temperature in *table 4.5* and *figure 4.25 a* and *b*, show the New Parameters experiment had an overall increase in the cool bias of Australian average air temperature compared to the Original Parameters experiment. The seasonal breakdown shows the New Parameters had: a marginal warm bias in austral summer compared to the marginal cool bias of the Original Parameters; a reduction in the cool bias of autumn; an increase in the cool bias of winter; and a reduction in the warm bias of spring. The spatial correlation of modelled and observed average air temperature shows higher correlation for the New Parameters experiment in all seasons, with the only exception a marginal decrease in winter.

The air temperature difference maps (*figure 4.26*) show the summer warming of the New Parameters experiment was focused in the north west of the continent, where the Original CSIRO experiment had a strong cool bias, and where the New Parameters had lower albedo and canopy resistance. The maps also show there were marginal reductions in summer warm biases in the south west and south east of the continent. The autumn maps show the New Parameters experiment had a general decrease in the cool bias of the Original CSIRO experiment over the

entire continent, with the winter maps showing a general increase in the cool bias over the entire continent. The spring maps are more geographically complex showing significant reductions in warm biases in the south west and south east, and a marginal decrease in the cool bias of the western inland.

Table 4.5 Evaluation of Australian average climate statistics for the New Parameters and the Original CSIRO Experiments against SILO observational data for the climate period 1975 – 1999. Seasons shown Annual; Austral Summer (DJF); Autumn (MAM); Winter (JJA); and Spring (MAM). Statistics shown are Australian climatic mean values and spatial correlations between Australian climatic mean maps of Model and SILO observations

Variable	Season	CSIRO	New Params	SILO	CSIRO Corr.	New Corr.
Air Temperature (^{O}C)	Annual	20.66	20.55	21.57	0.940	0.953
	DJF	27.23	27.45	27.27	0.919	0.953
	MAM	19.05	19.90	21.64	0.913	0.938
	JJA	13.18	12.35	14.85	0.931	0.923
	SON	23.19	22.49	22.15	0.970	0.977
Precipitation (mm/day)	Annual	1.40	1.72	1.23	0.814	0.753
	DJF	2.78	3.31	2.28	0.955	0.941
	MAM	1.32	1.83	1.16	0.664	0.585
	JJA	0.60	0.83	0.70	0.817	0.735
	SON	0.91	0.95	0.82	0.699	0.807
Mean Sea Level Pressure (hPa)	Annual	1017.20	1016.40	1015.50	0.976	0.984
	DJF	1010.40	1009.10	1010.30	0.973	0.983
	MAM	1019.10	1018.10	1016.50	0.982	0.987
	JJA	1022.10	1021.50	1020.10	0.983	0.982
	SON	1017.10	1017.10	1015.00	0.944	0.961

The seasonal analysis of precipitation in *table 4.5* and *figure 4.25 c* and *d*, shows the general increase in precipitation bias of the New Parameters experiment was largest in summer and autumn and much smaller in winter and spring. The spatial correlations of the modelled and observed average precipitation show the New Parameters experiment had lower overall spatial correlation, with the biggest seasonal decreases in autumn and winter. The decrease in summer spatial correlation was marginal, and there was a significant increase in spatial correlation for spring.

The precipitation maps (*figure 4.27*) show the summer increase in wet bias of the New Parameters experiment was largest in northern areas, with the increases amplifying the existing wet biases of the Original CSIRO experiment. The increase in wet bias in autumn also was largest in the north, but with a stronger westerly component reflecting the existing bias of the

Original Parameters experiment. The New Parameters experiment winter wet bias was centered in a band from the north west to the center of the continent, again amplifying a bias already present in the Original CSIRO experiment. In addition to the increase in wet biases there were decreases in dry biases across eastern Australia. The increase in the spring wet bias was the smallest of all seasons, with both experiments showing the same general patterns of bias. There also were some reductions in spring wet biases in the north, with increases in the central inland.

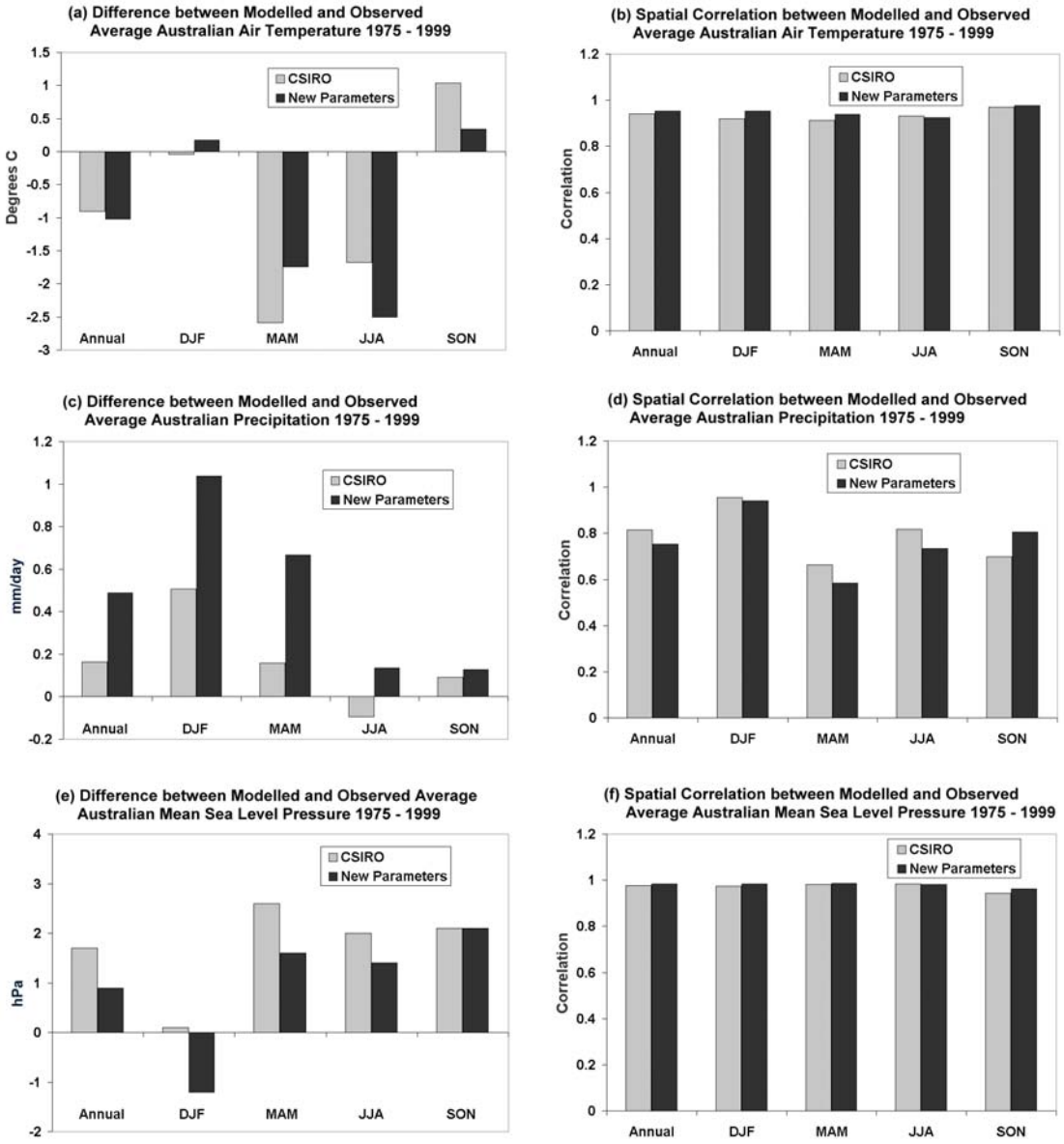

Figure 4.25 Seasonal model performance compared with Australian 1975 – 1999 observations: Differences and spatial correlations for the Original CSIRO and New Parameters experiments compared with observed average Australian temperature, precipitation and mean sea level pressure. Seasons shown are: Annual; Austral Summer (DJF); Autumn (MAM); Winter (JJA); and Spring (SON)

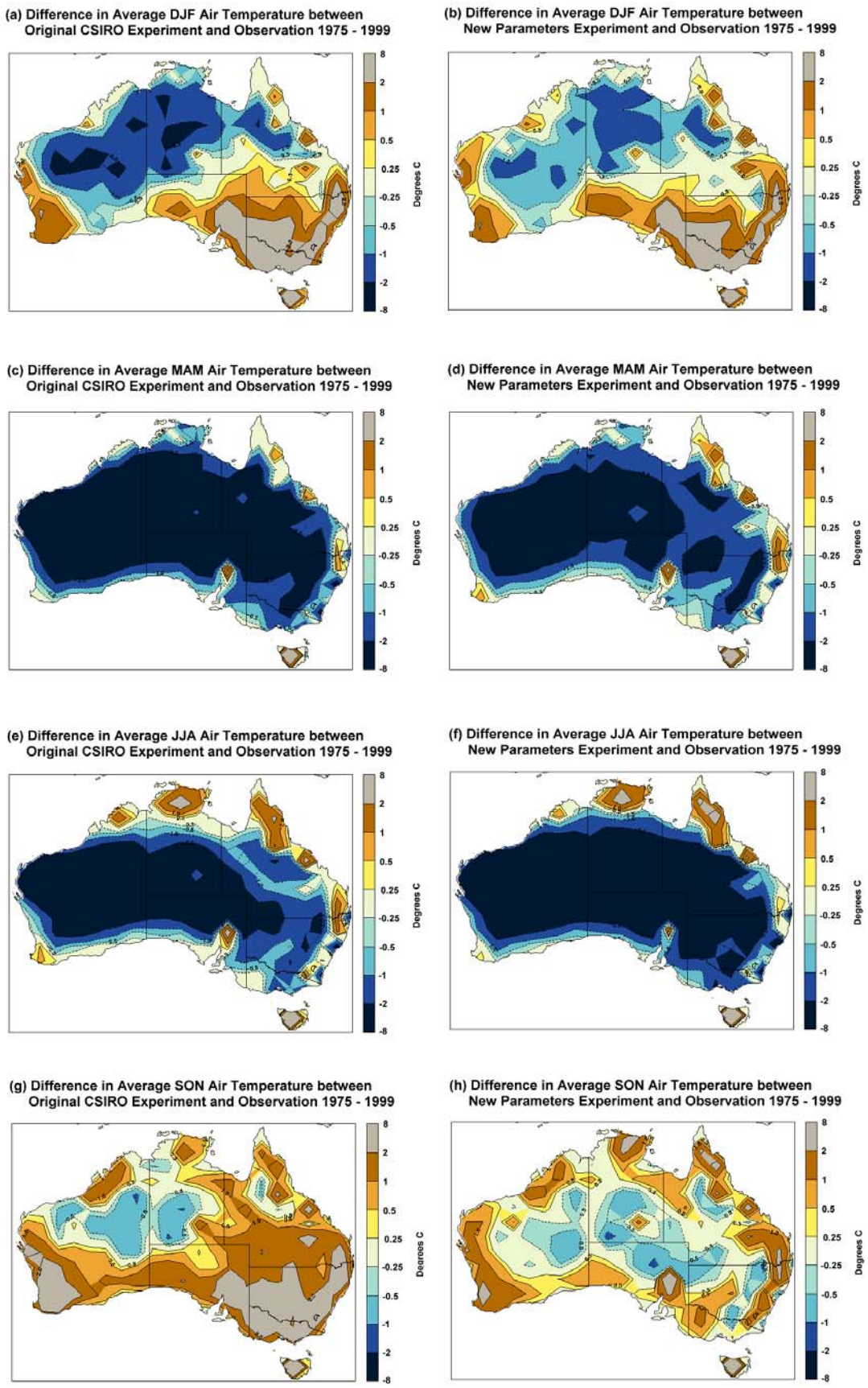

Figure 4.26. Average Air Temperature for Australia 1975 - 1999: Difference between Observed data from the SILO database, and the Original CSIRO and New Parameters Experiments for Austral Summer (DJF) (a) and (b); Autumn (MAM) (c) and (d); Winter (JJA) (e) and (f); and Spring (SON) (g) and (h)

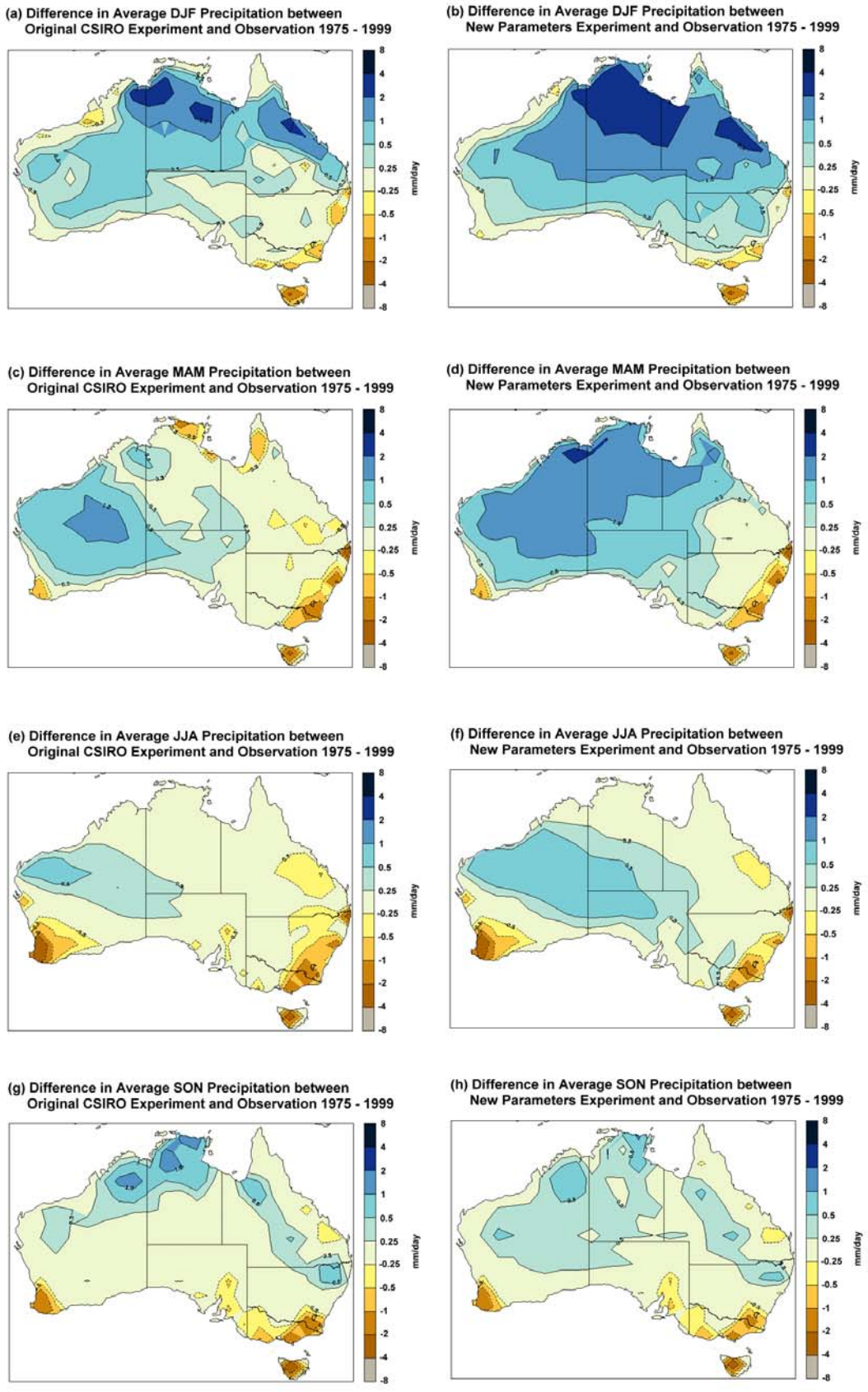

Figure 4.27. Average Precipitation for Australia 1975 - 1999: Difference between Observed data from the SILO database, and the Original CSIRO and New Parameters Experiments for Austral Summer (DJF) (a) and (b); Autumn (MAM) (c) and (d); Winter (JJA) (e) and (f); and Spring (SON) (g) and (h)

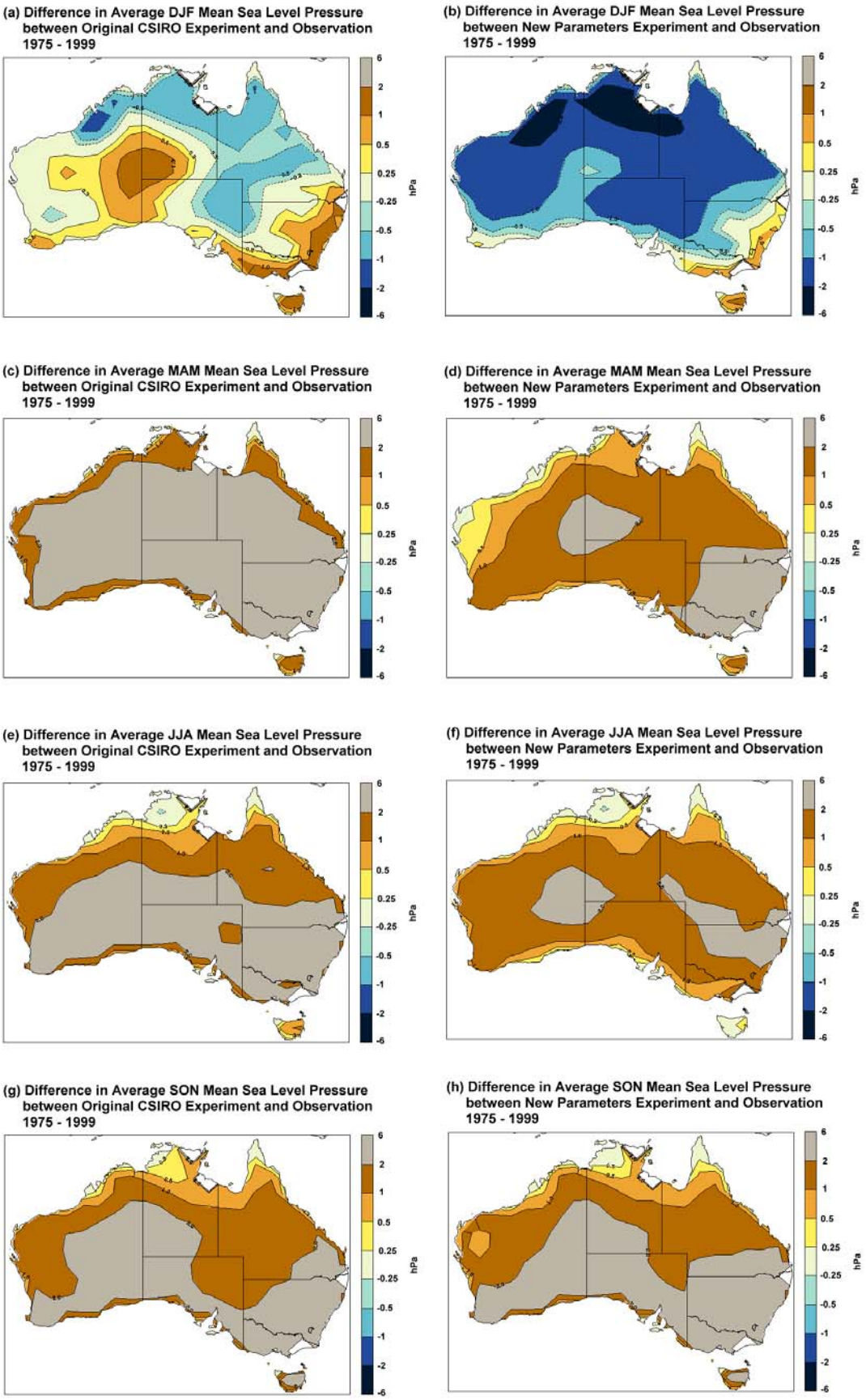

Figure 4.28 Average Mean Sea Level Pressure for Australia 1975 - 1999: Difference between Observed data from the SILO database, and the Original CSIRO and New Parameters Experiments for Austral Summer (DJF) (a) and (b); Autumn (MAM) (c) and (d); Winter (JJA) (e) and (f); and Spring (SON) (g) and (h)

The seasonal analysis of mean sea level pressure in *table 4.5* and *figure 4.25 e* and *f* shows there was an overall reduction in high pressure bias in the New Parameters experiment. The seasonal breakdown shows the New Parameters had: a low pressure bias in summer compared to a marginal high pressure bias in the Original Parameters experiment; reduced high pressure biases for autumn and winter; and a similar high pressure bias for spring. The spatial correlations of modelled and observed average mean sea level pressure show the New Parameters experiment had marginally higher correlation for all seasons except winter, where the New Parameters had a marginal decrease in spatial correlation.

The mean sea level pressure maps (*figure 4.28*) show that the summer low pressure bias of the New Parameters experiment had the same general patterns as the Original CSIRO experiment but with lower values. The general decrease in average pressure in the New Parameters had the effect of amplifying the existing low pressure biases over much of the continent. This decrease in pressure in the New Parameters experiment also greatly reduced or removed the high pressure biases of the Original Parameters experiment in central Australia and in the south east. The autumn and winter mean sea level pressure maps show that the New Parameters experiment had significantly reduced high pressure biases over the entire continent, while the spring maps show that the high pressure biases of the Original CSIRO experiment were relatively unchanged in the New Parameters experiment.

Overall the effect of the new parameters on simulation of Australian climate in the CSIRO GCM was to produce: a warmer, wetter austral summer and autumn, with lower pressure; a colder and wetter winter, again with lower pressure; and a cooler and marginally wetter spring with similar pressure. Compared to the observed climate for the same time period, the CSIRO GCM with the new parameters appears to improve the simulation of air temperature and mean sea level pressure, but degrades the simulation of precipitation.

4.4.5 Processes Driving Australian Differences

To investigate the possible mechanisms driving the changes in Australian climate in the New Parameters experiment, the global analysis was extended in more detail for the area surrounding Australia for austral summer (DJF) and winter (JJA). The differences between the two experiments for climate variables, model calculated land surface characteristics, and surface fluxes are shown for the area surrounding Australia in the differences maps of *figure 4.29*, *4.30* and *4.31*.

Austral Summer Analysis

The DJF air temperature in the New Parameters experiment was warmer in western and north eastern areas of Australia, but cooler over south eastern Australia and most of Asia (*figure 4.29 a*). For the same period the mean sea level pressure was lower over the Australian continent, and increased over Asia (*figure 4.29 e*). The differences in the DJF 850 hPa wind

fields (*figure 4.30 a*, *c* and *e*) show an increase in westerly winds through Indonesia with increased flow into northern Australia and into the South Pacific Convergence Zone (SPCZ). Associated with the increased westerly flow there is a decrease in the easterly winds from the Pacific Ocean into northern and central Australia. The more detailed wind field changes along with lower pressure and increased precipitation in northern Australia support the hypothesis made in the global analysis, that there was a strengthening of the north Australian monsoon for DJF in the New Parameters experiment.

The more detailed maps also show the differences in DJF surface short wave radiation flux (*figure 4.31 c*) were similar patterns to the January albedo difference maps (*figure 4.8 d*). As mentioned in the global analysis, there also were decreases in the DJF short wave radiation flux into the oceans to the north of Australia, and increases in the oceans to the south. As the cloud cover maps show little difference over these areas between the two experiments, it is speculated the changes in short wave radiation flux may result from changes in optical thickness of the cloud cover between the two experiments as described in the global analysis.

The more detailed maps show the changes in DJF short wave radiation flux directly flow on to sensible heat flux and air temperature over Australia, with areas of increased short wave radiation resulting in higher air temperature and sensible heat flux (*figure 4.31 c, 4.31 e,* and *4.29 a*). Over Australia, the differences in DJF latent heat flux between the two experiments were more complex, with differences in precipitation and soil moisture interacting with changes in vegetation fraction and canopy resistance to effect evaporation and transpiration rates (*figure 4.29 c*, *4.29 g*, *4.12 d*, and *4.16 d*).

In central Australia the increased precipitation of the New Parameters experiment increased soil moisture, which dominated the decreases in vegetation fraction and increases in canopy resistance, resulting in increased evaporation and transpiration and latent heat flux. Along the east coast of Australia the increased precipitation and soil moisture, combined with the decreased canopy resistance to increase latent heat flux. While in northern Australia, the decreases in vegetation fraction and the increases in canopy resistance resulted in reduced evaporation and transpiration despite the increased precipitation and soil moisture.

Austral Winter Analysis

The more detailed maps show the JJA air temperature of the New Parameters experiment was significantly cooler over Australia (*figure 4.29 b*). The maps also show DJF precipitation was significantly higher over central Australia and to the north west of the continent, but reduced to the north of Australia from Papua New Guinea through Indonesia (*figure 4.29 d*). The JJA mean sea level pressure was significantly lower over southern Australia, and over the Asian continent during the Asian monsoon, with significant increases in cloud cover over inland Australia (*figure 4.29 f* and *4.31 b*).

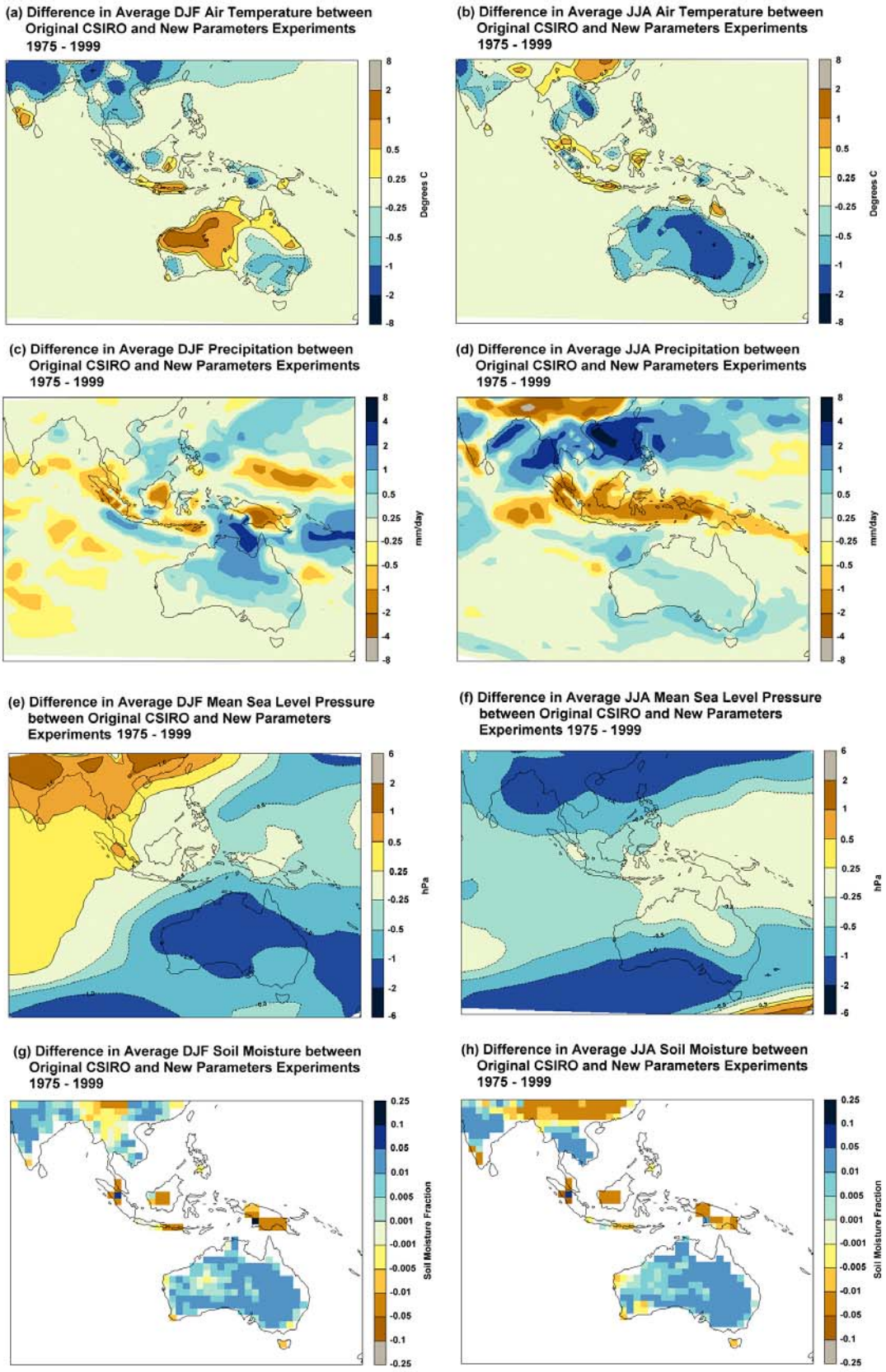

Figure 4.29 Differences in average climate between the Original CSIRO and New Parameters experiments for Australia – Asia Austral Summer (DJF) and Winter (JJA) 1975 – 1999 for: Average Air Temperature (a) and (b); Average Precipitation (c) and (d); Average Mean Sea Level Pressure (e) and (f); and Average Cloud Cover (g) and (h)

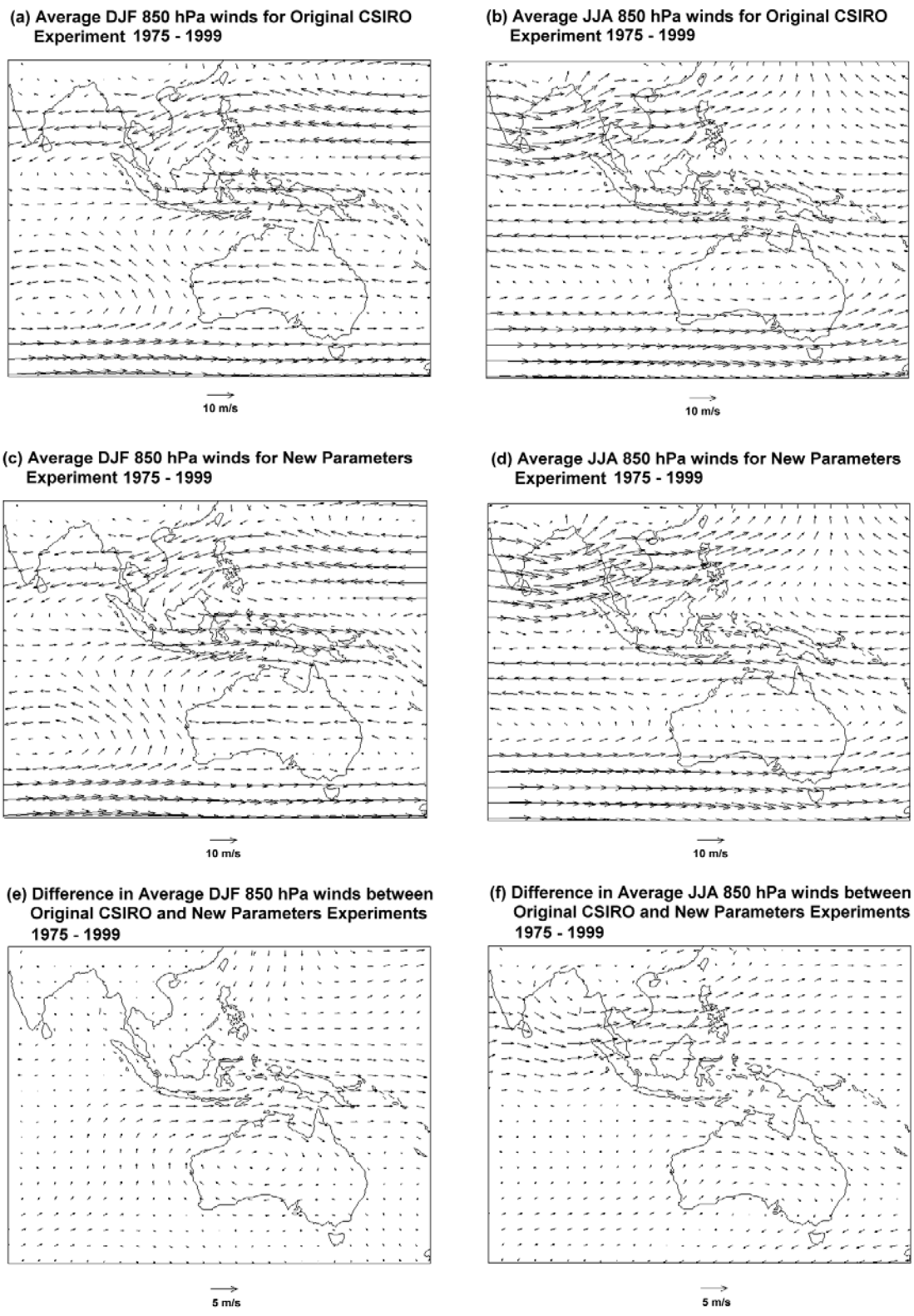

Figure 4.30 Average 850 hPa winds over Australia – Asia 1975 – 1999 for: The Original CSIRO experiment (a) Austral Summer (DJF) and (b) Winter (JJA); The New Parameters experiment (c) Summer (DJF) and (d) Winter; And the difference between the experiments (e) Summer (DJF) and (f) Winter (JJA)

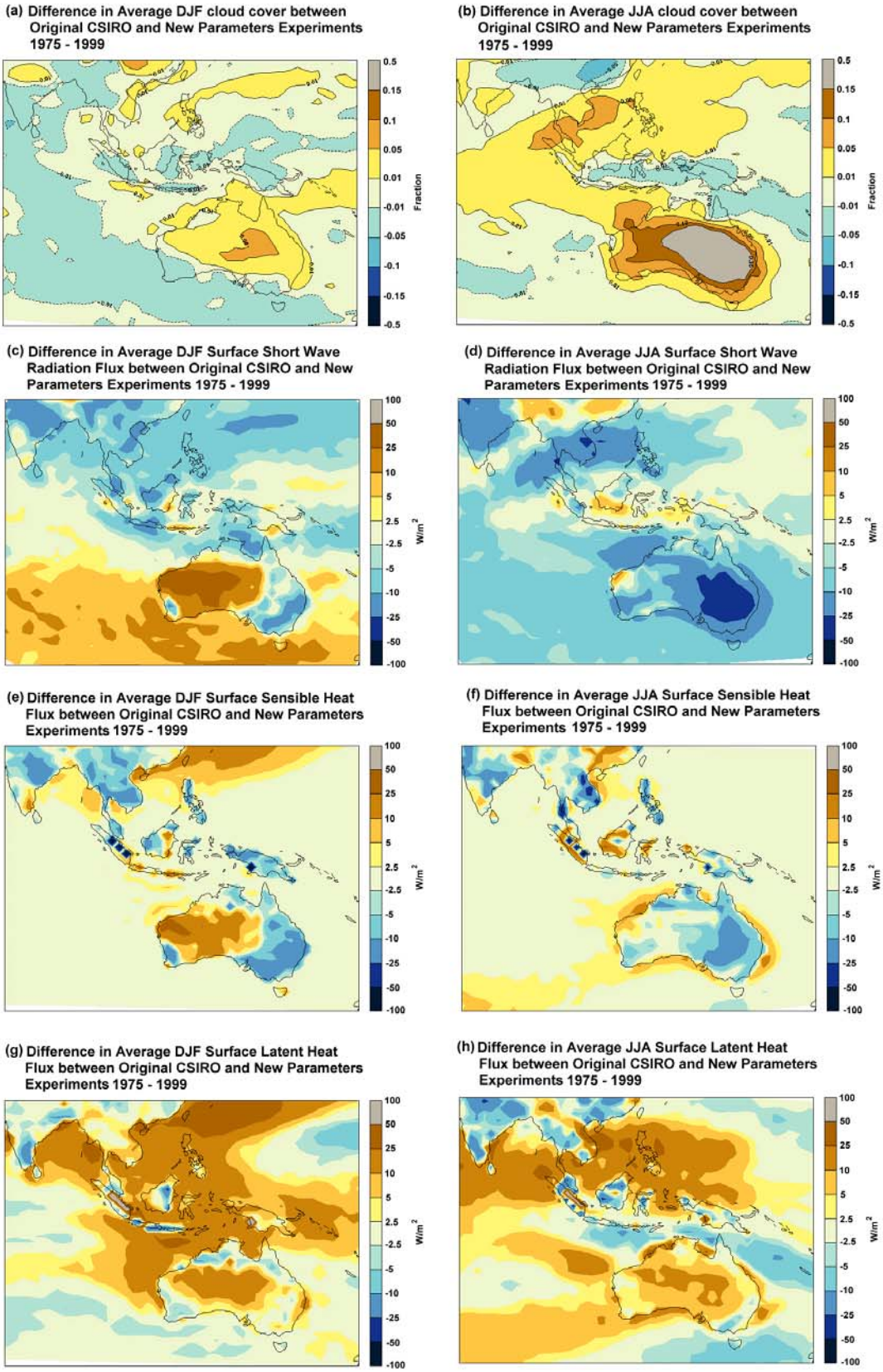

Figure 4.31 Surface energy flux differences over Australia – Asia between the Original CSIRO and New Parameters experiments for Austral Summer (DJF) and Winter (JJA) 1975 – 1999 for: Average Short Wave Radiation Flux (a) and (b); Average Sensible Heat (c) and (d); and Latent Heat Flux (e) and (f)

The JJA 850 hPa wind field differences show there was an increase in westerly winds flowing into south western Australia, with a stronger southerly component to these winds. The maps also show there was a decreased southerly component to the westerly winds flowing into south eastern Australia (*figure 4.30 b*, *d* and *f*). The increase in southerly winds flowing into south western Australia combined with the lower pressure, increased precipitation and increased cloud cover. This was highly supportive of the hypothesis made in the global analysis, that there was an increase in the penetration of mid latitude cyclones into the Australian continent in the New Parameters experiment. The 850 hPa wind field differences also show a decrease in easterly winds across northern Australia, Papua New Guinea and Indonesia, and a strengthening of westerly winds from India across South East Asia into the Pacific Ocean. The changes in wind fields, and pressure suggest there were significant changes to the Asian monsoon effecting precipitation across the Asian region in the New Parameters experiment.

Over Australia the changes in JJA surface energy balance were complex, with the decrease in short wave radiation not completely accounted for by the decrease in sensible and the increase in latent heat (*figure 4.31 d*, *f* and *h*). The net loss in surface energy may have been partly offset by warming from the surrounding oceans, with the sensible heat flux maps showing decreased sensible heat flux over most of the Australian continent and increased sensible heat flux over the near oceans (*figure 4.31 f*). Latent heat flux also was increased over most of Australia associated with increased precipitation and increased soil moisture (*figure 4.31 f*, *4.29 d* and *4.29 h*), which appeared to have larger impacts than the decreases in vegetation fraction and the increases in canopy resistance (*figure 4.12 h* and *4.16 h*). There was a small area in the south east, however, where latent heat flux was reduced even though the area had increased soil moisture. It is speculated that the given the high vegetation fraction over the area, the primary reason for this decrease was an increase in canopy resistance.

4.4.6 Section Summary

1. Two sensitivity experiments were conducted for 1975-1999 using the original and new land surface parameters to evaluate the model's ability to simulate observed climate with the new land surface parameters.
2. From the global and continental analyses of the sensitivity experiments, the new parameters where shown to increase the average cool air temperature bias over all land for both DJF and JJA, with the largest increases in cool biases in North America, Asia and Africa in DJF, and in Australia in JJA.
3. Over all land the new parameters reduced the average wet precipitation bias in DJF and increased the dry precipitation bias in JJA. The largest increase in wet bias was over Australia in DJF, and the largest increase in dry bias was over Africa in JJA.

4. It was speculated the strong DJF cooling of the Northern Hemisphere was caused by snow and albedo feedback at higher latitudes resulting in increased snow cover further south. The snow and albedo feedback was not present in JJA.
5. Increased albedo over Sahara resulted in increased subsidence, resulting in increased MSLP with reduced precipitation and cloud cover over central Africa for DJF and JJA. Increased canopy resistance over southern Africa also reduced JJA latent heat flux, reducing moist convection, with the result an increase in MSLP over the area. The higher MSLP combined with Saharan albedo induced increased MSLP to increase JJA MSLP over all of Africa.
6. Reduced canopy resistance over the Amazon resulted in increased latent heat flux, with associated increases in cloud and precipitation. Higher albedo and cloud cover resulted in reduced short wave radiation flux with associated cooling and increased MSLP for both DJF and JJA. The increased JJA MSLP over South America, combined with the increased MSLP over Africa increasing MSLP to the south of both continents into Southern Ocean.
7. Lower albedo over Australia increased DJF short wave radiation, with increased heating and thermal convection decreasing MSLP. Lower MSLP combined with increased MSLP over Asia to increase monsoon flow, resulting in increased precipitation and soil moisture.
8. Increased JJA MSLP in Southern Ocean perturbs JJA mid latitude westerly wind flow, increasing the westerly wind flow into southern Australia, with increased penetration of mid latitude cyclones. Increase in JJA moisture flux and mid latitude cyclones penetration, resulted in increased JJA precipitation and cloud cover over Australia. Increased cloud cover results in reduced short wave radiation flux, which combines with increased latent heat flux resulting in JJA cooling.
9. Global DJF changes in MSLP weaken DJF Antarctic mid latitude westerly wind flow, resulting in lower DJF MSLP over Antarctica with increased warming. Global JJA changes in MSLP also weaken the JJA Arctic mid latitude westerly wind flow, resulting in lower JJA MSLP over Arctic with increased warming.
10. Detailed Australian assessment of experiments with observed climate records show New Parameters in CSIRO GCM improve simulation of air temperature and MSLP over Australia, but degrade the simulation of precipitation. Analysis also shows Australian latent heat flux impacts are complex involving soil moisture, vegetation fraction and canopy resistance.
11. The sensitivity experiments demonstrate that the land surface parameters do have a strong influence on the climate simulated in the CSIRO GCM. The sensitivity experiments also demonstrate that the changes in land surface properties produce the

range of climate responses detailed in the literature both theoretically and from case study investigations.

12. The CSIRO GCM with the new land surface parameters simulates Australian climate and climatic processes with minimal increases in existing biases compared to the model with the original land surface parameters.

4.5 Chapter summary

The aim of this chapter was to develop a climate modelling framework, using the CSIRO GCM that could be used to investigate the climate impacts of the relatively fine-scale land cover changes described in Chapter 3. The CSIRO GCM was reviewed, and assessed as being suitable for investigating the climate impacts of land cover change as it could capture the fundamental properties of the land surface, and simulate how they interact with the atmospheric boundary layer, as well as simulating the dynamic feedbacks of the climate system through changes in atmospheric processes and circulation. Assessment of the current land surface representation in the CSIRO GCM, however, found the homogeneous allocation of GCM grid cells at the 1.875 degree grid increment was not capable of representing the relatively fine-scale land cover changes. In addition to this, the assessment found the land surface represented by recent satellite mapping projects, and parameterised through radiation and surface roughness models was significantly different to that specified by the original CSIRO GCM land surface parameters.

To overcome these limitations in the model, new land surface parameter generation methods were developed to integrate the best available land surface data into the land surface model of the CSIRO GCM. The methods used the two stream radiation model and the simplified roughness model in conjunction with satellite derived land surface data, to capture the heterogeneity and biogeophysics of the land surface. Linear aggregation rules were applied to the data to produce aggregated land surface parameters at the scale of the GCM. The new land surface parameters had large differences when compared to the original CSIRO land surface parameters. The major differences in the land surface parameters are listed in *table 4.6*.

The CSIRO GCM with the new land surface parameters was evaluated against the CSIRO GCM with the original land surface parameters for climate modelling performance over the 1969 to 1999 period. The experiments had the same initial conditions, with other sources of climate variability unrelated to the land surface kept consistent in both experiments by prescribing the same monthly observed sea surface temperatures and sea ice distributions. At the global and continental scale the climate simulated by the two experiments were compared to global historical weather records to assess the performance of the experiments in reproducing historical climate. Differences in a range of climate variables were compared to differences in land surface parameters at the global scale to investigate how the new land surface parameters influenced climate simulation in the CSIRO GCM. More detailed analysis was performed over

Australia to assess the suitability of using the CSIRO GCM with the new land surface parameters in the Australian land cover change experiments of Chapter 5.

Table 4.6 Differences in CSIRO GCM Land Surface Parameters between Original and New Parameters

Parameter	Evaluation of Differences
Albedo	*Global scale* - average values very close for all months but latitudinal discrepancies with dense vegetation and deserts. *Australian continent and regions* - new parameters significantly lower albedo for all months with inland arid regions showing the largest discrepancies.
Leaf Area Index	*Global scale* - new parameters are significantly lower than the old parameters for all months with different seasonal cycles. *Australian continent and regions* - larger discrepancies than at global scale but with similar seasonal patterns. Regionally, largest discrepancies are in the tropical savannas.
Vegetation Fraction	*Global scale* - similar differences to those found for leaf area index for all months. *Australian continent and regions* - similar average values to leaf area with strong regional differences in transition zone from coastal regions to arid interior.
Unrestrained Stomatal Resistance	*Global scale* - new parameters were significantly lower for all months. *Australian continent and regions* - new parameters were significantly lower for all months with largest regional differences in tropical savannas and coastal forests.
Unrestrained Canopy Resistance	*Global scale* - new parameters are lower than original parameters, with strongest difference in boreal summer, however, differences are not as great as for stomatal resistance. *Australian continent and regions* - new parameters have higher canopy resistance for all months with different seasonal cycles with the strongest differences in the sparsely vegetated arid interior.
Surface Roughness	*Global scale* - new parameters are marginally lower with slightly different seasonal cycle. *Australian continent and regions* - significantly lower with the biggest differences in Austral summer. Regionally, strong differences in the transitional zones from coast to interior

The climate modelling experiments demonstrated that the land surface parameters do have a strong influence on the climate simulated in the CSIRO GCM. The experiments also demonstrated that the CSIRO GCM reproduced the range of climate responses associated with changes in land surface properties that were detailed in the literature review of Chapter 2, with the conceptual model providing a robust explanation for differences in climate simulated in the two experiments. Finally the assessment of the CSIRO GCM with the new land surface parameters demonstrated that the new climate modelling framework developed to represent relatively fine-scale land cover change, simulates Australian climate and climatic processes with minimal increases in existing biases, completing the aims of the chapter.

CHAPTER 5.
CLIMATE IMPACTS OF AUSTRALIAN LAND COVER CHANGE EXPERIMENTS

5.1 Chapter Aims and Rationale

5.1.1 Aims and Structure

The aim of this chapter is to investigate the potential climate impacts of Australian land cover changes as described in Chapter 3, using the CSIRO GCM modelling framework developed in Chapter 4. The modelling framework is adapted to consistently represent the Australian land surface as it may have existed prior to clearing, and as it existed for current day (mid 1980s) after widespread clearing of the intensive land use zone. To ensure the only climate forcing introduced between the two experiments represents the historical Australian land cover changes, the climate modelling framework specifies all other sources of climate variability the same for both experiments (i.e. climate forcings such as sea surface temperatures, sea ice distributions and vegetation changes in other continents).

To address the key question of how do the changes in Australian land cover impact climate, the differences in the two climate experiments are analysed with robust statistical techniques for the Australian continent, and within Australia for regions of intense land cover change. To address the key question of whether the modelled changes reflected the observed changes, the modelled climate impacts of land cover change are compared to observed changes in precipitation for the past 100 years and the past 50 years. To address the other key questions of how do the land surface changes associated with land cover change directly and indirectly influence climate at a range of scales, analysis was performed to identify the differences in the climate of the two experiments in the larger context of the area surrounding Australia and globally. The results from the analyses were used to develop relationships that accounted for the climate changes of the experiments in the context of the conceptual model and the postulated relationships developed in Chapter 2.

The chapter is divided into two main sections. Section 5.2 defines the current and pre-clearing land cover data, and develops methods for extrapolating the biogeophysical properties of native land cover from the current remnant extent to the pre-clearing extent. These new methods are necessary to ensure consistency between pre-clearing and current land cover and land surface properties. The extrapolation methods are applied to the pre-clearing and current land cover data, using the current global land surface data described in Chapter 4. The aggregation methods presented in Chapter 4 are applied to the extrapolated land cover data to produce CSIRO GCM parameters representing the Australian pre-clearing and current day land surface. The differences between the pre-clearing and current land surface parameters are

assessed for the Australian continent, with three regions identified as requiring further investigation. The three regions are selected based on the intensity of historical land cover changes and the significance of historical changes in precipitation. The differences in land surface parameters of the three regions are assessed and compared to the land cover changes described in the Australian case studies of Chapter 2.

Section 5.3 performs two sensitivity experiments comparing the climate impacts of changing the land surface from the pre-clearing state to the current day state. The sensitivity experiments are the final modelling investigation of the research, and are performed to quantify the modelled climate impacts of land cover change in the intensive land use zone of Australia. The results of the two experiments are compared and statistically analysed for the Australia continent and the three Australian regions identified in Section 5.2. To assess whether the climate experiments reproduce the same changes in precipitation as were identified by *Manins et al.* (2001), the Australian continental and regional analyses are compared to historical changes in observed precipitation. The differences in the climate modelling experiments are analysed at the larger extents of the area surrounding Australia and globally for a range of climate variables to investigate the possible larger scale mechanism driving the changes in Australian climate. These analyses identify how direct local-scale processes as well as indirect changes in larger-scale atmospheric circulation and other feedbacks impact climate at a range of scales, based on the conceptual model and postulated relationships stated in Chapter 2.

5.1.2 Rationale

Following from Chapter 4, new land surface parameter generation methods were required to capture the fine-scale changes in Australian land cover change described in Chapter 3. To capture these changes, the land surface characteristics of native vegetation prior to clearing needed to be reproduced at the spatial scale of the vegetation mapping. To be consistent with the methods used to generate the land surface parameters for the current day, the seasonal dynamics of the native vegetation, as well as the physical processes, needed to be represented in the land surface parameters of the pre-clearing experiment as they were for the current experiment.

The current day land surface properties can be spatially and seasonally described by specifying vegetation cover and physiology from satellite imagery and field data. This is not possible for pre-clearing vegetation dynamics as the best available pre-clearing land surface data, consists of a limited number of speculative maps describing the possible extent of structural and floristic vegetation distributions. To develop consistent descriptions of the Australian land surface that may have existed prior to clearing therefore requires extrapolation of the seasonal dynamics of native vegetation cover and physiology from the current remnant extent to the pre-clearing extent.

For the extrapolation of land surface properties of remnant native vegetation to be realistically extended to larger pre-clearing extents, the remnant native vegetation needs to be

representative of the vegetation that existed prior to clearing. As shown in Chapter 3, there is good general agreement on the historical changes that have resulted from clearing of native vegetation for cropping and pastures, however there are large uncertainties in the land cover changes that have resulted from other forms of disturbance and land use. To ensure the land cover changes represented in the climate modelling experiments are as realistic as possible, only land cover changes that have high degrees of certainty in their nature and extent should be included in the land surface changes.

To avoid the problems reported by *Oleson et al.* (2004) in overstating of the magnitude and spatial extent of changes in land surface conditions prescribed in land cover change experiments, the most realistic representations of current and pre-clearing land surface conditions are required. By using the new methods developed in Chapter 4, the current land surface properties can be realistically described from finer scale, satellite derived land cover datasets, capturing sub-grid heterogeneity and land biogeophysics. By extrapolating these fine-scale land surface data realistically to well known and quantified pre-clearing extents, the sub-grid heterogeneity and land biogeophysics of the pre-clearing land surface can also be captured.

5.2 Australian Land Cover Change Data And Extrapolation Methods

5.2.1 Australian Land Cover Change Data

To remove as much of the uncertainty as possible, a conservative approach was taken to restrict land cover changes to those resulting from historical clearing. While this ignored a wide range of other possible sources of land cover change, the conservative approach ensured that the land cover change impacts on climate were understated as far as possible, preventing unrealistic representations of change between current and pre-clearing land surfaces in the climate modelling investigations. The rationale behind the conservative approach was to establish whether the most obvious and definitive changes in Australian land cover had an impact on climate before extending the research to the less well defined elements of land cover change.

Following this conservative approach, Australian land cover change was restricted to the clearing identified between the current and natural vegetation maps of *AUSLIG* (1990), as described in Chapter 3. While this definition of clearing excluded the recent clearing described by *Barson et al.* (2000) and *DNRM* (2003), the recent clearing at around 14,000 km^2 over Australia for 1990 to 1995, was deemed significantly smaller in extent, that the around 1,200,000 km^2 of historical clearing from 1780 to 1985.

The structural and floristic vegetation maps were simplified to produce current and natural land cover maps using the land cover classes of *Graetz et al.* (1995). The current and natural land cover maps are shown in *figure 5.1*, with the definitions for the land cover classes listed in *table 5.1*. To restrict land cover changes to only cleared areas, a new land cover map was produced with land cover mapped from the natural land cover values where the native

vegetation had been cleared and from current day values for all other areas. The new land cover map is referred to as the pre-clearing land cover map. The areas identified as being cleared are shown *figure 5.2 a*, with the pre-clearing land cover map shown in *figure 5.2 b*.

Table 5.1 Australian Land Cover Equivalence from the Classifications of Graetz et al. (1995) to Simple Biosphere biome classes

Land Cover Code	Structural Description	Overstorey Dominance	Simple Biosphere Biome
xTML4	Closed Forest	Other	Broadleaf-evergreen Trees
eTML3	Open Forest	Eucalyptus	Broadleaf-evergreen Trees
wTML3	Open Forest	Acacia	Trees with Groundcover
xTML3	Open Forest	Other	Trees with Groundcover
eM2	Woodland	Eucalyptus	Trees with Groundcover
wM2	Woodland	Acacia	Trees with Groundcover
xM2	Woodland	Other	Trees with Groundcover
eL2	Low Woodland	Eucalyptus	Trees with Groundcover
wL2	Low Woodland	Acacia	Trees with Groundcover
xL2	Low Woodland	Other	Trees with Groundcover
eM1	Open Woodland	Eucalyptus	Trees with Groundcover
wM1	Open Woodland	Acacia	Trees with Groundcover
xM1	Open Woodland	Other	Trees with Groundcover
eL1	Low Open Woodland	Eucalyptus	Trees with Groundcover
wL1	Low Open Woodland	Acacia	Shrubs with Groundcover
xL1	Low Open Woodland	Other	Shrubs with Groundcover
eS3	Shrubland	Eucalyptus	Shrubs with Bare Soil
wS3	Shrubland	Acacia	Shrubs with Bare Soil
xS3	Shrubland	Other	Shrubs with Bare Soil
eS2	Open Shrubland	Eucalyptus	Shrubs with Bare Soil
wS2	Open Shrubland	Acacia	Shrubs with Bare Soil
xS2	Open Shrubland	Other	Shrubs with Bare Soil
eS1	Sparse Shrubland	Eucalyptus	Shrubs with Groundcover
wS1	Sparse Shrubland	Acacia	Shrubs with Groundcover
xS1	Sparse Shrubland	Other	Shrubs with Groundcover
xZ3	Low Shrubland	Other	Shrubs with Bare Soil
xZ2	Low Open Shrubland	Other	Shrubs with Bare Soil
xZ1	Low Sparse Shrubland	Other	Shrubs with Groundcover
xH2	Hummock Grassland	Other	Groundcover Only
xG4	Dense Grassland	Other	Groundcover Only
xG3	Grassland	Other	Groundcover Only
xG2	Open Grassland	Other	Groundcover Only
xG1	Sparse Grassland	Other	Groundcover Only
xF4	Dense Crops and Pasture	Other	Agriculture
xF3	Crops and Pastures	Other	Agriculture
xF1	Sparse Grassland	Other	Groundcover Only
Littoral	Littoral	Other	Trees with Groundcover
Salt Lake	Salt Lake		Bare Soil
Lake	Lake		Water
Urban	Urban		Trees with Groundcover

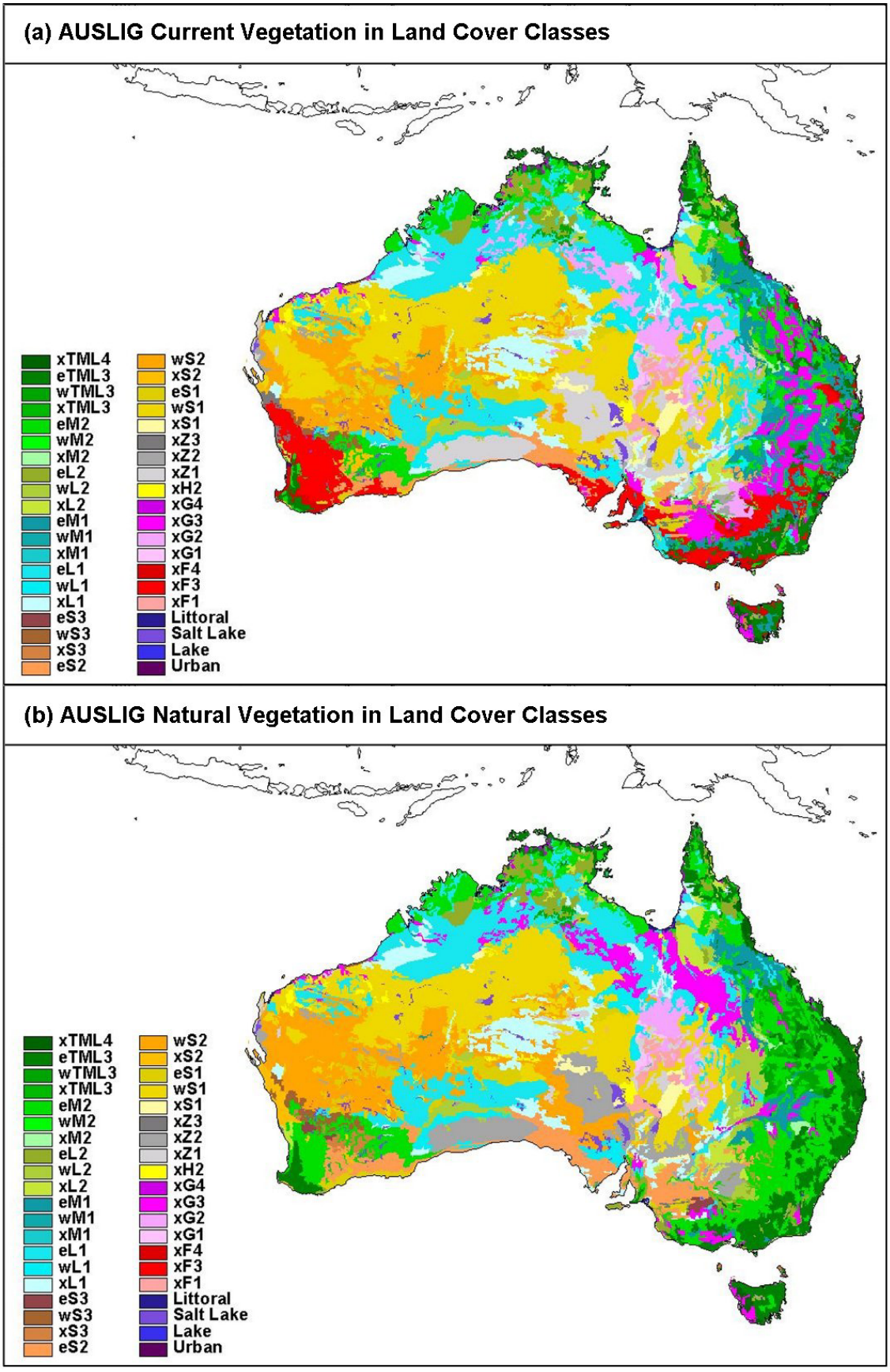

Figure 5.1 (a) Current AUSLIG (1990) Vegetation Map and (b) Natural Vegetation Map, in Land Cover Classes of Graetz et al. (1995)

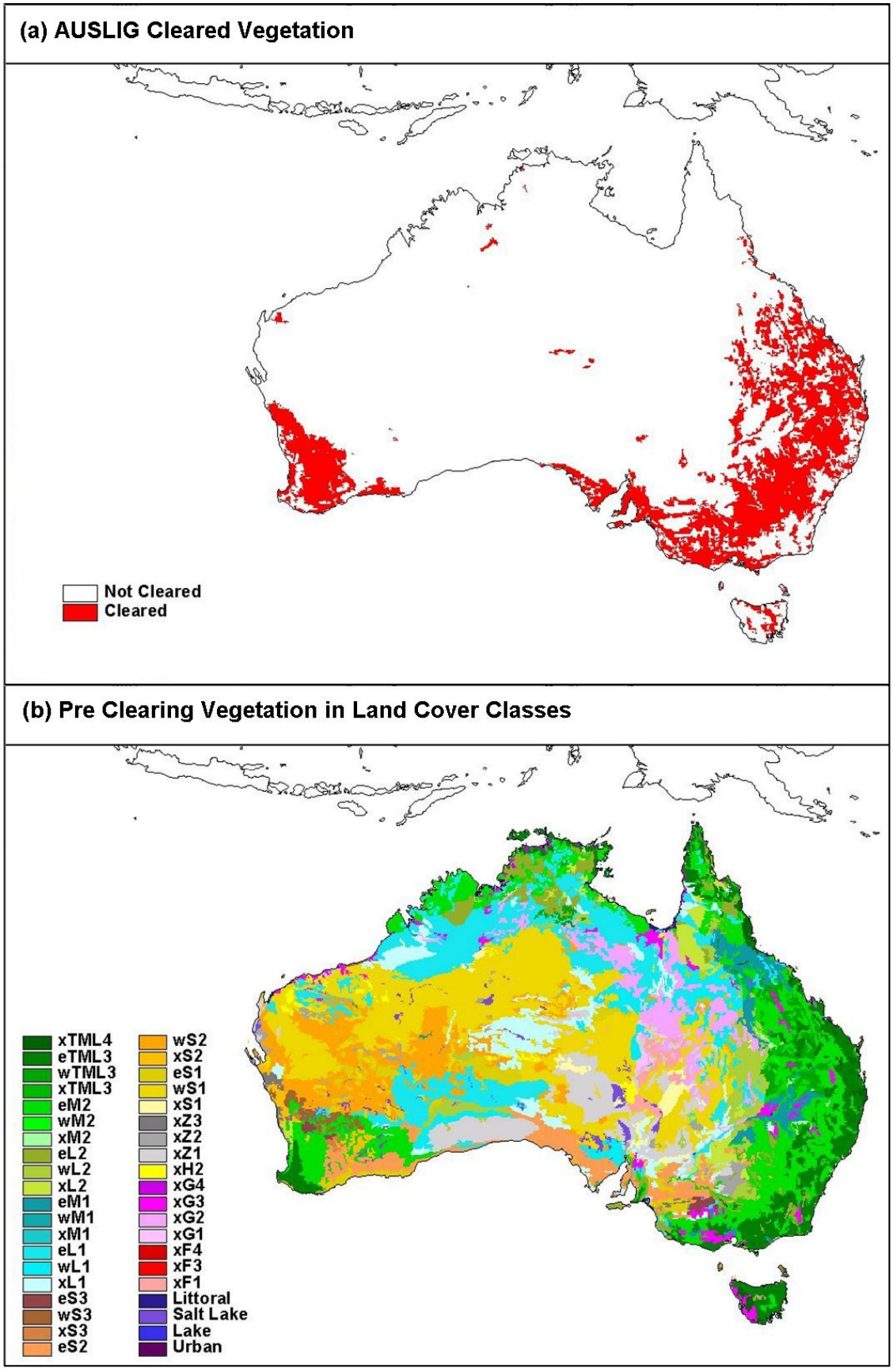

Figure 5.2 (a) Clearing Map developed in Chapter 3 and (b) Pre-clearing Vegetation Map in Land Cover Classes of Graetz et al. (1995)

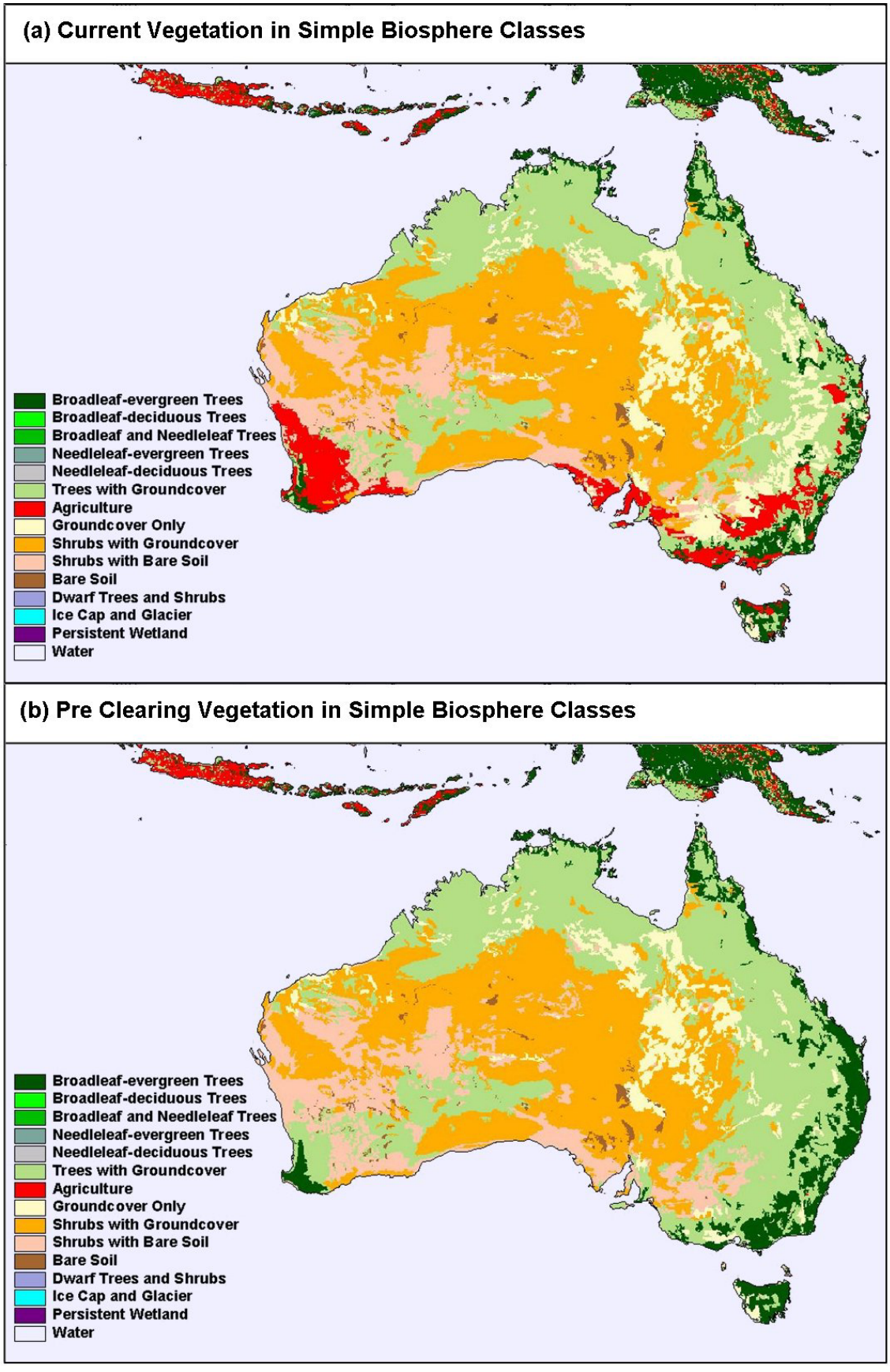

Figure 5.3 Current and Pre Clear Vegetation Maps in Simple Biosphere Classes. These maps are used for generating the vegetation specific parameters used in calculating the new CSIRO GCM land surface parameters

5.2.2 Land Surface Parameter Generation Methods

The current land surface parameters were generated with the methods developed in Chapter 4, using current vegetation mapping, with monthly satellite derived surface albedo and leaf area index. The vegetation mapping was modified from Chapter 4 by replacing the IGBP GLCC vegetation over Australia with the current Australian land cover map reclassified to Simple Biosphere (SiB) classes.

The reclassification of the current land cover classes to SiB classes followed equivalency relationships developed from the definitions of both classifications and spatial analysis of the current Australian land cover map (*figure 5.1 a)* with the IGBP GLCC vegetation map (*figure 4.1 b*). Equivalency was identified where the classifications were commonly mapped by both data sets and had similar structural definitions. The equivalence relationships between the land cover classes of *Graetz et al.* (1995) and the SiB classes are shown in *table 5.1*. The current land cover map reclassified in SiB classes is shown in *figure 5.3 a.*

The pre-clearing land surface parameters of surface albedo, vegetation fraction and leaf area index were generated by extrapolating the current monthly values of remnant native vegetation to the pre-clearing extents of each land cover class. The extrapolation was performed across Australia at the common 8 km resolution of the fine-scale data. The extrapolation technique ensured the seasonal dynamics captured by the satellite imagery were reflected in the monthly pre-clearing parameters.

Unrestrained stomatal resistance and surface roughness were calculated using the pre-clearing land cover map reclassified into the SiB classes using the equivalency relationships developed with the current land cover map. The unrestrained stomatal resistance was taken directly from the same SiB lookup tables used in Chapter 4. The monthly surface roughness was calculated using the simplified roughness model with canopy height specified from SiB look up values and LAI specified from the pre-clearing extrapolated monthly values. The pre-clearing land cover map reclassified in SiB classes is shown in *figure 5.3 b*.

5.2.3 Extrapolation

The extrapolation methods developed to generate the pre-clearing monthly albedo, vegetation fraction and leaf area index are shown graphically in *figure 5.4*. The methods were applied at the 8 km grid cell resolution of the source data before aggregation to the CSIRO GCM parameters following the aggregation rules developed in Chapter 4. For grid cells where the pre-clearing land cover class was the same as the current land cover class, the extrapolation method assigned the current monthly values directly to the pre-clearing values.

In cases where the current and pre-clearing land cover types were different, however, an expanding search box was used to find current monthly values from surrounding remnant land cover of the same type, with the average value from the surrounding remnant monthly values

assigned as the monthly pre-clearing value. The size of the search box was doubled each time remnant native vegetation of the same was not found in the search box. In areas were there was no remnant vegetation of the same type found in the surrounding area, the search was repeated using values from remnant land cover of a similar type.

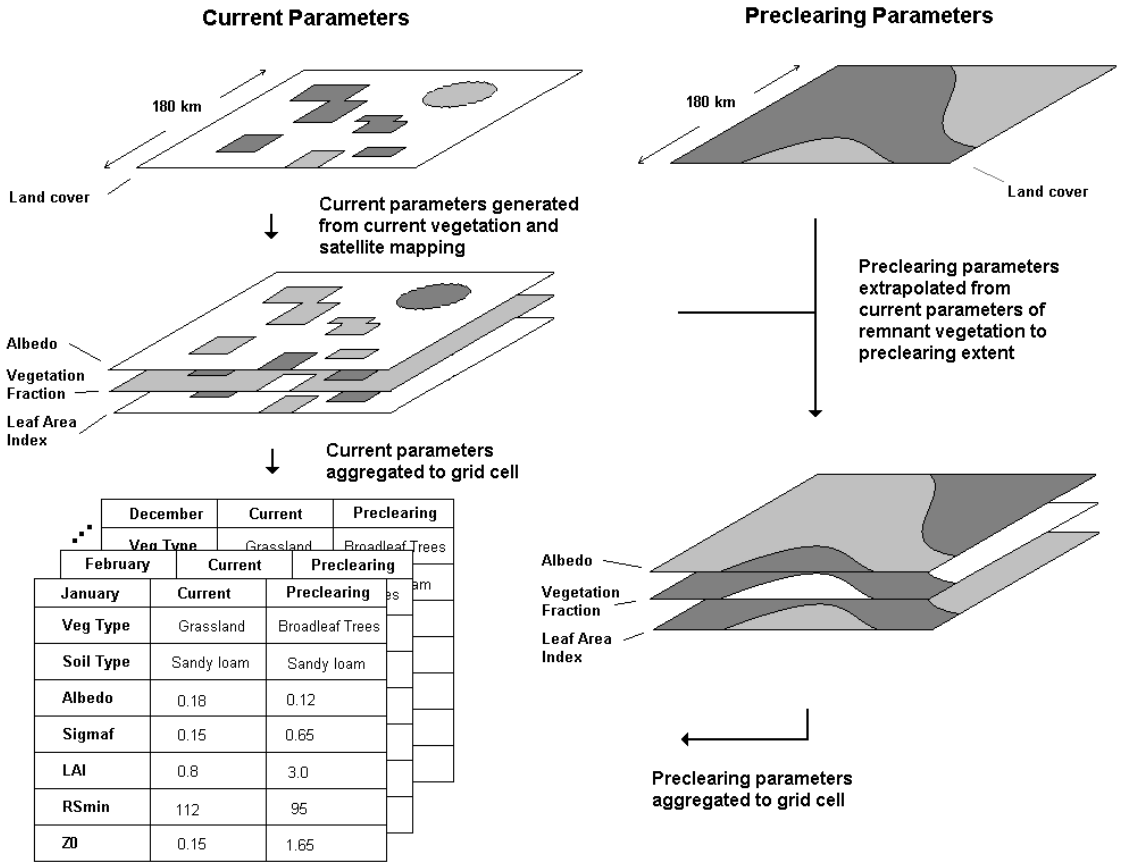

Figure 5.4 Extrapolation techniques for generating Pre-clearing land surface parameters from Current Parameters and Vegetation Maps. The parameterisation methods are shown for a single T63 Grid Increment (1.875 degree) GCM grid cell.

5.2.4 Fine-Scale Data Extrapolation Results

The extrapolated pre-clearing maps of January albedo, vegetation fraction, and leaf area index, along with differences between pre-clearing and current January values are shown in *figure 5.5*, *figure 5.6*, and *figure 5.7* respectively. The pre-clearing albedo maps (*figure 5.5*) show the native land cover was in general darker in January with lower albedo than the crops and pastures that replaced it. The difference in January albedo was largest in the south west of Australia where the native land cover was up to 0.1 lower, and smallest in inland eastern Australia where the differences were mixed with the native land cover between 0.02 higher to 0.02 lower.

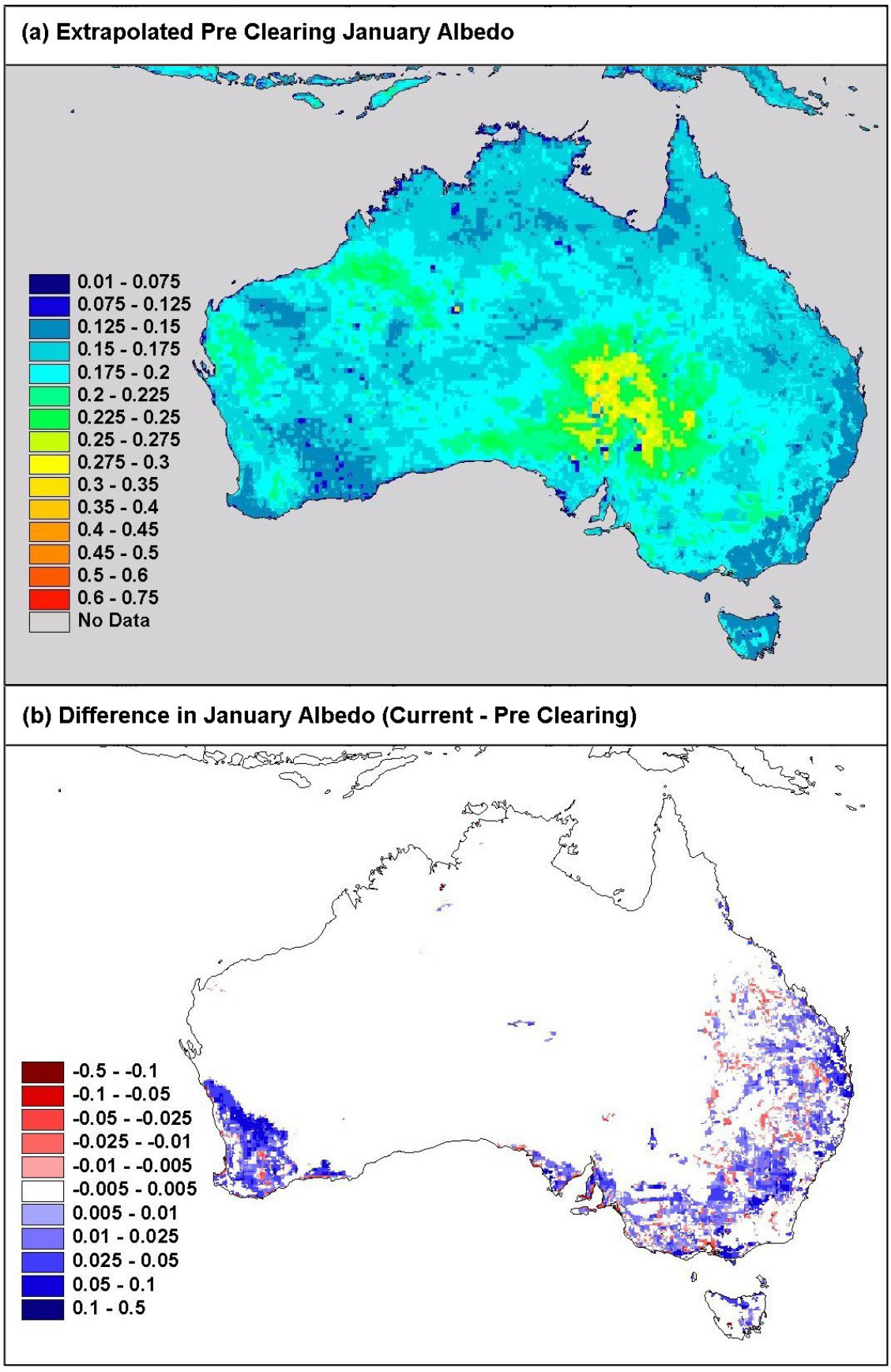

Figure 5.5 (a) Extrapolated Pre-clearing January Surface Albedo and (b) Difference between Pre-clearing and Current Albedo Maps

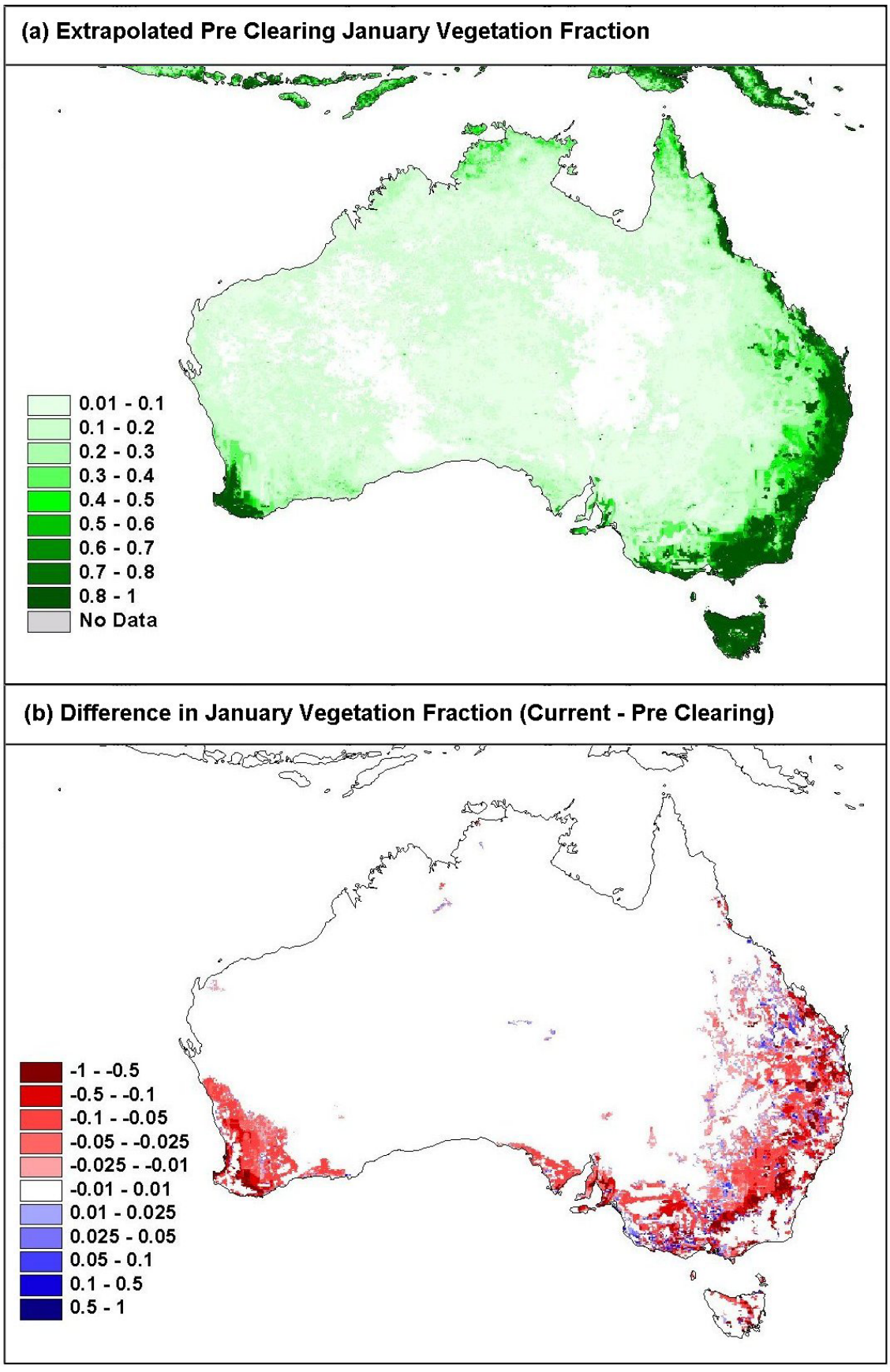

Figure 5.6 (a) Extrapolated Pre-clearing January Vegetation Fraction Map and (b) Difference between Pre-clearing and Current Vegetation Fraction Maps

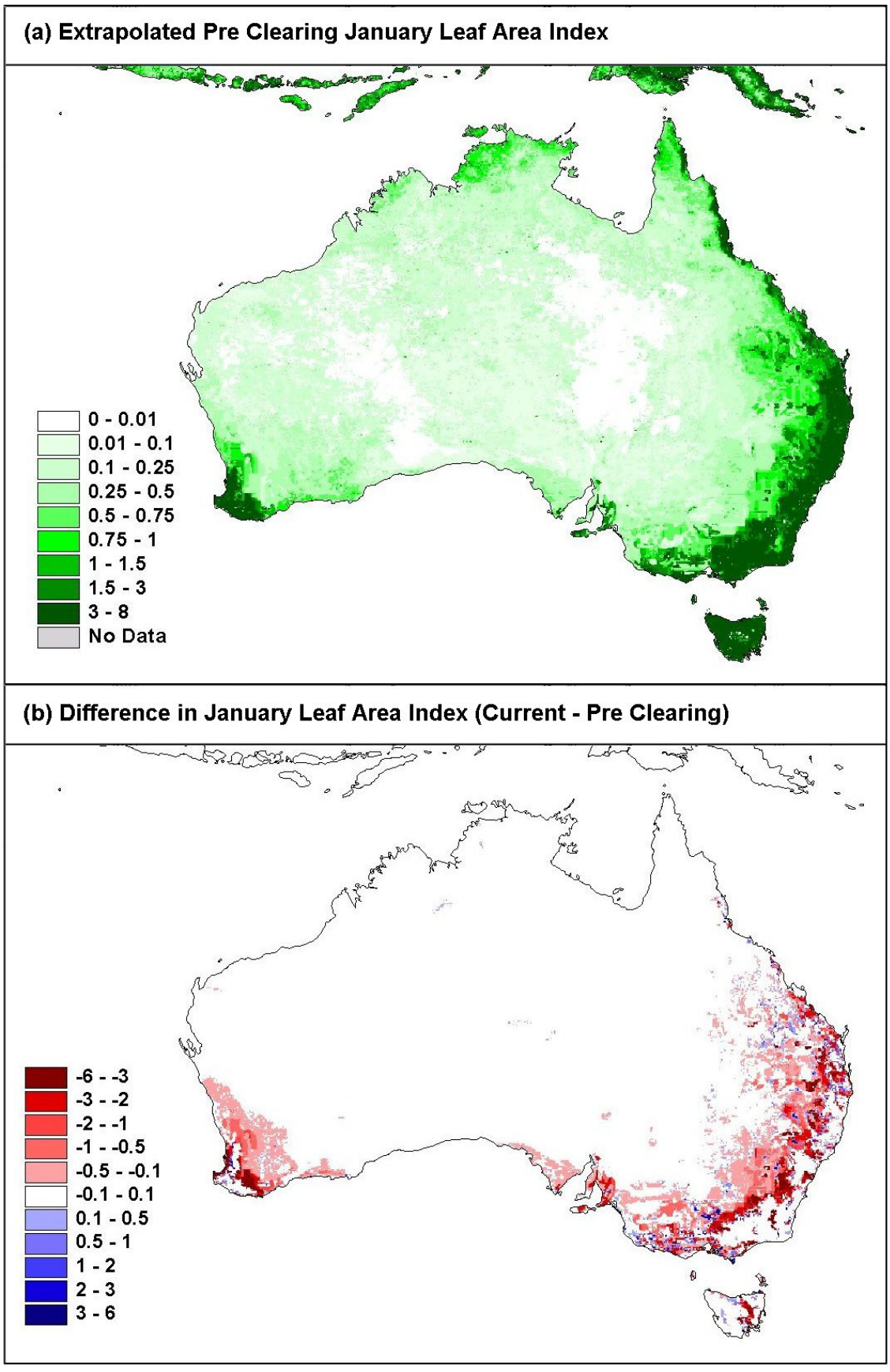

Figure 5.7 (a) Extrapolated Pre-clearing January Leaf Area Index Map and (b) Difference between Pre-clearing and Current Leaf Area Index Maps

The pre-clearing vegetation fraction maps (*figure 5.6*) show that the vegetation fraction was in general higher for the native land cover in January than the replacement land cover. The differences were greatest near the coast where the native land cover was densest, decreasing away from the coast as the native land cover density decreased. Near the coast the native land cover had January vegetation fraction up to 0.8 higher, where as in inland areas of Australia the differences were mixed, with native land cover having vegetation fraction between 0.2 higher and 0.2 lower than the replacement land cover.

The pre-clearing leaf area index maps (*figure 5.7*) show that LAI also was in general higher for the native land cover in January than the replacement land cover. Again the largest differences in LAI were near the coast where the native land cover was densest, with the differences decreasing away from the coast as the native land cover density decreased. Near the coast the native land cover had January LAI values up to 5 m^2m^{-2} higher, but in inland areas the LAI values were between 3 m^2m^{-2} higher and 2 m^2m^{-2} lower than the replacement land cover.

5.2.5 GCM Land Surface Parameters Results

The aggregation methods developed in Chapter 4 were applied to the finer scale pre-clearing and current land surface data to produce CSIRO GCM parameters for Australian pre-clearing and current day land cover. The differences between the pre-clearing and current land surface parameters were assessed for differences in Australian monthly values, to assess the representation of Australian land cover change in the CSIRO GCM land surface conditions. The results from these evaluations are shown for albedo, vegetation fraction, leaf area index, unrestrained stomatal resistance, unrestrained canopy resistance and surface roughness in the graphs of *figure 5.8*. The differences in Australian average values for these parameters are shown geographically for January and July in the Australian land surface differences maps of *figure 5.9* and *figure 5.10*.

Albedo

The monthly average Australian albedo graph (*figure 5.8 a*) shows that the average Australian current albedo was fractionally higher than the pre-clearing value for all months. The difference between the two sets of parameters was small, at around 0.002 (1 %). The differences were greatest in Austral summer and smallest in winter. The January and July albedo maps (*figure 5.9 a* and *5.10 a*) show that the differences in albedo were consistent for both months in the south west corner, however in the east the differences were larger in summer and significantly reduced in winter. The differences in albedo were influenced by changes in vegetation density, vegetation optical properties, the reflectivity of the underlying soils, and sun angle. This complexity resulted in the range of albedo changes from the land cover changes at different geographic localities.

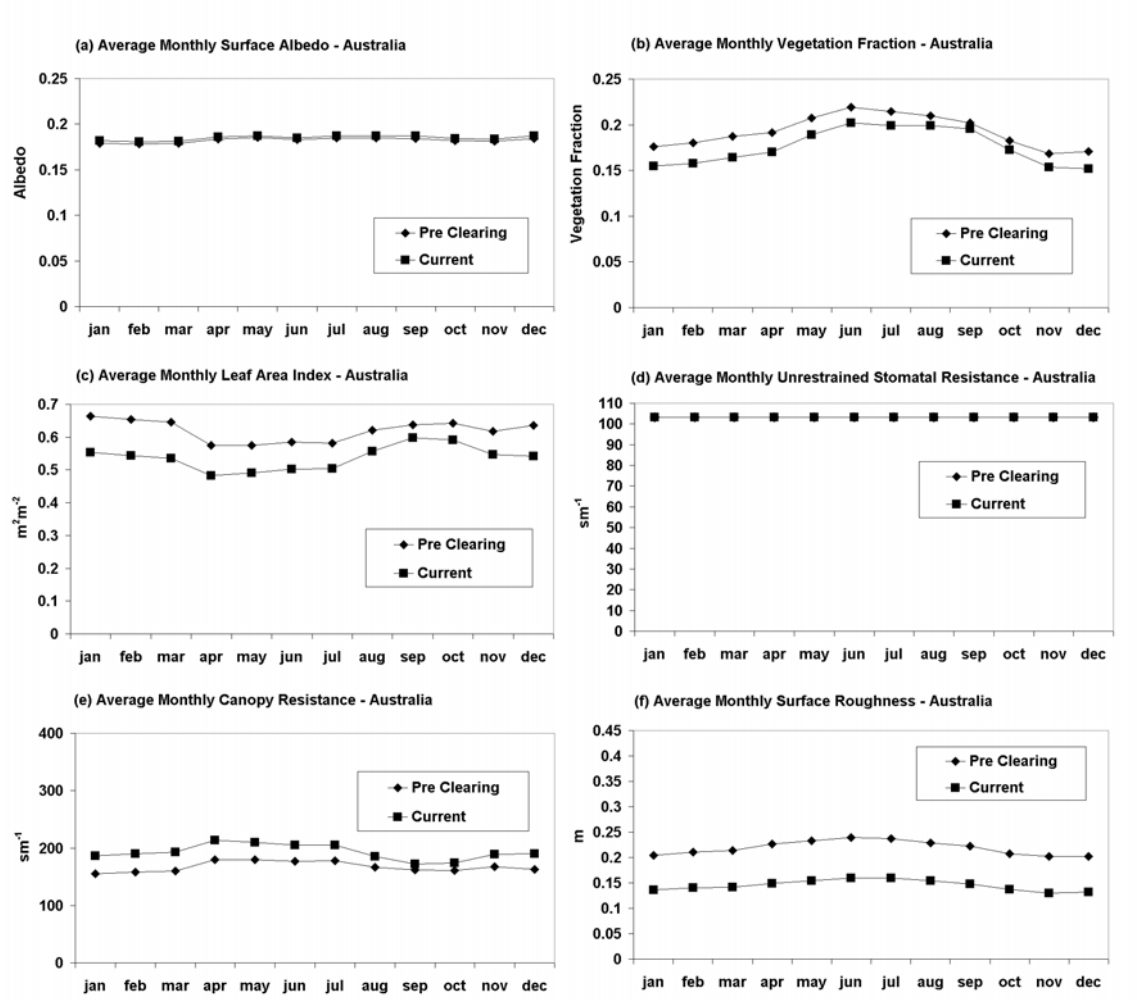

Figure 5.8 Average Australian Monthly Land Surface Parameters for Current and Pre-clearing Experiments

Vegetation Fraction

The monthly average Australian vegetation fraction graph (*figure 5.8 a*) shows that the average Australian current vegetation fraction was significantly lower than the current value for all months except September. The average Australian current vegetation fraction was 0.02 (15 %) lower than the current day value for February, but only 0.006 (3 %) lower for September. The differences between current and pre-clearing vegetation fraction were complex, as vegetation fraction was influenced by the optical properties of the vegetation, LAI, and sun angle. The contribution of LAI to the differences in vegetation fraction is evident for all months, with the largest differences in vegetation fraction coinciding with the largest differences in LAI. The January and July vegetation fraction maps (*figure 5.9 b* and *5.10 b*) show that for the south west and the south east the differences in vegetation fraction were largest in Austral summer and significantly reduced in winter. In central eastern areas, however, there were larger differences in winter than summer.

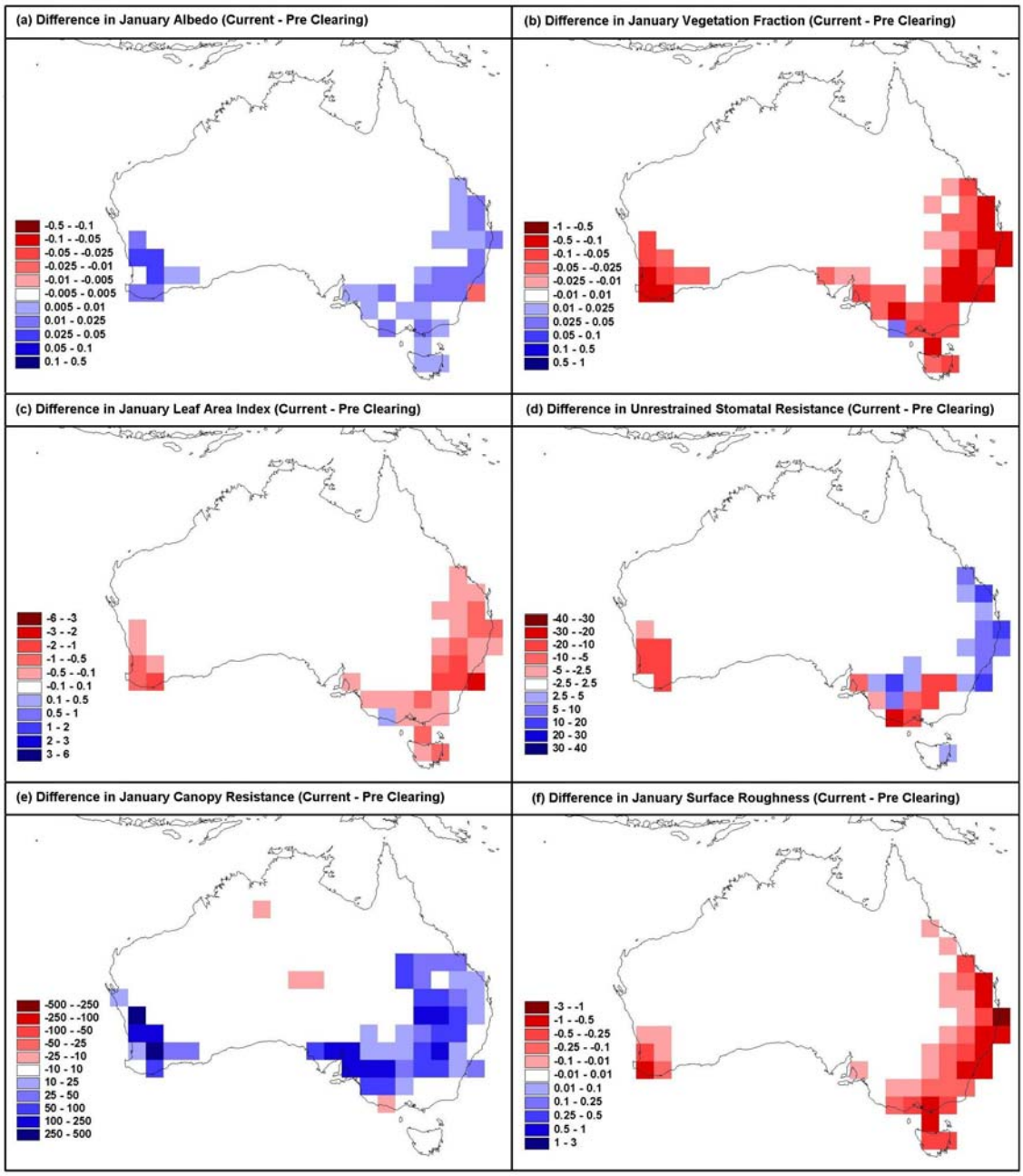

Figure 5.9 January Difference in Land Surface Parameters between Current and Pre-clearing Experiments

Leaf Area Index

The monthly average Australia LAI graph (*figure 5.8 c*) shows that the average Australian current LAI was significantly lower than the pre-clearing value for all months. The differences in LAI were greatest in Austral summer with the average Australian current LAI was 0.11 m^2m^{-2} (20 %) lower than the pre-clearing value for February. The differences in LAI were smallest in spring with average Australian current LAI only 0.04 m^2m^{-2} (6 %) lower than pre-clearing values for September. The January and July LAI maps (*figure 5.9 c* and *5.10 c*) show that like the vegetation fraction, the differences in LAI in the south west and the south east, were largest in Austral summer and were significantly reduced in winter. Again like the

vegetation fraction, the differences in LAI in central eastern areas were larger in winter than summer.

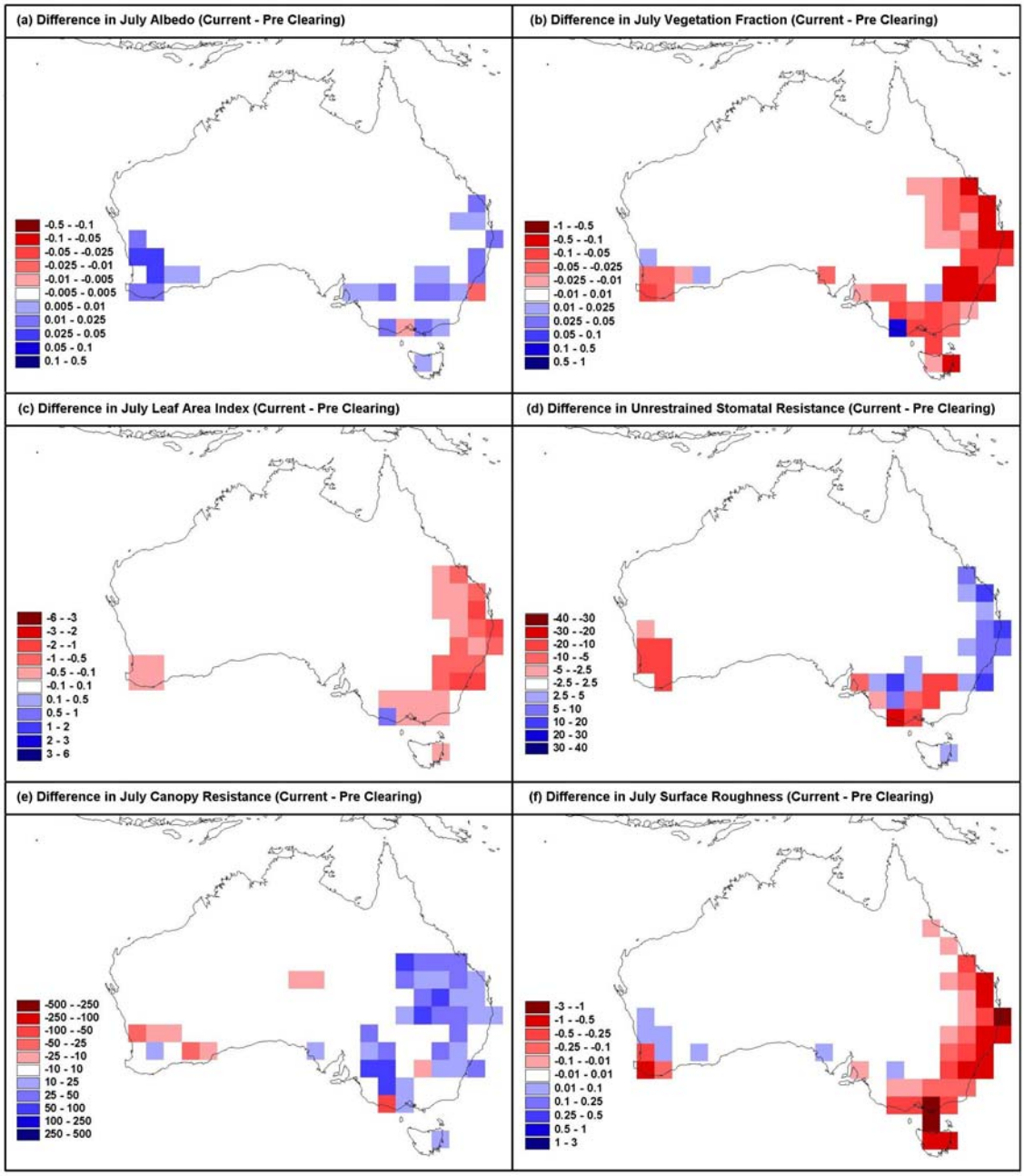

Figure 5.10 July Difference in Land Surface Parameters between Current and Pre-clearing Experiments

The seasonal patterns in the differences in LAI in southern and more northern areas suggest that the differences in LAI between the native land cover and the replacement land cover are strongly influenced by the dynamics of the different land cover types. In southern areas where the replacement land cover is predominantly cropping, the growing and fallow cycles of crops resulted in the differences in LAI being greatest in summer after harvest and smallest during spring with the growing crop. In more northern areas where the replacement

land cover is predominantly pastures the differences were more influenced by the relative responses of the two land cover types to moisture availability and temperature.

Unrestrained Stomatal Resistance

The monthly average Australian unrestrained stomatal resistance graph (*figure 5.8 d*) shows that the difference in average Australian stomatal resistance between the current and pre-clearing values was marginal, with current values only 0.25 sm^{-1} (0.2 %) higher than the pre-clearing value. The unrestrained stomatal resistance also was seasonally invariant for both current and pre-clearing values as it was directly prescribed from the SiB vegetation type of the two land cover maps.

The unrestrained stomatal resistance maps (*figure 5.9 d* and *5.10 d*) show for the south west, that the stomatal resistance of the native land cover was higher than the new land cover. In the south east, the differences in stomatal resistance were mixed and in the central east the native land cover had lower stomatal resistance than the new land cover. The changes in stomatal resistance associated with the land cover changes were directly related to the differences in stomatal resistance of the associated land cover types. In the south west and south east, where crops replaced woodlands, shrublands or grasslands, the stomatal resistance decreased. In the east where woodlands or pastures replaced forests, the stomatal resistance increased. In all other cases the stomatal resistance was unchanged.

Unrestrained Canopy Resistance

The monthly average Australian unrestrained canopy resistance graph (*figure 5.8 e*) shows that the average Australian canopy resistance was significantly higher for current land cover than pre-clearing for all months. The largest differences were in Austral summer where the average Australian current unrestrained canopy resistance was 30 sm^{-1} (20 %) higher than the pre-clearing value. The smallest differences were in spring where the current value was 10 sm^{-1} (6 %) higher. The strong influence of LAI to the differences in canopy resistance is evident for all months, with the differences in canopy resistance corresponded to the differences in LAI, primarily because the unrestrained stomatal resistance was invariant.

The unrestrained canopy resistance maps (*figure 5.9 e* and *5.10 e*) show for the south west, that the canopy resistance of the native land cover was significantly lower than the new land cover in Austral summer but significantly higher in winter. In the east however the maps show the native land cover canopy resistance was significantly lower than the new land cover for both seasons, with the difference largest in summer.

Surface Roughness

The monthly average Australian surface roughness graph (*figure 5.8 f*) shows that the average Australian surface roughness was significantly smaller for current land cover than pre-

clearing for all months. The differences in surface roughness were similar for all months with the average Australian current surface roughness around 0.07 m (50 %) lower than the pre-clearing value. The surface roughness maps (*figure 5.9 f* and *5.10 f*) show that in the south west the surface roughness of the native land cover was significantly higher than the new land cover in Austral summer but there were mixed differences between the land cover types in winter. In the east the maps show the surface roughness of the native land cover was significantly higher for summer and winter, with the largest differences in winter.

5.2.6 GCM Regional Land Surface Parameters Analysis

From the Australian continental analysis of parameters differences, three regions were identified for further investigation of land cover change and climate change in the climate modelling experiments. The regions were selected based on historical clearing patterns, the differences in land surface parameters, and the 50 and 100 year precipitation trend analysis of *Manins et al.* (2001). The regions selected are shown in *figure 5.11* as: south east Queensland; eastern New South Wales; and south west Western Australia. Regional analyses of changes in land surface properties associated with land cover change were performed on the mean monthly land surface parameter values of the two experiments for each region. These regions are also used for the regional analysis of climate impacts of Australian land cover change in the next section.

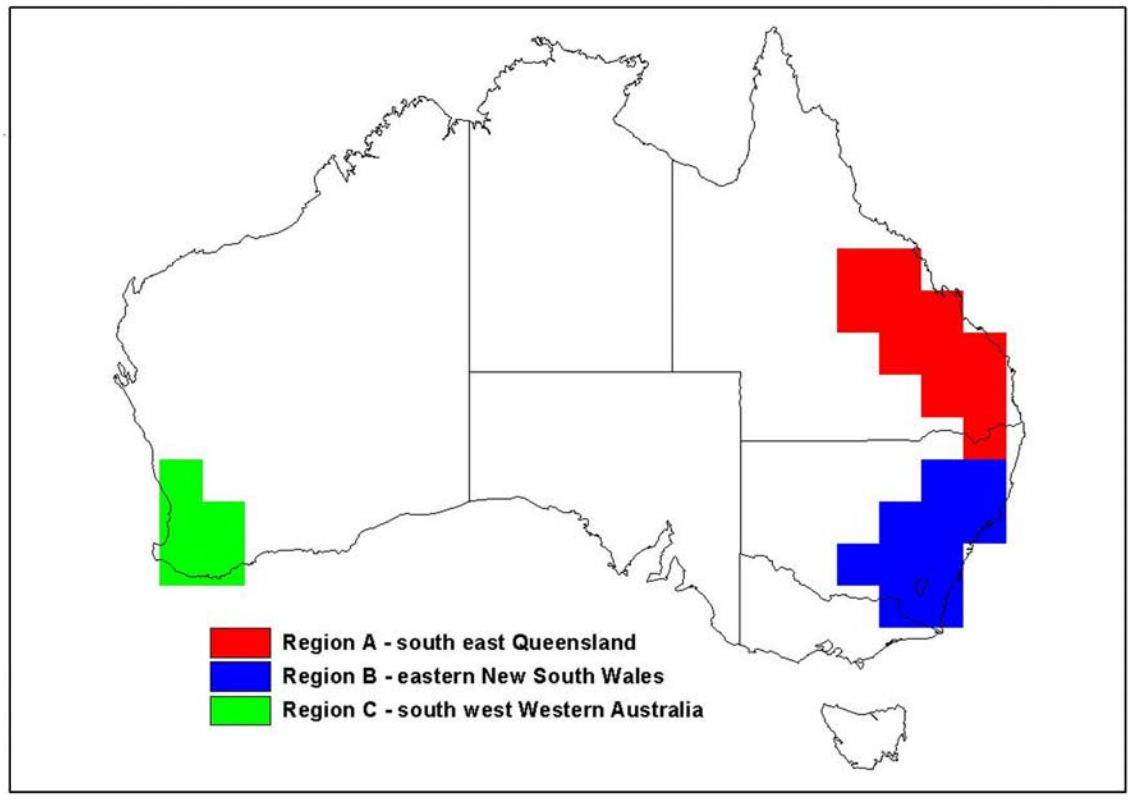

Figure 5.11 Australian Regions for Regional Investigation with Land Cover Change experiments and for Historical Climate Record Analysis

South east Queensland climate impacts

The south east Queensland region has experienced significant historical and ongoing clearing, as shown in Chapter 3, with the continental GCM land cover change analysis showing significant changes in January and July land surface parameter (*figure 5.9* and *5.10*). The 50 year precipitation trend analysis by *Manins et al.* (2001) also identified the region as having a strong decrease in precipitation since 1950 (*figure 1.1 d*).

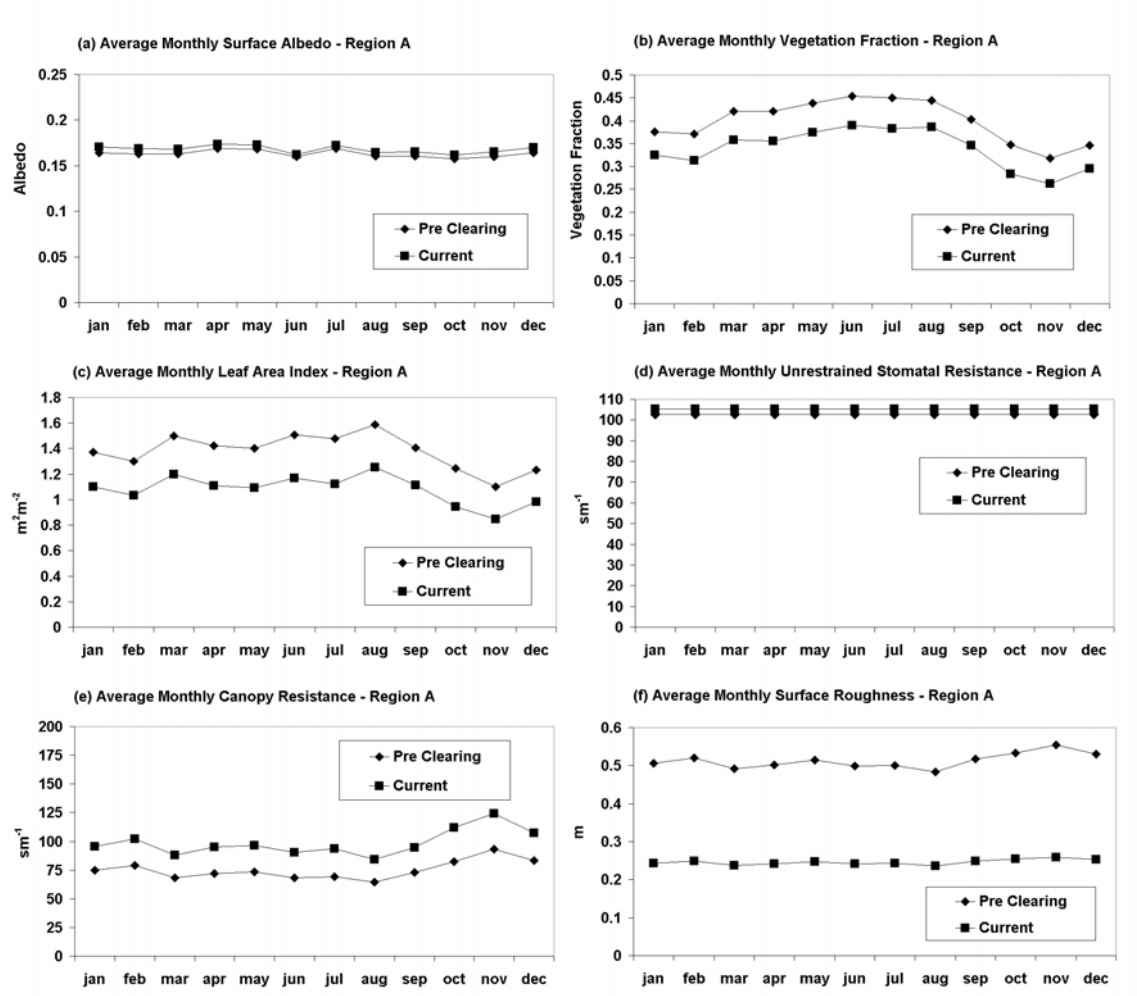

Figure 5.12 Average Monthly Land Surface Parameters for Current and Pre-clearing Experiments for South East Queensland

The average monthly land surface parameter values for the eastern Queensland region are graphed for the current and pre-clearing experiments in *figure 5.12*. The graphs show the current experiment had: average albedo values approximately 0.005 (2.9 %) higher for all months; average vegetation fraction values approximately 0.06 (14.9 %) lower for all months; average leaf area index values approximately 0.3 m^2m^{-2} (21.7 %) lower for all months; average stomatal resistance value 2.7 sm^{-1} (2.6 %) higher; average canopy resistance approximate 23.4 sm^{-1} (31.2 %) higher for all months; and average surface roughness values approximately 0.26 m (52%)

lower for all months. The graphs also show the seasonal patterns of all land surface parameters were the same for both experiments, with the exception of surface roughness, which showed stronger seasonal patterns in the pre-clearing experiment.

Eastern New South Wales climate impacts

The eastern New South Wales region has had significant historical clearing, but limited recent clearing, as shown in Chapter 3. The region also had significant changes in January and July land surface parameters, with the 50 year precipitation trend analysis by *Manins et al.* (2001) showing a strong decrease in precipitation for the region since 1950. The average monthly land surface parameter values for the eastern New South Wales region are graphed for the current and pre-clearing experiments in *figure 5.13*.

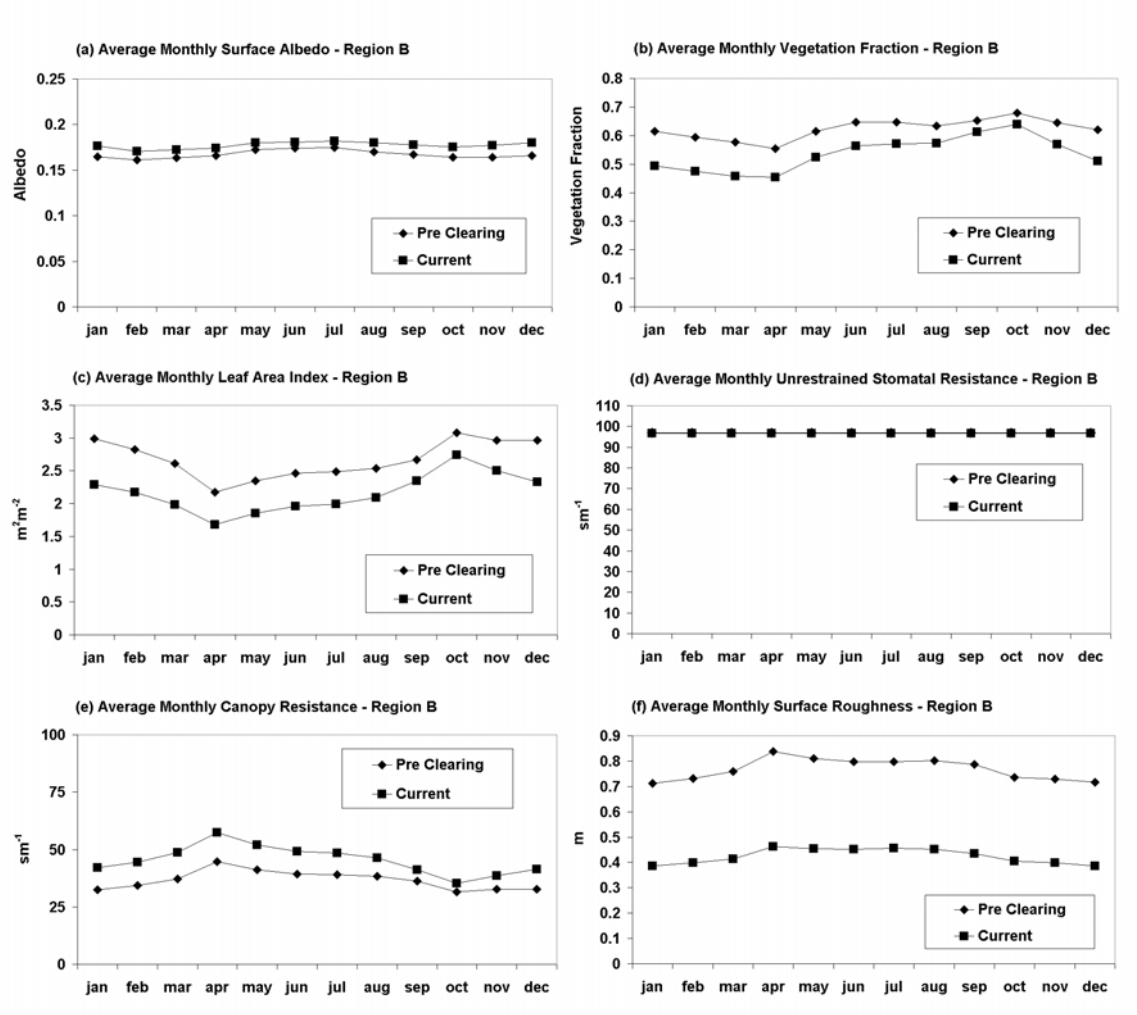

Figure 5.13 Average Monthly Land Surface Parameters for Current and Pre-clearing Experiments for Eastern New South Wales

Unlike the eastern Queensland region, the graphs show the differences between the experiments had significant seasonal cycles. The albedo values of the current experiment ranged from 0.014 (8.4 %) higher in December to 0.006 (3.6 %) higher in June. The vegetation fraction,

leaf area index and canopy resistance differences all showed similar seasonal cycles with the largest differences in January and the smallest differences in October. The vegetation fraction difference ranged from 0.04 (5.7 %) lower in October to 0.12 (19.8 %) lower in January; the leaf area index difference ranged from 0.32 m^2m^{-2} (10.8 %) lower in October to 0.69 m^2m^{-2} (23.2 %) lower in January; the stomatal resistance value was 0.26 sm^{-1} (0.2 %) lower; the canopy resistance difference ranged from 3.7 sm^{-1} (11.8 %) higher in October to 9.7 sm^{-1} (29.9 %) higher in January; and the surface roughness value was approximately 0.34 m (44.7 %) lower for all months, with the seasonal patterns of surface roughness the same for both experiments.

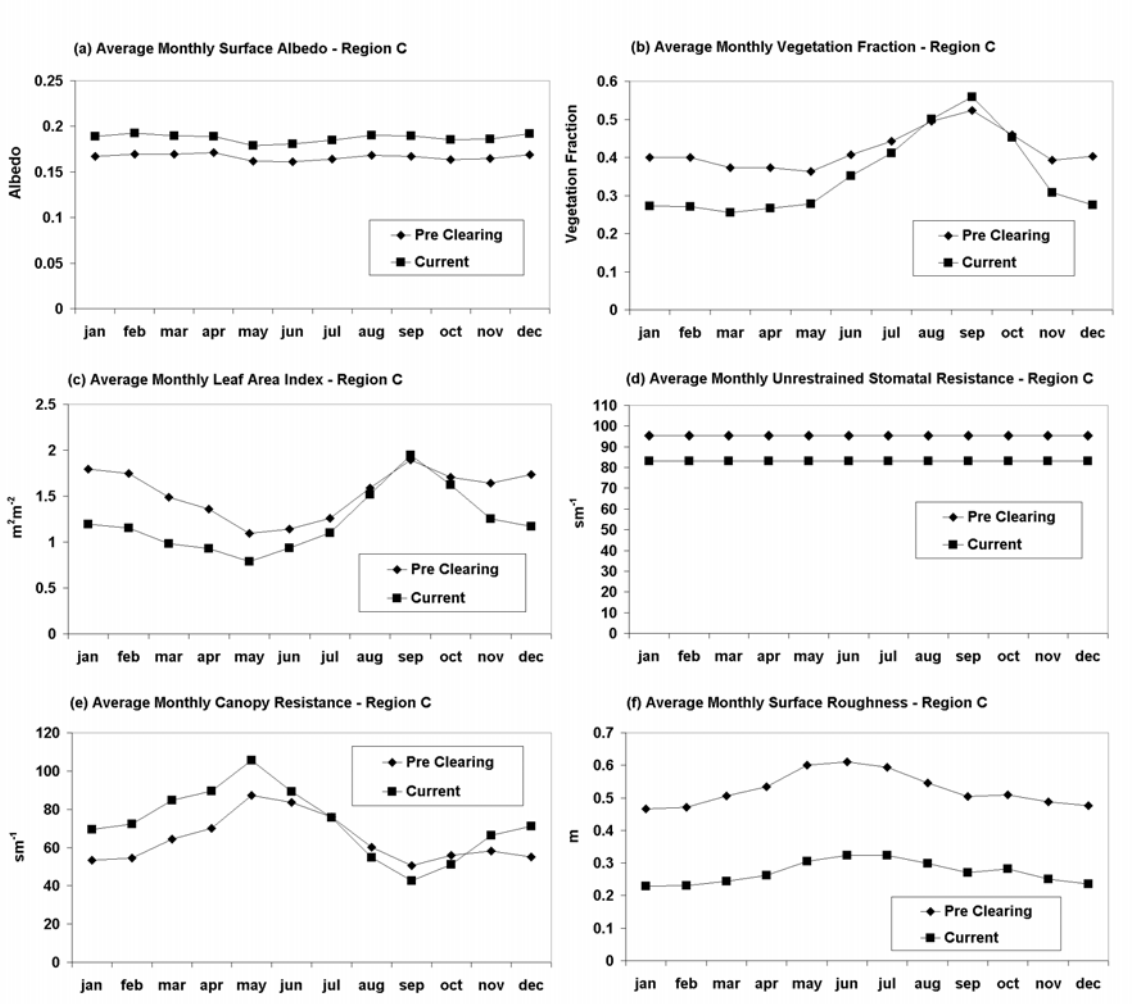

Figure 5.14 Average Monthly Land Surface Parameters for Current and Pre-clearing Experiments for South West Western Australia

South west Western Australian climate impacts

The South west Western Australia region experienced significant historical clearing as shown in Chapter 3, and as was shown in Chapter 2, has been extensively investigated for land cover change and climate change by *Xinmei et al.* (1995), *Lyons et al.* (1993) and *Ray et al.* (2003). The region also had significant changes in January and July land surface parameters,

with large decreases in the 50 and 100 year precipitation trend analysis by *Manins et al.* (2001). The average monthly land surface parameter values for the south west Western Australia region are graphed for the current and pre-clearing experiments in *figure 5.14*. The graphs show there are large differences between the experiments with pre-clearing and current land cover having significantly different seasonal cycles. The differences shown in the graphs reflect the differences observed between native vegetation and agricultural areas in the satellite and field studies of *Xinmei et al.* (1995), *Lyons et al.* (1993) and *Ray et al.* (2003).

The average albedo values of the current experiment were approximately 0.02 (12.7 %) higher for all months; the vegetation fraction difference ranged from 0.128 (32.0 %) lower in January to 0.036 (6.9 %) higher in September; the leaf area index difference ranged from 0.60 m^2m^{-2} (33.2 %) lower in January to 0.05 m^2m^{-2} (2.9 %) higher in September; the stomatal resistance value was 12.4 sm^{-1} (12.9 %) lower; the canopy resistance difference ranged from 16.2 sm^{-1} (30.4 %) higher in January to 7.7 sm^{-1} (15.4 %) lower in September; and the surface roughness value was approximately 0.25 m (48.5 %) lower for all months, with the seasonal patterns of surface roughness the same for both experiments. The vegetation fraction, leaf area index and canopy resistance differences all showed the same seasonal cycles with the largest differences in January and the smallest or marginally reversed differences in September.

5.2.7 Section Summary

1. Australian land cover changes were restricted to historical clearing identified by the differences in AUSLIG natural and current vegetation mapping, to eliminate land cover changes that had high degrees of uncertainty in their nature or extent.
2. The Australian land cover changes were represented in the land surface model of the CSIRO GCM by extrapolating the finer scale current land surface data from remnant native vegetation to pre-clearing extents. These methods captured the subgrid heterogeneity and biogeophysics of the pre-clearing land cover.
3. Australian average albedo was marginally higher (0.002) for all months in the current experiment. It was consistently higher for south west Western Australia (0.02), but in eastern Australia it was higher in summer (0.01) but with mixed differences in winter.
4. Australian average vegetation fraction was significantly lower for the current experiment, with the biggest differences in summer (15%) and smallest differences in spring (3%). In eastern Australia it was consistently lower (~15%), but in south west Western Australia it was significantly lower in summer (32%) but marginally higher in spring (7%).
5. Australian average LAI was significantly lower for the current experiment with largest differences in summer (20%), and smallest differences in spring (6%). In eastern Australia it was consistently lower (~20%) with marginally closer values in southern

areas in spring. In south west Western Australia it was significantly lower in summer (33%) but marginally higher in spring (3%).

6. Australian average stomatal resistance was marginally higher (0.2%) in the current experiment. In south eastern Queensland it was marginally higher (2.6%), in eastern New South Wales it was marginally lower (0.2%), and in south west Western Australia it was significantly lower (13%).
7. Australian average canopy resistance was significantly higher for all months, with the biggest difference in summer (20%) and smallest differences in spring (15.4%). In eastern Australia it was consistently higher with the biggest differences in summer (30%) and the smallest differences in spring (15%). In south west Western Australia canopy resistance was significantly higher in summer (30.4%) but significantly lower in spring (15.4%).
8. Australian average surface roughness was consistently significantly lower (50%) for all months, with the same seasonal patterns in current and pre-clearing experiments. The regional differences were consistent with the differences in the Australian average values.

5.3 Climate Impacts of Australian Land Cover Change Experiments

5.3.1 Experimental Methods

To evaluate the climate impacts of historical Australian land cover change, sensitivity experiments were performed, simulating the climate with the land surface parameters changed from the pre-clearing values to the current values in the CSIRO GCM, in a similar manner to the sensitivity experiments of Chapter 4. Like Chapter 4, the sensitivity experiments were performed as global simulations for 1969 to 1999, with the initial 6 years discarded as a "spin up" period. Again to ensure the only difference in climate forcings was that introduced by the land cover changes, other sources of climate variability were kept consistent by prescribing sea surface temperatures and sea ice distributions, and by setting other forcing factors constant between the two experiments. To assess the differences in the climate simulations, comparisons of the two experiments were performed using average climatological means for the 1975 to 1999 period for a range of climate variables, at a range of scales.

Scales of Analysis

Analysis was performed at four scales. At the scale of the Australian continent, seasonal differences in air temperature and precipitation were evaluated for spatial and temporal patterns across the Australian continent. The analysis involved mapping the differences of the climatological means between the two experiments at the grid increment of the CSIRO GCM, as well as statistical analysis of differences in Australian average air temperature and precipitation

through the modelling period. At the regional scale, the three regions identified in the analysis of the land surface parameter differences were investigated for regional changes in climate associated with land cover change. The climate response was assessed by analysing average annual and seasonal regional air temperature and precipitation using the same time series statistical methods as applied to the Australian continental averages. The final scales of analysis involved investigating the possible larger scale mechanism driving the changes in Australian climate by mapping the differences between the two experiments for a range of climate variables over the area surrounding Australia and globally for austral summer and winter. This was necessary in order to understand:

(i) to what extent climate impacts are the result of direct local-scale processes;
(ii) to what extent are local changes in climate the indirect result of changes in larger-scale atmospheric circulation; and
(iii) how far the climate impacts of Australian land cover change propagate from the Australian continent

Statistical Analysis

Following *Polcher and Laval* (1994), the statistical significance of the changes in average and seasonal Australian and regional air temperature and precipitation, were assessed relative to the inter-annual variance of the values, for the 1975 to 1999 period. The statistical analyses assessed the differences in the variance (standard deviation) about the mean values for both experiments through the Fisher's F test, and the differences in the means through the time series through the Student's T test. The statistical tests were performed using methods developed in S-Plus following the techniques of *Crawley* (2002).

The F test evaluated the probability that the null hypothesis, that the two time series had the same variance about the mean, was correct, with the probability presented as a p value. The T test was performed as a paired T test, with the difference between the two experiments for a given year or season the statistic of interest. The paired T test evaluated the probability that the null hypothesis, that the mean difference of the statistics were the same for the two time series was correct, again with the probability presented as a p value. The intention of the tests was to show that if the null hypotheses were false, then the alternative hypotheses that there were differences in the variance or in the means of the time series were correct. A 95 percent confidence interval was used as the limit for statistical significance on the null hypotheses, with p values of 0.05 indicated the null hypothesis was incorrect, implying the alternative hypothesis was correct within the 95 percent confidence interval.

Experimental Limitations

In addition to the conservative representation of Australian land cover change, the non-dynamic nature of the CSIRO GCM land surface model also requires the prescription of monthly climatologically mean vegetation properties for both the current and pre-clearing land cover. The non-dynamic vegetation does not incorporate responses in vegetation cover and distribution due to changes in longer term climate or changes in inter-annual climate variability in either of the two scenarios. The investigation of meso-scale atmospheric responses to land cover changes also are limited to phenomena with horizontal domains greater than the grid interval of the CSIRO GCM. This prevents investigation into meso-scale circulation changes, which have the potential to amplify or dampen the larger scale changes simulated in the experiments.

5.3.2 Australian Continental Results

The differences in the current and pre-clearing experiments for Australian air temperature and precipitation were compared to assess the modeled impacts of Australian land cover change on Australian continental climate. The annual and seasonal differences in air temperature and precipitation are shown in *table 5.2* for climatological means, standard deviations, and differences of the means over the climate modelling period. The table also shows the statistical significance of the differences of the mean values through the Student's T test p values and the statistical significance of the difference of the standard deviations of the mean values through the Fishers F Test p values. The seasonal differences in average air temperature and precipitation also are mapped for the Australian continent in *figure 5.15* and *5.16.*

*Table 5.2 Time Series analysis of Australian Average Air Temperature and Precipitation for Current and Pre-clearing Experiments 1975 –1999. Seasons shown are: Annual, Austral Summer (DJF), Autumn (MAM), Winter (JJA) and Spring (SON). * indicates statistical significant result*

Variable	Season	Current Mean	Pre Clear Mean	Diff of Means	F Test (p)	T Test (p)
Air Temperature (^{O}C)	Annual	20.48 (± 0.50)	20.50 (± 0.52)	-0.02	0.79	0.77
	DJF	27.42 (± 5.49)	27.24 (± 5.45)	0.18	0.98	0.00*
	MAM	19.84 (± 0.90)	20.05 (± 1.05)	-0.21	0.45	0.35
	JJA	12.31 (± 0.72)	12.14 (± 0.75)	0.17	0.85	0.40
	SON	22.39 (± 0.50)	22.58 (± 0.46)	-0.19	0.66	0.08
Precipitation (mm/day)	Annual	1.73 (± 0.03)	1.70 (± 0.39)	0.03	0.78	0.73
	DJF	3.27 (± 0.69)	3.36 (± 0.70)	-0.09	0.91	0.05*
	MAM	1.82 (± 0.50)	1.74 (± 0.74)	0.08	0.06	0.59
	JJA	0.84 (± 0.23)	0.79 (± 0.23)	0.05	0.99	0.36
	SON	0.97 (± 0.29)	0.93 (± 0.29)	0.03	0.93	0.48

The seasonal analysis of average Australian air temperature (*table 5.2*) shows that while the current experiment was marginally cooler overall (0.02 ^{O}C), there were larger seasonal differences between the two experiments, with the current experiment warmer for austral summer (0.18 ^{O}C) and winter (0.17 ^{O}C), but cooler in autumn (0.21 ^{O}C) and spring (0.19 ^{O}C). The time series statistical analysis shows the increase in summer air temperature was the only statistically significant difference in average Australian air temperature at the continental scale. The analysis also showed there were no statistically significant differences in the variance of average Australian air temperature between the experiments.

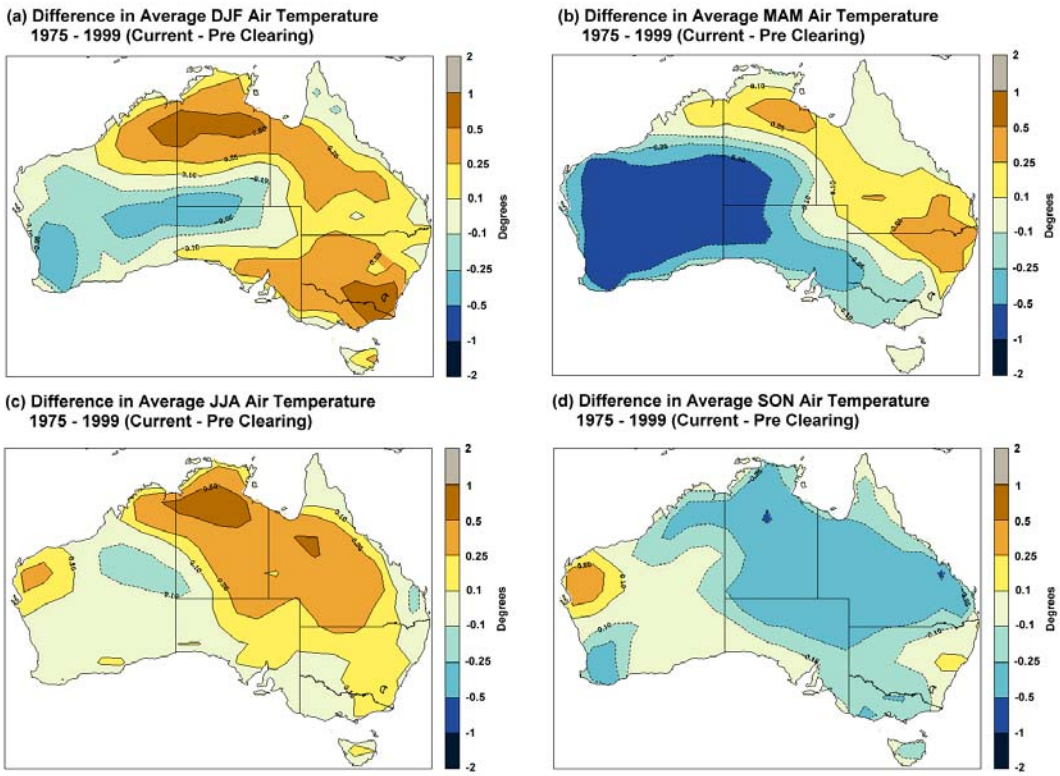

Figure 5.15 Average Air Temperature for Australia 1975 – 1999: Difference between Current and Pre-clearing Experiments for Austral Summer (DJF) (a), Autumn (MAM) (b), Winter (JJA) (c), and Spring (SON) (d)

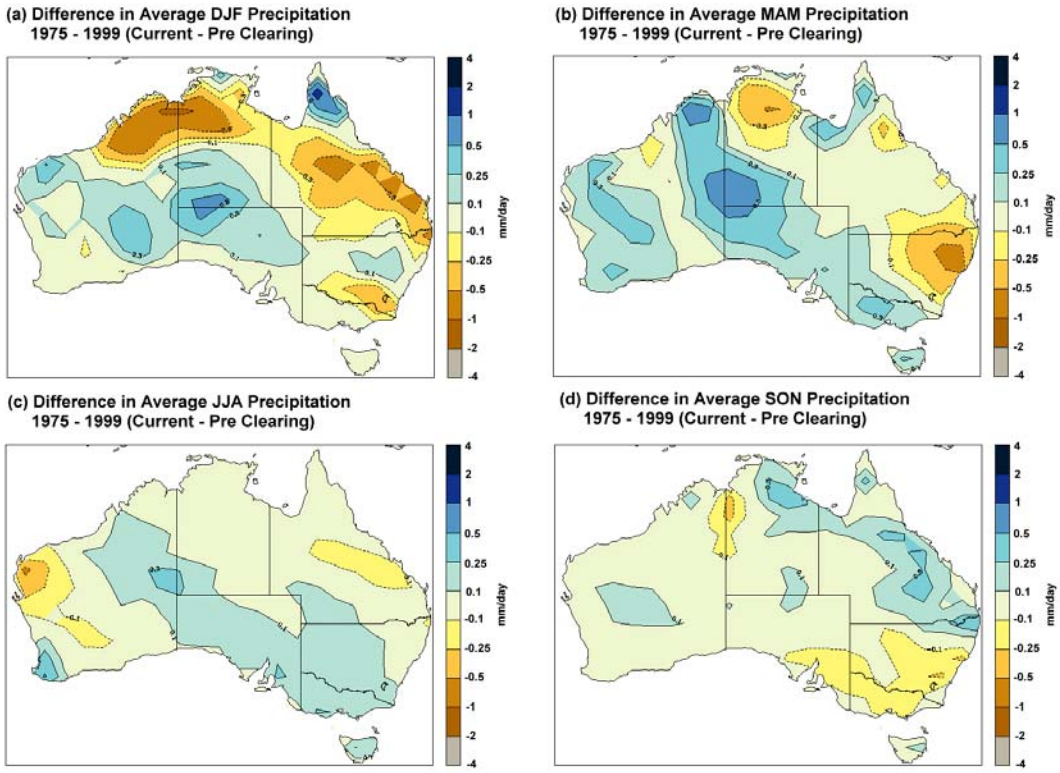

Figure 5.16 Average Precipitation for Australia 1975 – 1999: Difference between Current and Pre-clearing Experiments for Austral Summer (DJF) (a), Autumn (MAM) (b), Winter (JJA) (c), and Spring (SON) (d)

The summer air temperature difference map (*figure 5.15 a*) shows the higher summer air temperatures of the current experiment were focused across the north and south east of the continent, where temperatures were up to 1.0 ^{O}C warmer than for the pre-clearing experiment. In the south west and central areas of the continent the summer air temperature was cooler in the current experiment, with temperatures up to 0.5 ^{O}C lower.

The autumn air temperature difference map (*figure 5.15 b*) shows the cooler autumn air temperatures of the current experiments were focused across Western Australia into the center of the continent, where temperatures were up to 1.0 ^{O}C cooler than the pre-clearing experiment. The autumn map also showed the warmer areas of the summer map persisted in the north and the east, but the differences were reduced from the summer differences. The winter air temperature difference map (*figure 5.15 c*) shows like summer, the warmer winter air temperatures of the current experiment were focused in the north and eastern areas. Unlike summer however the cooling in the west was significantly reduced. The spring air temperature difference map (*figure 5.15 d*) shows the cooler air temperatures of the current experiment were focused across the north and east, with significant cooling over the south west corner.

The seasonal analysis of average Australian precipitation (*table 5.2*) shows that while the current experiment had marginally higher precipitation overall, there were larger seasonal differences between the two experiments, with the current experiment having lower precipitation for austral summer (0.09 mm/day), higher precipitation for autumn (0.08 mm/day),

winter (0.05 mm/day), and spring (0.03 mm/day). The time series statistical analysis of average Australian precipitation shows the decrease in summer precipitation was the only statistically significant difference in precipitation between the two experiments at the continental scale. The analysis also showed there was a near statistically significant difference in the variance of average Australian precipitation for autumn with the standard deviation of the current experiment lower than the pre-clearing experiment.

The summer precipitation difference map (*figure 5.16 a*) shows the lower summer precipitation of the current experiment was concentrated in the north and east, with precipitation up to 2 mm/day lower in these areas. The differences in summer precipitation also showed increases in central Australia of up to 1 mm/day, and in the far north east over Cape York of up to 2 mm/day. The autumn precipitation difference map (*figure 5.16 b*) shows the higher autumn precipitation of the current experiment was largest in central Australia, with precipitation up to 1 mm/day higher. There also were widespread increases in precipitation across the west and in the south east, with areas of lower precipitation in eastern Australia and the north, where precipitation was up to 1 mm/day lower.

The winter precipitation difference map (*figure 5.16 c*) shows the higher winter precipitation of the current experiment again was focused over central Australia, in a band from the north west to the south east, with increases up to 0.5 mm/day higher. There also was an increase in precipitation over the south west corner, again with increases up to 0.5 mm/day higher. The remainder of the Australian continent showed little change between the experiments with the exception of small decreases in precipitation in western and eastern areas. The spring precipitation difference map (*figure 5.16 d*) shows the higher spring precipitation of the current experiment was focused across the north east, with precipitation up to 0.5 mm/day higher. The maps also shows there was lower spring precipitation across the south east, however the precipitation was only up to 0.25 mm/day lower in these areas.

5.3.3 Australian Regional Results

South east Queensland climate impacts

The Australian air temperature and precipitation difference maps show south east Queensland had significant warmer and dryer summer, autumn, and winter, with a cooler and wetter spring in the current experiment. The annual and seasonal time series analyses of air temperature and precipitation for the south eastern Queensland region are shown in *table 5.3*.

*Table 5.3 Time Series analysis of south east Queensland average Air Temperature and Precipitation for Current and Pre-clearing Experiments. Seasons shown are: Annual, Austral Summer (DJF), Autumn (MAM), Winter (JJA) and Spring (SON). * indicates statistical significant result*

Variable	Season	Current Mean	Pre Clear Mean	Diff of Means	F Test (p)	T Test (p)
Air Temperature (^{O}C)	Annual	20.32 (± 0.59)	20.27 (± 0.53)	0.05	0.62	0.69
	DJF	26.16 (± 5.24)	26.01 (± 5.21)	0.15	0.82	0.00*
	MAM	20.29 (± 1.12)	20.10 (± 1.06)	0.18	0.79	0.50
	JJA	12.92 (± 1.14)	12.76 (± 0.91)	0.16	0.27	0.51
	SON	21.94 (± 0.50)	22.26 (± 0.63)	-0.33	0.25	0.02*
Precipitation (mm/day)	Annual	2.09 (± 0.49)	2.20 (± 0.49)	-0.11	0.96	0.37
	DJF	4.43 (± 0.95)	4.75 (± 1.00)	-0.31	0.82	0.00*
	MAM	1.79 (± 0.84)	1.86 (± 1.04)	-0.07	0.30	0.76
	JJA	0.71 (± 0.31)	0.80 (± 0.36)	-0.10	0.46	0.30
	SON	1.56 (± 0.48)	1.36 (± 0.45)	0.19	0.69	0.13

The air temperature T Test p values show that the 0.15 ^{O}C increase in the region's average summer air temperature, and the 0.33 ^{O}C decrease in average spring air temperature were the only statistically significant changes in mean values between the two experiments. The air temperature F Test p values show that there were no annual or seasonal statistically significant differences in inter-annual variance for the region's air temperature. The precipitation T Test p values show that the 0.11 mm/day decrease in the region's average summer precipitation was the only statistically significant difference in precipitation means between the experiments. The precipitation F Test p values show there were no statistically significant differences in inter-annual variance for the region's precipitation.

Eastern New South Wales climate impacts

The Australian air temperature and precipitation difference maps show eastern New South Wales had mixed differences in precipitation and air temperature for different seasons in the two land cover change experiments. The annual and seasonal time series analyses of air temperature and precipitation for the eastern New South Wales region are shown in *table 5.4*. The air temperature T Test p values show that the 0.4 ^{O}C increase in the region's average summer air temperature was the only statistically significant change in mean values between the two experiments. The air temperature F Test p values show that there were no annual or seasonal statistically significant differences in inter-annual variance for the region's air temperature.

*Table 5.4 Time Series analysis of eastern New South Wales Average Air Temperature and Precipitation for Current and Pre-clearing Experiments. Seasons shown are: Annual, Austral Summer (DJF), Autumn (MAM), Winter (JJA) and Spring (SON). * indicates statistical significant result*

Variable	Season	Current Mean	Pre Clear Mean	Diff of Means	F Test (p)	T Test (p)
Air Temperature (^{O}C)	Annual	14.68 (± 0.30)	14.53 (± 0.42)	0.15	0.12	0.11
	DJF	22.71 (± 4.54)	22.31 (± 4.47)	0.40	0.94	0.00*
	MAM	14.29 (± 0.74)	14.18 (± 0.70)	0.11	0.82	0.51
	JJA	6.80 (± 0.43)	6.67 (± 0.42)	0.12	0.90	0.28
	SON	14.93 (± 0.79)	14.95 (± 0.69)	-0.01	0.51	0.94
Precipitation (mm/day)	Annual	1.83 (± 0.26)	1.94 (± 0.31)	-0.11	0.42	0.16
	DJF	2.53 (± 0.53)	2.59 (± 0.54)	-0.06	0.91	0.22
	MAM	1.47 (± 0.56)	1.77 (± 0.80)	-0.30	0.09	0.13
	JJA	1.40 (± 0.40)	1.30 (± 0.37)	0.10	0.65	0.23
	SON	1.94 (± 0.54)	2.08 (± 0.57)	-0.14	0.78	0.35

The precipitation T Test p values show were no statistically significant difference in precipitation means between the experiments. The precipitation F Test p values show there was a near statistically significant increase in the inter-annual variance of autumn precipitation for the region's precipitation, with the standard deviation decreasing from 0.80 mm/day in the pre-clearing experiment to 0.56 mm/day in the current experiment.

South west Western Australian climate impacts

The Australian air temperature and precipitation difference maps show south west Western Australia had a significantly wetter autumn and winter, with a cooler summer, autumn and spring in the current experiment. The annual and seasonal time series analyses of air temperature for the south west Western Australia region are shown in *table 5.5*. The air temperature T Test p values show that the overall decrease of 0.35 ^{O}C in the region's average air temperature, as well as the decreases in summer, autumn and spring air temperature, were all statistically significant. The air temperature F Test p values show that there were no annual or seasonal statistically significant differences in inter-annual variance for the region's air temperature.

*Table 5.5 Time Series analysis of south west Western Australia Average Air Temperature and Precipitation for Current and Pre-clearing Experiments. Seasons shown are: Annual, Austral Summer (DJF), Autumn (MAM), Winter (JJA) and Spring (SON). * indicates statistical significant result*

Variable	Season	Current Mean	Pre Clear Mean	Diff of Means	F Test (p)	T Test (p)
Air Temperature (^{O}C)	Annual	16.73 (± 0.47)	17.08 (± 0.39)	-0.35	0.37	0.00*
	DJF	22.98 (± 4.60)	23.30 (± 4.66)	-0.32	0.95	0.00*

	MAM	16.81 (± 0.72)	17.51 (± 0.81)	-0.70	0.59	0.01*
	JJA	10.38 (± 0.66)	10.42 (± 0.50)	-0.04	0.18	0.73
	SON	16.77 (± 0.55)	17.09 (± 0.38)	-0.32	0.07	0.02*
Precipitation (mm/day)	Annual	1.10 (± 0.23)	0.98 (± 0.22)	0.12	0.91	0.09
	DJF	0.59 (± 0.15)	0.56 (± 0.14)	0.03	0.67	0.31
	MAM	1.33 (± 0.60)	1.13 (± 0.49)	0.21	0.36	0.22
	JJA	1.70 (± 0.39)	1.46 (± 0.29)	0.24	0.14	0.01*
	SON	0.75 (± 0.24)	0.73 (± 0.29)	0.02	0.29	0.78

The precipitation T Test p values show the only statistically significant difference in precipitation means was the 0.24 mm/day increase in winter, which resulted in the near significant increase in annual precipitation of 0.12 mm/day. The precipitation F Test p values show that there were no annual or seasonal statistically significant differences in inter-annual variance for the region's precipitation.

5.3.4 Observed Changes in Australian Annual Precipitation

To compare the changes in climate identified in the climate modelling experiments to observed changes in Australian climate, the analysis performed by *Manins et al.* (2001) into changes in Australian annual precipitation was repeated using precipitation data from the Queensland Department of Natural Resources and Mines' SILO database (*Jeffery et al.*, 2001). Linear regression analysis was performed for the Australian continent, and for the three regions identified in the land cover change parameter analysis for the 1900 to 1999 and the 1950 to 1999 time periods, using annual precipitation data at the 5km resolution of the SILO interpolated surfaces. The results of the linear regression analyses are mapped for Australia in *figure 5.17*, with comparative precipitation changes between the regression analysis and the modelling experiments shown in *table 5.6*.

*Table 5.6 Comparison of Modelled Precipitation Changes and Linear Regression of Historical Precipitation Records for Australia and Regions. Differences are shown as total changes in annual precipitation for the period investigated * indicates statistical significant result*

Region	Period	Modelled Difference (mm)	Extrapolated Difference (mm)	T Test (p)
Australia	1788 - 1990	9.8		0.73
	1900 - 1999		94.4	0.02*
	1950 - 1999		-6.6	0.92
South east Queensland	1788 - 1990	-40.8		0.37
	1900 - 1999		45.1	0.45
	1950 - 1999		-151.2	0.09

Eastern New South Wales	1788 - 1990	-39.9		0.16
	1900 - 1999		98.7	0.04*
	1950 - 1999		-104.5	0.14
South west Western Australia	1788 - 1990	43.0		0.09
	1900 - 1999		-70.6	0.03*
	1950 - 1999		-34.9	0.41

To make the changes in precipitation in the modelling experiments comparable to the changes in precipitation in the regression analyses, the total change in annual precipitation was extrapolated by multiplying the slope of the regression line by the time period the regression was calculated over. The significance of the regression slope also was calculated based on standard errors using the Student's T test, with a 95% confidence interval was used for statistical significance. From the T test, a p value less than 0.05 negated the null hypothesis that the regression slope was zero, implying the sign of the regression was statistically significant.

The results of the analyses identified no statistically significant changes in continental or regional annual precipitation in the climate modelling experiments, and few statistically significant trends in annual precipitation in the regression analysis. While not statistically significant, there were some corresponding trends in both the modelling and regression analysis. The modelled reductions in annual precipitation for south east Queensland (-40.8 mm), and eastern New South Wales (-39.9 mm) corresponded with the strong drying trends over the 1950 – 1999 period from the regression analysis for those areas (-151.2 mm and -104.5 mm). In south west Western Australia, however, the increase in annual precipitation from the modelling experiments (43 mm), was opposite to the observed changes for both the 1900 – 1999 period (-70.6 mm) and the 1950 – 1999 period (-34.9 mm).

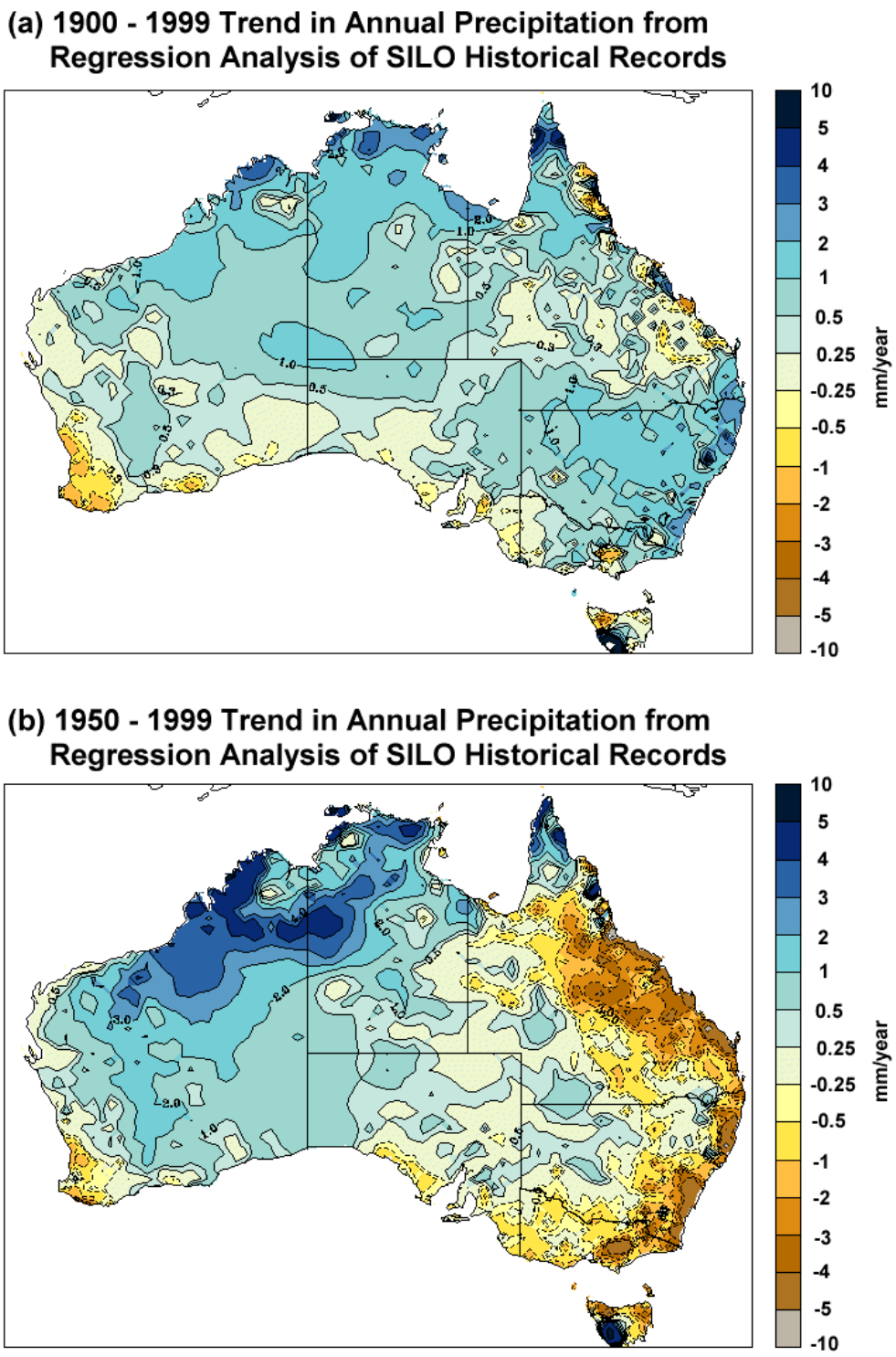

Figure 5.17 Annual Rainfall Trend Analysis from Linear Regression of SILO Rainfall Data for (a) 1900 – 1999 and (b) 1950 – 1999

Using regression trends to identify continental and regional long term trends in Australian precipitation was problematic, as the sign and magnitude of the trends shown were highly dependent on the time period selected. This complexity arose from the high variability in Australian annual precipitation and the issues of using regression analysis to detect change in a time series with multi-decadal and inter-decadal variability (*Crimp and Day*, 2003). The

magnitude of the variability in Australian precipitation is shown in the Australian annual precipitation time series graph of *figure 5.18*.

What is evident from both the annual precipitation and the 10 year running mean, is there is large variability in precipitation through the time period, with apparent cyclical patterns in the running means. One widely accepted influence on Australian precipitation is the El Niño-Southern Oscillation (ENSO), which has widespread impacts on eastern Australian rainfall and operates on inter-annual and quasi-biennial time scales (*McBride and Nicholls*, 1983). Another more recently identified source of variability is the inter-decadal oscillations in Pacific Ocean sea temperatures that appear to be correlated with the impact that ENSO has on eastern Australian rainfall (*Power et al.*, 1999).

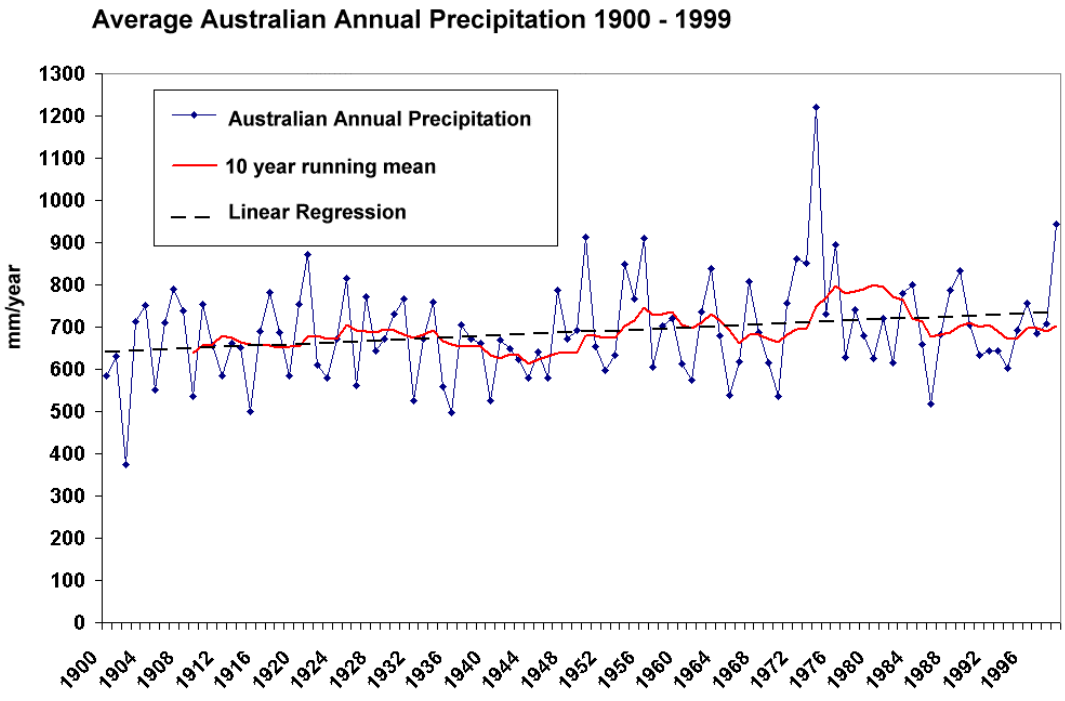

Figure 5.18 Yearly Average Annual Precipitation for Australia for 1900 – 1999 with 10 year running mean and regression line for the period

Wright and Jones (2003) also suggest that the decline in precipitation in south west Western Australia may be symptomatic of wider scale processes that are now influencing Tasmania, south eastern South Australia and southern Victoria. Analysis of Australian Bureau of Meteorology precipitation in their research indicated that since 1996 these areas have been subject to similar sharp declines in precipitation. *Wright and Jones* (2003) provided a number of possible sources of these declines. The first possibility raised by their study was that the precipitation decline is a product of poleward contraction of the mid latitude westerlies and Australian rain producing pressure systems as a result of global warming associated with increased greenhouse gas concentration. Another possibility raised followed recent work by

Thompson and Solomon (2002) indicating the growth of the Antarctic ozone hole over the past 20 to 25 years has strengthened the circumpolar vortex, again with a poleward contraction of the mid latitude westerlies and rain producing pressure systems.

Given there are so many other sources of variability influencing Australian precipitation it is difficult to isolate out the precipitation changes associated with land cover change from the back ground noise. This difficulty is compounded by the incremental nature of land cover change associated with the development of agriculture in Australia, as shown in Chapter 3. As a result of these difficulties it was not possible to directly attribute any statistically significant change in annual precipitation from the Australian land cover change modelling experiments to changes identified by *Manins et al.* (2001). It is important to note, however, that the comparative analysis was only performed on annual precipitation which had no statistically significant changes in the Australian land cover change experiments. There may be statistically significant trends in seasonal precipitation and other climate variables that have been recorded in climate records but were not assessed in this research.

5.3.5 Processes Driving Australian Results

To investigate the possible mechanisms driving the changes in Australian climate in the land cover change experiments, the differences between the two experiments were investigated over the area surrounding Australia for austral summer (DJF) and winter (JJA). The differences between the two experiments are shown for the area surrounding Australia in the average differences maps of *figure 5.19*, *5.20* and *5.21* for: climate variables; 850 hPa wind fields, model calculated land surface characteristics; and surface fluxes.

Austral Summer Analysis

The regional DJF climate impacts of land cover change were assessed by investigating differences in climate variables over the three Australian regions previously identified in the land surface parameter analysis. For DJF, all three regions in the current experiment had increased albedo and canopy resistance, and reduced vegetation fraction and surface roughness. These similar land cover changes had distinctly different climate responses for each region.

In south east Queensland the DJF climate of the current experiment was warmer (*figure 5.19 a*), with reduced precipitation (*figure 5.19 c*), mixed differences in mean sea level pressure (*figure 5.19 e*), lower soil moisture (*figure 5.19 g*), less cloud cover (*figure 5.21 a*), increased short wave radiation and sensible heat flux (*figure 5.21 c* and *e*), and reduced latent heat flux (*figure 5.21 g*). In eastern New South Wales the current experiment was warmer, with mixed precipitation differences, marginally higher mean sea level pressure, increased soil moisture, lower cloud cover, mixed short wave radiation and sensible heat flux differences, and reduced latent heat flux. While in south west Western Australia the current experiment was cooler, with

similar precipitation, marginally higher mean sea level pressure, increased soil moisture, reduced cloud cover, and reduced short wave radiation, sensible heat, and latent heat flux.

Looking at the larger scale, the differences in DJF climate variables between the current and pre-clearing experiments show that the climate impacts of land cover change were not limited in extent to the regions of land cover change, but propagated over the Australian continent and over other continents and oceans. The DJF air temperature difference map (*figure 5.19 a*) shows the warmer temperatures of the current experiment over northern and eastern Australia, corresponded with warmer temperatures over Indonesia and India, and cooler temperatures over the rest of the south east Asia. The DJF precipitation difference map (*figure 5.19 c*) shows the lower precipitation of the current experiment over northern and eastern Australia, extended in a band from the Tasman Sea to the east of Australia through Indonesia and into the Indian Ocean to the west. The map also shows there was an area of significantly higher precipitation to the north east of Australia over the South Pacific Convergence Zone (SPCZ), with increased precipitation also over the central Indian Ocean, and a latitudinal band of decreased precipitation from India to the Pacific Ocean.

Investigating the processes that produced the regional and larger scale changes in DJF climate from the Australian land cover changes, requires interpretation and conjecture as the immediate impacts of the land cover change on surface fluxes interact with feedbacks from changes in atmospheric circulation, cloud cover, and soil moisture over a range of spatial and temporal scales. To determine the immediate regional impacts of Australian land cover change, DJF surface fluxes of radiation, energy and moisture were investigated to describe changes in the primary land surface processes. The larger scale climate impacts were investigated by disentangling the direct and indirect feedback mechanisms shown by the DJF climate variable differences maps.

South east Queensland DJF Analysis

In south east Queensland, the DJF surface radiation budget was directly affected by the increased albedo prescribed in the current experiment. The net impact of the changes in surface properties combined with feedbacks, however, was an increase in short wave radiation flux. This increase in short wave radiation flux can be attributed to the decrease in cloud cover over the region which was a feedback with a larger impact than the increase in albedo. The DJF latent heat flux was directly affected by the increased canopy resistance, reduced vegetation fraction, and reduced surface roughness prescribed in the current experiment, which resulted in decreased latent heat flux over the region. The latent heat flux was further decreased through feedbacks by reduced soil moisture, reducing evaporation and transpiration. While the DJF sensible heat flux over the region was directly affected by the reduced surface roughness, the net impact of the changes in surface properties combined with feedbacks was an increase in sensible heat flux. The higher short wave radiation flux and lower latent heat flux appear to have more

influence on sensible heat flux than the reduced surface roughness, with the result increased DJF sensible heat flux and surface heating over the region.

The south east Queensland DJF feedbacks involved with the decreases in cloud cover, precipitation and soil moisture, were complex as the processes driving these feedbacks operated a range of scales. Following the theory of Chapter 2, at the local scale the changes in surface fluxes impacted air temperature, precipitation and cloud cover, through changes in the surface energy balance and through convective processes in the boundary layer. The net impact of the higher DJF sensible heat fluxes, and lower latent heat and moisture fluxes, were warmer DJF air temperatures with a deeper dryer boundary layer resulting in less cloud formation and precipitation. At the larger scale the changes in thermal convection and thermal gradients impacted larger scale circulation between the land and ocean, with the increased sensible heat flux increasing thermal convection and the thermal gradient between the land and the adjacent Pacific Ocean. The increased thermal convection and thermal gradient combine with the reduced surface roughness to increase the low level easterly wind flow from the Pacific Ocean into south east Queensland (*figure 5.20 e*).

The increased easterly wind flow into south east Queensland also had an increased southerly component which resulted in cooler more stable air masses from further south in the Pacific Ocean entering the region. The increased easterly wind flow also reduced the monsoon wind flow into northern Australia which reduced the transport of warm moist tropical air from north of Australia into the region. The net impact of these changes in air mass transport was a reduction in DJF moisture flux from both the north and east of Australia, resulting in reduced atmospheric moisture for precipitation and cloud cover. The changes in larger scale circulation and moisture flux combined with the impacts of the local processes to further reduce DJF precipitation and cloud cover. The reduction in precipitation also generating further feedbacks through reduced soil moisture further reducing evaporation and transpiration, which further decreased latent heat flux and increased sensible heat flux.

Eastern New South Wales DJF Analysis

The increase in DJF albedo was larger in eastern New South Wales than south east Queensland, with the net impact on short wave radiation flux over the region mixed. For much of the region the short wave radiation flux was the same for both experiments, however in the north and south of there were areas with increased short wave radiation fluxes and in the west there was an area with reduced short wave radiation flux. These differences in short wave radiation appear to be primarily the result of cloud cover feedbacks, with the areas of increased short wave radiation flux corresponding with the areas of greatest decrease in cloud cover, and the areas of decreased short wave radiation corresponding to areas with increases in cloud cover. In the other areas the decreases in cloud cover appear to be offset by the increase in albedo, with the result similar short wave radiation fluxes for both experiments.

Like south east Queensland, the eastern New South Wales DJF latent heat flux was directly affected by the increased canopy resistance, reduced vegetation fraction, and reduced surface roughness, with the net result decreased latent heat flux over the entire region. This decrease occurred despite an increase in soil moisture, suggesting the impact of the changes in surface properties were larger than the soil moisture feedback. The DJF sensible heat flux was directly affected by the reduced surface roughness, however the net impact of the changes in surface properties combined with feedbacks were mixed over the region. The sensible heat flux was increased in areas where the short wave radiation flux was increased or the latent heat flux decreased, and reduced in areas where the short wave radiation flux was reduced.

The eastern New South Wales DJF feedbacks involved with the changes in cloud cover, precipitation and soil moisture, were not as obvious as in south east Queensland due to the mixed differences in surface fluxes over the region. The net impact of the decreased DJF latent heat flux and the mixed sensible heat flux change was general warming over the region with the largest area of warming in the south associated with the largest decrease in latent heat flux. There also was a general reduction in cloud cover over the region, with mixed impacts for DJF precipitation.

South west Western Australia DJF Analysis

More than the other two regions, the DJF surface radiation budget of south west Western Australia was directly affected by the increased albedo prescribed in the current experiment, with short wave radiation flux significantly decreased over the region. The decrease in short wave radiation flux occurred despite the significant decrease in cloud cover over the region, indicating that the impacts from increased albedo were larger than the cloud cover feedbacks. This was supported by the largest decreases in short wave radiation flux occurring in areas that corresponded with the largest increases in albedo.

The DJF latent heat flux was marginally lower over the region, despite increased soil moisture, indicating the increased canopy resistance, reduced vegetation fraction, and reduced surface roughness had larger impact on latent heat flux, than the soil moisture and precipitation feedbacks. The sensible heat flux over the region also was significantly reduced, primarily as a result of reduced short wave radiation however reduced surface roughness also may have contributed to this decrease. The impact of the decreased DJF short wave radiation flux was cooler air temperatures over the region in the current experiment, with the largest cooling corresponding with the largest decrease in short wave radiation. The impacts on precipitation however were marginal, with both experiments having similar DJF precipitation for the region. Larger scale feedbacks are not obvious for the region in DJF, with wind fields over the region changing only marginally between the two experiments.

Other Australian Regions DJF Analysis

The changes in Australian land cover change experiments also showed changes in DJF climate in regions of Australia that had the same land surface properties in both experiments. In northern Australia the current experiment had warmer DJF air temperature and decreased precipitation for all areas except far north Queensland, which had increased precipitation and similar air temperature. In central Australia, the current experiment had cooler DJF air temperature and increased precipitation. As all these regions had the same land surface properties in both experiments, the changes in air temperature and precipitation were the result of feedbacks from the land cover changes in the other regions.

In northern Australia the largest influence on the DJF climate appears to be the changes in atmospheric circulation, with increased south easterly wind flow from the Pacific Ocean into eastern Queensland, and reduced monsoon flow from Indonesia into northern Australia. As occurred in south east Queensland, the change in wind flow resulted in changes in air mass transport, with a reduction in the DJF moisture flux from both the north and east of Australia into northern Australia. The reduced moisture flux resulted in reduced precipitation and cloud cover, with further feedbacks through reduced soil moisture and increased short wave radiation flux. The net outcomes from these feedbacks were the warmer air temperatures and the reduced precipitation over the region. In far north Queensland, the impacts of the changes in atmospheric circulation where different to the rest of northern Australia, as the altered monsoon flow resulted in increased moisture flux into this area with the net impact an increase in DJF precipitation.

In central Australia the largest influence on DJF climate appears to be the increased easterly wind flow across Australia. While this resulted in reduced moisture flux into eastern Queensland, the impact on the arid interior was increased moisture flux from the less arid east. The increased moisture flux resulted in increased precipitation and cloud cover, with further feedbacks from increased soil moisture and reduced short wave radiation flux. The increased latent heat fluxes and reduced short wave radiation flux resulted in the cooler DJF air temperature, and the increased latent heat flux combined with the increase moisture flux from the east to further increase precipitation and cloud cover.

Outside of Australia DJF Analysis

The difference maps demonstrate the changes in Australian land cover change impacted DJF climate beyond the Australian continent, with these changes appearing to have feedbacks on Australian climate as well. The largest change in DJF climate shown in the difference maps was the reduced monsoon flow into Australia, which resulted in increased monsoon flow over Papua New Guinea into the South Pacific Convergence Zone (SPCZ). The increased flow of warm, moist air into the SPCZ, resulted in increased precipitation and cloud cover in the area, with the increased moist convection resulting in decreased mean sea level pressure.

The lower pressure was a positive feedback on the monsoon flow, increasing the flow into the SPCZ, drawing more air from Indonesia and South East Asia. Another impact from the increased moist convection over the SPCZ was increased high level divergence of air above the SPCZ, which may have resulted in increased subsidence directly south of this region, which may explain the increased mean sea level pressure to the south east of Australia. This area of increased mean sea level pressure also corresponds with the DJF westerly wind flow from south east Australia into the Tasman Sea and it is possible that the decreased latent heat flux over south eastern Australia resulted in air with less moisture flowing into this area, further contributing to the decreased cloud cover and precipitation. The increased pressure to the south east of Australia may also have produced another feedback, through strengthening the easterly flow into eastern Queensland from the Pacific Ocean as well as giving the wind flow the stronger southerly component.

The changes in the monsoon flow into the SPCZ also appear to have impacted the atmospheric circulation over Asia and the Indian Ocean. These changes in circulation may explain the warmer DJF air temperatures over Indonesia and India, and the cooler air temperatures over the rest of the South East Asia. These changes in circulation also may explain the differences in DJF precipitation, cloud cover and mean sea level pressure over these areas. The net affect of the increased monsoon flow into the SPCZ appears to be decreased pressure over the western Pacific Ocean where the much of the increased monsoon flow is drawn from, with an increase in pressure over the Asian continent and the Indian Ocean in response to the decreased flow into Australia. The changes in wind flow also have impacts of the surface fluxes from the oceans surrounding Australia and on the cloud cover and soil moisture of the Asian continent.

Austral Winter Analysis

Like the DJF analysis, the regional JJA climate impacts of land cover change were assessed by investigating the differences in climate variables over the three Australian regions identified in the land surface parameter analysis. For JJA, there were differences in the land surface properties changes between the regions. South east Queensland and eastern New South Wales having marginally higher surface albedo, lower vegetation fraction, lower surface roughness, and higher canopy resistance in the current experiment, while south west Western Australia had significantly higher surface albedo, marginally lower vegetation fraction, lower surface roughness, and marginally lower canopy resistance in the current experiment.

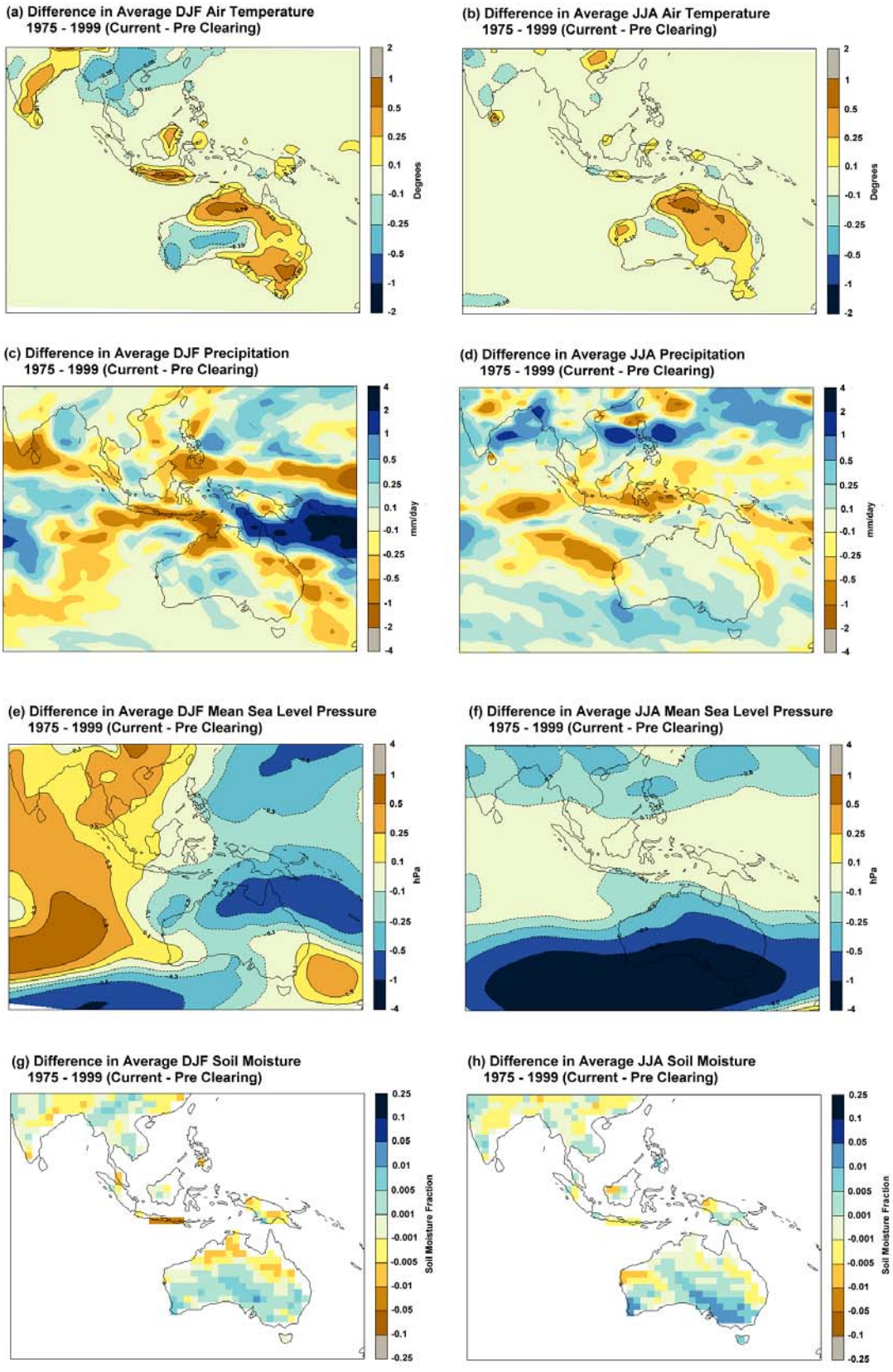

Figure 5.19 Differences in average climate between the Current and Pre-clearing experiments for Australia – Asia in Austral Summer (DJF) and Winter (JJA) 1975 – 1999 for: Average Air Temperature (a) and (b); Average Precipitation (c) and (d); Average Mean Sea Level Pressure (e) and (f); and Average Soil Moisture (g) and (h)

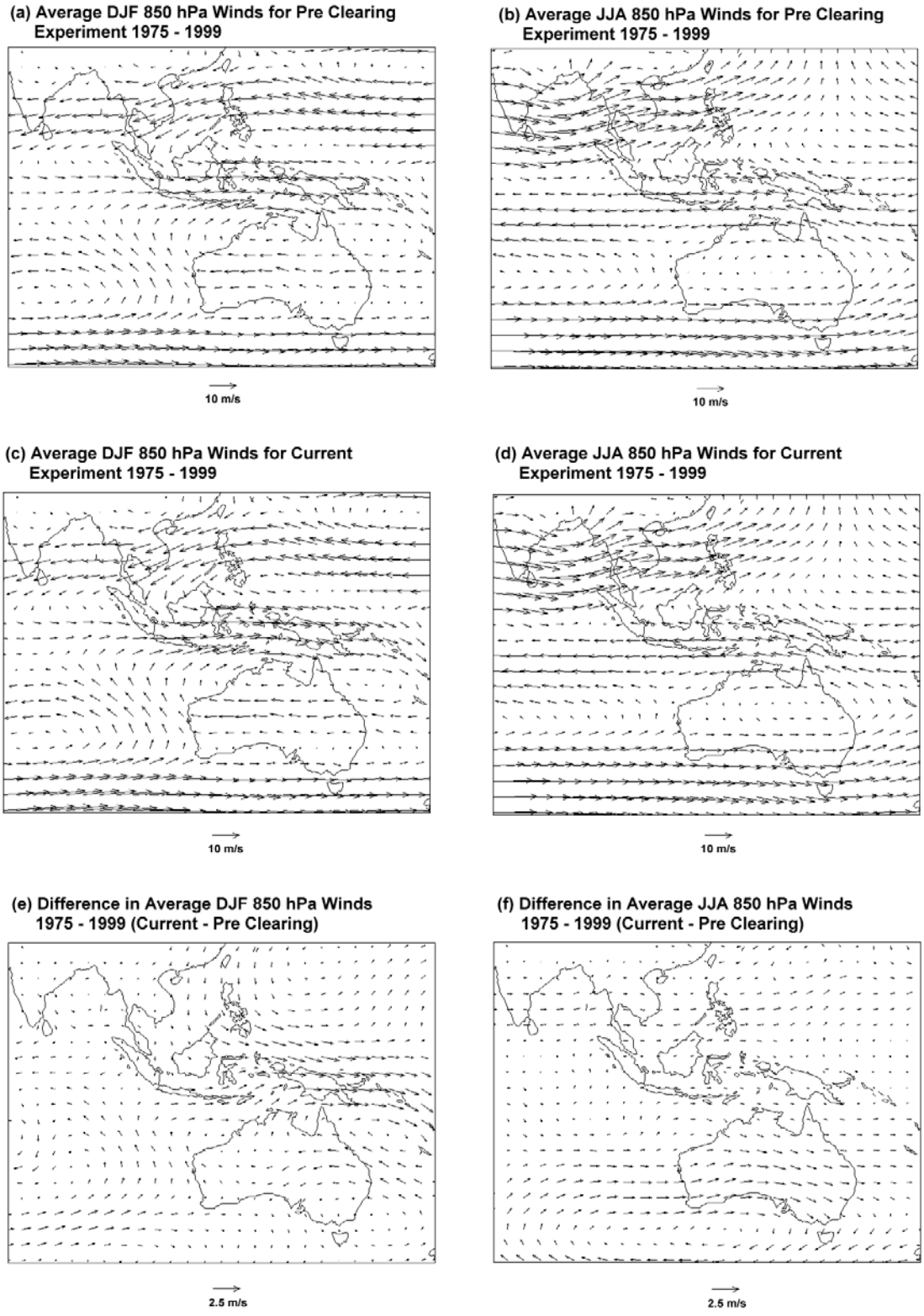

Figure 5.20 Average 850 hPa winds over Australia – Asia for: Pre-clearing experiment (a) Austral Summer (DJF) and (b) Winter (JJA); The Current experiment (c) Austral Summer and (d) Winter; And the difference between the experiments (e) Summer and (f) Winter

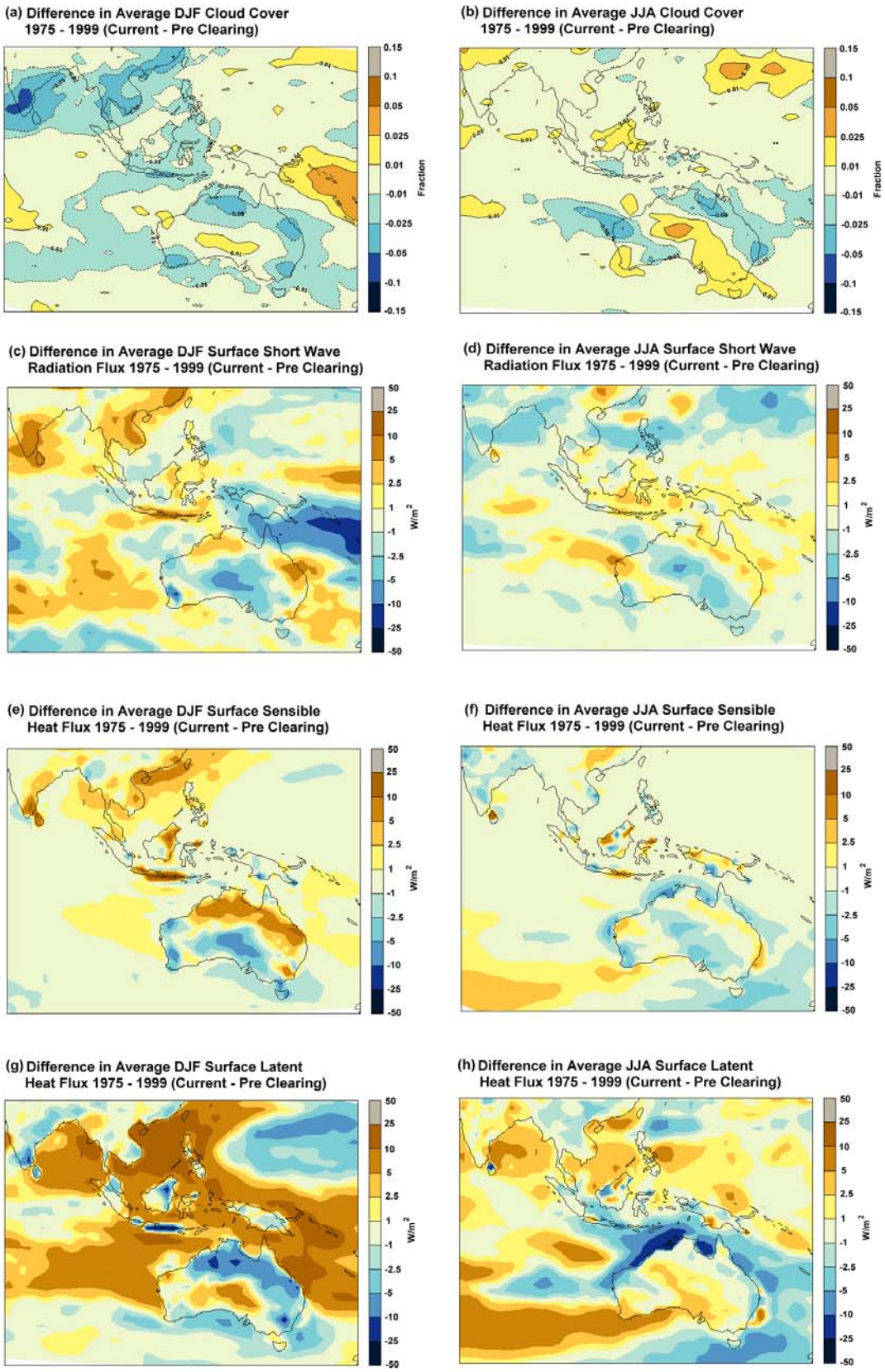

Figure 5.21 Surface energy flux differences over Australia – Asia between the Current and Pre-clearing experiments for Austral Summer (DJF) and Winter (JJA) 1975 –1999: for Average Cloud Cover (a) and (b); Short Wave Radiation Flux (c) and (d); Average Sensible Heat Flux (e) and (f); and Average Latent Heat Flux (g) and (h)

Again like the DJF analysis the climate impacts from the land cover changes were different in each region. In south east Queensland the current experiment had: warmer air temperature (*figure 5.19 b*); marginally reduced precipitation (*figure 5.19 d*); lower mean sea level pressure (*figure 5.19 f*); lower soil moisture (*figure 5.19 h*); less cloud cover (*figure 5.21 b*); increased short wave radiation (*figure 5.21 d*); increased sensible heat flux (*figure 5.21 f*); and reduced latent heat flux (*figure 5.21 h*). In eastern New South Wales the current experiment had: marginally warmer air temperature; mixed precipitation differences; significantly lower mean sea level pressure; increased soil moisture; mixed cloud cover; mixed differences of short wave radiation flux differences; mixed sensible heat flux differences; and reduced latent heat flux. While in south west Western Australia the current experiment had: similar air temperatures; significantly increased precipitation; significantly lower mean sea level pressure; increased soil moisture; increased cloud cover; reduced short wave radiation flux; reduced sensible heat flux; and increased latent heat flux.

Like the DJF analysis, the differences in JJA climate variables at the larger scale, show that the JJA climate impacts of Australian land cover change propagated over the Australian continent and over other continents and oceans. The JJA air temperature difference map (*figure 5.19 b*) shows that unlike the DJF analysis, the warmer temperatures in the current experiment over northern and eastern Australia were not accompanied by large changes in air temperature in South East Asia. The JJA precipitation difference map (*figure 5.19 d*) shows the increased precipitation of the current experiment over central Australia, corresponded with higher precipitation to the south and north west of Australia, and with lower precipitation to the north, west and east. The decrease in precipitation to the north was in a band from the Indian Ocean through Indonesia into the Pacific Ocean. To the north of this band there was another band of increased precipitation from the western Pacific through South East Asia.

Again like the DJF analysis, investigating the processes that produced the regional and larger scale changes in JJA climate, requires interpretation and conjecture as to how the change in surface fluxes interact with feedbacks through changes in atmospheric circulation, cloud cover, and soil moisture. Again the immediate regional impacts of Australian land cover change where investigated through changes in JJA surface fluxes of radiation, energy and moisture, with the larger scale climate impacts investigated by disentangling the direct and indirect feedback mechanisms shown by the JJA climate variable differences maps.

South east Queensland JJA Analysis

In south east Queensland, the JJA surface radiation budget was marginally affected by the increased albedo prescribed in the current experiment, however the largest impact was an increase in short wave radiation flux over the region attributed to the decrease in cloud cover. Like DJF, the JJA latent heat flux also was reduced by the increased canopy resistance, reduced vegetation fraction, and reduced surface roughness prescribed in the current experiment. The

reduction in latent heat flux due to the reduced soil moisture, however, was smaller than in DJF as the soil moisture differences were smaller, resulting in the total reduction in latent heat flux in the current experiment being significantly smaller than in DJF. The JJA sensible heat flux was marginally higher for the current experiment due to the increased short wave radiation flux and lower latent heat flux, however, the increase in sensible heat flux was significantly smaller than in DJF primarily due to the smaller differences in shortwave radiation and latent heat flux in JJA.

The smaller differences in JJA surface fluxes resulted in smaller direct changes in JJA climate in the current experiment, with larger scale changes in atmospheric circulation appearing to have had stronger influence on the regional climate. The increased westerly wind flow from central Australia, with an increased northerly component brought warmer dryer air into the region, which appears to be the primary source of the higher air temperatures and reduced precipitation over the region in the current experiment. The changes in latent and sensible heat flux also may have contributed to these changes, however, it appears this would have been to a lesser extent than in DJF.

Eastern New South Wales JJA Analysis

Like DJF, the increase in JJA albedo was larger in eastern New South Wales than south east Queensland, with the net impact on short wave radiation flux over the region again mixed. The short wave radiation differences appear to be primarily the result of differences in JJA cloud cover, as the northern areas of the region had increased short wave radiation flux and decreased cloud cover, and the southern areas had reduced short wave radiation flux and increased cloud cover. For the rest of the region the albedo differences appear to have been offset by the cloud cover differences with the short wave radiation flux similar both experiments.

The eastern New South Wales JJA latent heat flux was less affected by the increased canopy resistance, reduced vegetation fraction, and reduced surface roughness than in DJF, with the decreases in latent heat flux smaller over the region. The differences in soil moisture still appear to have influenced latent heat flux with the largest decrease occurring in the north of the region where soil moisture was reduced, and with similar JJA latent heat fluxes for both experiments over the rest of the region where increased soil moisture appears to have offset the changes in land surface properties. The JJA sensible heat flux differences also were smaller than in DJF, which appears to be related to the smaller differences in latent heat flux. The increased sensible heat flux of northern parts of the region corresponded with decreased latent heat flux, while the decreased sensible heat flux of the south corresponded with increased latent heat flux.

Like south east Queensland, the smaller differences in JJA surface fluxes of eastern New South Wales resulted in smaller direct changes in JJA climate, with larger scale changes in atmospheric circulation again appearing to have had stronger influence on the regional climate.

For northern parts of the region, the increased westerly wind flow from central Australia, with an increased northerly component brought warmer air into northern parts of the region, resulting in warmer air temperatures but with little impact on precipitation. In southern parts of the region, however, the increased westerly wind flow appears to be associated with increased moisture flux from the southern Indian Ocean and with lower mean sea level pressure, resulting in increased precipitation over this part of the region.

South west Western Australia JJA Analysis

Like DJF, the JJA surface radiation budget of south west Western Australia was more directly affected by increased albedo than the other two regions, with short wave radiation flux significantly decreased over the region. The decrease in short wave radiation flux also corresponded with a significant increase in cloud cover, which further contributed to the decrease in short wave radiation flux. The JJA latent heat flux was higher over the region in the current experiment, despite lower vegetation fraction, lower surface roughness, and marginally lower canopy resistance. The increased latent heat flux suggests that the lower canopy resistance and increased soil moisture had larger impact than the decreased vegetation fraction and surface roughness. The JJA sensible heat flux over the region also was significantly reduced, primarily as a result of the reduced short wave radiation and the increased latent heat flux, however reduced surface roughness also may have contributed to this decrease.

Like the other two regions, the direct changes in JJA climate from changes in surface fluxes are difficult to quantify, as the larger scale changes in atmospheric circulation appear to have had stronger influence on the regional climate. The JJA air temperature cooling that would have been expected to result from the decreased short wave radiation flux and increased latent heat flux appears to have been offset by increased warm moist westerly flow from the Indian Ocean (*figure 5.20 f*) with both experiments having similar JJA air temperature. The significant increase in precipitation, however, appears to be a combination of the increased latent heat flux over the region and the increased moist westerly flow, with the contribution from each source difficult to establish.

Other Australian Regions JJA Analysis

Like DJF, the Australian land cover changes experiments showed changes in JJA climate in regions of Australia that had the same land surface properties in both experiments. For most of northern and eastern Australia the current experiment had warmer JJA air temperature, while over the central and south eastern parts of Australia the current experiment had increased precipitation. Again like DJF, these regions had the same land surface properties in both experiments, so the changes in air temperature and precipitation were the result of feedbacks from the land cover changes in the other regions.

The major influence producing warmer JJA air temperatures in northern Australia appears to be the reduced easterly wind flow across northern Australia from the Pacific Ocean (*figure 5.20 f*). The reduced wind flow reduced the moisture flux across northern Australia, and allowed greater continental warming of the air over northern Australia before it was transported out of the continent. The major influence producing warmer JJA air temperatures in the remaining areas of eastern Australia was the increased westerly flow from central Australia, with an increased northerly component. In the north east, the warming of JJA air temperature also was enhanced by increased short wave radiation from reduced cloud cover, and from the reduced latent heat flux associated with reduced soil moisture. For other areas the warming occurred despite decreased short wave radiation associated with increased cloud cover, and increased latent heat flux associated with increased soil moisture.

The major influence producing the increased precipitation in central and south eastern areas of Australia appears to be the increased westerly wind flow and the lower pressure over the southern areas of the Australian continent. The increased westerly wind flow is associated with increased latent heat flux over the oceans to the south west of Australia, indicating increased moisture flux in the air masses transported by the wind flow. The increased moisture flux combined with the higher soil moisture and latent heat fluxes of central and south eastern areas of Australia, to produce increased precipitation and cloud cover over these areas. The lower pressure over these areas also suggests that the increased moisture resulted in increased moist convection, reducing the strength of JJA subtropical anti-cyclones developing over the continent, allowing mid latitude cyclones to penetrate further into the Australian continent, also contributing to the increased precipitation.

Outside of Australia JJA Analysis

Like DJF, the difference maps show the changes in Australian land cover change impacted JJA climate beyond the Australian continent, and again with the larger scale changes having feedbacks on Australian climate. The largest change in JJA climate shown in the difference maps was the significantly reduced mean sea level pressure over southern parts of Australia into the southern Indian Ocean, with the associated increase in westerly wind flow over southern Australian latitudes, and the decrease in easterly wind flow through central Australian latitudes. To the north of Australia, there also was a marginal decrease in pressure over India and South East Asia and an increase in the monsoon wind flow over these areas.

The increase in westerly winds over southern Australia and the accompanied lower pressure to the south of Australia, suggest that there was a northward shift in the JJA mid latitude westerly wind flow around Australia. This northward shift brought mid latitude cyclones further north with greater intensity over this region. The primary influence responsible for the northward shift in the mid latitude westerly wind flow appears to be the reduced strength

of JJA subtropical anti-cyclones over the Australian continent, due to the increased moist convection over central Australia and the warming over northern and eastern Australia.

The northward shift in mid latitude westerly wind flow also had impacts on the latent and sensible heat flux from the oceans surrounding Australia, with further impacts on the air masses that were transported over the Australian continent. The increased westerly flow over the south of the continent increased latent heat flux over oceans to the south west of Australia, and reduced latent heat flux from oceans to the south east, while the reduced easterly flow over the north of the continent reduced latent heat flux from oceans to the north east and north west.

The northward shift in the mid latitude westerly wind flow may also be responsible for the changes observed in the Asian monsoon flow, as well as the decreased mean sea level pressure over South East Asia. The changes in monsoon wind flow had further impacts on the surface fluxes from the oceans around South East Asia with increased latent heat flux associated with the increased flow. The higher latent heat flux and lower pressure appear to have impacted the precipitation, cloud cover and soil moisture over the Asian continent, with increased precipitation over the oceans and reduced precipitation and soil moisture over land.

5.3.6 Global Teleconnectioned Changes

Following *Pielke et al.* (2002), *Chase et al.* (2000), *Zhao et al.* (2001) and others, the changes in surface fluxes due to land cover change also may have global impacts through changes in global atmospheric circulation and moisture transport. To investigate global scale changes in climate in response to Australian land cover change, and to identify possible mechanisms driving these global changes, the land cover change experiments were analysed for differences in climate at the global scale. The differences between the two experiments are shown globally in the average differences maps of *figure 5.22*, *5.23*, *5.24* and *5.25* for Austral Summer (DJF) and Winter (JJA) for: climate variables; 850 hPa wind fields; model calculated land surface characteristics; and surface fluxes.

Austral Summer Analysis

The global DJF analysis identified regional changes in DJF air temperature in North America, Asia and Europe, that had larger extent and magnitude than were found over Australia (*figure 5.22 a*). The analysis also identified larger changes in DJF precipitation over the Pacific and Indian oceans, and over North America, South America and Africa, than were found over Australia (*figure 5.22 c*). Like the Australian analyses, investigating the processes that produced these changes in DJF global climate from the Australian land cover changes, required interpretation and conjecture to determine how changes in surface fluxes interacted with climate feedbacks to produce these changes at large distances from the Australian land cover changes.

Investigating the DJF global mean sea level difference map reveals large differences in mean sea level pressure over both the northern and southern hemispheres (*figure 5.22 e*). As

described in the Australian analysis, there was significantly lower DJF pressure to the north east of Australia in the South Pacific Convergence Zone (SPCZ). To the north of the SPCZ, over the western and northern Pacific, there was significantly lower pressure that extending into northern Asia, eastern Europe, and central North America. This area of lower pressure corresponded with significantly higher DJF pressure over western Europe, the northern Atlantic Ocean, and northern parts of North America. There was higher DJF pressure over the Indian Ocean and over central Asia, while in the southern Pacific, Indian and Atlantic oceans there were large areas with significantly lower pressure, corresponding with higher pressure over Antarctica.

From the DJF 850 hPa wind flow maps (*figure 5.23 a*, *c*, and *e*) the decrease in pressure over the northern Pacific Ocean appears to be in response to the increased monsoon flow into the SPCZ, with the increased monsoon flow drawing more air from the northern Pacific Ocean. The decreased pressure appears to have strengthened the Aleutian Low over the northern Pacific, with impacts on the mid latitude westerly wind flow into North America, resulting in increased flow with an increased southerly component to the flow. The increased flow also appears to be responsible for the increased precipitation across the northern Pacific Ocean, the warmer temperatures and increased precipitation over western areas of North America, and the decreased precipitation over southern areas of North America.

The changes in the mid westerly wind flow appear to propagate over North America and the Atlantic Ocean to add a strong northerly component to the wind flow in the eastern Atlantic Ocean and over western Europe. The increased northerly component of the westerly wind flow may account for the colder air temperatures over western Europe, and down into central Asia. The colder air temperatures may also account for the higher pressure over these areas. The increased mid latitude westerly flow over the northern Pacific Ocean also appears to impact the DJF easterly wind flow across the central Pacific, resulting in the significantly reduced precipitation over this area. In the western Pacific the easterly wind flow also appears to be influenced by the increased monsoon flow into the SPCZ, also resulting in reduced precipitation over that area.

The increased DJF monsoon flow into the SPCZ resulted in the increased precipitation and lower pressure over this region, as described in the Australian analyses. The increased moisture flux from the increased monsoon flow also appears to increase DJF precipitation to the south east of the SPCZ, across the southern Pacific Ocean. The 850 hPa wind flow maps suggest that the lower pressure associated with the increased moist convection, disturbed the mid latitude westerly wind flow over this area. The changes in westerly wind flow propagated to the east over the southern area of South America, and to a lesser extent over areas south of Africa and south west of Australia. The changes in westerly wind flow impacted mean sea level pressure with significantly lower pressure surrounding the southern area of South America and over the southern Atlantic and Indian oceans.

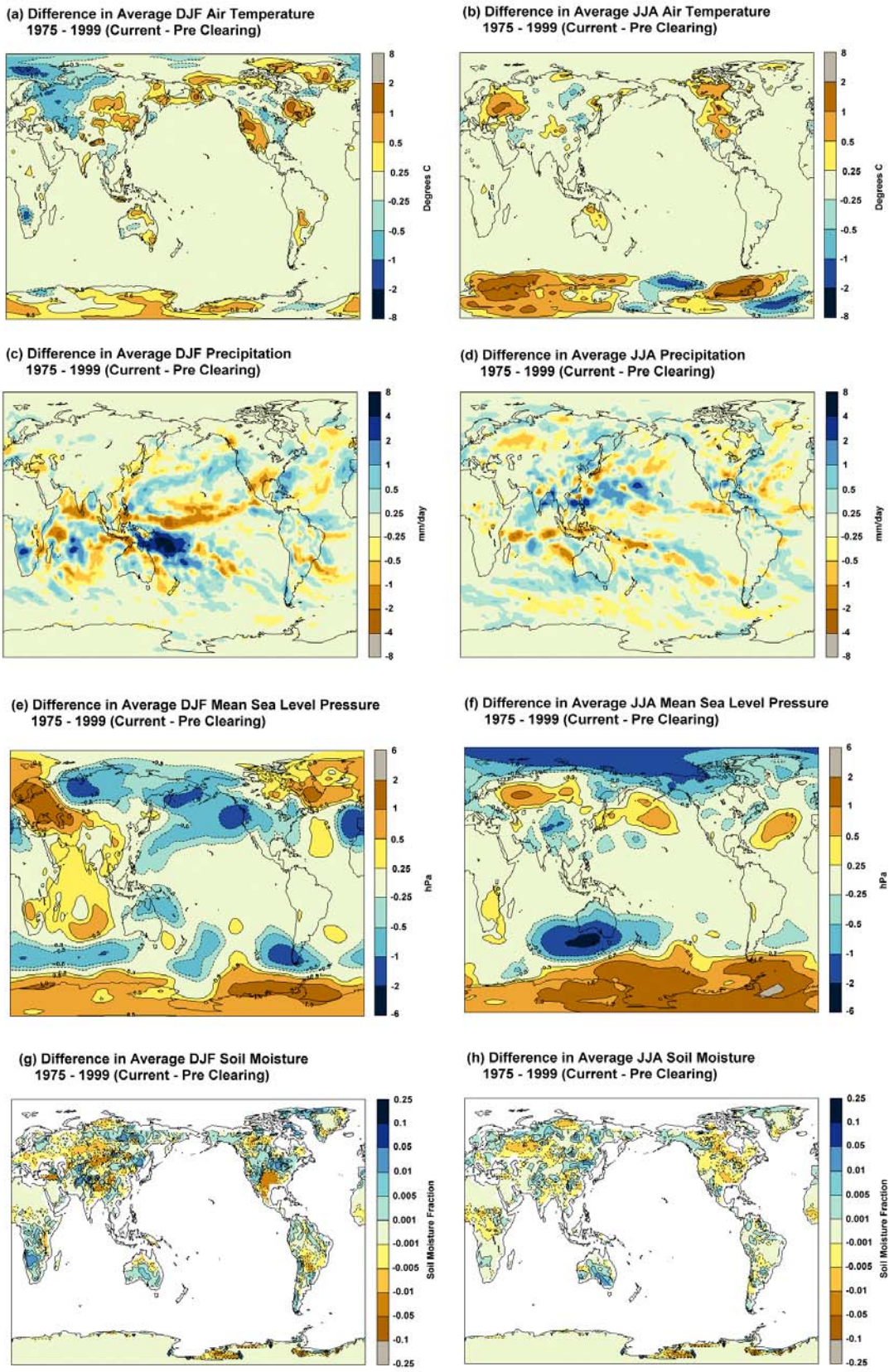

Figure 5.22 Global Differences in average climate between the Current and Pre-clearing experiments for Austral Summer (DJF) and Winter (JJA) 1975 – 1999 for: Average Air Temperature (a) and (b); Average Precipitation (c) and (d); Average Mean Sea Level Pressure (e) and (f); and Average Cloud Cover (g) and (h)

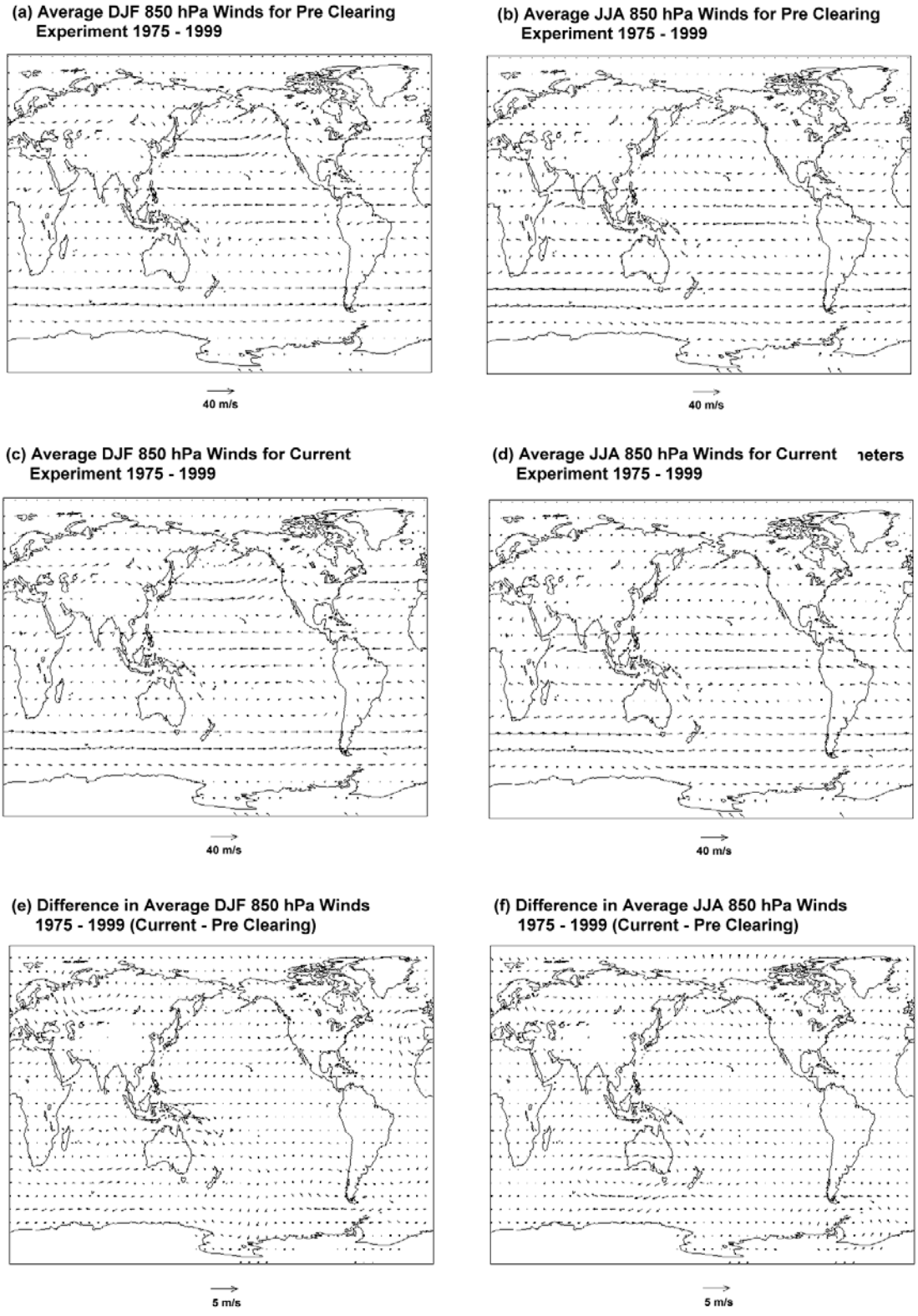

Figure 5.23 Global 850 hPa wind fields for 1975 – 1999 for: the Pre-clearing experiment for (a) Austral Summer (DJF) and (b) Winter (JJA); the Current experiment for (c) Austral Summer (DJF) and (d) Winter (JJA) and the Difference between the experiments (Current – Pre-clearing) for (e) Austral Summer (DJF) and (f) Winter (JJA)

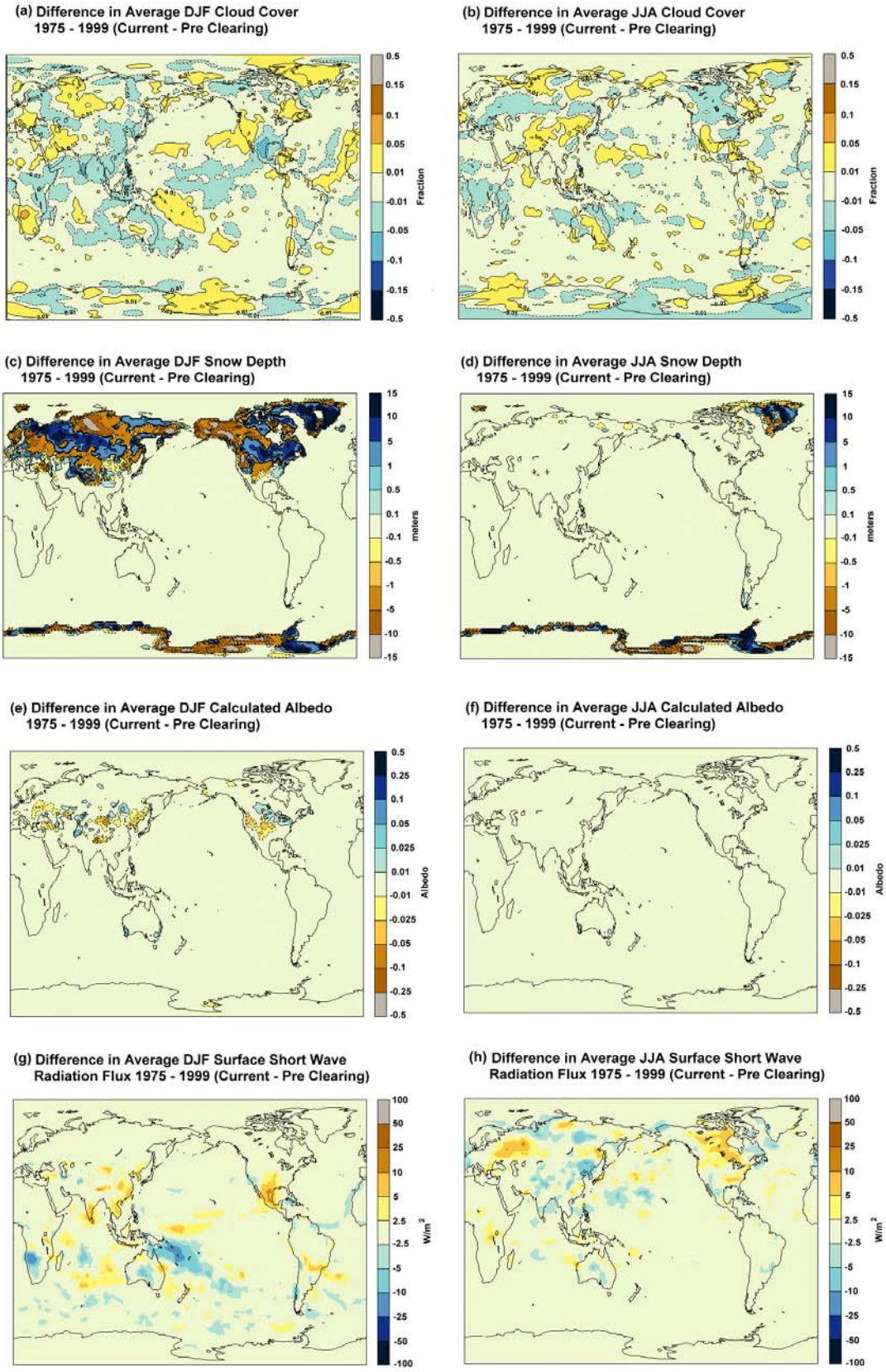

Figure 5.24 Global Differences in average climate between the Current and Pre-clearing experiments for Austral Summer (DJF) and Winter (JJA) 1975 – 1999 for: Average Air Temperature (a) and (b); Average Precipitation (c) and (d); Average Mean Sea Level Pressure (e) and (f); and Average Cloud Cover (g) and (h)

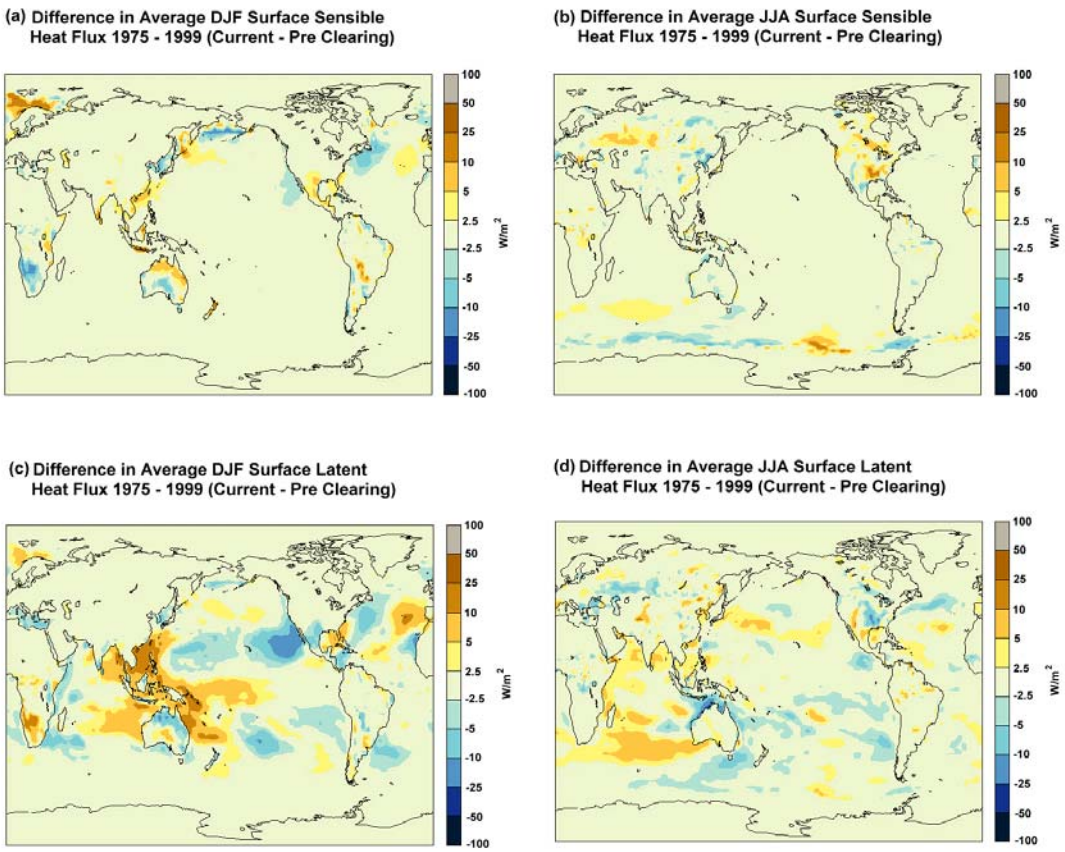

Figure 5.25 Surface energy flux differences over Australia – Asia between the Current and Pre-clearing experiments for Austral Summer (DJF) and Winter (JJA) 1975 –1999: for Average Short Wave Radiation Flux (a) and (b); Average Sensible Heat Flux (c) and (d); and Average Latent Heat Flux (e) and (f)

The changes in air temperature and precipitation in these areas also had influences on DJF snow pack depth in the northern hemisphere. The changes in snow cover, however, had marginal influence on DJF calculated albedo, short wave radiation flux or sensible heat flux. The largest changes in DJF surface fluxes were in latent heat flux from the oceans, with increased latent heat flux from the oceans surrounding Australia, and decreased latent heat flux in central and southern areas of the Pacific Ocean. The impact on latent heat flux over land was significantly smaller than over oceans with the soil moisture impacts only significant over Australia, and southern Africa.

Austral Winter Analysis

Like DJF, the land cover change experiments had larger changes in JJA air temperature over other continents than over Australia, with significantly warmer air temperature over central Europe, North America and Antarctica (*figure 5.22 b*). The analysis also identified there were larger changes in JJA precipitation outside the Australian continent than over it, with a significant increase in JJA precipitation over the southern Indian and south western Pacific oceans, decreased precipitation across the Indian Ocean, Indonesia and the South Pacific Convergence Zone (SPCZ), and increased precipitation over the northern Indian Ocean, India,

South East Asia and the western Pacific Ocean (*figure 5.22 d*). Again, investigating the processes that produced these changes in JJA global climate from the Australian land cover changes, required interpretation and conjecture to determine how changes in surface fluxes interacted with climate feedbacks.

The differences in the JJA mean sea level pressure map (*figure 5.22 f*) shows the lower pressure over southern Australia, extended over the southern Indian Ocean and over the south western Pacific Ocean, and corresponded with increased pressure over Antarctica. The lower pressure over South East Asia also extended into central Asia and corresponded with higher pressure over northern Asia, central Europe and the northern Pacific Ocean. Corresponding to these increases in pressure there also was increased pressure over the northern Atlantic Ocean and significantly lower pressure over the Artic.

The global JJA 850 hPa wind flow maps (*figure 5.23 b*, *d*, and *f*) supported the northward shift in JJA mid latitude westerly wind flow around Australia suggested in the Australian analysis, with the global maps also showing significant weakening in the westerly wind flow closer to Antarctica. The lower pressure over Asia also suggests a northward shift in the Asian monsoon, with the decreased precipitation in southern areas and the increased precipitation in northern areas further supporting this suggestion. The 850 hPa wind flow maps show there was increased monsoon flow over India and South East Asia. The lower pressure over central Asia also increased the wind flow from the northern Pacific into the Asian continent. The disturbance in the JJA mid latitude westerly wind flow around Australia also appears to propagate to the east, with impacts on the westerly wind flow south of South America. The increased southerly wind flow south of Australia and South America appear to be the primary reason for the increased JJA air temperatures and pressure over Antarctica in these areas.

The warmer JJA air temperatures over North America and central Europe appear to be due to decreased cloud cover, increasing short wave radiation flux, and reduced soil moisture reducing latent heat flux. The higher pressure over northern Asia, central Europe and the northern Pacific Ocean appear to be related to the northward shift in the Asian monsoon and the associated lower pressure over central Asia. The lower pressure over the Artic and the higher pressure over the northern Atlantic also appear to be related to this northward shift in the Asian monsoon.

Unlike DJF, the changes in JJA air temperature and precipitation had little influence on snow pack depth, with the exception of Greenland and the Antarctic coast, and even in these areas there was no influence on JJA calculated albedo. Despite the similarity in snow cover, the JJA short wave radiation flux differences, as well as the sensible and latent heat flux differences were larger in central Europe, North America, and Asia than they were in Australia. Even in Australia the differences in JJA surface fluxes were greater in areas with unchanged land surface parameters, than in areas with land cover change. This suggests that the JJA climate

impacts from feedback mechanisms were significantly greater that the impacts from changes in land surface properties associated with Australian land cover change.

5.3.7 Section Summary

1. Two sensitivity experiments were conducted for 1975-1999 with the only change between the experiments replacement of land surface parameters representing Australian land cover as it may have existed pre-clearing with how it existed for current day. The differences in climate simulated in the two experiments were evaluated to assess the modelled climate impact of historical Australian land cover change.
2. Overall the model experiments showed Australian climate with the current land cover was cooler and marginally wetter than with pre-clearing land cover. Statistical analysis, however showed that the only statistically significant changes in average Australian climate were for austral summer (DJF), which was warmer (+0.15 ^{O}C p = 0.00) and dryer (-0.09 mm/day p = 0.05)
3. Regional analysis showed statistically significant changes in average climate for: South east Queensland, where summer was warmer (+0.15 ^{O}C p = 0.00) and dryer (-0.31 mm/day p = 0.00), and spring was cooler (-0.33 ^{O}C p = 0.02); Eastern New South Wales, where summer was warmer (+0.4 ^{O}C p = 0.00) and; South west Western Australia, where it was overall cooler (-0.35 ^{O}C p = 0.00), with summer cooler (-0.32 ^{O}C p = 0.00), autumn cooler (-0.7 ^{O}C p = 0.01), winter wetter (+0.24 mm/day p = 0.01), and spring cooler (-0.32 ^{O}C p = 0.02).
4. None of the statistically significant trends in annual precipitation identified from linear regression were found to be statistically significant in the climate modelling experiments. The modelled reductions in annual precipitation for south east Queensland (-40.8 mm), and eastern New South Wales (-39.9 mm), however, corresponded with the strong drying trends in those areas for 1950 – 1999 (-151.2 mm and -104.5 mm). In south west Western Australia, the modelled increase in annual precipitation (43 mm), was opposite to the observed changes for both 1900 – 1999 (-70.6 mm) and 1950 – 1999 (-34.9 mm)
5. Analysis of historical precipitation records showed the sign and magnitude of changes detected from linear regression were highly dependent on the start and end dates of the analysis period for both Australian and regional annual precipitation changes. The large range of sources of variability in Australian precipitation and the incremental nature of land cover change suggested comparison of historical trends and model results was complex as the two changes detected by the analyses were not temporally equivalent.
6. The impacts of changes in surface albedo on the short wave radiation budget appear to be significant only in south west Western Australia, where the increased albedo corresponded to decreased short wave radiation flux for both summer (DJF) and winter

(JJA). In south east Queensland and eastern New South Wales the short wave radiation flux increased or was similar despite increases in albedo, and in other areas of Australia there were similar changes in short wave radiation flux with out changes in albedo. The primary cause of these changes was thought to be changes in cloud cover and optical thickness.

7. The impacts of changes in vegetation fraction and canopy resistance on latent heat flux were significant for all three regions, with increased canopy resistance and reduced vegetation fraction resulting in reduced latent heat flux even in areas with increased soil moisture. The opposite was also true in south west Western Australia in winter, where reduced canopy resistance resulted in increased latent heat flux.
8. There were larger changes in latent heat flux in areas of Australia with unchanged land surface parameters, suggesting soil moisture was a strong feedback mechanism in these areas. There also were large changes in latent heat flux over the oceans surrounding Australia due to changes in atmospheric circulation changing wind flows.
9. Changes in sensible heat flux were primarily driven by changes in short wave radiation flux and latent heat flux, with increased short wave radiation or reduced latent heat flux resulting in increased surface heating and sensible heat flux, while reduced short wave radiation or increased latent heat flux had the opposite impact.
10. Precipitation and air temperature were impacted by both changes in surface fluxes, and changes in atmospheric circulation through changes in air mass transport. It was not possible to quantify the contribution to each influence from the experimental analyses.
11. The largest changes in summer (DJF) atmospheric circulation around Australia were the reduced monsoon flow into northern Australia, associated with the increased monsoon flow in to the South Pacific Convergence Zone, and the increased south easterly wind flow into eastern Queensland. The largest changes in winter (JJA) circulation around Australia resulted from the northward shift in the mid latitude westerly winds over southern Australia and over the southern Indian Ocean. Again it was not possible to quantify the influence of changes in surface fluxes and the influences from other feedback mechanisms.
12. Global analysis identified larger changes in air temperature and precipitation over continents and oceans at distance from Australia, than occurred over Australia. The changes in climate in these areas were traced to changes in global atmospheric circulation and feedbacks from altered cloud cover, soil moisture, and snow cover and depth. These feedback mechanisms also resulted in larger changes in surface fluxes of short wave radiation, sensible heat, and latent heat in these areas with unchanged land cover, than occurred over the areas of Australian land cover change.

5.4 Chapter Summary

The aim of this chapter was to investigate potential climate impacts of historical Australian land cover change using the CSIRO GCM modelling framework developed in Chapter 4. To achieve this, historical Australian land cover change was defined as the historical changes in vegetation associated with clearing of native vegetation for replacement with cropping, pastures and urban development as described by *AUSLIG* (1990) in Chapter 3. The land surface properties of pre-clearing land cover were extrapolated from current day satellite observation and mapping using methods that were consistent with the modelling framework of Chapter 4. Sensitivity experiments were performed using the climate modelling framework, with the pre-clearing and current Australian land surface parameters. The modelled climate impacts of historical Australian land cover change were assessed by comparing the differences in the climate simulated in the two experiments.

The restriction of Australian land cover change to the clearing of native vegetation removed the uncertainties involved with land cover changes from extensive land use such as grazing, and from changes land cover related to disturbance such as altered fire regimes and invasions by exotic animals and plants. The use of the *AUSLIG* (1990) vegetation mapping also excluded more recent clearing identified by *Barson et al.* (2000) and *DNRM* (2003), however, this was deemed to be acceptable given the extent of the recent clearing was estimated to be less than the 5% of the historical clearing in the vegetation mapping. The extrapolation and aggregation techniques ensured the subgrid heterogeneity and biogeophysics captured in the satellite imagery was consistently recreated for the pre-clearing land cover.

To assess the land cover changes represented in the CSIRO GCM for the modelling experiments, the pre-clearing and current land surface parameters were analysed for differences in average Australian monthly values, as well as, average regional monthly values. The general differences found in these analyses are listed in *table 5.7* for Australian values, and for south east Queensland, eastern New South Wales and south west Western Australia regional values. The differences identified between the pre-clearing and current parameters in south west Western Australia, reflected the differences observed between native vegetation and agricultural areas from the numerous satellite and field studies performed by *Xinmei et al.* (1995), *Lyons et al.* (1993) and *Ray et al.* (2003). This confirmed that the methods used to extrapolate the pre-clearing land cover characteristics from remnant vegetation captured the physical properties of the native vegetation as well as the seasonal dynamics.

The differences in climate simulated in the pre-clearing and current experiments were analysed using climatological means and statistical analysis of means relative to inter-annual variance. The analysis was performed at the four spatial scales of: The Australian continent; the Australia regions identified in the parameter analysis; the larger context of the area surrounding Australia and; the global context.

Table 5.7 General Differences in CSIRO GCM Land Surface Parameters between Pre-Clearing and Current Experiments

Parameter	Evaluation of Differences
Albedo	*Australia* - average albedo was marginally higher for all months. *South east Queensland* - higher in summer with mixed differences in winter. *Eastern New South Wales* - higher in summer with mixed differences in winter. *South west Western Australia* - consistently higher for all months.
Leaf Area Index	*Australia* - average LAI was significantly lower for all months with largest differences in summer and smallest differences in spring. *South east Queensland* - consistently lower for all months. *Eastern New South Wales* was consistently lower for all months, with marginally closer values in spring. *South west Western Australia* - significantly lower in summer but marginally higher in spring.
Vegetation Fraction	*Australia* - average vegetation fraction was significantly lower for all months, with the biggest differences in summer and smallest differences in spring. *South east Queensland* - consistently lower for all months. *Eastern New South Wales* - consistently lower for all months. *South west Western Australia* - significantly lower in summer but marginally higher in spring.
Unrestrained Stomatal Resistance	*Australia* - average stomatal resistance was marginally higher. *South eastern Queensland* - was marginally higher. *Eastern New South Wales* - was marginally lower. *South west Western Australia* - was significantly lower.
Unrestrained Canopy Resistance	*Australia* - average canopy resistance was significantly higher for all months, with the biggest difference in summer and smallest differences in spring. *South eastern Queensland* - was consistently higher with the biggest differences in summer and the smallest differences in spring. *Eastern New South Wales* - was consistently higher with the biggest differences in summer and the smallest differences in spring. *South west Western Australia* - was significantly higher in summer but significantly lower in spring.
Surface Roughness	*Australia* - average surface roughness was consistently significantly lower for all months. *All three regions* – same as Australian average surface roughness, with values consistently lower for all months.

The Australian continental and regional analysis demonstrated that Australian land cover change did have statistically significant impacts on air temperature and precipitation simulated in the CSIRO GCM. While none of the statistically significant trends in annual precipitation identified from linear regression of historical precipitation records were found to be statistically significant in the climate modelling experiments, the modelled reductions in annual precipitation for south east Queensland and eastern New South Wales corresponded with the strong drying trends in those areas for 1950 – 1999. In south west Western Australia, however, the modelled increase in annual precipitation was opposite to the observed drying trends of both 1900 – 1999 and 1950 – 1999. Further analysis of historical Australian precipitation data identified that the sign and magnitude of continental and regional precipitation trends were highly dependant on the period selected for analysis. This was attributed to the high variability in Australian precipitation, and suggested that any long term trends in Australian precipitation needed to be provided in the context of the natural inter-annual and inter-decadal variability, as well as in the light of other sources of Australian climate change.

Larger scale analysis of differences in mean climate variables around the Australian continent suggested the local changes in surface fluxes had strong impacts on atmospheric circulation. The largest changes in austral summer (DJF) circulation resulted from the reduced monsoon flow into northern Australia, corresponding with increased monsoon flow into the South Pacific Convergence Zone and increased south easterly wind flow into eastern Queensland. These changes in circulation influenced DJF moisture flux into northern and eastern Australia, which intensified the direct warming and drying impact caused by the reduced transpiration from the land cover change in eastern Queensland. The largest changes in winter (JJA) circulation resulted from the northward shift of mid latitude westerly wind flow over southern Australia and over the surrounding oceans. This shift increased the JJA moisture flux into southern Australia and increased the penetration of mid latitude cyclones into the continent. The increased moisture flux and cyclone penetration combined with higher latent heat fluxes from reduced canopy resistance over south west Western Australia and the increased soil moisture over southern and central Australia, to increase precipitation over southern and central Australia.

The global analysis identified global scale changes in atmospheric circulation responding to the changes in circulation around Australia. The DJF changes in monsoon flow appeared to influence the wind flow across the Indian and Pacific oceans, with impacts on air temperature and precipitation in Asia, Europe and North America. The changes in cloud cover, soil moisture and snow cover over these continents resulted in changes in surface fluxes that were greater in magnitude than resulted from the land cover change in Australia. The JJA northward shift in mid latitude westerly wind flow also had impacts further to the north, resulting in a northward shift and increased flow in the Asian monsoon. The increased Asian monsoon flow impacted the wind flow and circulation over the Indian and Pacific oceans, with impacts on air temperature, and precipitation over Asia, Europe and North America. Again the changes in cloud cover and soil moisture over these continents resulted in changes in surface fluxes greater in magnitude than over Australia.

CHAPTER 6.
EVALUATION AND CONCLUSION

6.1 Chapter Aims and Rationale

The aim of this chapter is to evaluate and draw conclusions from the research to show how this thesis addresses the original problem statement raised in Chapter 1, and verifies the postulated relationships between Australian land cover change and climate generated in Chapter 2. The original problem statement identified that: the impacts of Australian land cover change on regional and continental climate had not been studied with larger-scale atmospheric circulation changes and associated feedbacks, or with longer term soil moisture feedbacks accounted for.

To address this problem statement, the primary aim of the thesis was to investigate and identify possible causal explanations for changes in climate resulting from historical Australian land cover change using the CSIRO General Circulation Model (GCM). The CSIRO GCM was selected as the climate model for these investigations as it could incorporate the indirect climate impacts of larger-scale atmospheric circulation feedbacks and longer term soil moisture feedbacks, as well as the direct impacts of changes in surface fluxes. As part of this research, the secondary aim was to investigate how land cover and land surface properties were represented in the CSIRO GCM and explain how this representation affected simulation of climate in model.

The outcomes of the research are discussed in the context of the postulated relationships of the climate impacts of Australian land cover change with the outcomes identified as a series of conclusions addressing the primary and secondary aims of the thesis. The chapter concludes with a discussion of the implications of the outcomes of the research and the future research requirements raised by these outcomes.

6.2 Thesis Conclusions

The conclusions to the thesis are structured around the postulated relationships of Chapter 2, with the findings from each component of the thesis integrated in a discussion for that relationship. The conclusions and the discussion form the basis for the implications of the research and the future work requirements that follow.

6.2.1 Postulated Relationship 1

The first postulated relationship was that Australian land cover change modified Australian land surface properties of: surface albedo; vegetation fraction; unrestrained canopy resistance to transpiration; canopy moisture storage capacity; canopy interception rate for precipitation and dew; and surface roughness and displacement heights.

Discussion

As was shown in the Australian climate and land cover change review of Chapter 2 and the Australian land cover change review of Chapter 3, Australian land cover and Australian land surface properties have been significantly altered since European settlement with a strong consensus from a range of studies. The reviews show historical land cover change was concentrated in the relatively fertile and climatically favourable areas of the continent, with native vegetation in these areas replaced or modified primarily for cropping and intensive animal production. In the remaining areas of the continent, the vegetation was shown to be largely intact but disturbed from grazing by cattle and sheep, changed fire regimes, and invasion from introduced plants and animals.

The reviews of international and Australian literature and case studies of land cover change and climate in Chapter 2, established that Australian land cover change would have impacts on key land surface attributes. The review of the existing research into Australian land cover change impacts on climate, identified that there had been extensive field and satellite monitoring campaigns in south west Western Australia that showed there were large changes in vegetation density and the seasonal cycles of the vegetation. The reviews also demonstrated that recent satellite monitoring detected the high land clearing rates continued through out Australia through the 1990s, with the largest areas concentrated in central and southern Queensland. These reviews showed that clearing still was predominantly for grazing and agriculture, with clearing rates many time greater than regeneration. The satellite monitoring also demonstrated the dynamic nature of Australian land cover over months and years, as the vegetation responds to seasonal climatic cycles, and to droughts and above average precipitation.

Following the international and Australian land cover change and climate reviews, the CSIRO GCM was reviewed and adapted to capture Australian land cover change from Australian and global land surface data in Chapter 4. The review assessed that while the CSIRO GCM as suitable for investigating the climate impacts of land cover change, the homogeneous allocation of GCM grid cells at the 1.875 degree grid increment was not suitable for representing the relatively fine-scale land cover changes. In addition to this, the land surface detailed by recent satellite mapping projects, and parameterised through radiation and surface roughness models was significantly different to the land surface specified by the original CSIRO GCM land surface parameters.

To overcome these limitations, the model was modified and new land surface parameter generation methods developed to integrate the best available land surface data into the land surface model of the CSIRO GCM. The two stream radiation model and the simplified roughness model were used with monthly vegetation cover and physiology from satellite imagery and field data, to capture the heterogeneity and biogeophysics of the land surface.

Aggregation rules were applied to the fine-scale data to produce land surface parameters at the scale of the GCM.

The changes in Australian land surface characteristics from land cover change were investigated by comparing the land surface properties of native vegetation prior to clearing to the modified land surface properties that replaced it. To remove the uncertainties involved with land cover changes from extensive land use such as grazing, and from land cover changes related to changes in disturbance regimes, Australian land cover change was restricted to the historical clearing of native vegetation as described by the *AUSLIG* (1990) vegetation mapping. This restriction also excluded more recent clearing identified by *Barson et al.* (2000) and *DNRM* (2003), however, the extent of the recent clearing was estimated to be less than the 5% of the historical clearing. The rationale behind this approach was to investigate the climate impacts of the most obvious and definitive changes in Australian land cover before extending the research to the less well defined elements of land cover change.

The pre-clearing land surface properties were extrapolated from the current monthly values of remnant native vegetation to the pre-clearing extents of each land cover class at the resolution of the fine-scale data. The current and pre-clearing CSIRO GCM land surface parameters were generated from the relatively fine-scale land surface data using the aggregation rules of Chapter 4. The extrapolation and aggregation techniques ensured the subgrid heterogeneity and biogeophysics captured in the satellite imagery was consistently recreated for Australian current and pre-clearing land cover. The pre-clearing and current land surface parameter analysis of Chapter 5 demonstrated that the differences from Australian land cover had associated changes in land surface properties for both continental and regional Australia values. Specifically Australian land cover change has changed Australian land surface characteristics so that:

1. Australian average albedo was marginally higher in the current experiment, with south west Western Australia consistently higher, and eastern Australia higher in summer but with mixed differences in winter;
2. Australian average vegetation fraction was significantly lower for the current experiment, with the biggest differences in summer and smallest differences in spring. In south west Western Australia it was significantly lower in summer and marginally higher in spring. In eastern Australia it was consistently lower;
3. Australian average LAI was significantly lower for the current experiment with largest differences in summer and smallest differences in spring. In south west Western Australia it was significantly lower in summer and marginally higher in spring. In eastern Australia it was consistently lower, with marginally closer values in southern areas in spring.

4. Australian average stomatal resistance was marginally higher in the current experiment. In south west Western Australia it was significantly lower. In south eastern Queensland it was marginally higher. In eastern New South Wales it was marginally lower;
5. Australian average canopy resistance was significantly higher, with the biggest difference in summer and smallest differences in spring. In south west Western Australia it was significantly higher in summer but significantly lower in spring. In eastern Australia it was consistently higher with the biggest differences in summer and the smallest differences in spring; and
6. Australian average surface roughness was significantly lower, with the regional differences consistent with the differences in the Australian average values.

The differences identified between the pre-clearing and current parameters in south west Western Australia, were consistent with the differences observed between native vegetation and agricultural areas from the numerous satellite and field studies performed by *Xinmei et al.* (1995), *Lyons et al.* (1993) and *Ray et al.* (2003). This confirmed that the methods used to describe current land cover and to extrapolate pre-clearing land cover characteristics from remnant vegetation captured the physical properties of the native vegetation and agricultural lands as well as the seasonal dynamics.

The changes in albedo, LAI, and surface roughness for south west Western Australia and eastern New South Wales, were significantly smaller in magnitude, than the changes described in *Narisma and Pitman* (2003) for these areas. There also were significant differences in the seasonal cycles between the experiments. The smaller changes in surface properties and the seasonal cycles associated with land cover changes were consistent with the differences suggested by *Oleson et al.* (2004) between climate modelling experiments using satellite-derived land cover change datasets, compared to experiments conducted with biome-derived datasets at the model grid increment.

The land surface parameter analysis of Chapter 4, also showed there were large differences in the new land surface parameters when compared to the original CSIRO land surface parameters. The differences between the land surface parameters of new parameter and the original parameter experiments were larger than the differences between the Australian pre-cleared and current experiments both for Australian continental and regional land surface properties. There also were large global and continental differences in land surface parameters between the new parameter and the original parameter experiments outside of the Australian continent.

Conclusions

The conclusions to this postulated relationship were therefore:

1. Australian land cover change has modified the Australian continental and regional land surface properties of surface albedo; vegetation fraction; unrestrained canopy resistance to transpiration; canopy moisture storage capacity; canopy interception rate for precipitation and dew; and surface roughness and displacement heights;
2. The differences in CSIRO GCM land surface parameters between pre-clearing and current Australia, however, were smaller in magnitude than those described in *Narisma and Pitman* (2003), and smaller than the differences between the original CSIRO GCM parameters and the new satellite derived land surface parameters; and
3. The smaller magnitude of land surface parameters differences of the Australian land cover change experiments did not reduce the ability of the CSIRO GCM to investigate the climate impacts of Australian land cover change, however, it did suggest that there may be implications for climate modelling experiments that represent the land surface with biome-derived datasets at the model grid increment.

6.2.2 Postulated Relationship 2

The second postulated relationship was that Australian land cover change modified Australian land surface and lower atmosphere interaction processes through changes in: surface radiation budget; surface hydrology; the surface energy balance; and mechanical turbulence in the turbulent surface layer, with all impacting the surface fluxes of latent, sensible and ground heat.

Discussion

As was shown in the Australian climate and land cover change review of Chapter 2, the influences of Australian land cover change would have impacts on key land surface attributes, with impacts on the interaction of the land surface with the near earth atmosphere, and the associated fluxes of radiation, moisture, energy and momentum. The review of the existing research into Australian land cover change impacts on climate, identified that in regional climate modelling experiments, the extensive changes in vegetation density and the seasonal cycles of the vegetation changed land surface properties with significant impacts on surface fluxes. The investigation by *Narisma and Pitman* (2003) into the near surface climate impacts of Australian land cover change also demonstrated statistically significant changes in surface heating and surface fluxes resulted from replacing pre-European land cover with current day land cover.

Analysis of the Australian land cover change experiments in Chapter 5 showed there were significant changes in surface fluxes and near earth atmospheric processes associated with

Australian land cover changes. The analysis also showed the direct impacts of changes in land surface properties on surface fluxes interacted strongly with other feedback mechanisms at a range of scales. Isolating the direct impacts of changes in land surface properties from the feedback mechanisms therefore required interpretation and conjecture. From the analysis and interpretation of Chapter 5, the following relationships between land cover changes and regional changes in surface fluxes, surface hydrology and near earth atmospheric processes were developed from the Australian land cover change experiments.

South east Queensland

The marginal increase in albedo over south east Queensland associated with the change from pre-clearing to current land cover, did not correspond with reduced short wave radiation flux for either DJF or JJA. This suggested that other feedback mechanisms such as cloud cover had larger influence on the radiation budget in this region. The increase in canopy resistance, decrease in vegetation fraction, and decrease in surface roughness, however, did correspond with reduced evaporation and transpiration, with a significantly larger reduction in DJF than JJA.

The increased short wave radiation flux and reduced evaporation and transpiration directly impacted latent heat flux, surface hydrology and the surface energy balance. The increased short wave radiation flux and reduced latent heat flux resulted in surface warming and increased sensible heat flux, again with the largest changes in DJF. The reduced evaporation and transpiration directly impacted the surface hydrology by reducing the soil moisture extracted from the soil profile, however, the net impact of the changes in surface properties and other feedback mechanisms was decreased soil moisture for both DJF and JJA. This suggested the decrease in soil moisture from reduced precipitation infiltration was greater than the reduced soil moisture extraction from reduced evaporation and transpiration.

The surface flux analysis for south east Queensland in the investigation by *Narisma and Pitman* (2003) showed that there were mixed changes in short wave radiation flux between the experiments with the magnitude of changes significantly larger in January than July. The analysis also showed latent heat flux was in general increased for the region, again with the increases in January larger than the increases in July. The mixed changes in January air temperature suggested that there was little difference in January sensible heat flux, with the marginal cooling in July suggesting a marginal decrease in July sensible heat flux. The January differences in surface fluxes were significantly larger in magnitude than the CSIRO GCM surface flux differences, however, the July differences were of the same magnitude.

Eastern New South Wales

The larger increase in albedo over eastern New South Wales resulted in mixed changes in short wave radiation flux for both DJF and JJA. The changes in short wave radiation flux

corresponded to changes in cloud cover, with much of the region having similar short wave radiation in both experiments, despite reduced cloud cover. Only in areas where cloud cover was significantly reduced was the short wave radiation flux increased. The increase in canopy resistance, decrease in vegetation fraction, and the decrease in surface roughness resulted in reduced evaporation and transpiration over the entire region for DJF, even in areas where the soil moisture was increased. In JJA evaporation and transpiration was the same or marginally increased in areas where soil moisture was higher, with evaporation and transpiration reduced only in areas where soil moisture was lower.

The changes in evaporation and transpiration resulted in changes in latent heat flux, which combined with changes in short wave radiation flux to have mixed impacts on the surface energy balance. There was surface warming and increased sensible heat flux in areas where short wave radiation flux was increased or latent heat flux decreased, and surface cooling and reduced sensible heat flux where latent heat flux was increased. The changes in evaporation and transpiration also had impacts on the surface hydrology, with impacts on soil moisture. In general the reduced evaporation and transpiration resulted in increased soil moisture where changes in precipitation infiltration where not significant.

The surface flux analysis for eastern New South Wales by *Narisma and Pitman* (2003) showed there was a general reduction in short wave radiation flux between the experiments with changes significantly larger in January than July. The analysis also showed latent heat flux was significantly reduced, with the decreases larger in January than July. The reduced latent heat flux had larger impacts than the short wave radiation resulting in significantly warmer air temperature in the current experiment, again with significantly larger increases in January than July. The air temperature increases suggested increased sensible heat flux for both months. Like south east Queensland, the January differences in surface fluxes were significantly larger in magnitude than the CSIRO GCM experiments, with the July differences of the same magnitude.

South west Western Australia

The increase in albedo over south west Western Australia was larger than the other two regions, resulting in reduced short wave radiation flux for both DJF and JJA over the region. The DJF reduced short wave radiation flux occurred despite a decrease in cloud cover, while the JJA reduced short wave radiation flux was further reduced by increased cloud cover. The DJF increase in canopy resistance, decrease in vegetation fraction and decrease in surface roughness resulted in reduced evaporation and transpiration, despite higher soil moisture. The JJA marginal decrease in canopy resistance and higher soil moisture had larger impacts on evaporation and transpiration than the decreased vegetation fraction surface roughness, with the net impact of the changes increased evaporation and transpiration.

In DJF the decreased short wave radiation flux appears to have the greatest influence on the surface energy balance, resulting in surface cooling and decreased sensible heat flux, despite

decreased latent heat flux from reduced evaporation and transpiration. In JJA the decreased short wave radiation flux and increased latent heat flux had a combined impact on the surface energy balance, again resulting in surface cooling and reduced sensible heat flux. The reduced evaporation and transpiration in DJF impacted the surface hydrology, with less moisture being extracted from the soil profile, resulting in higher soil moisture. For JJA the higher moisture extraction from increased evaporation and transpiration did not result in lower soil moisture, suggesting that the increased infiltration from precipitation had greater impact on surface hydrology than the increased evaporation and transpiration. This also suggested that the increase in soil moisture from increased precipitation had a larger impact on evaporation and transpiration than the decrease in canopy resistance.

Like eastern New South Wales, the surface flux analysis for south west Western Australia by *Narisma and Pitman* (2003) showed a general reduction in short wave radiation flux between the experiments with changes significantly larger in January than July. Again, the analysis showed latent heat flux was significantly reduced, with the decreases larger in January than July. The reduced latent heat flux had larger impacts than the short wave radiation with significantly warmer air temperature in the current experiment, with significantly larger increases in January than July. The air temperature increases suggested increased sensible heat flux for both months. Like the other two regions, the January differences in surface fluxes were significantly larger in magnitude than the CSIRO GCM experiments, and the July differences were of the same magnitude.

Other Land Surface Changes in Australia

Changes in short wave radiation flux between the Australian land cover change experiments where as large or larger in regions of Australia without land cover changes, suggesting that cloud and short wave radiation feedbacks had similar magnitude impacts as changes in albedo associated with land cover change. The changes in evaporation and transpiration also were as large or larger in other regions of Australia, suggesting precipitation and soil moisture feedbacks had similar magnitude impacts to the changes in canopy resistance, vegetation fraction and surface roughness associated with land cover change. These changes in other regions indicated that the Australian land cover change had similar magnitude impacts on the CSIRO GCM surface fluxes, surface energy balance, and surface hydrology as the feedback mechanisms that respond to the land cover changes.

The surface flux analysis of *Narisma and Pitman* (2003) showed that the surface flux differences from Australian land cover change were restricted to the immediate locality of the land cover change, with minimal feedbacks in other regions. The climate analysis of Chapter 4, also showed differences in surface fluxes, surface hydrology and surface energy budget between the new parameter and the original CSIRO parameter experiments were larger than the differences between the Australian pre-cleared and current experiments. There also were larger

global and continental differences in land surface processes between the new parameter and the original CSIRO parameter experiments outside of the Australian continent than occurred between the Australian pre-cleared and current experiments.

Conclusions

The conclusions to this postulated relationship were therefore:

1. Australian land cover change has modified Australian land surface and lower atmosphere interaction processes through changes in: surface radiation budget; surface hydrology; and the surface energy balance, which has impacted the surface fluxes of latent, sensible and ground heat;

2. These changes in surface fluxes had direct impacts on the near surface air temperature modelled in the CSIRO GCM, with the most apparent changes surface warming over south east Queensland and eastern New South Wales, associated with reduced latent heat flux, and the surface cooling over south west Western Australia associated with reduced short wave radiation flux;

3. It was not possible to assess how changes in surface roughness impacted mechanical turbulence in the turbulent surface layer from the analysis of the Australian land cover change experiments, as all land surface changes were applied simultaneously in the experiments, so this component could not be individually investigated;

4. The Australian and global changes in regions that were not affected by land cover change, indicated that the changes from Australian land cover change had similar magnitude impacts on CSIRO GCM surface fluxes, surface energy balance, and surface hydrology as the feedback mechanisms that responded to the land cover changes;

5. The changes in land surface processes between pre-clearing and current Australia, were smaller in magnitude than those identified in *Narisma and Pitman* (2003) for DJF, which was inline with the changes in land surface properties, however, the changes were of a similar magnitude for JJA, despite the significantly smaller land surface parameter differences; and

6. The changes in land surface processes were smaller than those produced in the CSIRO GCM with the original CSIRO parameters and the new land surface parameters. Again, this did not reduce the ability of the CSIRO GCM to investigate the climate impacts of Australian land cover change, however, it confirmed that there are implications for climate modelling experiments that represent the land surface with biome-derived datasets at the model grid increment.

6.2.3 Postulated Relationship 3

The third postulated relationship was that Australian land cover directly influenced the atmospheric boundary layer and troposphere through changes in local scale fluxes of moisture and energy affecting the atmospheric boundary layer, meso-scale circulation, and moisture transport, with impacts on the convective processes within the boundary layer, cloud formation and precipitation.

Discussion

As was shown in the Australian climate and land cover change review of Chapter 2 and the evaluation of the previous postulated relationship, the changes in surface processes and fluxes to the near earth atmosphere from Australian land cover change, would have had direct impacts on the processes of the atmospheric boundary layer, and from those the processes of the troposphere. The review of the existing research into Australian land cover change impacts on climate, identified that in regional climate modelling experiments, the changed land surface processes and fluxes to the near earth atmosphere did have significant impacts on boundary layer structure, cloud formation and potentially precipitation.

The modelling investigation into the climate impacts of land cover change in south west Western Australia by *Xinmei et al.* (1995), found the higher latent heat flux from native vegetation in summer and agricultural lands in winter had significant impacts on atmospheric profiles compared to those of the adjacent land cover type. The modelling experiments showed that the increased latent heat flux resulted in higher convective available potential energy (CAPE), lower lifting condensation levels, and lower levels of condensation and free convection in the atmospheric profile. These changes suggested that the increased latent heat flux resulted in higher cloud formation potential and therefore higher precipitation potential.

The investigation by *Narisma and Pitman* (2003) into the near surface climate impacts of Australian land cover change found the changes in surface fluxes had impacts on the vertical profile of the atmosphere, with the warming of summer air temperatures over south west and south east Australia propagated to around 2.6 km in altitude, with net cooling above this level. The changes in atmospheric profile, however, produced no consistent changes in precipitation over these regions in the experiments.

The grid increment of the CSIRO GCM in the Australian land cover change experiments in Chapter 5 prevented investigation into local and meso-scale circulation impacts from the land cover changes, as the sub-grid heterogeneity of land cover change could not be explicitly specified in the experiments. While the impact of land cover changes on subgrid processes could not be investigated, the cumulative impacts of changes in surface fluxes of moisture, energy and momentum could be investigated at the grid cell increment, where these changes impacted the average gridscale surface and boundary layer processes in the GCM. The net impacts of the changes in atmospheric boundary layer and troposphere processes were assessed

by analysing changes in cloud cover, precipitation and mean sea level pressure. The analysis showed that these properties were strongly impacted by other feedback mechanisms at a range of scales, and required interpretation and conjecture to disentangle the direct impacts of changes in land surface fluxes from the feedback mechanisms. From the analysis and interpretation of Chapter 5, the following relationships between land cover changes and changes in atmospheric boundary layer and troposphere processes were developed from the Australian land cover change experiments.

South east Queensland

It is speculated the increased DJF sensible heat flux and decreased DJF latent flux produced a deeper dryer boundary layer, with less cloud cover and precipitation. It also was speculated the smaller magnitude of the increases in JJA sensible heat flux and decreases in JJA latent heat flux had significantly weaker impacts on the boundary layer and therefore cloud formation and precipitation in JJA.

The primary cause of the reduced latent heat flux in both cases was the increased canopy resistance, reduced vegetation fraction and reduced surface roughness. The larger differences in soil moisture in DJF, however, suggested that the soil moisture feedback was a large contributor to the larger surface flux changes in DJF. It was also difficult to isolate the impacts from surface fluxes on precipitation and cloud cover from those of changes in larger scale atmospheric circulation. The warmer dryer boundary layer, lower precipitation and cloud cover, however, were shown to be the major drivers of the soil moisture and the DJF atmospheric circulation changes, suggesting the primary source for most of these changes, was the original change in surface fluxes.

Eastern New South Wales

It was speculated the decreased DJF latent heat flux and mixed sensible heat flux changes may have had some drying impacts on the boundary layer over the region contributing to the reduced cloud cover and mixed precipitation differences. The JJA latent and sensible heat fluxes, however, were similar for the region for both experiments despite the changes in land surface properties. The reason suggested for the smaller changes in surface fluxes with similar land cover changes to south east Queensland, was that the feedback mechanisms in eastern New South Wales appear to be negative, in that they produce the opposite affects to the surface flux changes.

The decreases in latent heat flux associated with increased canopy resistance, reduced vegetation fraction and reduced surface roughness, resulted in higher soil moisture, which acted to offset the decrease in latent heat flux. Similarly the decreases in cloud cover acted to offset the increase in surface albedo resulting in little change in short wave radiation flux. There also were feedbacks from changes in larger scale atmospheric circulation for both DJF and JJA.

Unlike south east Queensland, however, the changes in circulation appear to originate from land cover changes in other regions. It was therefore difficult to assess the direct impacts of the changes in surface fluxes of the region as the surface fluxes and the atmospheric processes were negated by various feedbacks mechanisms.

South west Western Australia

It was speculated that the marginally lower DJF latent heat flux and significantly lower DJF sensible heat flux resulted in a shallower boundary layer with less CAPE under the current land cover conditions. The cumulative impact of DJF surface flux changes and feedbacks was reduced cloud cover, and a marginal increase in precipitation. It was also speculated that the the significantly higher JJA latent heat flux and significantly lower sensible heat flux produced a wetter, shallower boundary layer with increased CAPE. The increased moisture and CAPE would have promoted increased cloud formation and precipitation, which contributed to the significant increases in JJA cloud cover and precipitation for the region.

The DJF decrease in latent heat flux and marginal increase in precipitation also resulted in higher soil moisture over the region. This was a negative feedback on the decrease of precipitation as the higher soil moisture offset the further decreases in latent heat flux. The JJA increased soil moisture extraction associated with increased latent heat flux, however, was smaller than the increase in precipitation infiltration resulting in higher soil moisture. This was a positive feedback on the increase in precipitation as the higher soil moisture further contributed to the increased latent heat flux. The higher soil moisture despite increased latent heat flux also indicated that the changes in atmospheric circulation and soil moisture feedbacks were larger in magnitude than the original increase in latent heat flux from reduced JJA canopy resistance.

Other Land Surface Flux Changes in Australia

The DJF changes in surface fluxes in other areas of Australia would have had impacts on the boundary layer structure and atmospheric processes in those areas. Over northern Australia, the decrease in DJF latent heat flux and increase in sensible heat flux would have produced a deeper dryer boundary layer, less conducive to cloud formation and precipitation. Over central Australia, the increase in DJF and JJA latent heat flux and associated decreases in sensible heat flux would have produced shallower moister boundary layers with higher CAPE, that were more conducive to cloud formation and precipitation. In each of these cases the cloud cover and precipitation changes did correspond to the changes in surface fluxes, often with positive soil moisture and radiation feedbacks.

The atmospheric analysis of *Narisma and Pitman* (2003) showed that the while surface flux differences produced changes in atmospheric structure and meso-scale circulations in the immediate locality of the land cover change, there were minimal feedbacks in other regions due to the prescription of larger scale atmospheric circulation from analysis data. The climate

analysis of Chapter 4 also showed the differences in surface fluxes of the new parameters and original CSIRO parameters experiments, resulted in changes in atmospheric pressure, precipitation, and cloud cover over in both Australia and other parts of the world. The difference between the new parameter and the original CSIRO parameter experiments were as large or larger than those that occurred between the pre-cleared and current experiments for regions with land cover change.

Conclusions

The conclusions to this postulated relationship were therefore:

1. From the CSIRO GCM modelling experiments, Australian land cover directly influenced the atmospheric boundary layer and troposphere in the model through changes in local scale fluxes of moisture and energy affecting the atmospheric boundary layer, and moisture transport, with impacts on the convective processes within the boundary layer, cloud formation and precipitation;
2. Due to the nature of the experiments it was not possible to quantify the impacts of the land cover change induced surface fluxes alone, as changes in atmospheric circulation, cloud, and soil moisture produced radiation and evaporation and transpiration feedbacks at various spatial and temporal scales; and
3. The grid increment of the CSIRO GCM preventing investigations into local and meso-scale circulations that respond from the finer scale changes in surface fluxes, as the model could only represent the cumulative impacts of changes in surface fluxes at the grid cell increment.

6.2.4 Postulated Relationship 4

The fourth postulated relationship was that Australian land cover change indirectly influenced climate at a distance beyond the location of the land cover changes through changes in larger scale atmospheric circulation with impacts on humidity and temperature of the air masses under the altered atmospheric circulation, and changes in larger-scale synoptic pressure systems.

Discussion

Larger scale analysis in Chapter 5 suggested the local changes in surface fluxes had strong impacts on atmospheric circulation. The largest changes surrounding Australia in DJF were the reduced monsoon flow into northern Australia, corresponding with increased monsoon flow into the South Pacific Convergence Zone (SPCZ) and increased south easterly wind flow into eastern Queensland. The largest change surrounding Australia in JJA was the northward shift of mid latitude westerly wind flow over southern Australia and over the surrounding

oceans. The changes in circulation impacted the air masses that were brought into the Australian continent which combined with the changed surface fluxes to impact precipitation, air temperature and convection. The global analysis identified changes in global atmospheric circulation responding to the changes in circulation around Australia. The global circulation changes impacted cloud cover, soil moisture and snow cover over other continents and oceans, resulting in changes in surface fluxes of greater magnitude than resulted from the land cover change in Australia.

From the analysis of Chapter 5, the driving force behind the change in the DJF monsoon flow into northern Australia appear to be complex with a range of feedback mechanisms operating. As discussed in the previous postulated relationship, the reduced latent heat flux associated with land cover change over south east Queensland, resulted in less cloud and precipitation, with increased short wave radiation, which resulted in increased warming and drying over the region. The warmer dryer air over the region produced an increased thermal gradient between the land and ocean to the east resulting in increased south easterly flow into south east Queensland.

The increased south easterly flow offset the monsoon flow into northern Australia, resulting in reduced DJF moisture flux from the South East Asia and the oceans to north of Australia. The reduced moisture flux reduced the cloud and precipitation, resulting in warming and drying over northern Australia. The reduced monsoon flow into northern Australia also resulted in increased monsoon flow into the SPCZ, with increased moisture flux into that region. The increased moisture flux also resulted in increased precipitation and cloud cover, as well as increased moist convection over the SPCZ. The increased convection further increased the monsoon flow into the SPCZ and away from northern Australia, as well as producing increased subsidence to the south over the Tasman Sea. The increased subsidence increased pressure over this region reinforcing the south easterly flow into eastern Australia.

The driving forces behind the JJA northward shift in mid latitude westerly wind flow over southern Australia also were elusive, as it was difficult to establish the extent to which the changes in atmospheric circulation were in response to increased JJA latent heat flux over south west Western Australia from lower JJA canopy resistance. The year round increase in precipitation over central Australia resulted in increased latent heat flux in response to increased soil moisture over that region as well. The increased latent heat flux of both these regions would have resulted in shallower moisture boundary layers developing, producing increased precipitation and cloud cover as well as increased moist convection. The increased moist convection appeared to have reduced the intensity of continental sub-tropical anti-cyclones developing over Australia, allowing the mid-latitude cyclones to penetrate further into the continent with increased intensity.

The global impacts that resulted from the local changes in Australian land surface fluxes were initially unexpected, but given the changes in DJF monsoon flow and the JJA mid-latitude

westerly wind flow, the larger scale atmospheric circulation changes could be rationalised. Research by *Goswami* (1998) and *Wang et al.* (2004) into the impact of SSTs on the variability of the Australian and Asian monsoons showed the impacts of regional-scale fluctuations in SSTs were comparable to the influence of larger scale SST fluctuations such as ENSO. It was not unrealistic therefore to expect the influences from changes in regional-scale surface fluxes and atmospheric circulation from Australian land cover change to be of the same magnitude as changes from region-scale fluctuations in SSTs.

Given that the regional changes from Australian land cover change had influences on the Australian and Asian monsoon flows, it also was reasonable to expect these changes in atmospheric circulation would have propagated from the Australian continent across the Indian and Pacific oceans with impacts in climate in Europe, Asia and North America. These influences in global climate from changes in Australian and Asian monsoons were consistent with the changes observed in studies of historical monsoon flows and climate departures in Europe, Asia and North America by *Webster et al.* (1998) and *Webster and Yang* (1992).

Conclusions

The conclusions to this postulated relationship were therefore:

1. From the CSIRO GCM modelling experiments, Australian land cover indirectly influenced climate at a distance beyond the location of the land cover changes through changes in larger scale atmospheric circulation with impacts on humidity and temperature of the air masses under the altered atmospheric circulation, and changes in larger-scale synoptic pressure systems;
2. The atmospheric circulation change impacts interacted with precipitation induced soil moisture feedbacks and cloud induced short wave radiation feedbacks to intensify the atmospheric circulation change impacts at large distances beyond the Australian land cover changes; and
3. The atmospheric circulation changes to the Australian and Asian monsoon flows had impacts on global climate consistent with the climate impacts shown in observational studies of Australian and Asian monsoon variability and global climate impacts.

6.2.5 Postulated Relationship 5

The fifth postulated relationship was that Australian land cover change indirectly influenced climate through feedback mechanisms through changes in cloud cover impacting the surface radiation budget, and changes in precipitation impacting soil moisture with impacts on evaporation and transpiration.

Discussion

As discussed in the previous postulated relationships, the majority of the climate impacts evident from Australian land cover change in the CSIRO GCM modelling experiments, were not the direct result directly from changes in surface fluxes but were the result of these changes operating in combination with various feedback mechanisms. Due to the nature of the experiments performed it was not possible to disentangle the direct impacts on climate from changes in surface fluxes from the indirect impacts through feedback mechanisms. The larger scale analysis of global climate impacts showed the largest changes in DJF surface fluxes were in latent heat flux from the oceans. The impacts on DJF latent heat flux over land were significantly smaller than over oceans with the soil moisture impacts only significant over Australia, and southern Africa.

Over North America and central Europe, warmer JJA air temperatures appeared to be due to decreased cloud cover increasing short wave radiation flux, and reduced soil moisture reducing latent heat flux. The JJA short wave radiation flux differences, as well as the sensible and latent heat flux differences were larger in central Europe, North America, and Asia than they were in areas of Australia land cover change. In Australia the differences in JJA surface fluxes also were greater in areas with unchanged land surface parameters than in areas with land cover change.

The larger changes in surface fluxes at distance from the land cover change suggested the impacts from feedback mechanisms on surface conditions were significantly greater that the direct impacts of changes in land surface properties associated with Australian land cover change. In closely related work *Zeng* (1998) suggests that GCMs have high regional climate sensitivity to land cover change, and that different parameterisation schemes within different GCMs can give rise to a range of climate responses for the same tropical deforestation land cover change. This is an important consideration when assessing the Australian land cover change experiments in Chapter 5, given that the feedback mechanisms in the CSIRO GCM produced larger surface fluxes changes than were produced by the initial land cover changes.

Conclusions

The conclusions to this postulated relationship were therefore:

1. From the CSIRO GCM modelling experiments, Australian land cover indirectly influenced climate through feedback mechanisms through changes in cloud cover impacting surface radiation budgets, and changes in precipitation impacting soil moisture with impacts on transpiration and evaporation;
2. The changes in surface fluxes were larger in many areas at a distance from the land cover change than in the immediate locality of the land cover change, suggesting the impacts from feedback mechanisms on surface conditions were larger that the direct impacts of Australian land cover change; and

3. Investigations into tropical deforestation demonstrate that the same land cover change can have significantly different climate impacts, depending on the parameterisations used in the climate model used in the modelling experiments.

6.3 Implications

The statistically significant DJF warming and drying modelled over south east Queensland, with causal links back to historical land cover change in the region, has significant implications for the region. This region has experienced strong drying trends over the last 50 years with significant impacts on agriculture, water storage and supply for urban areas and industry, and for ecosystem functions limited by water availability and temperature (*Crimp and Day*, 2003 and *McKeon et al.*, 2000). This region and the areas to the north and west, continue to be actively cleared, accounting for the majority of current land clearing occurring across Australia. While these modelled climate impacts need to be verified through further research, the modelling results indicate that the climate impacts of ongoing clearing may be significantly contributing to the observed drying over eastern Queensland. If this is the case then the climate impacts of land cover change need to be incorporated into land use management planning as a significant outcome of current land clearing in Queensland.

The statistically significant increase in JJA precipitation over south west Western Australia had significant implications for the region, as it increased the annual precipitation, which was opposite to the observed drying trends identified from 100 and 50 year analyses. This result demonstrated that the increased JJA latent heat fluxes over agricultural land from decreased canopy resistance had the potential to increase precipitation despite increased albedo over the region. This finding also supported the observation of *Ray et al.* (2003), which showed winter latent heat fluxes were higher over agricultural land than over adjacent native vegetation, and preferentially formed cumulus clouds with higher water content than over the native vegetation. The modelling results therefore suggest the strong drying trend over south west Western Australia has been in response to other climatic forcing such as those suggested by *Wright and Jones* (2003), rather than from historical land cover change.

The strong influence of feedback mechanisms such as changes in atmospheric circulation, changes in soil moisture, and changes in cloud cover had significant implications for modelling experiments that do not include these processes. The modelled impacts of feedback mechanisms demonstrated that experiments that did not include these processes were unable to describe the range of climate impacts resulting from land cover change. These investigations with out the complexity of feedback mechanisms however are essential as they provide a framework for investigating how changes in land surface properties directly impact land surface fluxes, and how changes in surface fluxes directly impact atmospheric processes.

The significantly smaller land surface property changes obtained from satellite-derived land cover change compared to the biome-derived datasets used in experiments such as those of

Narisma and Pitman (2003), had significant implications for representing Australian land cover change in climate modelling experiments. The large differences in the satellite-derived land surface properties and the original CSIRO land surface parameters also had significant implications for the modelling experiments using the CSIRO GCM with the original parameters. The differences between the satellite-derived parameters and the original parameters were significantly larger in magnitude than the Australian land cover changes, with the differences in the parameters having global extent.

6.4 Future Research

The evaluation of differences in climate in the modelling experiments of Chapter 4 and 5 show the climate impacts of Australian land cover change are inherently complex as the climate system responds on a range of time and space scales to changes in surface conditions through processes involving the atmosphere, radiation, soil moisture and snow cover. To describe the Australian land cover change impacts on climate, therefore required separating the direct land surface flux changes from the feedbacks, to develop causal relationships between changes in land surface properties and changes in climate in the climate modelling experiments.

The theorectical impacts of land cover change on surface fluxes and soil moisture require validation with experimental data from field studies and satellite observation in eastern and central Australia as they have been in south west Western Australia. To remove the possible model dependent climate impacts suggested by *Zeng* (1998) the experiments need to be repeated in an independent modelling framework with different land surface and atmospheric parameterisations to ensure that the modelling results found in this research are not a product of the CSIRO GCM parameterisations.

The modelling studies also need to be extended to investigate the climate impacts of recent and ongoing Australian land cover change, as well as incorporating the less well defined land cover changes associated with extensive grazing, altered fire regimes and invasions by introduced animals and plants. The climate impacts of historical and current land cover change need to be assessed in relation to the precipitation and temperature impacts on agriculture, urban and industrial development, and environmental management. These impacts also need to be assessed in the context of other sources of climate change such as those due to increased greenhouse gas concentrations in the atmosphere, and changes in the intensity and frequency of ENSO events.

One approach to evaluating the wide range of responses the climate system has to Australian land cover change would be to represent the same land cover change across a range of experiments with each experiment investigating either the influence of scale or the impact of additional feedback processes. Such an investigation would require a range of climate models with the same land surface parameterisations, but which could include different levels of

freedom in atmosphere, ocean and biosphere processes over different spatial and temporal domains.

This investigation would commence with the regional climate modelling experiments such as those performed by *Narisma and Pitman* (2003) to demonstrate how the changes in surface characteristics impact surface fluxes and regional atmospheric processes with out feedbacks. The complexity of these changes could be increased as well as the scale at which the processes operate by incorporating models with atmosphere and soil moisture feedbacks. These feedbacks would be extended to incorporate changes in sea surface temperatures and sea ice distributions through dynamic ocean and ice models. The investigation would be further extended to include dynamic vegetation to incorporate changes in community composition and vegetation structure in response to changes in moisture availability and temperature from land cover change. The final component of such a study would involve the carbon cycle with enhanced anthropogenic greenhouse gas concentrations to evaluate the climate impacts of Australian land cover changes in potential future climate conditions.

APPENDICES

A. Two stream radiation model

Dickinson (1983) reviewed the work of *Meador and Weaver* (1980) to provide a two-stream approximation of the dynamics of short wave radiation within vegetation canopies by representing the canopy as a cloud of leaves. The canopy cloud approximation represented the leaves as partially transparent isotropic scattering objects that behaved similarly to the particles of clouds (*Sellers*, 1985). In this model intercepted light is assumed to be absorbed, reflected or transmitted dependant on the optical properties of the leaf for the wavelengths of the radiation, and the position and orientation of the leaf within the canopy.

Direct beam solar radiation and diffuse sky scattered radiation are explicitly calculated as they travel through the leaves of the vegetation canopy to the underlying soil and are reflected back through the canopy. The radiation dynamics of visible and near-infrared wavelengths are calculated independently for each of the direct and diffuse components so the differences in the optical properties of the leaves for each spectral band can be incorporated.

The attenuation of direct beam radiation as it passes through the vegetation canopy is calculated according to Beer's exponential extinction law under the assumption the direct beam radiation is incident with a homogeneous plane-parallel canopy. This relationship between the direct beam flux (F_L) at a depth within the canopy specified by the cumulative the leaf area (L), is dependent on the direct beam flux incident on the canopy (F_0), and the optical depth of the direct beam per unit leaf area (K), which is equal to $G(\mu)/\mu$, where μ is the cosine of the zenith angle of the incident beam and $G(\mu)$ is the projected area of leaf elements in the direction of the incident beam.. This relationship is written as:

$$F_L = F_0 e^{-KL} \qquad \text{(A.1)}$$

In the model, the direct beam radiation that is removed by the canopy is divided into radiation absorbed by leaves, radiation reflected by leaves as upward diffuse radiation, and radiation transferred through leaves as downward diffuse radiation. The direct beam radiation that reaches the soil is either absorbed by the soil or reflected back from the soil as upward diffuse radiation.

The transfer of diffuse radiation through the canopy and its reflection from the underlying soil is calculated using upward and downward fluxes of diffuse radiation in a similar manner to that of atmospheric scattering. The work of *Meador and Weaver* (1980) has been adapted to describe the rate of change of upward and downward fluxes of diffuse radiation in the vegetation canopy as the cumulative leaf area index increases. The relationship of these rates of change can be calculated for the upward ($I\uparrow$) and downward ($I\downarrow$) fluxes of diffuse radiation at the cumulative leaf area index (L), using the scattering coefficient of the leaves (ω), the

upscatter parameters of the leaves for diffuse (β) and direct (β_0) beam radiation, and the average inverse diffuse optical depth per unit leaf area ($\bar{\mu}$). These relationships are written as:

$$\frac{dI\uparrow}{dL} = \frac{1}{\bar{\mu}}\left[1-(1-\beta)\varpi\right] I\uparrow - \frac{\varpi}{\bar{\mu}}\beta\, I\downarrow - \varpi K\beta_0 e^{-KL} \qquad \text{(A.2)}$$

$$\frac{dI\downarrow}{dL} = -\frac{1}{\bar{\mu}}\left[1-(1-\beta)\varpi\right] I\downarrow + \frac{\varpi}{\bar{\mu}}\beta\, I\uparrow + \varpi K(1-\beta_0)e^{-KL} \qquad \text{(A.3)}$$

The terms on the right hand side of *equations A.2* and *A.3* represents the change in diffuse radiation flux caused by the leaf upscattering for the diffuse radiation in each direction and for the direct beam radiation. *Equations A.2* and *A.3* can be solved for boundary conditions at the top of the canopy where the downward component of diffuse radiation from the direct beam radiation is 0, and at the soil surface where the upward component is equal to the reflected downward components. *Sellers* (1985) provides general numerical solutions from these boundary conditions that allow for the calculation of net diffuse radiation fluxes in both directions for the direct beam solar radiation and diffuse sky scattered radiation components. The specific solutions for these net fluxes of diffuse radiation depend upon:

1. the scattering coefficient for the leaves (ω)
2. the soil reflectance (a_s)
3. the leaf area index (L)
4. the leaf angle distribution factor (χ_L)
5. the solar zenith angle (θ)

Albedo and Radiation Absorption in Vegetation

From the net fluxes of diffuse radiation leaving the canopy, and the net fluxes of solar radiation entering the canopy, the surface albedo can be calculated for a given solar zenith angle and spectral band. The net fluxes of direct and diffuse radiation reaching the soil and leaving the canopy also can be used to calculate the net flux of radiation absorbed by the soil and the vegetation individually for the solar zenith angle and spectral band.

The scattering coefficients, leaf angle distribution, and leaf area index of the vegetation are determined by the vegetation physiology, which determine the radiation dynamics through the canopy. Changes in the radiation dynamics alter the surface radiation budget by changing the broadband surface albedo. *Figure A.1* plots the broadband surface albedo (α) for different vegetation physiological characteristics over a range of leaf area index values and solar zenith angles.

The differences between the plotted relationships of *figure A.1* show the relative importance of the vegetation and soil optical properties. Where the vegetation absorbs more radiation than the soil (*a*, *b*, and *d*), increases in vegetation density (LAI) result in general decreases in broadband surface albedo, but where the soil is more absorbing than the vegetation (*c*), this relationship is reversed. Investigation into the sensitivity of these relationships to changes in the leaf angle distribution factor, suggests that this parameter is of secondary importance relative to the relationship between the leaf scattering coefficients and the soil reflectivity, with large changes in the leaf angle distribution factor having relatively less influence on the overall nature of the surface albedo plots.

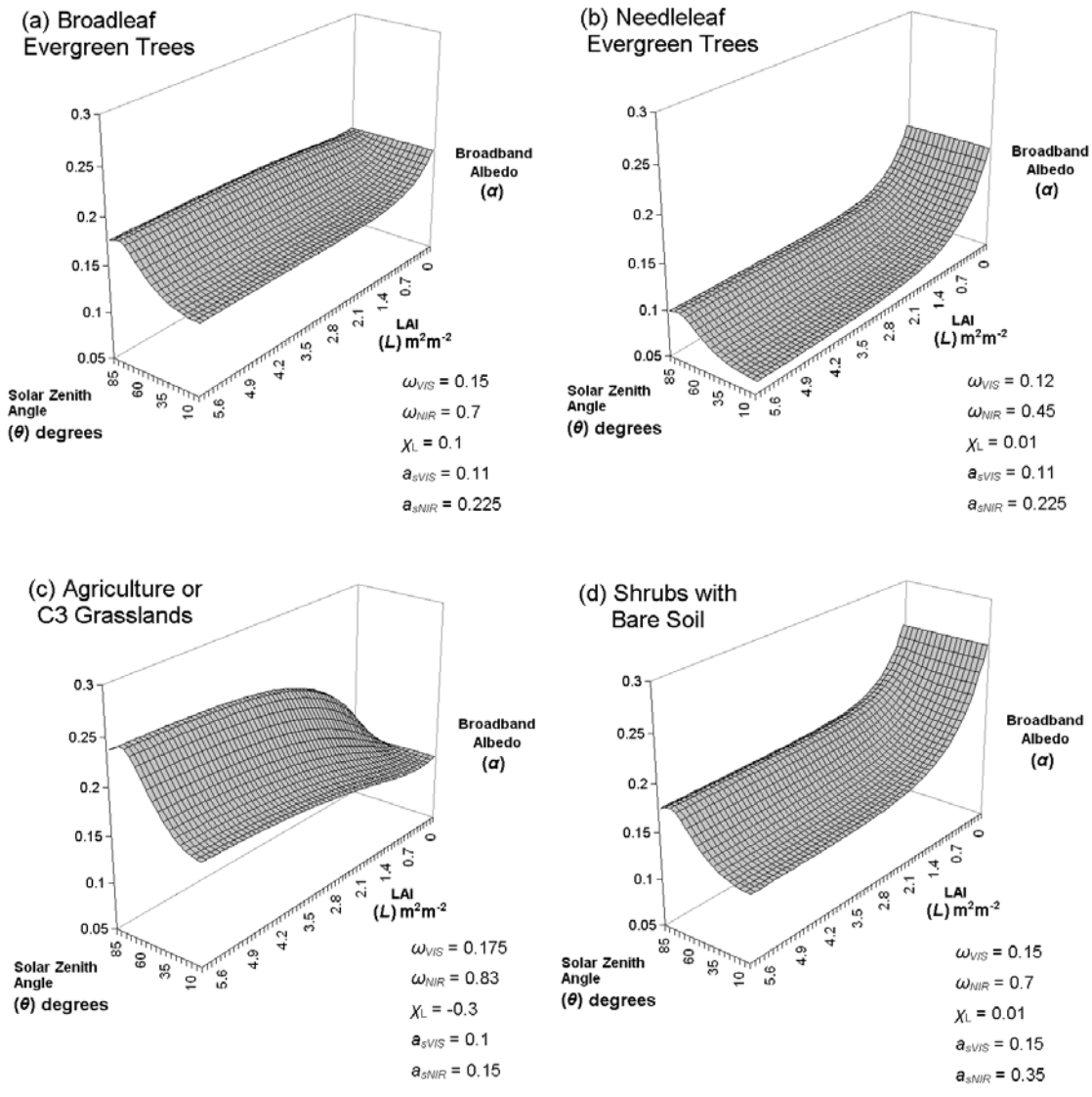

Figure A.1 Broadband Surface Albedo (α) plotted against Solar Zenith Angle (θ) and Leaf Area Index (L) using the Two-Stream Radiation model solutions of Sellers (1985) with Clear Sky Radiation calculated from the methods of Dorman and Sellers (1989) and Vegetation Parameters taken from Sellers et al. (1996a).

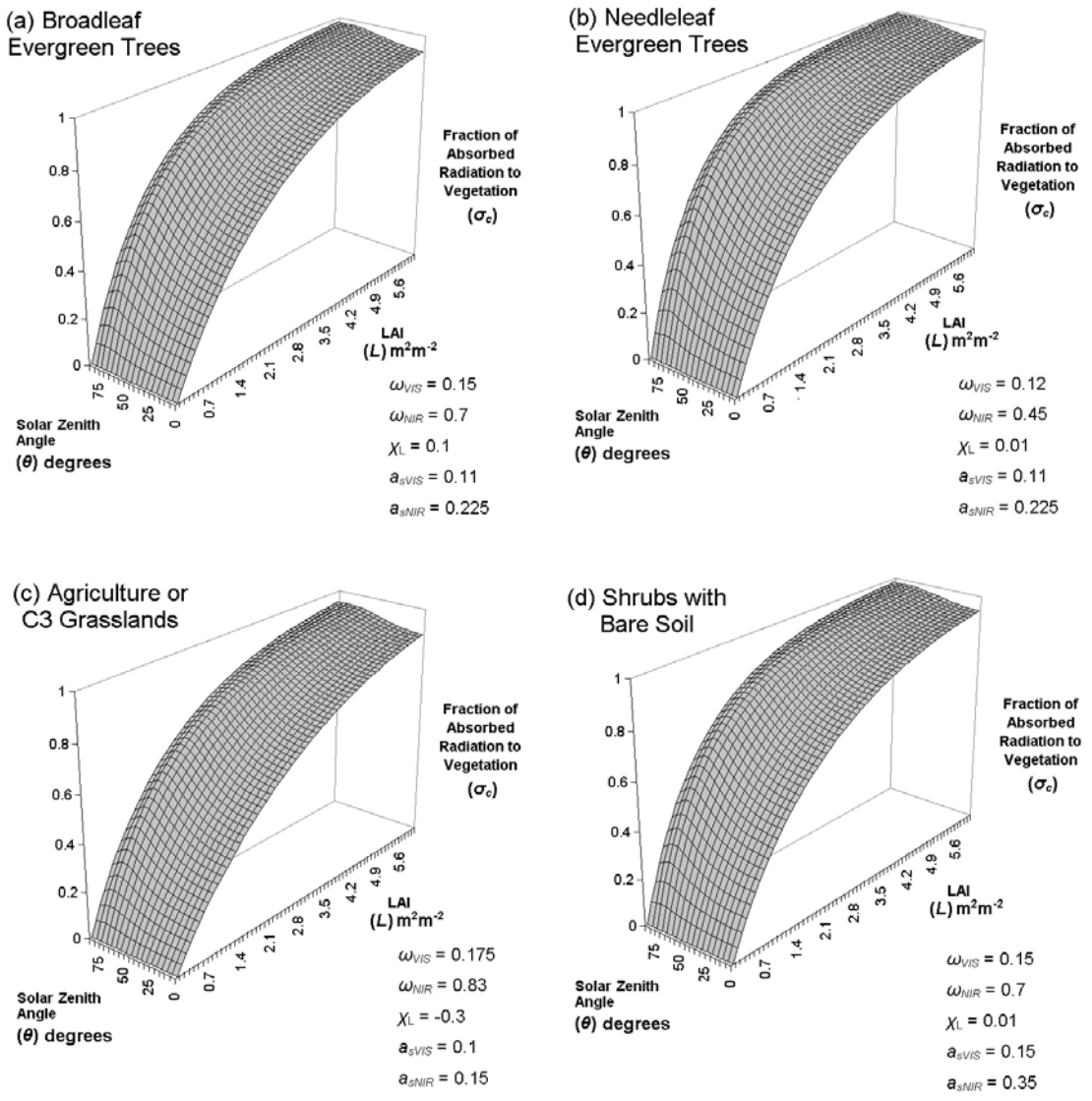

Figure A.2 Fraction of absorbed short wave radiation, absorbed by the vegetation (σ_c) plotted against Solar Zenith Angle (θ) and Leaf Area Index (L) using the Two-Stream Radiation model solutions of Sellers (1985) with Clear Sky Radiation calculated from the methods of Dorman and Sellers (1989) and Vegetation Parameters taken from Sellers et al. (1996a).

The magnitude of the relationship between leaf scattering coefficients, soil reflectivity and surface albedo are highly dependent on the absolute difference in the leaf and soil optical properties. *Figure A.1 a* and *b* show that Needleleaf Evergreen Trees have larger decreases in broadband surface albedo with increases in vegetation density than Broadleaf Evergreen Trees over soil with the same reflectivity. The differences in the leaf optical properties show that leaves in Needleleaf Evergreen Trees absorb more radiation in the visible spectrum (ω_{VIS} = 0.12 compared to ω_{VIS} = 0.15) and significantly more radiation in the near infrared spectrum (ω_{VIS} = 0.45 compared to ω_{VIS} = 0.7).

This relationship between leaf scattering coefficients, soil reflectivity and surface albedo, also can be seen for vegetation with similar leaf scattering coefficients over soils with different reflectivity. *Figure A.1 a* and *d* show that Shrubs with Bare Soil have larger decreases in albedo with increases in vegetation density than Broadleaf Evergreen Trees. The leaf scattering

coefficients of the two vegetation types are the same, however, the typical soil under Shrubs with Bare Soil is more reflective in the visible spectrum (a_{sVIS} = 0.15 compared to a_{sVIS} = 0.11) and significantly more reflective in the near infrared spectrum (a_{sNIR} = 0.35 compared to a_{sNIR} = 0.225).

The distribution of short wave radiation absorbed at the ground and in the vegetation is more strongly dependant on leaf area index, than scattering coefficients, leaf angle distributions or soil reflectance. *Figure A.2* plots the fraction of total radiation absorbed at the surface that is absorbed by the canopy (σ_c) for different vegetation physiological characteristics over a range of leaf area index values and solar zenith angles. The similarity of the plots for each vegetation type highlights the dependence of the split of radiation into the canopy and the ground on the leaf area index. The influence of the leaf area index, leaf angle, and leaf optical properties of the vegetation on short wave radiation result in changes the surface radiation budget and on the distribution of radiation energy between the ground and the vegetation.

B. Canopy Transpiration Model

Trenberth (1992), *Monteith and Unsworth* (1990), *Gurevitch et al.* (2002), and others detail how the transpiration flux from the canopy is a product of the exchanges of moisture, carbon dioxide, and oxygen involved in photosynthesis. *Figure C.1* illustrates the how the photosynthetic processes involved in a C3 plant leaf use photosynthetically active radiation (PAR) to combine water and carbon dioxide to produce glucose and oxygen. The concentration of carbon dioxide within the sub-stomatal cavity is reduced by photosynthesis and requires the air within the cavity to be exchanged with air in the surrounding atmosphere to maintain the supply of carbon dioxide.

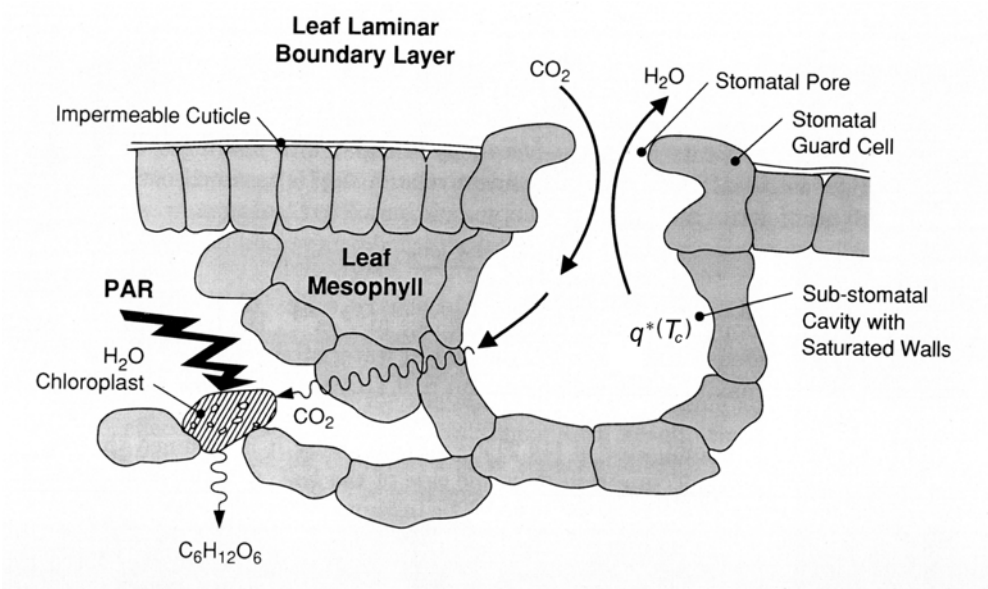

Figure C.1 Schematic of stomatal gas exchanges and photosynthesis within a C3 plant leaf (after Trenberth (1992))

The difference in the moisture concentrations between the air within sub-stomatal cavity, where the air is at saturated specific humidity $q^*(T_c)$, and the surrounding atmosphere is called the vapour pressure deficit. The difference in moisture concentrations results in a transpirational flux of moisture associated with the photosynthesis driven exchanges of air. The rate of the flux of moisture is determined by the vapour pressure deficit, and the rate of exchange the air, which is controlled by the stomatal pore at the opening of the sub-stomatal cavity.

To regulate the moisture and carbon dioxide exchanges, the stomata are optimised to maximise carbon assimilation and minimise water loss through opening and closing in response to environmental stresses. *Jarvis* (1976) provided a stomatal conductance (g_s) model for the behaviour of stomata on illuminated leaves that is a function of temperature, vapour pressure deficit, leaf water potential, ambient carbon dioxide concentration and photosynthetic rate.

Sellers (1985), *Noilhan and Planton* (1989) and others, have used the reciprocal of the stomatal conductance as a stomatal resistance (r_s) term, which can be added to the canopy boundary layer resistance (r_b) to produce a single resistance value for the flux of moisture from

inside the sub-stomatal cavity to the canopy air space. By integrating across all leaves in the canopy, the stomatal resistance model can be extended to a canopy resistance (r_c) model for use in calculating canopy transpiration rates. The canopy transpiration flux is calculated as:

$$E_{ctrans} = \rho \frac{\left(q^*(T_c) - q_0\right)}{r_c + r_b} \tag{B.1}$$

The canopy transpiration model of *Noilhan and Planton* (1989) uses a minimum stomatal resistance term (r_{smin}) to represent the unstressed stomatal resistance of each leaf to transpiration, with the unstressed value specified for each vegetation type from experimental data. The canopy resistance expression is written as:

$$r_c = \frac{r_{s\min}}{L} F_1 F_2^{-1} F_3^{-1} F_4^{-1} \tag{B.2}$$

where environmental stress functions are used to scale the unstressed stomatal resistance to account for the effect of photosynthetically active radiation (F_1), the effect of water availability in the root zone (F_2), the effect of vapour pressure deficit (F_3), and the effect of high or low temperatures (F_4). The stomatal resistance is divided by leaf area index (L) to integrate it across the canopy to calculate the bulk canopy resistance to transpiration.

C. Canopy Interception of Precipitation and Dew Model

The evaporative flux from the canopy (E_c) is split between evaporation from the fraction of the canopy covered by intercepted precipitation or dew (E_{cwet}), and transpiration from the remaining dry fraction of the canopy (E_{ctrans}). *Deardorff* (1978) suggested that the moisture retained in the canopy from precipitation and dew could be used as a wetness fraction for calculating the relative fractions of these evaporative and transpiration fluxes, where the wetness fraction of the canopy (δ) is a function of canopy water content (W_c) and the maximum amount of moisture that could be retained in the canopy (W_{cMax}). These relationship are written as:

$$E_c = \delta E_{cwet} + (1-\delta) E_{ctrans} \tag{C.1}$$

$$\delta = \left(\frac{W_c}{W_{cMax}} \right)^{2/3} \tag{C.2}$$

Dickinson (1983) suggested that the maximum moisture store in the canopy was 0.2mm per unit leaf area index (L), with the maximum precipitation and dew interception by vegetation a function of leaf area index. This equation is written as:

$$W_{cMax} = 0.2L \tag{C.3}$$

The evaporative flux from the wet fraction of the canopy (E_{cwet}) occurs at the potential evaporation rate, as the water is freely available on the surface of the leaves. The potential evaporative rate from the canopy is calculated from the saturated specific humidity $q^*(T_c)$ at canopy temperature (T_c), the specific humidity (q_0) within the canopy air space water, and the canopy boundary layer resistance (r_b). This is written as:

$$E_{cwet} = \rho \frac{\left(q^*(T_c) - q_0 \right)}{r_b} \tag{C.4}$$

The water balances for the soil moisture store and the canopy moisture store can be evaluated independently based on evaporative and transpiration fluxes, precipitation, and runoff for each store. The changes in soil moisture store (ΔW_s) and the canopy moisture store (ΔW_c) are written as:

$$\Delta W_s = P_g + D_c - E_g - (1-\delta) E_{ctrans} - R_s \tag{C.5}$$

$$\Delta W_c = P_c - D_c - \delta E_{cwet} \tag{C.6}$$

where P_g and P_c are the effective precipitation rates for the ground and canopy, D_c is the drainage rate from the canopy to the ground, E_g is the evaporative surface flux from soil moisture, and R_s is the surface runoff and deep soil drainage rate.

Sellers (1986) suggests the interception of precipitation can be estimated by adapting the Beer's exponential extinction law for radiation to represent the precipitation as vertical radiation falling on leaves with emissivity of unity. In this representation the effective precipitation for the canopy and soil can be expressed as functions of the actual precipitation rate (P), the leaf area index (L), and the optical depth of the long wave radiation per unit leaf area (K) calculated in the same manner as the long wave radiation. These relationships are written as:

$$P_g = Pe^{-KL} \tag{C.7}$$

$$P_c = P\left(1 - e^{-KL}\right) \tag{C.8}$$

The drainage rate from the canopy can be evaluated as the amount of precipitation intercepted by the canopy that is over the maximum amount that can be retained in the canopy. This relationship is written as:

$$D_c = 0 \qquad \text{if } P_c <= W_{cMax} - W_c$$

$$D_c = P_c - \left(W_{cMax} - W_c\right) \qquad \text{if } P_c > W_{cMax} - W_c \tag{C.9}$$

D. Soil Moisture Evaporation Model

Kondo et al. (1990) provides two solutions for estimating the bare soil evaporative flux from soil moisture contained within the soil matrix near the surface. The alpha method uses the soil moisture availability (α_{sm}) as a scaling factor to calculate the specific humidity at the soil surface as a fraction of the saturated specific humidity at the soil temperature (T_g). The beta method uses the soil moisture availability (β_{sm}) as a limit on the flux of moisture to a fraction of the potential evaporation that would occur if the soil were saturated.

In both cases the soil moisture availability term is strongly controlled by the molecular diffusivity of water at the surface temperature (D_{atm}), the soil moisture content (η), the saturation soil moisture content (η_{sat}), and the atmospheric resistance within the turbulent surface layer (r_a). Both fluxes are written for the soil moisture evaporative flux (E_g) as:

$$E_g = \rho \frac{\left(\alpha_{sm} q^*\left(T_g\right) - q_a\right)}{r_a} \qquad \text{(D.1)}$$

$$E_g = \rho \beta_{sm} \frac{\left(q^*\left(T_g\right) - q_a\right)}{r_a} \qquad \text{(D.2)}$$

Lee and Pielke (1992) reviewed a range of empirically derived methods for evaluating soil moisture availability for both the α and β methods. The beta method was suggested as the most practical formulation, primarily as the alpha method requires the calculation of the beta term to determine the transport of the moisture from the soil surface to the roughness height for moisture. *Lee and Pielke* (1992) adapted the alpha method of *Noilhan and Planton* (1989) to produce a simple method for deriving the β term from the soil moisture content (η), and the field capacity soil moisture content (η_{fc}). The new method was compared with experimental results for a range of soils and soil moisture contents, and showed good agreement for all soils. The expression for the moisture availability terms is written as:

$$\beta_{sm} = \frac{1}{4}\left[1 - \cos\left(\frac{\eta}{\eta_{fc}}\pi\right)\right]^2 \qquad \text{if } \eta < \eta_{fc}$$

$$\beta_{sm} = 1 \qquad \text{if } \eta >= \eta_{fc} \qquad \text{(D.3)}$$

E. Surface Roughness Model

The relationships between vegetation height and structure, with surface roughness and displacement height have been extensively examined through experiment and theory by *Raupach* (1992), *Shaw and Pereira* (1982), and others. *Raupach* (1994) provides simplified expressions for surface roughness normalised by height (z_0/h) and the displacement height normalised by height (d/h) that can be determined from canopy height (h) and leaf area index (L), with experimentally derived shelter and drag coefficients. These relationships are written as:

$$\frac{z_0}{h} = \frac{h-d}{h}\exp(\psi_h)\exp(-k\gamma) \tag{E.1}$$

$$\frac{d}{h} = 1 - \frac{1-\exp\left(-\sqrt{c_{d1}L}\right)}{\sqrt{c_{d1}L}} \tag{E.2}$$

where

$$\psi_h = \ln(c_w) + 1 - \frac{1}{c_w} \tag{E.3}$$

$$\gamma = \frac{u_*}{u(h)} = \min\left[\left(C_S + C_R L/2\right)^{1/2}, \gamma_{\max}\right] \tag{E.4}$$

with values set for the wind profile departure function constant (c_w) = 2, the element drag coefficient (C_R) = 0.3, the surface drag coefficient (C_S) = 0.003, the d/h coefficient (c_{d1}) = 7.5, and the maximum value for the frictional velocity divided by the velocity at canopy height h ($\gamma_{\max}$) = 0.3.

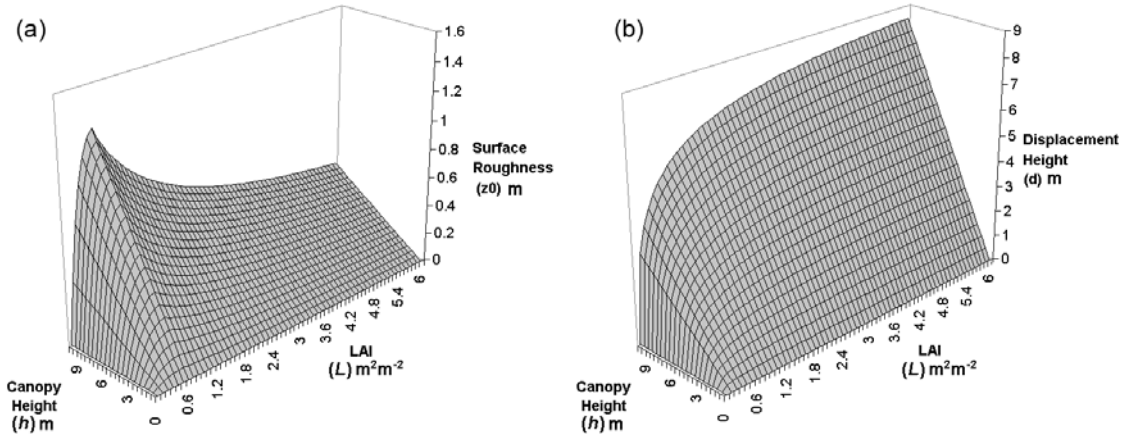

Figure E.1 (a) Surface Roughness (z0) and (b) Displacement Height (d) plotted against Canopy Height (h) and Leaf Area Index (L) using the simplified expressions of Raupach (1994)

The relationships between leaf area index and canopy height with surface roughness length and displacement height are shown in the plots of *figure E.1*. The plot of surface roughness length shows that as leaf area index (LAI) increases the surface roughness length increases to maximum value at LAI = 0.58. Beyond the maximum value the height of the surface roughness length added to the displacement height remains nearly constant, however, the value of surface roughness length decreases as the displacement height increases. The plot of displacement height shows that as LAI increases the displacement height increases to a maximum value around 85% of the canopy height.

BIBLIOGRAPHY

Arain, A.M., W.J. Shuttleworth, Z.L. Yang, J. Michaud, and A.J. Dolman, Mapping surface-cover parameters using aggregation rules and remotely sensed cover classes, *Quarterly Journal of the Royal Meteorological Society*, *123*, 2325-2348, 1997.

AUSLIG, *Atlas of Australian resources: Vegetation*, Commonwealth Government Printer, Canberra, 1990.

Avissar, R., Scaling of land-atmosphere interactions: An atmospheric modelling perspective, *Hydrological Processes*, *9*, 679-695, 1995.

Avissar, R., and Y. Liu, Three-dimensional numerical study of shallow convective clouds and precipitation induced by land surface forcings, *Journal of Geophysical Research*, *101*, 7499-7518, 1996.

Avissar, R., and T. Schmidt, An evaluation of the scale at which ground-surface heat flux patchiness affects the convective boundary layer using large-eddy simulations, *Journal of Atmospheric Science*, *55*, 2666-2689, 1998.

Baidya Roy, S., and R. Avissar, Scales of response of the convective boundary layer to land-surface heterogeneity, *Geophysical Research Letters*, *27* (4), 533-536, 2000.

Barson, M., L. Randall, and V. Bordas, Land cover change in Australia, Bureau of Rural Sciences, Canberra, 2000.

Beard, J.S., and M.J. Webb, *Vegetation Survey of Western Australia*, University of Western Australia Press, Nedlands, 1974.

Berry, S.L., and M.L. Roderick, CO2 and land-use effects on Australian vegetation over the last two centuries, *Australian Journal of Botany*, *50*, 511-531, 2002a.

Berry, S.L., and M.L. Roderick, Estimating mixtures of leaf functional types using continental-scale satellite and climatic data, *Global Ecology and Biogeography*, *11*, 23-39, 2002b.

Betts, A.K., J.H. Ball, A.C.M. Beljaars, M.J. Miller, and P. Viterbo, The land surface-atmosphere interaction: A review based on observational and global modeling perspectives, *Journal of Geophysical Research*, *101* (D3), 7209-7225, 1996.

Betts, R.A., Offset of the potential carbon sink from boreal forestation by decreases in surface albedo, *Nature*, *408*, 187-190, 2000

Blackadar, A.K., The vertical distribution of wind and turbulent exchange in a neutral atmosphere, *Journal of Geophysical Research*, *67*, 3095-3102, 1962.

Bounoua, L., G.J. Collatz, S.O. Los, P.J. Sellers, D.A. Dazlich, C.J. Tucker, and D.A. Randall, Sensitivity of Climate to Changes in NDVI, *Journal of Climate*, *13*, 2277-2292, 2000

Bounoua, L., R.S. DeFries, G.J. Collatz, P.J. Sellers, and H. Khan, Effects of land cover conversion on surface climate, *Climatic Change*, *52*, 29-64, 2002.

Buermann, W., J. Dong, X. Zeng, R.B. Myneni, and R.E. Dickinson, Evaluation of the utility of satellite-based vegetation leaf area index data for climate simulations, *Journal of Climate*, *14* (17), 3536-3550, 2001.

Burrows, W.H., B.K. Henry, P.V. Back, M.B. Hoffmann, L.J. Tait, E.R. Anderson, N. Menke, T. Danaher, J.O. Carter, and G.M. McKeon, Growth and carbon stock change in eucalypt woodlands in northeast Australia: ecological and greenhouse sink implications, *Global Change Biology*, *8*, 769-784, 2002.

Brovkin, V., A. Ganopolski, M. Claussen, C. Kubatzki, and V. Petoukhov, Modeling climate response to historical land cover change, *Global Ecology and Biogeography*, *8*, 509-517, 1999

Charney, J.G., Dynamics of deserts and drought in the Sahel, *Quarterly Journal of the Royal Meteorological Society*, *101* (428), 193-202, 1975.

Chase, T.N., R.A. Pielke, T.G.F. Kittel, R.R. Nemani, and S.W. Running, Sensitivity of a general circulation model to global changes in leaf area index, *Journal of Geophysical Research*, *101* (D3), 7393-7408, 1996

Chase, T.N., R.A. Pielke, T.G.F. Kittel, R.R. Nemani, and S.W. Running, Simulated impacts of historical land cover changes on global climate in northern winter, *Climate Dynamics*, *16*, 93-105, 2000.

Chase, T.N., R.A. Pielke, T.G.F. Kittel, M. Zhao, A.J. Pitman, S.W. Running, and R.R. Nemani, Relative climatic effects of landcover change and elevated carbon dioxide combined with aerosols: A comparison of model results and observations, *Journal of Geophysical Research*, *106*, 31685-31691, 2001.

Crawley, M.J., *Statistical Computing: An Introduction to Data Analysis using S-Plus*, John Wiley and Sons, Ltd, Chichester, 2002.

Crimp, S.J., and K.A. Day, Evaluation of multi-decadal variability in rainfall in Queensland using indices of El Nino-Southern Oscillation and inter-decadal variability, in *National Drought Forum 2003*, edited by R. Stone, and I. Partridge, Brisbane, 2003.

Deardorff, J.W., Efficient Prediction of Ground Surface Temperature and Moisture, with Inclusion of a Layer of Vegetation, *Journal of Geophysical Research*, *83*, 1889-1903, 1978.

DeFries, R.S., and J.R.G. Townshend, NDVI-derived land cover classifications at a global scale, *International Journal of Remote Sensing*, *15*, 3567-3586, 1994.

DeFries, R.S., C.B. Field, I. Fung, C.O. Justice, S.O. Los, P.A. Matson, E. Mathews, H.A. Mooney, C.S. Potter, K. Prentice, P.J. Sellers, J.R.G. Townshend, C.J. Tucker, S.L. Ustin, and P.M. Vitousek, Mapping the land surface for global atmosphere-biosphere models: toward continuous distributions of vegetation's functional properties, *Journal of Geophysical Research*, *100* (D10), 20867-20882, 1995.

DeFries, R.S., J.R.G. Townshend, and M.C. Hansen, Continuous fields of vegetation characteristics at the global scale at 1km resolution, *Journal of Geophysical Research*, *104* (D14), 16911-16923, 1999.

DeFries, R.S., M.C. Hansen, J.R.G. Townshend, A.C. Janetos, and T.R. Loveland, A new global 1-km dataset of percentage tree cover derived from remote sensing, *Global Change Biology*, *6*, 247-254, 2000.

DeFries, R.S., L. Bounoua, and G.J. Collatz, Human modification of the landscape and surface climate in the next fifty years, *Global Change Biology*, *8*, 438-458, 2002.

Dickinson, R.E., Land surface processes and climate-surface albedos and energy balance, *Advances in Geophysics*, *25*, 305-353, 1983.

DNR, Land Cover Change in Queensland 1991-1995, pp. 52, Queensland Department of Natural Resources, Brisbane, 1999a.

DNR, Land Cover Change in Queensland 1995-1997, pp. 54, Queensland Department of Natural Resources, Brisbane, 1999b.

DNR, Land Cover Change in Queensland 1997-1999, pp. 57, Queensland Department of Natural Resources, Brisbane, 2000.

DNRM, Land Cover Change in Queensland 1999-2001, pp. 78, Queensland Department of Natural Resources and Mines, Brisbane, 2003.

Dorman, J.L., and P.J. Sellers, A Global Climatology of Albedo, Roughness Length and Stomatal Resistance for Atmospheric General Circulation Models as Represented by the Simple Biosphere Model (SiB), *Journal of Applied Meteorology*, *28*, 833-855, 1989.

Field, C.B., and R. Avissar, Bidirectional Interactions between the Biosphere and the Atmosphere - Introduction, *Global Change Biology*, *4*, 459-460, 1998.

Forestry and Timber Bureau, D.o.N.D., *The use of trees and shrubs in the dry country of Australia*, Australian Government Publishing Service, Canberra, 1972.

Garratt, J.R., *The atmospheric boundary layer*, Cambridge University Press, Cambridge, 1992.

Goddard, NOAA/NASA Pathfinder AVHRR Land Data Set User Manual, National Oceanic and Atmospheric Administration, Greenbelt, 1994.

Gordon, H.B., L.D. Rotstayn, J.L. McGregor, M.R. Dix, E.A. Kowalczyk, S.P. O'Farrell, A.C. Waterman, A.C. Hirst, M.A. Wilson, I.G. Collier, I.G. Watterson, and T.I. Elliot, The CSIRO Mk3 Climate System Model, pp. 62, CSIRO, Melbourne, 2002.

Goswami, B. N., Interannual variations of Indian summer monsoon in a GCM: External conditions versus internal feedbacks. *Journal of Climate, 11*, 501-522, 1998.

Goudriaan, J., *Crop Micrometeorology: A Simulation Study*, Wageningen Center for Agricultural Publishing and Documentation, Wageningen, 1977.

Graetz, R.D., The Terrestrial Carbon Pools of the Australian Continent: an assessment of their size, dynamics and tractability, CSIRO Earth Observation Centre, Canberra, 1998.

Graetz, R.D., R.P. Fisher, and M.A. Wilson, *Looking Back: The changing face of the Australian continent, 1972-1992*, CSIRO Office of Space Science & Applications, Canberra, 1992.

Graetz, R.D., M.A. Wilson, and S. Campbell, *Looking Around: A contemporary assessment of landcover disturbance for the Australian continent*, CSIRO Office of Space Science & Applications, Canberra, 1995a.

Graetz, R.D., M.A. Wilson, and S.K. Campbell, Land Cover Disturbance over the Australian Continent: A Contemporary Assessment, Department of Arts, Sports and Territories, Canberra, 1995b.

Groves, R.H., Origins of Western Environmentalism, *Scientific American*, *267* (1), 42-47, 1992.

Gurevitch, J., S.M. Scheiner, and G.A. Fox, *The Ecology of Plants*, Sinauer Associates, Inc., Sunderland, 2002.

Hagemann, S.H., M. Botzet, L. Dumenil, and B. Machenhauer, Derivation of global GCM boundary conditions from 1 km land use satellite data, pp. 1-34, Max Planck Institute for Meteorology, Hamburg, 1999.

Hales, K., and J.D. Neelin, Sensitivity of Tropical Land Climate to Leaf Area Index: Role of Surface Conductance versus Albedo, *Journal of Climate*, *In Press*, 2002.

Henderson-Sellers, A., and K. McGuffie, *A Climate Modelling Primer*, John Wiley & Sons Ltd., Wiltshire, 1987.

Huggett, R.J., *Environmental Change, The Evolving Ecosystem*, 377 pp., Routledge, London, 1997.

Jarvis, P.G., The interpretation of the variations in leaf water potential and stomatal conductance found in canopies in the field, *Philosophical transactions of the Royal Society of London. Series B*, *273*, 593-610, 1976.

Jeffery, S.J., J.O. Carter, K.B. Moodie, and A.R. Beswick, Using spatial interpolation to construct a comprehensive archive of Australian climate data, *Environmental Modelling and Software*, *16* (4), 309-330, 2001.

Kabat, P., M. Claussen, P.A. Dirmeyer, J.H.C. Gash, L. Bravo de Guenni, M. Meybeck, R.A. Pielke Sr., C.J. Vorosmarty, R.W.A. Hutjes, and S. Lutkemeier, *Vegetation, Water, Humans and the Climate: a New Perspective on an Interactive System*, Springer, Berlin, Heidelberg, New York, 2004.

Kimes, D.S., Modeling the directional reflectance from complete homogeneous vegetation canopies with various leaf orientation distributions, *Journal of the Optical Society of America, A.*, *1*, 725-737, 1984.

Kistler, R., E. Kalnay, W. Collins, S. Saha, G. White, J. Woollen, M. Chelliah, W. Ebisuzaki, M. Kanamitsu, V. Kousky, H. van den Dool, R. Jenne, and M. Fiorino, The NCEP-NCAR 50-year reanalysis: Monthly means CD-ROM and documentation, *Bulletin of the American Meteorological Society*, *82* (2), 247-267, 2002.

Kondo, J., N. Saigusa, and T. Sato, A Parameterization of Evaporation from Bare Soil Surfaces, *Journal of Applied Meteorology*, *29*, 385-389, 1990.

Koster, R., and M.J. Suarez, A comparative analysis of two land surface heterogeneity representations, *Journal of Climate*, *5*, 1379-1390, 1992.

Kulcher, A.W., World map of natural vegetation, in *Goode's World Atlas*, pp. 16-17, Rand McNally, 1983.

Lawton, R.O., U.S. Nair, R.A. Pielke, and R.M. Welch, Climate impact of tropical lowland deforestation on nearby montane cloud forests, *Science*, *294*, 584-587, 2001.

Lee, T.J., and R.A. Pielke, Estimating the Soil Surface Specific Humidity, *Journal of Applied Meteorology*, *31*, 480-484, 1992.

Li, D., H. Komiyama, K. Kurihara, and Y. Sato, Case studies of the impact of landscape changes on weather modification in Western Australia in summer, *Journal of Geophysical Research*, *15* (D10), 12,303-12,315, 2000.

Lofgren, B.M., Sensitivity of Land-Ocean Circulations, Precipitation, and Soil Moisture to Perturbed Land Surface Albedo, *Journal of Climate*, *8*, 2521-2542, 1995.

Loveland, T.R., B.C. Reed, J.F. Brown, D.O. Ohlen, Z. Zhu, L. Yang, and J.W. Merchant, Development of a global land cover characteristics database and IGBP DISCover from 1km AVHRR data, *International Journal of Remote Sensing*, *21* (6 & 7), 1303-1330, 2000.

Lyons, T.J., P. Schwerdtfeger, J.M. Hacker, I.J. Foster, R.C.G. Smith, and H. Xinmei, Land-Atmosphere interaction in a semiarid region: The bunny fence experiment, *Bulletin of the American Meteorological Society*, *74* (7), 1327–1334, 1993.

Manins, P., R. Allan, T. Beer, P. Fraser, P. Holper, R. Suppiah, and K. Walsh, Atmosphere, Australia State of the Environment Report (Theme Report), Department of Environment and Heritage, Canberra, 2001.

McAlpine, C.A., R. Fensham, and S. McIntire, Sustainable Management of Queensland Landscapes: Linking the Science and Action, *The Rangeland Journal*, *24* (1), 3-5, 2002.

McKeon, G.M. et al., Learning from history: land and pasture degradation episodes in Australia's rangelands, Brisbane, 2000.

McVicar, T.R., J. Walker, D.L.B. Jupp, L.L. Pierce, G.T. Byrne, and R. Dallwitz, Relating AVHRR vegetation indices to in situ measurement of leaf area index, pp. 56, CSIRO, Canberra, 1996.

Meador, W.E., and W.R. Weaver, Two-stream approximations to radiative transfer in planetary atmospheres: A unified description of existing methods and a new improvement, *Journal of Atmospheric Science*, *37*, 630-643, 1980.

Monteith, J.L., and M.H. Unsworth, *Principles of Environmental Physics*, Routledge, Chapman and Hall, Inc., New York, 1990.

Moore, N., and S. Rojstaczer, Irrigation's influence on precipitation: Texas High Plains, U.S.A, *Geophysical Research Letters*, *29* (16), 2-1 - 2-4, 2002.

Myneni, R.B., G. Asra, and E.T. Kanemasu, The theory of photon transport in leaf canopies, in *Theory and Application of Optical Remote Sensing*, edited by G. Asra, pp. 142-204, Wiley and Sons, 1989.

Myneni, R.B., R.R. Nemani, and S.W. Running, Estimation of Global Leaf Area Index and Absorbed Par Using Radiative Transfer Models, *IEEE Transactions on Geoscience and Remote Sensing*, *35* (6), 1380-1393, 1997.

Narisma, G.T., and A.J. Pitman, The Impact of 200 Years of Land Cover Change on the Australian Near-Surface Climate, *Journal of Hydrometeorology*, *4*, 424-437, 2003.

NLWRA, Australian Agriculture Assessment 2001, National Land and Water Resources Audit, Canberra, 2001a.

NLWRA, Australian Native Vegetation Assessment 2001, National Land and Water Resources Audit, Canberra, 2001b.

Noilhan, J., and S. Planton, A Simple Parameterization of Land Surface Processes for Meteorological Models, *Monthly Weather Review*, *117*, 536-549, 1989.

Oke, T.R., *Boundary layer climates*, 435 pp., Routledge, New York, 1987.

Oleson, K.W., G.B. Bonan, S. Levis, and M. Vertenstein, Effects of land use change on U.S. climate: Impact of surface datasets and model biogeophysics, *Climate Dynamics (in Prep)*, 2004.

Oleson, K.W., G.B. Bonan, C. Schaaf, F. Gao, Y. Jin, and A.H. Strahler, Assessment of global climate model land surface albedo using MODIS data, *Geophysical Research Letters*, *30* (8), 1443-1447, 2003.

Orlanski, I., A subdivision of scales for atmospheric processes, *Bulletin of the American Meteorological Society*, *56*, 527-530, 1975.

Peixoto, J.P., and A.H. Oort, *Physics of Climate*, 520 pp., American Institute of Physics, New York, 1992.

Pielke, R.A., Earth System Modeling - An Integrated Assessment Tool for Environmental Studies, in *Present and Future of Modeling Global Environmental Change: Toward Integrated Modeling*, edited by T. Matsuno, and H. Kida, Terra Scientific Publishing, Tokyo, 2001a.

Pielke, R.A., Influence of the spatial distribution of vegetation and soils on the prediction of cumulus convective rainfall, *Reviews of Geophysics*, *39* (2), 151-177, 2001b.

Pielke, R.A., and R. Avissar, Influence of landscape structure on local and regional climate, *Landscape Ecology*, *4* (2/3), 133-155, 1990.

Pielke, R.A., R. Avissar, M.R. Raupach, A.J. Dolman, X. Zeng, and A.S. Denning, Interactions between the atmosphere and terrestrial ecosystems: influence on weather and climate, *Global Change Biology*, *4*, 461-475, 1998.

Pielke, R.A., G. Marland, R.A. Betts, T.N. Chase, J.L. Eastman, J.O. Niles, D. Niyogi, and S.W. Running, The influence of land-use change and landscape dynamics on the climate

system: relevance to climate-change policy beyond the radiative effect of greenhouse gases, *Philosophical transactions of the Royal Society of London. Series A*, *360*, 1-15, 2002.

Pielke, R.A., P.L. Vidale, J.L. Eastman, G.E. Liston, R.L. Walko, G. Dalu, A. Barr, and C. Ziegler, Influence of landscape on boundary layer atmospheric processes, in *Symposium on the Boundary Layers and Turbulence (Land Surface). 77th AMS Annual Meeting*, pp. 10-14, Long Beach, California, 1997.

Pitman, A.J., Simulating heterogeneous vegetation in climate models. Identifying when secondary vegetation becomes important, *Hydrological Processes*, *9*, 719-728, 1995.

Polcher, J., and K. Laval, A statistical study of the regional impacts of deforestation on climate in the LMD GCM, *Climate Dynamics*, *10*, 205-219, 1994.

Ramankutty, N., J.A. Foley, and N.J. Olejniczak, Changes in Global Croplands During the 20th Century: Implications for Food Security, *Ambio*, 2000.

Raupach, M.R., Drag and drag partition on rough surfaces, *Boundary Layer Meteorology*, *60*, 375-395, 1992.

Raupach, M.R., Simplified expressions for vegetation roughness length and zero-plane displacement as functions of canopy height and area index, *Boundary Layer Meteorology*, *71*, 211-216, 1994.

Raupach, M.R., and J.J. Finnigan, Scale issues in boundary-layer meteorology: Surface energy balances in heterogeneous terrain, *Hydrological Processes*, *9*, 589-612, 1995.

Ray, D.K., U.S. Nair, R.M. Welch, Q. Han, J. Zeng, W. Su, T. Kikuchi, and T.J. Lyons, Effects of land use in Southwest Australia: 1. Observations of cumulus cloudiness and energy fluxes, *Journal of Geophysical Research*, *108* (D14), 4414-4434, 2003.

Rayner, N.A., E.B. Horton, D.E. Parker, C.K. Folland, and R.B. Hackett, Version 2.2 of the Global sea-Ice and Sea Surface Temperature Data Set, 1903-1994, Hadley Centre, 1996.

Reale, O., and P.A. Dirmeyer, Modeling the effects of Vegetation on Mediterranean Climate During the Roman Classical Period. Part I: Climate History and Model Sensitivity, pp. 1-48, Center for Ocean-Land-Atmosphere Studies, Calverton, 1998.

Reynolds, C.A., T.J. Jackson, and W.J. Rawls, Estimating Available Water Content by Linking the FAO Soil Map of the World with Global Soil Profile Databases and Pedo-transfer Functions, in *AGU 1999 Spring Conference*, Boston, MA., 1999.

Schaaf, C.B., F. Gao, A.H. Strahler, W. Lucht, X. Li, T. Tsang, N.C. Strugnell, X. Zhang, Y. Jin, and J.-P. Muller, First operational BRDF, albedo nadir reflectance products from MODIS, *Remote Sensing of Environment*, *83* (1-2), 135-148, 2002.

Sellers, P.J., Canopy reflectance, photosynthesis and transpiration, *International Journal of Remote Sensing*, *6* (8), 1335-1372, 1985.

Sellers, P.J., Modelling the exchanges of water, energy and carbon between continents and the atmosphere, *Science*, *275*, 1997.

Sellers, P.J., S.O. Los, C.J. Tucker, C.O. Justice, D.A. Dazlich, G.J. Collatz, and D.A. Randall, A Revised Land Surface Parameterization (SiB2) for Atmospheric GCMs. Part II: The Generation of Global Fields of Terrestrial Biophysical Parameters from Satellite Data, *Journal of Climate*, *9*, 706-737, 1996a.

Sellers, P.J., B.W. Meeson, J. Closs, G.J. Collatz, F. Corprew, F.G. Hall, Y. Kerr, R. Koster, S.O. Los, K.E. Mitchell, J. McManus, D. Myers, K.J. Sun, and P. Try, An Overview of the ISLSCP Initiative I Global Data Sets, pp. 34, NASA/GSFC, Greenbelt, 1995.

Sellers, P.J., D.A. Randall, G.J. Collatz, J.A. Berry, C.B. Field, D.A. Dazlich, C. Zhang, G.D. Collelo, and L. Bounoua, A Revised Land Surface Parameterisation (SiB2) for Atmospheric GCMs. Part I: Model Formulation, *Journal of Climate*, *9*, 676-705, 1996b.

Shaw, R.H., and A.R. Pereira, Aerodynamic roughness of a plant canopy: a numerical experiment, *Agricultural Meteorology*, *26*, 51-65, 1982.

Shuttleworth, W.J., The Modellion concept, *Reviews of Geophysics*, *29*, 585-606, 1991.

Specht, R.L., Vegetation, in *The Australian Environment*, edited by G.W. Leeper, CSIRO in assoc. with Melbourne University Press, Melbourne, 1970.

Stohlgren, T.J., T.N. Chase, R.A. Pielke, T.G.F. Kittel, and J.S. Baron, Evidence that local land use practices influence regional climate, vegetation, and stream flow patterns in adjacent natural areas, *Global Change Biology*, *4* (5), 495-504, 1998.

Sturman, A., and N. Tapper, *The weather and climate of Australia and New Zealand*, 476 pp., Oxford University Press, Melbourne, 1996.

Thompson, D.W.J., and S. Solomon, Interpretation of recent Southern Hemisphere climate change, *Science*, *296*, 895-899, 2002.

Trenberth, K.E., *Climate system modeling*, 788 pp., Cambridge University Press, London, 1992.

Wang, B., I. Kang, and J. Lee, Ensemble Simulations of Asian–Australian Monsoon Variability by 11 AGCMs, *Journal of Climate*, *17*, 803–818, 2004.

Webster, P.J., and S. Yang, Monsoon and ENSO, *Quarterly Journal of the Royal Meteorological Society*, *118*, 877-926, 1992.

Webster, P.J., V.O. Magana, T.N. Palmer, J. Shulka, R.A. Tomas, M. Yanai, and T. Yasunari, Monsoons: Processes, predictability, and the prospects of prediction, *Journal of Geophysical Research*, *103*, 14451-14510, 1998.

Wigley, T.M.L., and B.D. Santer, Statistical Comparison of Spatial Fields in Model Validation, Perturbation, and Predictability Experiments, *Journal of Geophysical Research*, *95* (D1), 851-865, 1990.

Willmott, C.J., and S.M. Robeson, Climatologically Aided Interpolation (CAI) of Terrestrial Air Temperature, *International Journal of Climatology*, *15*, 221-229, 1995.

Wright, W.J., and D.A. Jones, Long-term rainfall declines in southern Australia, in *Science for drought*, edited by R. Stone, and I. Partridge, pp. 35-39, Brisbane, 2003.

Xinmei, H., and T.J. Lyons, Estimation of Land Surface Parameters using Satellite Data, *Hydrological Processes*, *9*, 631-643, 1995.

Xinmei, H., T.J. Lyons, and R.C.G. Smith, Meteorological impact of replacing native perenial vegetation with annual agricultural species, *Hydrological Processes*, *9*, 645-654, 1995.

Yang, Z.L., Investigating impacts of anomalous land-surface conditions on Australian climate with an advanced land-surface model coupled with the BMRC GCM, *International Journal of Climatology*, *15*, 137-174, 1995.

Zeng, N., Understanding climate sensitivity to tropical deforestation in a mechanistic model. *Journal of Climate*, *11*, 1969-1975, 1998.

Zhang, H., A. Henderson-Sellers, and K. McGuffie, Impacts of Tropical Deforestation. Part I: Process Analysis of Local Climatic Change, *Journal of Climate*, *9*, 1497-1517, 1995.

Zhao, M., A.J. Pitman, and T.N. Chase, The impact of land cover change on the atmospheric circulation, *Climate Dynamics*, *17*, 467-477, 2001.